Alma Mater Studiorum · Università di Bologna

facoltà di scienze matematiche, fisiche e naturali

Dottorato di Ricerca in
Biologia Cellulare Molecolare e Industriale
Ciclo XXIV

Settore scientifico disciplinare di afferenza: MED/04
Settore concorsuale di afferenza: 06/A2

Genetic Analysis of Tumour Initiation and Progression in a *Drosophila* Model of Epithelial Cancer

Presentata da
Francesca Froldi

Coordinatore:
Prof. Michela Rugolo

Relatore
Prof. Annalisa Pession

Esame Finale anno 2012

Abstract

Neoplastic overgrowth depends on the cooperation of several mutations ultimately leading to major rearrangements in cellular behaviour. The molecular crosstalk occurring between precancerous and normal cells strongly influences the early steps of the tumourigenic process as well as later stages of the disease. Precancerous cells are often removed by cell death from normal tissues but the mechanisms responsible for such fundamental safeguard processes remain in part elusive.

To gain insight into these phenomena I took advantage of the clonal analysis methods available in *Drosophila* for studying the phenotypes due to loss of function of the neoplastic tumour suppressor *lethal giant larvae* (*lgl*). I found that *lgl* mutant cells growing in wild-type imaginal wing discs are subject to the phenomenon of cell competition and are eliminated by JNK-dependent cell death because they express very low levels of dMyc oncoprotein compared to those in the surrounding tissue. Indeed, in non-competitive backgrounds *lgl* mutant clones are able to overgrow and upregulate dMyc, overwhelming the neighbouring tissue and forming tumourous masses that display several cancer hallmarks. These phenotypes are completely abolished by reducing dMyc abundance within mutant cells while increasing it in *lgl* clones growing in a competitive context re-establishes their tumourigenic potential.

Similarly, the neoplastic growth observed upon the oncogenic cooperation between *lgl* mutation and activated Ras/Raf/MAPK signalling was found to be characterised by and dependent on the ability of cancerous cells to upregulate dMyc with respect to the adjacent normal tissue, through both transcriptional and post-transcriptional mechanisms, thereby confirming its key role in *lgl*-induced tumourigenesis. These results provide first evidence that the dMyc oncoprotein is required in *lgl* mutant tissue to promote invasive overgrowth in developing and adult epithelial tissues and that dMyc abundance inside *versus* outside *lgl* mutant clones plays a key role in driving neoplastic overgrowth.

Contents

Chapter 1

Introduction

Multicellularity has originated in many instances since life has appeared on Earth leading to the evolution of increasingly complex organisms, capable of self-replication, in which different cell types perform specialised functions integrated by sophisticated and finely tuned regulatory circuits [1]. As complexity increased, a plethora of strategies have evolved to keep proliferation, differentiation, adhesion and migration of each and every cell of the organism under strict control to ensure the correct and harmonious development of multicellular beings, their ability to adapt to the environment and thus increase their chances of survival. Nevertheless, along with undeniable advantages, evolution of multicellularity has its downside: breakdown of regulatory circuits can lead to escape from developmental constraints, uncontrolled proliferation and altered behaviour of cells, a disease known as cancer.

Cancer is the leading cause of death in developed countries and the second leading cause of death in developing countries [2]. Despite the huge effort in terms of biomedical and pharmacological research, it has been estimated that about 12.7 million cancer cases and 7.6 million cancer death have occurred in 2008 worldwide [2]. The reason for this lies in the complexity and heterogeneity of this disease. It is now widely accepted that it results from the clonal accumulation and cooperation of various genetic and epigenetic lesions which cause the progressive transformation of normal somatic cells into malignant derivatives which can grow, invade and migrate uncontrollably [3].

Two general classes of genes are typically affected in cancer cells: oncogenes and tumour suppressor genes (TGS). The first are aberrantly activated and thus represent dominant gain of function mutations of genes (proto-oncogenes) generally

involved in growth and division promotion and protection against programmed cell death. On the other hand, tumour suppressor genes are inactivated in cancer cells (commonly in the form of recessive loss of function mutations), resulting in the loss of normal cellular functions, such as accurate DNA damage repair, control over the cell cycle, cell polarity and adhesion within tissues [3].

Cancer can arise in virtually any organ but those of epithelial origin, namely carcinomas, are the most frequent form, representing about 90% of all human malignant tumours. The first carcinogenic events generally lead to local hyperproliferation/metaplasia or dysplasia that then evolves into *in situ* carcinoma, which already exhibit strong alterations in cell physiology and behaviour, such as loss of differentiation, apical-basal cell polarity and tissue organisation, but the lesion is still confined within the basement membrane (BM), a specialised sheet of extracellular matrix that underlies epithelial tissues. At this stage, tumour-induced angiogenesis and vascularisation of the cancerous mass is also observed. Finally the tumour becomes invasive when basement membrane degradation occurs and cells disseminate to neighbouring tissues. These cells can eventually intravasate into lymph or blood vessels, allowing their passive transport to distant organs. At secondary sites, carcinoma cells can extravasate seeding micrometastases that in some cases will form secondary lesions, the final step of this sequence of events often termed invasion-metastasis cascade (Fig. 1.1) [3].

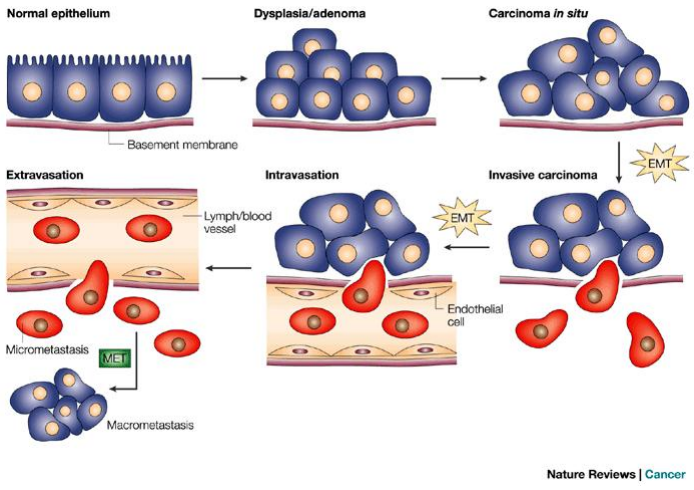

Figure 1.1: Main stages of epithelial tumour progression from dysplasia to metastasis [4]. A detailed description is given in the text.

1.1 The Hallmarks of Cancer

The heterogeneity and complexity of cancer led to the widely accepted notion that it represents a large group of different diseases with a common outcome rather than a single pathological condition [5]. Tumourigenesis can indeed be seen as a Darwinian evolutionary process: it founds itself on random genetic variation and evolves by means of natural selection within the organism. Mutant cancerous cells compete for space and resources and are under a strong selective pressure to evolve strategies which will allow them to evade the organism defensive mechanisms and to be able to proliferate, migrate and colonise. All those acquired features, leading to an increased fitness of the cancerous cell, will result in an enhanced "reproductive" success, a growth advantage, and thus will be favourably selected [5, 6].

There are more than 100 distinct types of cancers and a myriad of organ- and tissue-specific subtypes, everyone characterised by a set of genetic and epigenetic lesions that may differ even within each subtype. But, despite this remarkable diversity, it is still possible to identify a handful of essential physiologic alterations that cells need to acquire in order to progress towards malignancy. A huge effort in this sense has been made by Hanahn and Weinberg to provide a conceptual framework for understanding the complex biology of cancer [5, 7]; the authors have identified six hallmarks that are shared by most if not all human tumours: sustaining proliferative signals, evading growth suppressors, resisting cell death, enabling replicative immortality, inducing angiogenesis and activating invasion and metastasis (Fig. 1.2). Two emerging hallmarks have been added in the more up to date review [7]: reprogramming energy metabolism and evading immune destruction (Fig. 1.3).

Self-Sufficiency in Growth Signals Abnormal proliferation is probably the most striking feature of cancer. Cell proliferation in a healthy tissue is carefully controlled and depends on the release of growth-promoting factors which activate membrane receptors and their downstream signalling pathways stimulating growth, cell cycle entry and cell division. There are several ways cancerous cells can gain independence from physiological mitogenic signals and paroxystically activate proliferative programs. These cells may be able to produce growth factors and thus induce proliferation in an autocrine fashion or stimulate the tumour-associated stroma to release them. Alternatively growth signal receptors can be overexpressed resulting in higher sensitivity towards the ligands. Nevertheless, the most common way in

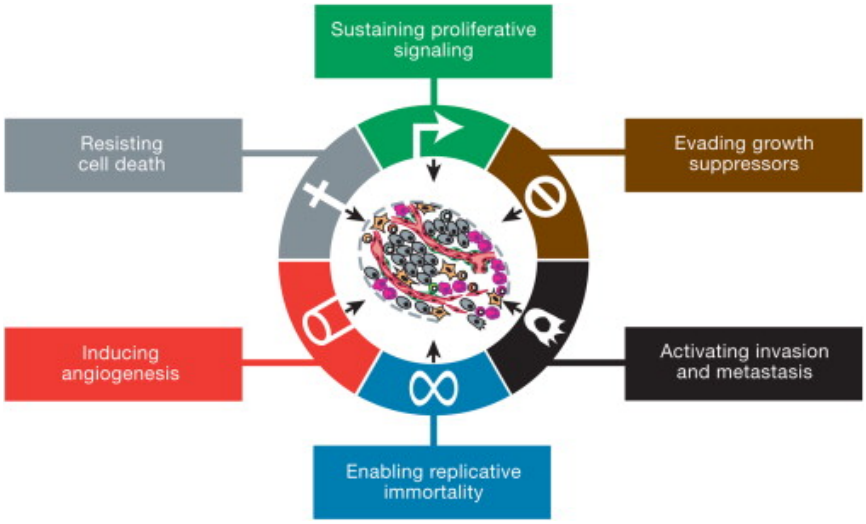

Figure 1.2: The six hallmarks of cancer proposed by Hanahan and Weinberg in 2000 [5].

which cancer cells become independent of mitogenic factors is the constitutive activation of components of proliferation-promoting pathways (or the loss of negative regulators) [5, 7]. This is probably best exemplified by the Ras/MAPK (Mitogen Activated Protein Kinase) signalling cascade as activating mutations of its members are found in a significant percentage of human cancers [8]. This key signalling pathway and its relevance to cancer will be discussed in greater detail in Section 1.3.

Insensitivity to Anti-Growth Signals Tissue homeostasis is also maintained by means of powerful antiproliferative programs that cancer cells need to circumvent for unrestrained proliferation to occur. In physiological conditions proliferation is inhibited by two distinct mechanisms: cells may enter a quiescent state (the so-called G_0 phase), a reversible condition that allows re-entry into the cell cycle upon mitogenic signalling, alternatively cells can permanently block proliferative programs by committing them-selves to a specific cell fate and entering the post-mitotic state. Relief of proliferation inhibition is generally achieved through loss of function of tumour suppressor genes, the key players in these processes, and inactivating mutations of these genes are indeed a common feature of all tumours. At the same time some oncogenes are known to inhibit terminal differentiation allowing mutant cells to switch back to a fully proliferative phenotype [5, 7].

Cell Death Evasion Programmed cell death is a major safe-guard mechanism employed in the control of the balance between cell proliferation, differentiation and death. Besides ensuring the correct patterning and development of the organism it also serves the elimination of damaged and potentially harmful cells. Apoptosis, arguably the best characterised form of programmed cell death, is known to be triggered in response to many stresses cancerous cells face in the course of tumour development, including hyperproliferation, elevated levels of oncogene signalling and DNA damage. In normal conditions both intra- and extracellular stresses are perceived by molecular sensors which can elicit adequate responses or, if the damage is not reversible, trigger cell death. Unsurprisingly many of these sensors belong to the tumour suppressor genes category and are found inactivated in human cancers, being p53 a well-known example. Increased expression of antiapoptotic regulators or pro-survival signals or downregulation of proapoptotic molecules are also strategies cancer cells may use to prevent cell death [5, 7].

Limitless Replicative Potential It has been established that normal cells are able to undergo only a limited number of growth and division cycles before irreversibly entering a non-proliferative status named senescence. This phenomenon is particularly evident when cells are propagated in culture: they pass through a certain number of cell divisions and then become senescent. Senescence seems to be linked to the telomere ends. Each cell division telomeres undergo progressive shortening untill they reach a critical length and proliferation is inhibited. Inducing cells to circumvent this barrier by forcing cell proliferation leads to telomere loss and thus genomic instability; as a consequence cells enter a crisis phase characterised by high levels of cell death; rare variants may emerge from this crisis and acquire limitless replicative potential, a status termed immortalisation. Senescence and crisis, much like programmed cell death, are self-defence mechanism against uncontrolled proliferation that cancer cells need to overcome to acquire limitless replicative potential and give rise to a tumour. Immortalisation of cells which will eventually proceed towards malignancy seems to depend on their ability to maintain telomeric DNA at a length sufficient to avoid triggering of senescence or apoptosis. This is generally achieved by upregulating the activity of telomerase, a specialised DNA polymerase that adds telomere repeat units to the chromosomal ends, usually absent in nonimmortalised cells [5, 7].

Sustained Angiogenesis Beyond a critical tumour volume, diffusion of oxygen and nutrients becomes insufficient to sustain the metabolic requirements of the growing mass and cells suffer from hypoxia. This hypoxic condition triggers the so-called angiogenic switch: the normally quiescent vasculature is induced to proliferate, expand and sprout new vessels which penetrate into the tumour supplying it with oxygen and nutrients as well as evacuating its metabolic waste. A sustained angiogenesis is thus an essential step in tumour progression and also provides cancer cells with an access to the blood stream allowing them to spread and metastasise to distant sites. Angiogenesis is generally activated by cancer cells upon the secretion of proangiogenic factors such as VEGF (Vascular Endothelial Growth Factor) and FGF (Fibroblast Growth Factor) which are normally responsible for regulating blood vessel growth during development as well as in physiologic conditions in the adult (i.e. wound healing) [5, 7].

Recent findings seem to prove that angiogenesis can start very early in tumour development, before hypoxia occurs. This "early angiogenesis" is triggered by the cancer-initiating cells or cancer stem cells (CSC), which have potent pro-angiogenic capabilities. CSC are characterised by high plasticity and multipotency of differentiation; interestingly, they are able to transdifferentiate into several cell types, including endothelial cells, and to form a vascular-like structure which supplies blood to the tumour in the early stages of cancer development, called vasculogenic mimicry (VM). It was proposed that only later VM is replaced by endothelium-dependent vasculature via a transition phase where vessels are a mosaic of cancer and endothelial cells. Indeed, a significant proportion of the tumour-associated vascular endothelium has been proved to be of neoplastic origin [9].

Invasion and Metastasis More than 90% of cancer mortality is not attributable to the growth of the primary tumour, often successfully removable by surgical resection, but to the development of metastases which, due to their systemic nature and resistance to therapeutic agents, are still largely incurable. In the last decade of research substantial progress has been made towards the understanding of the molecular mechanisms behind the invasion-metastasis cascade, in particular regarding carcinomas, but a lot still needs to be achieved to fully address this pivotal hallmark.

It is now clear that epithelial cells acquire the ability to invade, migrate and

disseminate by activating the epithelial-mesenchymal transition (EMT), a developmental regulatory program involved, in physiologic conditions, in various aspects of embryonic morphogenesis and wound healing, which consists in loss of cell adhesion, acquisition of a fibroblastic-like morphology, secretion of matrix-degrading enzymes, increased motility and resistance to apoptosis. Secretion of proteases, such as matrix-metalloproteinases (MMPs), able to degrade matrix components, allows carcinoma cells freed from cell-adhesive ties to branch the basement membrane and directly invade the stroma. Besides the mesenchymal-like invasion characteristic of EMT, two other mechanisms of invasion have been identified: collective invasion, where cells migrate in clusters, and ameboid invasion in which individual cells slide through existing interstices. Once in the stroma, by virtue of their motility, cancer cells can directly access the systemic circulation by entering either lymphatic or blood vessels, being these latter the most common option. Intravasation is facilitated by the abnormal leakiness which characterises the tumour-associated neovasculature. When in the blood stream cancer cells need to resist multiple stresses as anchorage loss, hemodynamic shear forces and immune system attacks and they seem to be able to overcome these threats by interacting with platelets and forming emboli, a process akin to normal blood coagulation.

Robust clinical evidence proved that individual types of carcinomas form metastasis in only a limited subset of target organs, a phenomenon called tissue tropism. It is still unclear what the reasons for this selectivity are and two main hypotheses have been proposed. The first envisions a passive mechanical explanation according to which circulating cancer cells arrest within the capillary beds of certain organs due to vessel diameter restrictions and are thus unable to reach more distant territories. The alternative hypothesis is that cancer cells posses intrinsic characteristics that determine their ability to interact with specific microenvironments. Extravasation may also play a role in organ tropism: microvessels in normal tissues, distant from the primary tumour, are functional and posses an extremely low permeability, moreover while some organs result relatively accessible, some other are protected by additional physical obstacles (i.e. the blood-brain barrier). Nevertheless circulating cancer cells are known to be able to secrete specific factors able to perturb physical barriers and increase vascular permeability.

In order to form micrometastases tumour cells must survive in a new environment and may adapt to new conditions via the establishment of a “premetastatic

niche" induced by systemic signals released by the primary tumour, but more generally, disseminating cancer cells seem to employ very complex local strategies to modify their new microenvironment as well as trigger cell-autonomous mechanisms to adapt to it.

It has been estimated that less then 0,01% of cancer cells that enter into the systemic circulation develop into clinically detectable metastases. Micrometastasis formation is certainly a rate-limiting step but the most prominent one appears to be colonisation. In fact, the vast majority of the carcinoma cells that do manage to land in distant sites are probably either poorly adapted to the new environment, experience high levels of cell death that counterbalance possible high levels of cell proliferation or enter a quiescent state that may persist for years after seeding. Nevertheless, certain organs seem to offer a more hospitable environment to certain types of cancer cells (the well-known seed-and-soil model of metastatic dissemination) giving yet another explanation for the phenomenon of tissue tropism.

Substantial progress is currently being made to define a metastatic signature of gene expression changes which correlates with the establishment of macroscopic metastases in specific tissues. This will also help clarify how metastasis-promoting genetic alterations are selected within the primary tumour: whether these mutations are also beneficial to primary growth and thus are fixed before cells start to disseminate or whether they are stochastically accumulated as "passenger" mutations that will only subsequently give an advantage and be fixed. Alternatively, cells may leave the tumour in a partially metastatic-competent condition and further evolve once they experience the new environment-associated pressure. Indeed, an increasing body of evidence seems to point towards a parallel progression model for certain types of carcinomas, according to which mutant cells disseminate relatively early, from pre-neoplastic lesions, and undergo genetic diversification and selection within the distant target organs thus showing a rather different genetic profile with respect to the primary tumour [7, 10].

Enabling Characteristics Acquisition of the hallmarks described above relies on the recurrence of genetic alterations that may, by chance, provide cells with novel advantageous capabilities and thus be favourably selected and fixed. In normal conditions spontaneous mutation rate is extremely low thanks to very efficient genome maintenance systems capable of detecting and repairing DNA damages and

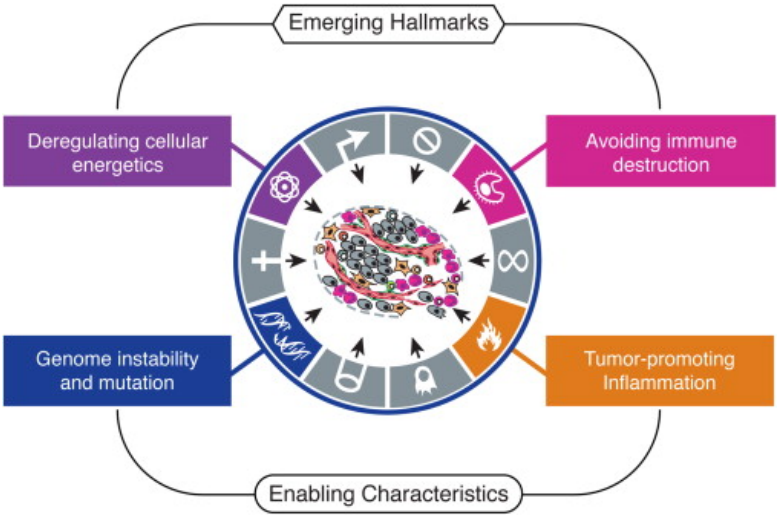

Figure 1.3: The emerging hallmarks and enabling characteristics Hanahan and Weinberg added to their conceptual framework of cancer biology in 2011 [7].

defects. Mutation rate must therefore somehow be increased to explain how cancer cells are able to accumulate a sufficient number of lesions to develop a malignant behaviour. A higher mutability can be achieved by precancerous cells through impairment of the genome maintenance systems them-selves or of those circuits which monitor genome integrity and force damaged and potentially dangerous cells into apoptotic cell death. Indeed, many genes belonging to these two categories can be classified as tumour suppressor genes and are often found inactivated in most, if not all, human cancers. In addition, a certain degree of genomic instability initially generated upon telomeric ends loss (before telomerase activity is restored) in the process of immortalisation may further promote accumulation of genetic lesions. It is therefore clear that high genomic instability is to be considered an enabling characteristic as it endows the row material on which natural selection can act and, as a consequence, drive tumour progression.

Another distinctive trait that all neoplastic lesions share is the presence, at various degrees, of immune system cells. Counterintuitively, a large body of compelling evidence has unquestionably led in recent years to the conclusion that the tumour-associated inflammatory response has tumour-promoting rather than anticancer effects. Immune cells have been proved to contribute to the acquisition of multiple hallmarks by releasing a wide range of molecules among which growth and

prosurvival factors thus sustaining growth and limiting cell death, by producing matrix metalloproteinases and pro-angiogenic molecules facilitating angiogenesis and stimulating cancer cells to undergo EMT, invasion and metastasis. Moreover inflammatory cells can also contribute to genomic instability by releasing reactive oxygen species (ROS), potent mutagenic agents [7].

The Emerging Hallmarks It has been known for long time that cancer cells have peculiar metabolic charcteristics, despite their higher energetic requirements, even in presence of oxygen these cells switch to a much less efficient glycolytic metabolism, the well-known Warburg effect. Glycolysis can be upregulated both by certain oncogenes such as Myc and Ras and by hypoxic condition but the biological significance of this metabolic reprogramming remains elusive. According to some interpretations glycolytic intermediates can be redirected into various biosynthetic pathways, including those of aminoacids and nucleotides, contributing to sustain the high proliferation rate. Nevertheless, it still needs to be clearly established whether deregulation of energy metabolism belongs to the core hallmarks or it merely is a secondary effect of proliferation-inducing oncogenes activity and/or excessive growth.

A second still disputed issue again involves the immune system. There is some evidence that an actual anti-tumoral immune response exists that cancer cells need to avoid to survive and be able to expand. This immune surveillance seems to be mediated mainly by T and B lymphocytes and macrophages but further work needs to be done to ascertain whether or not antitumour immunity plays a significant role in contrasting cancer development [7].

The tumour-promoting role played by immune system cells is paradigmatic of the fundamental concept that cancer must not be considered as a cell-autonomous disease, instead progression towards malignancy is unavoidably based on the crosstalk between cancer cells and their microenvironment. Besides those belonging to the immune system, many other cell types contribute to the emergence of neoplastic traits in mutant cells: a notable example of the importance of these interactions is given by carcinomas where neoplastic epithelial cells coexist with a variety of cell types such as fibroblasts and endothelial cells which, together with the immune system cells, form the tumour stroma. Indeed stromal cells are leading players in cancer initiation and progression and contribute to the acquisition of nearly all

the hallmarks described above. To take an example, tumour associated fibroblasts can stimulate cell proliferation through release of growth factors, hormones and cytokines; they can convey survival signals and proangiogenic factors and promote invasion and metastasis by inducing EMT of tumour epithelial cells as well as secreting BM-remodelling factors [7, 11].

Further to this, it is becoming clear that tumour development also depends on systemic interactions between cancer cells and distant tissues and organs [12]. An increasingly large body of evidence is thus contributing to the understanding of the tumour-enhancing abilities of the tumour microenvironment, nevertheless very little is known about its tumour-suppressing ones. For earlier stages of cancer development, the probability of progression is lower than for more advanced stages of disease [13] and this clearly suggests the existence of safeguard mechanisms able to avoid the expansion of precancerous lesions.

1.2 Modelling Cancer in *Drosophila*

Most aspects of human carcinogenesis can be profitably investigated employing *Drosophila* as an *in vivo* model. The first tumour-causing mutation was indeed described in the fruit fly by Elizabeth Gateff in the 60's [14]; this mutation affected a *locus* named *lethal giant larvae*, *lgl*, that acted in a recessive manner and was thus the first tumour suppressor gene to be identified, even before the first human transforming oncogenes were described [15]. In subsequent years, also thanks to the possibility to easily conduct wide genetic screens, several other tumour suppressor genes were identified in *Drosophila* that caused uncontrolled proliferation leading to tumorous growth and proved not only to be functionally conserved in mammals but also were found to be altered in human cancers. Thanks to the high degree of conservation of most signalling pathways, analyses of the fly tumour suppressors and proto-oncogenes have produced substantial contribution towards understanding the basic cell biology of tumourigenesis [16]. Nowadays *Drosophila* represents an invaluable model in cancer research as the fine genetic tools available allow to study the clonal effects of multiple genetic manipulations on populations of cells which are embedded in and interact with the surrounding normal tissue; these effects can be examined in the context of a whole organ or even the whole animal and with remarkable resolution [17].

1.2.1 *lethal giant larvae* Tumour Suppressor Gene

Although almost all human tumour suppressors have a fly homologue, conventionally only those genes that cause overproliferation in *Drosophila* can be defined as fly tumour suppressor genes (TGS). They are classified into two main categories: hyperplastic and neoplastic [15].

Hyperplastic Tumour Suppressor Genes Belong to this category those genes that when mutated display extensive overproliferation of imaginal epithelia, but overall tissue monolayer organisation and cell shape are not affected and mutant tissue is able to differentiate into adult organs. Examples are given by loss of function of the Hippo (Hpo) pathway genes, involved in organ size control (see Section 1.2.1.2).

Neoplastic Tumour Suppressor Genes On the other hand, are classified as neoplastic those TGS that, when mutated, cause excessive proliferation accompanied by loss of apical-basal cell polarity and organ structure and in mutant tissues differentiation never occurs. Furthermore, when transplanted into adult hosts, tissues mutant for neoplastic TSG are able to overgrow, spread metastases and kill the host.

Among the neoplastic tumour suppressors so far identified, *lethal giant larvae*, *discs large* (*dlg*) and *scribble* (*scrib*) are of particular interest as they encode conserved proteins involved in the establishment and maintenance of epithelial apical-basal polarity as well as in proliferation control [15]. The regulation of epithelial cell polarity is a crucial issue in cancer biology as its loss is a key feature of carcinomas. As reported in Section 1.1, it well correlates with invasive and metastatic abilities of cancer cells and is strongly associated to a negative prognosis [18, 19].

1.2.1.1 *lgl* in Epithelial Cell Polarity

The plasma membrane of epithelial cells is subdivided into two functionally distinct domains: apical and basolateral domains, by means of epithelial cell junctions (Fig. 1.4). The basolateral domain interconnects neighbouring cells while the apical domain forms a specialised surface usually not in permanent contact with other cells. This distinct polarisation along the apical-basal axis is essential for the adhesion,

communication, vectorial transport, permeability and morphogenetic properties of epithelia [18, 20].

Apical and basolateral domains are separated by an adhesive belt that encircles the cell just below the apical surface, which is called the *zonula adherens* (ZA), made of adherens junctions (AJs). At the core of AJs, E-cadherins mediate cell-cell adhesion through homophilic interactions between their extracellular domains; the cadherin cytoplasmic portion binds β-catenin, (Armadillo in *Drosophila*), that links to α-catenin which in turn binds to F-actin connecting ZA to the cytoskeleton. Vertebrate epithelial cells develop tight junctions (TJs) apical to the ZA. In *Drosophila* epithelial cells no TJs are observed; instead the septate junctions (SJs) lie basal to the ZA and form a region of close membrane contacts that extends over large parts of the lateral plasma membrane domain. SJs and TJs share however some functions in establishing solute barrier as well as regulating paracrine transport. Vertebrates also posses a third epithelial junction, absent from invertebrate tissues, the desmosomes, which mediate adhesion by linking intermediate filament network to the plasma membrane. At cell basement, both in vertebrates and invertebrates, Intergrins and Dystroglycan provide attachment to the basement membrane mainly contacting one of its major components, Laminin [20, 21].

Extensive genetic analysis in *Drosophila* has led to the notion that establishment and maintenance of cell polarity is mediated by the antagonising activity of three main protein complexes: the Crumbs/Stardust/PatJ (apical), the Bazooka/Par6/aPKC (sub-apical) and the Scribble/Dlg/Lgl (basolateral) complexes (Fig. 1.5). Given the pivotal importance of epithelial cell polarity in animal development and homeostasis, it is not surprising that the vast majority of the proteins involved in its regulation are extremely conserved through evolution.

The Crumbs/Stardust/PATJ Complex This complex establishes the apical identity of polarised cells and is required for AJs formation both in *Drosophila* and mammalian epithelial cell lines. It consists of three main components: a transmembrane protein, Crumbs (Crb), and two adaptor proteins Stardust (Sdt) and PATJ. *Drosophila* Crb is characterised by a large extracellular portion with thirty epithelial growth factor (EGF)-like and four laminin A G-domain-like repeats and a small conserved cytoplasmic region. In mammals three homologous genes have been

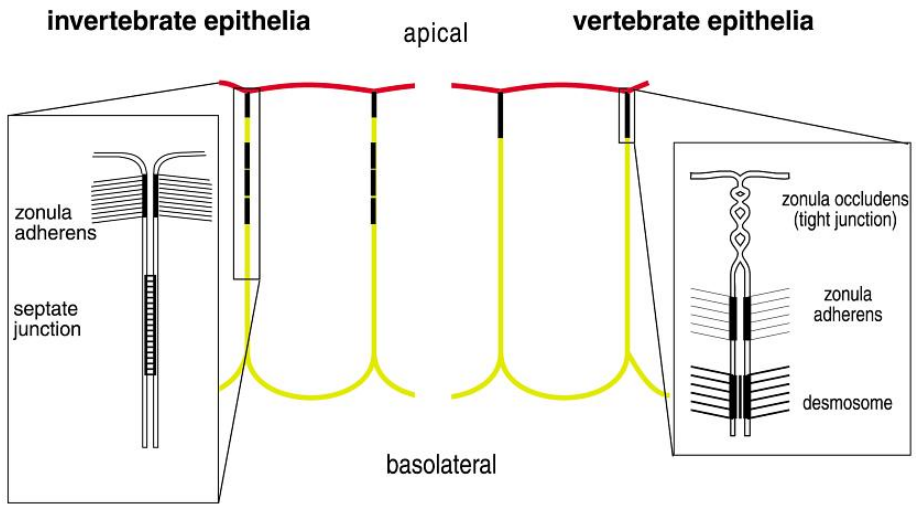

Figure 1.4: Basic epithelial cell structure in invertebrates and vertebrates. The apical and basolateral domains are marked in red and yellow respectively. Schematics of the lateral cell junctions are also shown [20].

identified (*CRB* 1-3); they show tissue specific expression patterns (CRB3 is the most widely expressed in epithelial tissues) and high levels of sequence identity with *Drosophila* Crumbs are observed in the cytoplasmic domain. *std* encodes a MAGUK (Membrane-Associated with GUanylate Kinase domain) protein with a PDZ (PSD-95/Dlg/ZO-1), a SH3 (Src homology region 3) and a GUK (GUanylate Kinase-like) domain which binds Crb intracellular domain. Similarly, CRB3 complexes with the PDZ domain of Std mammalian homologue Pals1 (protein associated with lin seven 1). The third component is encoded by *dpatj* gene in *Drosophila* and two mammalian homologues, *PATJ* (Pals-associated tight junction protein) and *MUPP1* (multi-PDZ domain protein) are also known to interact with Crb intracellular portion [18, 21].

The Bazooka/Par6/aPKC Complex In *Drosophila*, below the Crumbs/ Stardust/PATJ Complex at the sub-apical region, lies a complex composed of two scaffold proteins, Bazooka (Baz) and Par6, both containing PDZ domains as well as other protein-protein interaction motifs and an atypical protein kinase C, aPKC. Genetic analysis has revealed that they are mutually dependent for proper localisation and ZA formation. In mammals one Baz homologue (Par3), three Par6 homologues (Par6α, β and γ) and two aPKC homologues (aPKcλ/ι and aPKCζ) have been

found with differential expression patterns but mostly redundant functions.

In mammalian cells this complex localises to tight junctions and is required for AJs formation as it is in *Drosophila* [18, 21].

The Scribble/Discs Large/Lethal Giant Larvae Complex In *Drosophila* the three neoplastic TSG show identical loss of function (LOF) phenotypes as well as a strong genetic interaction. Indeed, genetic analysis demonstrated that they act in a common pathway linking cell polarity and cell proliferation control in epithelial cells [22]. They all encode scaffolds rich in protein-protein interaction domains. Scribble belongs to the LAP (Leucine-rich repeats And PDZ domain) family and has four PDZ domains at the C-terminus and sixteen LRR (Leucine-Rich Repeats) at the N-terminus; it is encoded by a single gene both in *Drosophila* and mammals. Dlg is a MAGUK protein and contains three PDZ an SH3 and a GUK domain. Four mammalian homologues of *Drosophila* Dlg have been identified so far (Dlg 1-4). *lethal giant larvae* encodes a protein, Lgl, rich in WD40 repeats predicted to fold into two β-propeller domains at the N-terminus. The mammalian genome encodes two *Drosophila* Lgl homologues: Lgl-1 and Lgl-2 (also known as Hugl-1 and Hugl-2) which also contain WD40 repeats and have distinct expression patterns [18, 21]. Fly and human proteins show the significant global sequence similarity of 62.5% if conservative aminoacid changes are taken into account and conclusive evidence of the functional conservation between the two proteins is found in the full rescue of the null *lgl* mutant by the human *Lgl-1* cDNA [23]. Analogous rescuing ability has been demonstrated also for rat *Dlg* [24] and human *Scrib* [25].

In *Drosophila* it has been demonstrated that the three proteins are mutually dependent for correct localisation [22] although direct physical interactions have never been proved. Dlg and Scrib localise at the membrane cortex, at *Drosophila* septate junctions. Lgl colocalises with Dlg and Scrib at septate junctions but its localisation is not restricted to the cortex but it is also found in the cytoplasm. In neuronal synapses Scrib has been shown to bind Dlg via a protein named GUK Holder. In mammalian epithelial cells they are also localised in the basolateral domain of the plasma membrane and, similarly to the fly counterparts, the exact nature of their physical interaction has yet to be established; so far direct binding has only be proven for Scrib and Lgl-2 [18, 21].

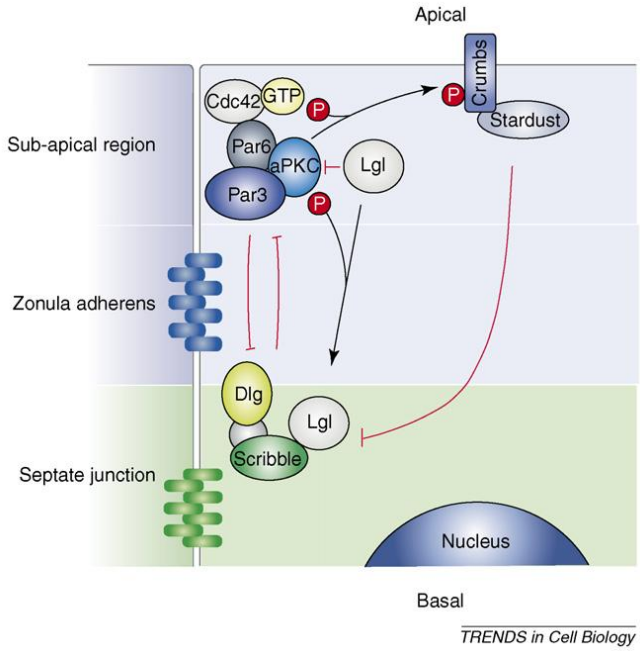

Figure 1.5: Schematic representation of *Drosophila* polarity complexes. The Crumbs/Stardust complex identifies the apical domain of the plasma membrane; the Bazooka(Par3)/Par6/aPKC localises at the subapical region while the Scribble/Dlg (Discs Large)/Lgl (Lethal Giant Larvae) complex lies in the basolateral domain. Details on how apical-basal cell polarity is regulated by these complexes are given in the text. Apical and basal sides as well as cell junctions are indicated [26].

Regulation of Cell Polarity The Scrib/Dlg/Lgl complex functions in establishing basolateral domain identity antagonising the activity of the other two polarity complexes. Their mutually exclusive activity is required for the correct formation and positioning of cell junctions, which in turn provide cells with a correct apical-basal and cytoskeletal structure [18] (Fig. 1.5).

The mechanism through which these complexes regulate each other was initially investigated in *Drosophila* neuroblasts, the larval neuronal progenitors [27]. These cells do not have cell junctions but require a compartimentalisation of membrane domains in order to perform asymmetric cell division. These membrane complexes are required for proper positioning of cell fate determinants that will differentially segregate into the daughter cells giving origin to a new stem cell (self-renewal) and to a ganglion mother cell (GMC), the neuron/glia precursor. Failure to segregate

cell fate determinants due to *lgl* LOF results in excessive self-renewal and thus abnormal expansion of the neuroblast population [28]. It was demonstrated that Lgl localisation at the plasma membrane depends on its phosphorylation in conserved residues by aPKC of the Baz complex [27]. Phosphorylated Lgl assumes an autoinhibited conformation in which protein interaction domains are masked and is thus excluded from the cortex. Lgl in turn counteracts aPKC activity by sequestering it in an inactive Lgl/aPKC/Par6 complex from which Bazooka is excluded [29]. The phenotype observed in $lgl^{-/-}$ tissues can indeed be reproduced by expanding aPKC activity domain in neuroblasts. The expression of a prenylated form, which is targeted to the entire cell cortex, results in impairment of asymmetric cell division leading to an excess of self-renewal and abnormal increase in neuroblast population similarly to what happens in $lgl^{-/-}$ individuals [30].

The same is true for epithelial tissues. The lateral spreading of aPKC activity causes cytoplasmic release of Lgl from the basolateral membrane leading to hyperproliferation and massive overgrowth in the wing disc and deep morphogenetic alterations in the adult wing [31]. Moreover, reduced aPKC levels can suppress $lgl^{-/-}$ phenotype in the imaginal discs [32] and a non-phosphorylatable form of Lgl completely fails to rescue mutant phenotype in embryos lacking both maternal and zygotic *lgl* [33]. The Crb complex is recruited by the Baz complex to the apical domain and seems to further antagonise the activity of the lgl complex by blocking its spreading along the lateral membrane domain. Crb is phosphorylated by aPKC and this event is required for its correct apical localisation [18].

As expected from the high level of functional conservation, mammalian Lgl-1 and Lgl-2 are also excluded from the apical domain due to aPKC phosphorylation and bind Par6 and aPKC preventing their association with Par3 and thus the basolateral spreading of apical complexes [18].

Lgl is also part of the actin cytoskeleton network, linking it to the cell cortex, as it interacts with non-muscle myosin II heavy chain both in *Drosophila* and human cells [29, 34]. Furthermore, it was observed in fly neuroblasts a negative genetic interaction between *lgl* and *zipper* (*Drosophila* myosin II gene): delocalisation of basal determinants in $lgl^{-/-}$ cell can be rescued reducing the dosage of *zipper* [35]. Nevertheless, the importance of Lgl in Myosin regulation and the effects of Lgl loss in cytoskeletal architecture in epithelial cells have yet to be elucidated.

Lgl yeast homologues SRO7 and SRO77 have been shown to bind the t-SNARE

protein Sec9p, involved in the fusion of transport vesicles at plasma membrane and SRO7/SRO77 double mutants show accumulation of post-Golgi vesicles within the cytoplasm [36]. An intriguing possibility is that Lgl may contribute to generation and maintenance of basolateral domain identity regulating polarised exocytosis of vesicles containing specific proteins. There is evidence of Lgl being involved in Decapentaplegic (Dpp) signal exocytosis, the fly TGF-β (Transforming Growth Factor β) homologue, as *lgl* activity seems to be required in those cells producing Dpp and not in those which respond to the morphogen, and to function downstream *dpp* transcription and upstream Dpp receptor, Thickveins [37]. Direct demonstration of Lgl involvement in vesicle trafficking has however yet to be found in *Drosophila* and mammalian cells.

1.2.1.2 *lgl* in Tumourigenesis

lethal giant larvae was the first *Drosophila* tumour suppressor described in literature: it was identified by Hadorn in 1938 and its neoplastic phenotype was characterised in depth by Elizabeth Gateff following the isolation of a spontaneous *locus* deletion named lgl^4 [14] and the gene, located in the sub-telomeric region of the second chromosome's left arm, cytologic position 21A, was cloned and characterised by Mechler in 1985 [38].

lgl loss of function causes neoplastic overproliferation of both imaginal epithelia and neuroblasts of the larval brain. These structures not only show excessive growth but also loss of apical-basal polarity and tissue architecture which result in an extended larval period and pre-pupal lethality. Cell growth appears to be slow in *lgl* mutants; 5 days-old $lgl^{-/-}$ wing discs indeed contain about one third cells with respect to the wild-type counterpart [15]; despite this, since $lgl^{-/-}$ cells are unable to exit cell cycle, after many additional days of proliferation, discs reach an enormous cell number and eventually form large amorphous masses which fail to form proper cellular contacts and do not differentiate (Fig. 1.6). *lgl* mutants also show loss of positional clues since, in *lgl* defective discs, cells straddle the anterior-posterior compartment boundary [39], which separates two independent developmental units that never intermix. Moreover they are able to fuse with nearby tissues, i.e. haltere and third leg discs, so displaying local invasiveness [14]. $lgl^{-/-}$ larval brains are twice as big as wild-type ones and overproliferating neuroblasts spread to all regions causing a disorganised brain structure and never differentiate into neurons [30].

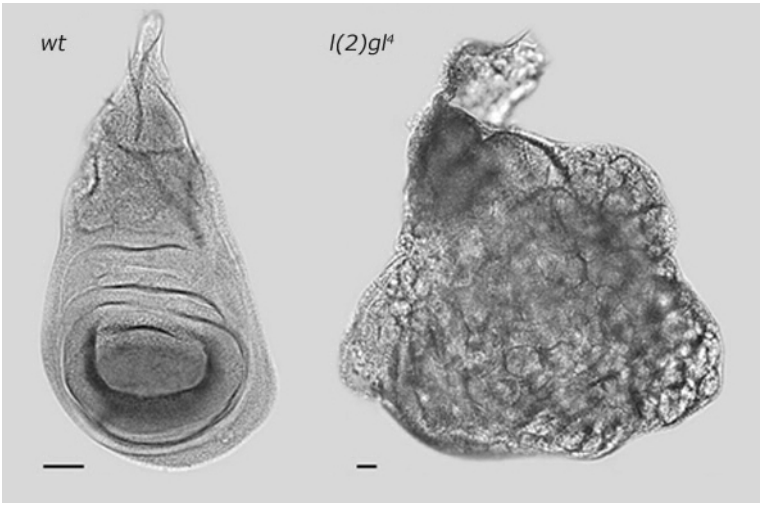

Figure 1.6: A wild-type (left) and a lgl^4 (right) imaginal wing disc. Overgrowth and loss of monolayered organisation and tissue architecture are evident in *lgl* mutant epithelium.

***lgl* and Proliferation** Understanding how loss of cell polarity and control of cell proliferation are linked would represent a relevant advance in the comprehension of the molecular bases of cancer development. Overgrowth might be hypothesised to be a direct consequence of loss of cell polarity in *lgl* mutant tissues. Loss of membrane compartimentalisation could indeed alter distribution of diffusible signals that regulate proliferation and their receptors, delocalisation of signalling molecules both on cell surface and within the cytoplasm could result in simultaneous deregulation of several different pathways so triggering changes in cell metabolism and proliferation rate. Moreover, disruption of the adherens junctions could impinge on contact inhibition, known to restrict cell division. Nevertheless, several lines of evidence exist that demonstrate a specific signalling function of the Dlg/Lgl/Scrib module in proliferation control. First of all, disruption of polarity by other means does not induce overproliferation in imaginal discs, mutation of E-cadherin being the best example [40]. Furthermore, alleles of *lgl*, *scrib* and *dlg* were identified in a screening for dominant suppressors of a hypomorphic mutation of *cyclin E*, a key regulator of G1-S phase transition [41], implying a direct role in negative regulation of cell cycle. Indeed $lgl^{-/-}$ clones in the eye disc (see below) show ectopic Cyclin E expression and

thus ectopic S-phases without losing apical-basal polarity [42] demonstrating that loss of proliferation control is not a direct consequence of polarity loss, at least in this context.

Recently it was demonstrated that the proliferative defects in the eye disc described above are due to the deregulation of the Hpo pathway, a very conserved signalling network that plays a central role in the control of epithelial tissues proliferation, establishing for the first time a direct link between *lgl* and cell proliferation control [43].

The Hpo pathway (Fig. 1.7) is composed of two core kinases, Hpo and Wts (Warts), the adaptors Sav (Salvador) and Mats (Mob As a Tumour Suppressor) and the transcriptional co-activator Yki (Yorkie) and it is modulated by numerous upstream factors among which the cytoskeletal proteins Ex (Expanded) and Mer (Merlin) and the atypical cadherins Ft (Fat) and Ds (Dachsous). When the pathway is active Hpo can phosphorylate and activate Wts which in turn phosphorylates Yki sequestering it in the cytoplasm; on the other hand, upon its inactivation unphosphorylated Yki can translocate to the nucleus and activate the transcription of its target genes involved in cell growth, proliferation and resistance to apoptosis such as *cyc E*, *dMyc*, *dIAP1* (*Drosophila Inhibitor of APoptosis 1*) and the microRNA *bantam*. Yki is thus a growth promoter, whereas the upstream components act as tumour suppressors by antagonising the growth-promoting activity of Yki [44].

Lgl was indeed shown to take part in the regulation of this pathway: *lgl* mutant cells in the eye imaginal disc show upregulation of Hpo pathway target genes as *cyc E* and *dIAP1* as well as genes belonging to the negative feedback loops such as *ex*; consistently in $lgl^{-/-}$ cells Yki was found to localise also in the nucleus and the phosphorylated form levels were reduced. Removal of one copy of *yki* partially reduced Hpo target genes upregulation as well as the ectopic S-phases phenotype previously described [42], indicating that Yki activity is required for $lgl^{-/-}$ proliferative defects. Yki activation in $lgl^{-/-}$ cells seems to be due to Hpo mislocalisation and to the hypothetical formation of an inactive complex with RASSF (Ras associated factor), another regulator of the pathway, also mislocalised in mutant cells [43].

lgl-dependent regulation of Yki has also been observed in the wing imaginal disc but it was proposed to occur through a different mechanism [45]. *lgl* depletion-dependent tumours were generated by specifically knocking down *lgl* transcript in the posterior compartment of the wing disc leading to overgrowth and loss of cell

polarity. In these posterior cells Yki was mainly localised to the nucleus and Hpo pathway reporter genes were upregulated. Indeed knockdown of Yki or overexpression of Wts in this context blocked the overgrowth and resulted in discs with reduced posterior compartment and high levels of cell death suggesting that Yki activity is required for growth and survival of *lgl*-depleted cells. Interestingly Yki activation was found to be due to JNK (c-Jun N-terminal kinase) signalling, a conserved stress-induced pathway the activation of which is a common feature of neoplastic TSG loss [46] (see Section 1.2.2 for a detailed discussion of JNK functions in tumour development). Two explanations have been proposed to account for this differences in Yki regulation upon *lgl* depletion in the eye *vs* wing imaginal discs: first, in the experimental conditions employed in the wing disc cell polarity was lost whereas this was not the case in the eye disc (in addition Hpo seems to have a different localisation pattern in the two tissues); second, wing and eye discs seem to have a different sensitivity to JNK signalling since its direct activation is able to regulate Yki in the wing disc only [45]. *lgl* may thus regulate cell proliferation by influencing the Hpo pathway in a tissue specific manner through JNK-dependent and independent pathways. *scrib* loss of function however induces JNK-independent impairment of the Hpo pathway both in eye and wing imaginal discs [47]. It thus seems that the cross-talk between cell polarity proteins, JNK signalling and the Hpo pathway are complex and possibly context dependent and further work is needed to clarify this.

***lgl* and Invasion/Migration** Involvement of the Scrib/Dlg/Lgl complex in migratory behaviour has been proven in different epithelial contexts. Maybe the most striking example is given by the migratory behaviour displayed by mutant epithelia upon transplantation into naive hosts [48]. Indeed both $lgl^{-/-}$ brain and imaginal tissues show this capability.

An attempt to quantify this metastatic potential was made by E. Woodhouse and colleagues: marked brain fragments were found to be highly metastatic, giving rise to 1-6 secondary tumours in 87% of transplanted hosts, mainly in the thorax and abdomen (gut and ovaries) but also in head, wing and leg. Transplanted imaginal discs formed secondary lesions in 43% of hosts, mostly in the abdomen where they invaded gut and ovaries. Lineage analysis of these $lgl^{-/-}$ suggests that only a small fraction of the cancer cells (less than 2%) displayed this metastatic behaviour [48]. Since the open circulatory system of the insect calls into question the possibility of

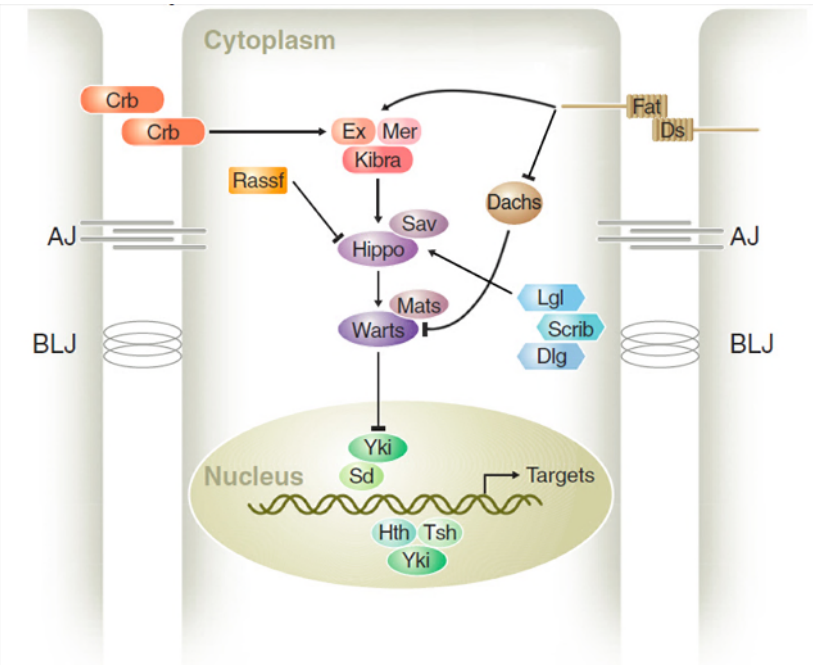

Figure 1.7: Schematic representation of the Hpo pathway. The core of the pathway composed of the kinases Hippo and Warts and the adaptors Salvador (Sav) and Mats converges on the phosphorylation of the transcriptional co-activator Yki preventing it from translocating to the nucleus where it binds its alternative partners Scalopped (Sd), Homothorax (Hth) and Teashirt (Tsh) and activates target genes. Some of the upstream modulators of the pathway are also represented: the atypical cadherins Fat and Dachsous (Ds); the unconventional myosin Dachs, the adaptor proteins Rassf, Kibra, Merlin and Expanded, and the apical (Crumbs) and basolateral (Lgl, Scrib and Dlg) polarity complexes. AJ: Adherens Junctions, BLJ: Basolateral Junctions. Adapted from [44].

a passive transport of cancer cells to distant sites, a second and more reliable *in vivo* assay to test metastatic abilities of cancer cells was developed [49]. Only those metastases occurring in the host's ovaries were taken into account. The *Drosophila* ovary consists of 16-20 ovarioles surrounded by a peritoneal sheath of cells. Each ovariole is in turn surrounded by a muscle layer allocated between two layers of extracellular matrix flanking the basement membrane of the follicular epithelium. Since cancer cells have to pass through all these continuous layers to colonise the ovaries, the recovery of metastases within these organs is stricter evidence of active invasion. Transplanted *lgl* mutant cells formed metastases in 15.8% of ovarioles analysed and all of the hosts examined had at least one ovariole invaded. By extend-

ing the proliferation time of primary tumours through serial transplantations into multiple hosts, the frequency of metastases increases significantly. This, together with lineage analysis (see above), highlights the possible requirement of additional genetic lesions to promote invasion, very similarly to what happens in mammalian tumourigenesis. Karyotypic instability, including increased polyploidy and aneuploidy, was also observed in *lgl* mutant tumour cells after serial transplantations into adult hosts [14].

Secretion of Collagenase IV [50] and Matrix Metallo-Proteinase 1 (MMP1) [51] has also been observed in $lgl^{-/-}$ mutant tissues: these two proteins are involved in basement membrane type IV collagen degradation and have been implicated in several stages of tumour progression in mammals such as angiogenesis, proliferation and metastasis (see Section 1.1). MMP1 appears to be essential for $lgl^{-/-}$ cells spreading because *lgl*; MMP1 double mutant cells show a strong reduction in the ability to leave primary lesions [51].

$lgl^{-/-}$ invasive phenotype was taken as a starting point from which to isolate novel genes involved in tumour formation and metastasis. A mutagenesis screening was carried out to search for second *locus* mutations that regulated *lgl* malignant behaviour upon transplantation of larval tissues into adult wild-type hosts. Interestingly, one of the genes identified to be required for metastasis formation is *semaphorin 5c* (*sema5c*). Sema5c protein contains extracellular thrombospondin type I repeats, known to regulate TGF-β signalling in mammals. Indeed, whereas *lgl* null mutant primary tumours show an increased *Drosophila* TGF-β homologue Dpp signalling, in *lgl*; *sema5c* double mutants Dpp signalling levels are comparable to wild-type tissue. This implicates the Dpp/TGF-β signalling pathway in cancer emergence as it is known to happen for many types of human malignancies, where TGF-β appears to switch from an antiproliferative, pro-apoptotic function to an oncogenic role during cancer progression [52].

The employment of temperature sensitive *lgl* alleles has allowed to investigate this gene's phenotypes also during early embryonic development when the heterozygous mother can supply enough protein to sustain early stages of development thus masking the LOF effects. Development of embryos from eggs laid at 29°C by lgl^{ts3} homozygous females was blocked at germ band shortening resulting in a so called "shrimp-shaped" embryo, where head involution and dorsal closure were also affected [22, 53].

In the follicular epithelium, mutation of *lgl* and *dlg*, besides resulting in loss of apical-basal cell polarity and overproliferation, causes cells to actively migrate across the germ line [22, 53, 54]. These movements resemble that of normal border cells (BCs) migration; BCs are a follicular epithelium subpopulation which udergoes a very stereotyped migration from the anterior pole of the egg chamber towards the oocyte. During normal BC migration, however, adherens junctions are retained (partial EMT) and cells migrate as a cluster, while *lgl* and *dlg* mutant follicular cells adherens junctions become diffusely redistributed and cells invade mainly as a stream and less frequently as highly disorganised clusters [54]. Also in this case, control of cell polarity, proliferation and invasion seem to be independent functions exerted by the proteins since partial LOF *dlg* mutants cause follicle cells to accumulate in multilayers without invading; these cells indeed lose polarity implying that this phenomenon is not sufficient to induce migration [55]. Furthermore, proliferation does not appear to be essential for invasion, as clusters of $dlg^{-/-}$ cells are observed to delaminate and migrate without overproliferating, also indicating that these movements are active and not a mere mechanical consequence of cell stacking [54, 55]. Loss of cell polarity in follicular cells due to LOF of members of any other polarity complex (i.e Bazooka, Crumbs and E-cadherin complexes) does not induce invasion [54], confirming a direct role for the Scrib/Dlg/Lgl complex in repression of migration during oogenesis. Indeed, $lgl^{-/-}$ and $dlg^{-/-}$ BCs are also shown to migrate faster than wild-type cells [56]

Zhao and colleagues [57] performed a wide genetic screen to identify pathways downstream of the basolateral complex. They screened for *loci* enhancing invasion in a *dgl* hypomorphic background and identified *lgl*, *scrib* and two genes not previously associated: *roughened eye* (*roe)* and *warts*. Interestingly, *scrib* displayed a less strong enhancement than *lgl* implying that the two might not be physiologically equivalent in this context. *roe* encodes a zinc-finger protein of the Krüppel-family, possibly a transcription factor and may thus represent the first identified nuclear target of the complex. *warts* encodes a serine-threonine kinase known to act as a tumour suppressor in imaginal epithelia belonging to the Hpo pathway (see above). It is particularly interesting as it shows a strong genetic interaction with *dlg* (comparable to that of *scrib*) but, in the follicular epithelium, it seems to act downstream of the Scrib/Dlg/Lgl complex, independently of the Hpo pathway. Phenotypic analysis revealed that *scrib*, *wts* and *roe*, differently from *lgl* and *dlg*, act only in repressing

EMT and proliferation but not in repressing motility [57].

***lgl* and the Tumour Microenvironment** As reported in Section 1.1, the interactions occurring between mutant cells and their microenvironment are proving to play a key role in tumour development. In *Drosophila* an extremely powerful genetic tool, namely clonal analysis [58], is available to generate marked patches of homozygous mutant tissue in an otherwise heterozygous background, allowing to investigate the complex crosstalk between mutant and wild-type tissue. Indeed *lgl* LOF clonal behaviour appears to be quite different compared to that of the whole mutant animal, at least in some contexts.

In the eye imaginal disc, $lgl^{-/-}$ clones show ectopic proliferation but maintain apical-basal cell polarity. Overall clonal size is however not affected since increased cell death is also observed. If clones are induced in a background heterozygous for a *Minute* mutation, prominent loss of cell polarity occurs and several individuals undergo extended larval period and die as giant larvae very similarly to the homozygous mutant [42]. The *Minute* mutations are dominant, homozygous lethal, LOF mutations of different ribosomal proteins. Heterozygous *Minute* cells are viable but display a slow growing phenotype [59] (see Section 1.4.3). The authors hypothesise that this background, delaying development, induces several extrarounds of cell proliferation in $lgl^{-/-}$ clones, completely depleting maternal protein. This would suggest the existence of a threshold level of Lgl protein, sufficient to sustain the function in cell polarity maintenance but not that in proliferation control [42].

A different clonal behaviour in the eye disc was also observed for *scrib* LOF: clones lose polarity and overproliferate but very little mutant tissue is recovered in the adult eye as it is removed during development by JNK-mediated apoptosis (see Section 1.2.2). Blocking JNK pathway in these clones greatly increases the amount of mutant tissue and results in lethality. Interestingly, cell death is induced in a non-autonomous manner by the surrounding wild-type tissue since upon its removal *scrib* clones viability is rescued [60].

A mechanism to explain JNK non-autonomous activation in *scrib* or *dlg* clones was provided by Igaki and colleagues [61] who linked the elimination of mutant cells to a phenomenon they named Intrinsic Tumour Suppression (ITS) which consists in the endocytic activation of Eiger (Egr), *Drosophila* TNF (Tumour Necrosis Factor), a known activator of JNK pathway. $scrib^{-/-}$ or $dlg^{-/-}$ clones generated in an *egr* null

background no longer die but overgrow and develop into tumours; the same effect was observed in the wing imaginal disc. Mutant cells were found to have increased endocytic activity and Egr was mislocalised and enriched at the endocytic vesicles. Egr localisation correlated with intense phosphorylated and thus activated JNK staining. Indeed inhibition of endocytosis by means of a dominant negative form of Rab5 (an early endosomal marker) abolished JNK activation and mutant clones elimination, allowing tumorous growth. Ablation of surrounding wild-type tissue prevented endocytosis upregulation and Egr/JNK-dependent cell death in *scrib*$^{-/-}$ implying the existence of tumour suppressive mechanisms able to sense polarity deficient cells and trigger their elimination [61].

The differences between *lgl*$^{-/-}$ clones and whole mutant tissues are even more striking in the imaginal wing disc. X-rays induced clones generated in a wild-type background do not show aberrant growth or morphological abnormalities at all in adult wing, possibly due to extensive cell death of mutant cells [62]. Again, generation of clones in a *Minute* background results in aberrant cell-cell interactions, straddling of the anterior-posterior border, failure to differentiate and abnormal growths in adult wings [39]. These differences clearly underline the great impact that interactions between mutant and wild-type tissue have in tumour progression.

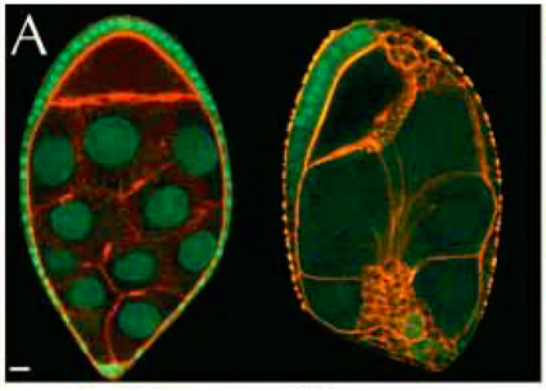

Figure 1.8: A Wild-type egg chamber (left) and an egg chamber of the same stage bearing *lgl* loss of function clones; *lgl* mutant follicular cells grow as a multilayer and invade the germ line territory [15].

Interestingly, differently to what happens in eye and wing imaginal tissues, *lgl* clonal behaviour in the follicular epithelium appears to be rather similar to that of the whole mutant tissue. Indeed, $lgl^{-/-}$ clones overproliferate to form large multilayers with loss of cell polarity and invade between nurse cells [15, 22] (Fig. 1.8). A two-fold increase in the number of S-phase follicle cells is observed in mutant clones with respect to wild-type tissue; phosphorylation of H3 histone (a marker for mitotic cells) persists after stage 6, when wild-type cells have already exited cell cycle, and increased cyclin E is also detected. Moreover, in agreement with their viability, $lgl^{-/-}$ clones upregulate dIAP1 [57].

These data suggest that also the context in which the interaction between mutant and wild-type tissue takes place has great relevance in clonal output.

Mammalian Lgl-1 and Lgl-2 Several lines of evidence showing mislocalisation, decreased expression or loss of Lgl-1/2 in primary human tumours seem to indicate that they play a role in mammalian tumourigenesis. Indeed *Lgl-1* transcript results decreased or completely absent in a wide variety of human epithelial malignancies such as breast, lung, prostate, ovarian cancers and melanomas [23, 63]. It has also been implicated in colorectal cancer progression where it was found to be associated with advanced stages and lymph node metastases [64]. Its loss has been correlated with reduced survival in glioblastoma [65] and the occurrence of aberrant splicing variants with hepatocellular carcinoma progression [66]. Moreover Lgl-1 subcellular localisation seems to play a crucial role as its cytoplasmic localisation correlates to aPKC lateral spreading and to cancer progression in ovarian carcinomas [31]. This clearly drives a strong parallel with the phenotypes observed in *Drosophila lgl* epithelial cancers. Interestingly, pronounced similarities with *Drosophila lgl* mutant were also found in Lgl-1 knock-out (KO) mice. $Lgl\text{-}1^{-/-}$ individuals presented at birth severe brain dysplasia due to an abnormal expansion in the number of progenitor cells, unable to exit cell cycle and to differentiate. These cells formed neuroepithelial rosette-like structures, similar to the neuroblastic rosettes found in human primitive neuroectodermal tumors (PNETs) occurring at pediatric age [67]. Noticeably, human *Lgl-1* gene maps to 17p11.2, a region often shown to undergo chromosomal breakage in human PNETs [34]. *Lgl-2* has been found to be a negative target of ZEB1, a master regulator of EMT [68] suggesting that its loss in epithelial cells may favour the acquisition of mesenchymal, migration-prone behaviour.

All these data strongly support the notion that also mammalian *lgl* homologues act as TSG so giving a major relevance to *Drosophila lgl* mutant in the study of human tumourigenesis.

1.2.2 Cooperative Oncogenesis

The definitive confirmation of *Drosophila* as a model for cancer research came with the development of the MARCM (Mosaic Analysis with a Repressible Cell Marker) technique [69] which allows to induce somatic clones in which LOF mutations of tumour suppressor genes and overexpression/activation of oncogenes are simultaneously present. This, together with classic clonal analysis experiments, allowed to demonstrate that also in *Drosophila* transformation requires the accumulation of multiple genetic lesions and debunked the previously accepted view of the "single-hit" tumourigenesis model derived from observation of whole mutant tissues' phenotypes of the neoplastic TSGs (see above).

The first models Two seminal studies published in 2003 unveiled a strong cooperation between *scrib*, *lgl* and *dgl* mutations and the constitutively activated form of *ras* proto-oncogene, Ras^{V12}, in tumour growth and metastatic behaviour [60, 70]. In the first one Brumby and colleagues [60] showed that GFP-marked clones mutant for *scrib* generated in the eye disc grew poorly and were eliminated by JNK-dependent cell death (see above), however when Ras^{V12} was expressed within mutant clones, these where able to overgrow in three dimesions and formed large masses that never differentiated and fused with nearby tissues leading to the death of the individuals as giant larvae. Clones expressing Ras^{V12} alone overgrew but formed non invasive tumours. The authors observed the same effect on *scrib* null cells upon activated Notch expression (found to be dependent on Ras activity) but not upon the expression of other growth-promoting pathways such us Dpp and Wg (Wingless, *Drosophila* WNT homologue), indicating a specific cooperation between $scrib^{-/-}$ and activated Ras. Interestingly, expression of a constitutively activated form of Raf (Raf^{ACT}), one of Ras signalling effectors which acts upstream of the MAPK cascade (see Section 1.3.1) in *scrib* mutant clones fully recapitulated the $scrib^{-/-}$; Ras^{V12} phenotype, whereas overexpression of PI3K (Phosphatidyl Inositol 3 Kinase), the other main downstream effector, did not, indicating the key role of the MAPK branch

in cooperating with *scrib* loss. Cell cycle promoters such as CycE and E2F were found to be necessary to the tumorous phenotype but not sufficient to drive it if overexpressed in $scrib^{-/-}$ clones, even in the presence of apoptosis inhibitors. The activity of specific targets downstream of Ras signalling and not its generic ability to promote proliferation while inhibiting cell death may thus be required to promote this oncogenic cooperation [60].

Pagliarini and colleagues [70] obtained very similar results in an attempt to identify mutations able to promote metastatic behaviour of non-invasive Ras^{V12} expressing clones in the eye disc. Indeed when the expression of activated Ras was combined with *scrib*, *dlg* or *lgl* null mutations, clones grew aggressively and became highly metastatic. They displayed a consistent invasion of the ventral nerve cord, an area of the larval brain not immediately adjacent to the eye disc, active basement membrane degradation was observed and cancer cells (Fig. 1.9) were also found to spread and colonise other tissues, including the tracheal system. Similar phenotypes were obtained upon the inactivation of other polarity regulators underlining the key role of cell polarity loss in inducing metastatic behaviour. In fact, malignant cells also showed a lowered expression of E-cadherin, a hallmark of EMT, and its overexpression was sufficient to block invasion in $scrib^{-/-}$;Ras^{V12} clones; E-cadherin deprivation however was not sufficient to drive invasion of activated Ras-expressing cells. Again, expression of proliferation promoters, such as Myc, Akt or E2F as well as apoptosis inhibitors in *scrib* mutant clones, despite increasing clone size failed to induce the metastatic behaviour observed for $scrib^{-/-}$;Ras^{V12} cells [70].

The oncogenic cooperation between *scrib* loss and constitutively active Ras was shown to be conserved in organotypic cultures of human epithelial cells. Non-transformed MCF10A breast epithelial cells, when cultured in reconstituted basement membrane, differentiate into polarised, hollow acini. Coexpression of Ras^{V12} (or Raf^{ACT}) and a *Scribble* knock-down construct ($Scribble^{KD}$) in these cells induced invasive behaviour through the extracellular matrix with formation of protrusions that projected out from the acinar structure [71].

The role of JNK signalling As reported above and in Section 1.2.1 *scrib* mutant cells grown in a clonal context are eliminated by non-autonomous JNK-induced cell death [60, 61]. JNK signal transduction pathway is an evolutionarily conserved stress-induced MAPK cascade that has roles in multiple cellular processes includ-

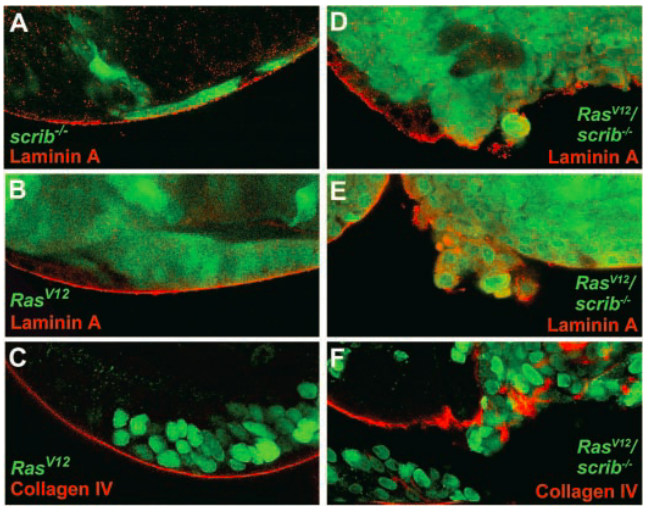

Figure 1.9: The oncogenic cooperation between *scrib* loss of function and activated Ras reported by Pagliarini and colleagues. As shown by Laminin A and Collagen IV stainings (red), *scrib*$^{-/-}$; *Ras*^{V12} cells (GFP^{+} in D-F) are able to degrade the basement membrane indicating that these cells have acquired an invasive behaviour. The two genetic alterations alone (GFP^{+} in A-C) are not sufficient to provide mutant cells with these properties [70].

ing proliferation, differentiation, morphogenesis, and most of all, apoptosis, and has been implicated in several aspects of tumour development. The *Drosophila* only JNK protein Basket (Bsk) is phosphorylated and activated by the upstream JNK kinase (JNKK) Hemipterous (Hep) which is in turn a substrate for several upstream JNKKKs that respond to a variety of internal and environmental stimuli. Activation of this cascade results in phosphorylation of several JNK targets among which the AP-1 family transcription factors Jun and Fos and is negatively regulated through a negative feedback loop by the phosphatase Puckered that is itself a Jun/Fos transcription target [46].

With the aim of understanding the possible role of JNK signalling in tumour development Uhlirova and colleagues [72] analysed the effect of constitutive activation of the pathway in the Raf^{ACT}; *scrib*$^{-/-}$ context. While increased JNK signalling further enhanced the elimination of *scrib* mutant clones in the eye disc giving rise to a wild-type adult eye, its effect on *Raf*^{ACT}; *scrib*$^{-/-}$ was rather peculiar. Increasing apoptotic cell death reduced clone size and abolished aggressive expansion of mutant cells and thus pupal lethality but adult heads and eyes of these flies displayed massive hyperplasia of wild-type tissue. This might be due to the non-autonomous compen-

satory proliferation induced by JNK activation in adjacent cells to replace the dying ones, as demonstrated in other contexts [73], in addition to a cell-autonomous effect in promoting apoptosis; activated Raf would in this case attenuate JNK-dependent apoptosis delaying cell death and thus boosting compensatory proliferation of the surrounding wt tissue [72].

Nevertheless, the experimental paroxistic activation of JNK signalling in Raf^{ACT}; $scrib^{-/-}$ clones, by inducing massive amounts of cell death, might have masked the cell-autonomous role of this signalling cascade in tumour development. Indeed a few papers were subsequently published which demonstrated that JNK signalling activation due to *scrib* loss is the key factor in this oncogenic cooperation and it switches from pro-apoptotic, and thus tumour suppressive, to tumour promoting in presence of oncogenic Ras signalling [74–77]. Similarly to *scrib* LOF clones, also in $scrib^{-/-}$;Ras^{V12} malignant clones JNK pathway is strongly activated but while blocking it in $scrib^{-/-}$ cells abolished cell death and allowed overgrowth [60], blocking it in the *scrib*, *lgl* or $dlg^{-/-}$;Ras^{V12} background completely abolished invasion of the VNC, dramatically reduced growth and restored differentiation. Thus cell polarity loss results in JNK activation which, if constitutive Ras signalling is present to abolish its pro-apoptotic effect, induces invasive behaviour and stimulates growth.

Several lines of evidence seem to indicate that JNK signalling promotes invasion by upregulating MMP1 expression in a Fos-dependent manner and thus basement membrane degradation: inhibition of MMP activity either by genetic inactivation or by expression of MMP inhibitors also abolished invasiveness of mutant clones [75, 76]. Moreover growth and invasion seem to be separable effects since inhibition of MMP1 activity blocked invasion without affecting growth [74, 75] and vice versa insulin signalling disruption inhibited growth but did not inpinge on the metastatic capabilites of cancerous cells [74]. Whether JNK activation is *per se* sufficient to cooperate with Ras in inducing invasion may depend on the strength of the activation itself (too high levels would induce massive cell death and mask the effect) and thus remains a matter of debate [74, 75, 77, 78].

Concerning the growth promoting capability of JNK activation, a mechanism through which it is achieved was identified in its ability to activate JAK-STAT signalling, a conserved proliferation-promoting pathway. $scrib^{-/-}$;Ras^{V12} (but also $lgl^{-/-}$;Ras^{V12}) clones showed upregulation of the *unpaired* (*upd*) genes which encode JAK/STAT-activating cytokines and JNK-dependent activation of a JAK-STAT re-

porter. Not only reduction of JAK-STAT activity completely abolished growth and invasion of mutant clones, but *upd* genes overexpression was sufficient to cooperate with Ras to give large invasive tumours which were insensitive to Bsk depletion, placing cytokines production and JAK-STAT activation downstream of JNK signalling in this cooperation model. The authors also demonstrated that STAT function is required in the compensatory proliferation induced by *scrib* mutant cells elimination in the eye disc as adult eyes are smaller in size if mutant clones are induced in a $STAT^{-}$ background and thus propose that JAK-STAT activation downstream of JNK represents a mechanism to ensure recovery after damage through compensatory proliferation that explains the development of $scrib^{-/-}$; Ras^{V12} tumours [79]. Interestingly, similar results were obtained even when *scrib* loss of function and Ras activation occurred in adjacent clones rather than in the same cells. JNK signalling induced in *scrib* mutant cells was proven to be able to propagate (also explaining the non-autonomous JNK activation often observed upon *scrib* clonal loss [60]) and promote Upd production in adjacent Ras^{V12}-expressing cells thus sustaining growth even after *scrib* deficient cells were eliminated by JNK-dependent cell death (see above) [79]. This indicates that oncogenic cooperation can also occur when genetic lesions do not coexist in the same cell and since it is well known that human cancers are often composed of genetically heterogeneous cell populations, this findings might be relevant to gain a better understanding of the interactions between these populations.

Overgrowth has also been proposed to be a consequence of the extended larval period that $scrib^{-/-}$;Ras^{V12} clones-bearing animals undergo and thus would be due to the JNK-dependent block in differentiation rather than to a direct effect in cell growth [78].

Notably, a role in disrupting epithelial cell polarity has also been suggested for JNK signalling activity downstream of *lgl* loss of function, despite not in a clonal context. Upon inhibition of the Hep/JNK/Fos cascade, besides reversion of the tumour-like phenotype (overgrowth and invasion), localisation of polarity markers as well as epithelial folding were also partially restored in whole $lgl^{-/-}$ imaginal discs [80]. Similar results were also obtained by Sun and Irvine [45]. Nevertheless, rescue of polarity defects was not observed upon JNK inhibition in a *scrib* LOF clonal context [47] and JNK activation alone is not sufficient to induce loss of cell polarity [45]; further analysis will therefore be required to fully address this aspect of JNK

function.

Since JNK signalling is implicated in human cancer development [81] it is likely that this oncogenic cooperation model represents a relevant tool for a better understanding of the mechanisms behind JNK function in tumourigenesis.

The role of the Hpo pathway Similarly to what has been demonstrated for *lgl* and *scrib* loss of function phenotypes (see Section 1.2.1.2), deregulation of the Hpo pathway also seems to contribute, at least in part, to the overgrowth that characterises the oncogenic cooperation between activated Ras/Raf and polarity genes loss [47, 82, 83]. Dogget and colleagues found that Yki target genes were upregulated in *scrib*$^{-/-}$; *Raf*$^{\mathrm{ACT}}$ (or *Ras*$^{\mathrm{V12}}$) tumours in the eye imaginal disc and inhibition of Yki activity significantly reduced tumour growth. However, despite this reduction of tumorous mass, mutant clones were still able to invade and differentiation remained blocked indicating that Hpo pathway impairment does not contribute to these phenotypes. Moreover the fact that the growth of these clones was not totally abrogated by blocking Yki function suggests that other pathways may also be involved in driving *scrib*$^{-/-}$; *Raf*$^{\mathrm{ACT}}$ cells clonal expansion in this context [47].

In another study analysis of large overgrown and fast-proliferating *lgl*$^{-/-}$; *Ras*$^{\mathrm{V12}}$ clones in the wing disc revealed an evident Yki nuclear staining and, accordingly, a strong upregulation of its target genes *dIAP1* and *dMyc*. The authors did not test whether Yki was required for the overgrowth of *lgl*$^{-/-}$; *Ras*$^{\mathrm{V12}}$ clones but showed that its expression within *lgl*$^{-/-}$ clones is sufficient to promote it [82]. Similarly *scrib*$^{-/-}$; *Ras*$^{\mathrm{V12}}$ clones in the wing disc also showed upregulation of Yki target genes and Yki overexpression was able to promote overgrowth of *scrib* mutant cells [83].

The role of PI3K signalling Several lines of evidence seem to indicate that the Raf/MAPK pathway is the downstream branch of Ras signalling involved in the cooperation with polarity genes loss [47, 60, 72]. While activated Raf fully recapitulates Ras-mediated phenotypes, induction of PI3K signalling pathway (the other main branch, see Section 1.3.1) can only moderately increase *scrib*$^{-/-}$ clone size but is not sufficient to promote their malignant growth [60, 70, 74]. Its ability to promote growth but not invasion is confirmed by the reduction in tumour size upon its disruption in *scrib*$^{-/-}$;*Ras*$^{\mathrm{V12}}$ clones which however still display metastatic capabilities [74].

Interestingly, in a screening attempting to identify genes required for neoplastic tumour growth which employed a modified version of the *scrib*$^{-/-}$; *Ras*^{V12} tumour model, PI3K signalling was found to be absolutely indispensable for tumorous growth [84]. The authors induced overgrowth by coexpressing *Ras*^{V12} and a *dlg* RNA interference construct (*dlg*RNAi) throughout the eye disc (using the Flp-out technique [85]); silencing PI3K or other downstream members of the pathway, such as Akt, severely reduced growth in this context resulting in eye discs much smaller than the wild-type ones and, accordingly, knockdown of the negative regulator, PTEN, enhanced overgrowth. On the other hand manipulation of the pathway in wild-type discs only had mild effects. These results were also confirmed inducing *dlg*RNAi; *Ras*^{V12}; *pi3k*$^{-/-}$ MARCM clones. This dependency on PI3K signalling was neither observed in *Ras*^{V12} or *dlg*RNAi eye discs nor in large overgrown discs obtained coexpressing *dlg*RNAi, *Yki* and *Upd* where reduction of PI3K levels had a less pronounced effect, indicating that it is a specific feature of *dlg*RNAi; *Ras*^{V12} cells. Surprisingly *dlg*RNAi; *Ras*^{V12} discs showed low levels of activated Akt suggesting that *Ras*^{V12} expression is not able to activate PI3K pathway if cell polarity is compromised; according to the authors this paradoxical result could indicate that PI3K signalling is rate-limiting in *dlg*RNAi; *Ras*^{V12} tissue overgrowth and hence explain the sensitivity to its alterations they observed [84].

Interactions with the immune system In 2008 the interesting observation that *scrib*$^{-/-}$;*Ras*^{V12} clones in the eye disc displayed many cells on their surface that did not belong to the tumour led to the discovery that *Drosophila* innate immune system cells, the hemocytes, specifically associate with the tumorous mass [86]. They were mainly found to adhere to areas where basement membrane was compromised and consistently they were also found on *scrib* mutant tissues, where BM degradation is observed, but not on *Ras*^{V12} clones. Mechanical disruption of BM as well as expression of MMP1 also caused hemocytes recruitment confirming the role of BM alteration in this process. Interestingly, the number of circulating hemocytes in *scrib*(or *lgl*)$^{-/-}$;*Ras*^{V12} and *scrib* mutant larvae was dramatically increased; the authors demonstrated that JNK activation in the tumour induced local as well as systemic activation of JAK-STAT signalling, through the production of cytokines, that was in turn responsible for hemocytes hyperproliferation. This mechanism was also proved to be true for tissue damage-dependent JNK activation pointing towards

the existence of an innate mechanism of response to tissue damage that can be triggered both by tumours and wounds [86].

Some indications were also given that hemocytes recruitment functioned in restricting tumorous growth of *scrib* mutant imaginal disc but definitive evidence for a role of hemocytes in tumour development came in a subsequent paper where Cordero and colleagues [87] demonstrated that tumour associated hemocytes are stimulated to produce Eiger that is sufficient to induce MMP expression in tumour cells and may have two different outcomes according to the context. *lgl* mutant clones in the wing disc display increased viability and aberrant morphology upon hemocytes-specific *egr* knockdown indicating that in this case it functions in eliminating mutant cells probably by activating JNK as it was demonstrated for *scrib* mutant clones [61] (although in that case Eiger activation was attributed to autocrine production of Egr itself). On the contrary Egr depletion, blocking JNK activation, completely abolished invasion and MMP1 expression and restored pupation of $scrib^{-/-}$;Ras^{V12} clones-bearing larvae, confirming that Egr/JNK signalling acquires a tumour-promoting role in presence of oncogenic Ras. In this latter case, however, for technical reasons, *egr* function was abrogated in the whole individual and thus a specific role for hemocytes-produced Eiger can only be speculated by the observation that transfusion of $egr^{+/+}$ hemocytes was sufficient to induce MMP1 expression in $scrib^{-/-}$;Ras^{V12} clones generated in $egr^{-/-}$ individuals [87]. These data add evidence to support the notion that tumour cells hijack organismal self-defence mechanisms to promote growth and invasion.

Other Ras^{V12} cooperators Besides polarity regulators, other genes have been recently added to the list of *Ras*-cooperating tumour suppressors. Loss of function of genes belonging to the Class C VPS (Vacuolar Protein Sorting) pathway, involved in lyosomes delivery and degradation, cooperate with Ras^{V12} to promote growth and invasion. This cooperation was found to be specific as it did not occur with dMyc or Insulin pathway activation. The authors were also able to confirm the role of lysosomes degradation impairment in oncogenic cooperation by showing that administration of drugs that block this process promoted tumour progression and metastasis of cells expressing oncogenic *Ras* [88].

A genome-wide screen for enhancers of Ras^{V12} hyperplastic phenotype in the eye imaginal disc allowed to identify several genes among which *Rac1*, *Rho1* and

RhoGEF2, all involved in cell morphology regulation, that when overexpressed clonally cooperated with activated *Ras* to induce overgrowth and invasion [78].

Interestingly the cooperation between Ras^{V12} and both loss of function of lysosomal delivery genes and gain of function of morphology regulators depends on JNK activation since growth, invasion and differentiation blockade are abolished upon coexpression of a dominant negative form of Bsk, further underlining the key role of this pathway in tumour development [78, 88]. It will be interesting to investigate how JNK signalling is activated in these contexts.

1.3 Ras Signalling Pathway

Ras family proteins are membrane-associated guanine nucleotide-binding proteins involved in extracellular signals transduction. They belong to the small GTPase proteins (or G proteins) class and function by switching from GDP-bound to GTP-bound state. Extracellular signals are received by membrane-bound receptors which activate guanine-nucleotide-exchange factors (GEFs). GEFs are in turn able to transiently activate Ras by promoting its association with GTP. Activated GTP-bound Ras undergoes a conformational change and is able to recruit and activate its downstream effectors. Under physiological conditions Ras signalling is terminated when bound GTP is hydrolysed to GDP and the bound effectors are released. GTP hydrolysis is stimulated by GTPase-activating proteins (GAPs) [89, 90].

Ras signalling has been shown to promote a wide variety of cellular functions among which cell growth and proliferation, survival, migration and differentiation, hence it is not surprising that Ras-activating mutations are found in approximately 30% of human malignancies. Tumour-associated Ras mutations cause persistent GTP binding and thus constitutive signalling to downstream effector proteins; one of the best examples is the glycine-to-valine mutation at residue 12 which results in the highly oncogenic Ras^{V12} variant [89, 90].

Mammalian genomes contain three *Ras* proto-oncogenes which encode H-Ras, K-Ras and N-Ras proteins, highly related to each other [89, 90]; *Drosophila* has three Ras homologues, but only Ras1 (also known as *Ras* oncogene at 85D and hereafter referred as Ras) has substantial homology to mammalian Ras proteins (75% identity) [91] and the same effectors [92].

1.3.1 Ras Effectors

Given its undisputed involvement in tumourigenesis, *Ras* proteins are perhaps the best studied molecules in molecular oncology and among the first transforming oncogenes to be identified [93]. The continuously increasing body of work produced to understand the mechanisms behind its pleiotropic effects demonstrated that GTP-bound Ras can interact with and activate a wide range of molecules depending on cell context but the two main downstream effectors, both in *Drosophila* and mammals, are the Raf/MAPK signalling cascade and the PI3K pathway [94] (Fig. 1.10).

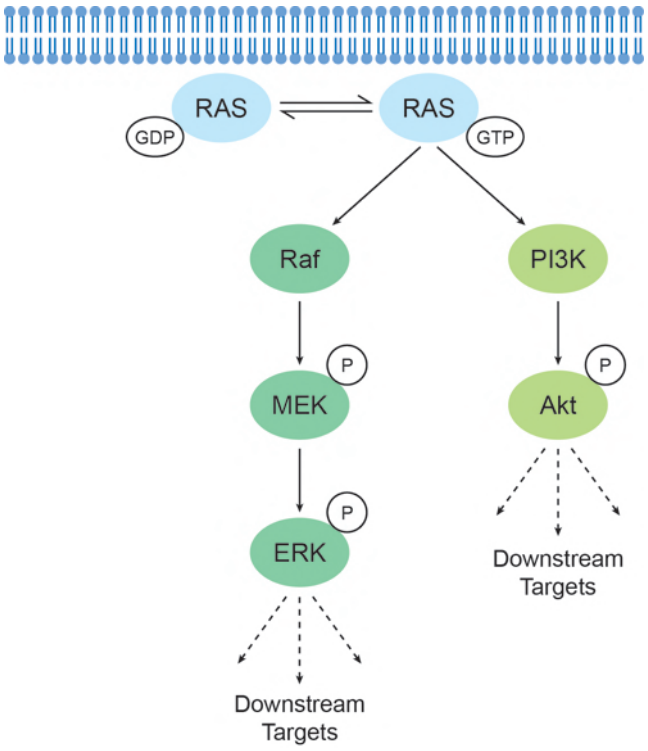

Figure 1.10: The two main pathways activated downstream of GTP-bound Ras: the Raf/MAPK and PI3K cascades. P indicates phosphorylation. Details are in the text.

The Raf/MAPK signalling pathway is perhaps the best characterised Ras downstream effector. Raf proteins are serine/threonine kinases that activate the MEK-MAPK kinase cascade. Activated MAPKs (or Extracellular signal Regulated Ki-

nases, ERKs) can phosphorylate both cytosolic and nuclear substrates, which include transcription factors such as JUN and FOS. Activation of these transcriptional regulators can lead to the expression of proteins that control cell-cycle progression, cell survival and many other processes. The importance of this pathway downstream of Ras-mediated tumourigenesis is highlighted by the fact that activated Raf and MEK are able to transform different cell types and Raf-activating mutations are frequent in human cancers and may be equivalent to those of *Ras* genes as their occurrence never overlap [95].

GTP-bound Ras is able to directly bind the catalytic subunit of type I PI3Ks, a family of kinases involved in intracellular Insulin signal transduction. This binding results in the translocation of PI3K to the plasma membrane and subsequent activation. Active PI3K phosphorylates membrane phosphatidylinositol-4,5-bisphosphate (PIP_2) thus generating a second messenger, phosphatidylinositol-3,4,5-triphosphate (PIP_3), which in turn recruits and activates downstream effectors such as Akt by binding to their pleckstrin homology (PH) domains. Akt is a protein kinase B (PKB) that promotes growth and survival in many cell types regulating glucose and lipid import and nutrient storage as well as inhibiting pro-apoptotic molecules. Similarly to MAPK/ERK, PI3K pathway is also found deregulated in many human cancers and has shown in different contexts to be required for Ras-induced transformation [95, 96].

Drosophila activated-Ras also signals through Raf/MAPK and PI3K signalling although it does not seem to be required, with some exceptions, to maintain physiological levels of this latter [92, 97].

Among the other pathways activated by mammalian Ras there is also the JNK signalling cascade, however, this does not seem to be the case for *Drosophila* counterparts [74].

Both in flies and mammals Ras signalling affects very different aspects of cell physiology and behaviour. In *Drosophila*, Ras has been shown to promote processes as diverse as proliferation, migration and differentiation even in the same cell type. Just to give a few examples, it regulates cell fate and patterning of follicular cells [98], it is required for photoreceptors differentiation [99] and in the imaginal wing disc it promotes both proliferation [100, 101] and cell fate determination [102]; in adult life it is involved in maintenance and proliferation of intestinal stem cells [103, 104]. The specificity of these effects depends on the cellular context: different cell-

specific regulators and downstream targets as well as specific subcellular localisation of pathway components can influence the outcome, moreover also the amplitude and duration of the signalling impact on its effects [105–107].

1.3.2 Mechanisms of Oncogenesis

Extensive analysis of the effects of oncogenic Ras signalling on cell behaviour of the past decades has unveiled its capacity to contribute to most of the hallmarks of cancer discussed in Section 1.1 [90].

Sustained Proliferation The ability to promote cell cycle entry in absence of growth factors in mammalian cells was attributed to constitutive Ras activity since the very early studies. It was subsequently shown that it is able to promote proliferation in several ways including transcriptional upregulation of growth factors and their receptors, activation of transcription factors that regulate genes involved in cell cycle progression such us c-Myc and CycD1, activation of pathways that regulate the stability of these genes' products and inhibition of cell cycle inhibitors [90].

Similarly, also activated *Drosophila* Ras promotes cell proliferation. In the wing and eye imaginal disc cells Ras^{V12} ectopic expression is sufficient to drive cell proliferation and cause hyperplastic growth of the tissue [100]. Its clonal expression in the wing disc has been shown to increase cell size and growth rates and to promote G1/S transition. These effects are mediated by its ability to increase post-transcriptional levels of dMyc (see Section 1.4.2) and Cyc E [101]. Moreover Ras is required for proliferation and maintenance of *Drosophila* adult intestinal stem cells and it is involved in regeneration upon tissue damage downstream of EGFR (Epidermal Growth Factor Receptor) in the adult midgut [103, 104].

Evasion of Cell Death Ras ability to promote cell survival is well documented in mammalian cells. Both Raf/MAPK and PI3K signalling pathways contribute by inhibiting a wide range of pro-apoptotic factors as well as activating anti-apoptotic ones [90].

In *Drosophila* one major target for the anti-apoptotic activity of Ras is the pro-apoptotic Head Involution Defective (Hid) protein. Active Hid induces apoptosis by binding to and inhibiting dIAP1, an essential inhibitor of Caspases in *Drosophila*,

through stimulation of its auto-ubiquitination. Hid is transcriptionally downregulated as well as post-transcriptionally inactivated via phosphorylation by MAPK signalling [108, 109]. It has also been proposed that inhibition of JNK signalling contributes to Ras anti-apoptotic effects [110].

Angiogenesis As mentioned in Section 1.1, hypoxic cancer cells can induce proliferation of endothelial cells and sprouting of new blood vessels by releasing VEGF. Under physiological conditions, low oxygen tension leads to stabilisation of the pro-angiogenic transcription factor HIF1α (Hypoxia-Inducible Factor 1α) by inhibiting the prolyl hydroxylases which would otherwise prime it for degradation. HIF1α is a potent activator of VEGF promoter. Secreted VEGF triggers angiogenesis by binding and activating VEGFR downstream signalling in endothelial cells [111]. Indeed, oncogenic Ras signalling is able to upregulate VEGF, via HIF1α and other VEGF regulators, as well as other endothelial growth factors such as FGF2. Moreover Ras activity promotes angiogenesis by producing inflammatory cytokines that contribute to the recruitment of angiogenic growth factors-releasing immune cells [90].

In *Drosophila* oxygen is transported to the tissues through a tracheal system that consists of an interconnected tubular network made of epithelial monolayered tubes, the regulation of which shares significant similarities with that of mammalian angiogenesis, with *Drosophila* FGF/FGFR (FGF Receptor) cascade performing a function analogous to that of VEGF/VEGFR [112, 113]. *Drosophila* Ras signalling has shown to be cell-autonomously required for tracheal cells migration [114] but no evidence exists for a role in tracheogenesis.

Tracheal network development begins during embryogenesis and depends on three main processes: directional cell migration, cell rearrangements and cell shape changes. Clusters of tracheal cells in the embryo are specified by the expression of the transcription cofactor, Trachealess (Trh) [115] a direct target of STAT [116]; Trh is phosphorylated by Akt and this event is required for its nuclear localisation and transactivating abilities [117]; Trh in turn activates the transcription of *breathless* (*btl*) gene which encodes the *Drosophila* FGFR. Surrounding epithelial cells produce the FGF ligand (encoded by *branchless*, *bnl*) which activates Btl and stimulate directional migration and branching of tracheal cells by activating Ras signalling through a tracheal-specific adaptor protein called Dof (Downstream-Of-EGFR, also

known as Stump) [112–114]. The FGF/FGFR signalling pathway is also involved in later phases of tracheal development, during larval life, and is required for proliferation and migration of tracheoblasts of the air sac, a sac-like structure which develops attached to the wing imaginal discs and will originate large reservoirs connected with the flight muscles of the adult fly. Air sac cells are induced to proliferate by, migrate and extend filopodia towards a group of FGF/Bnl-expressing epithelial cells of the wing imaginal disc; also in this case FGFR/Btl signalling in tracheal cells requires downstream Ras activity and the transcription factor Pointed [118]; despite being essential, Ras activation is however not sufficient to promote FGF/Bnl dependent cell migration, indicating that additional downstream effectors might be required to induce chemotactic movements of tracheal cells [114]. Recently it has also been demonstrated that heparan sulphate proteoglycans (HSPGs) are necessary to respond to FGF/Bnl [119].

Drosophila tracheal network has also been shown to respond to oxygen requirements: while shape and size of the tubes are genetically determined, fine terminal branches form in response to local hypoxic conditions. Oxygen deprivation induces FGF/Bnl expression which acts as a chemoattractant for terminal branches. The mechanism is strikingly similar to that of mammalian angiogenesis: hypoxia is sensed by prolyl hidroxilases that stabilise Sima, *Drosophila* HIF1α, which then activates FGF/Bnl expression to attract new terminal branches towards the expressing cells [113]. Terminal branching of tracheal cells depends on the formation of long cytoplasmic processes with intracellular lumen which connect to the lumen of the main branches and are regulated by *blistered*, the fly homologue of serum response factor (SRF), known to regulate sprouting in mammalian angiogenesis [120]. It is however still not known how FGF signalling coordinates these cell rearrangements.

Migration and Metastasis Many metastatic tumours contain Ras mutations and oncogenic Ras signalling has been implicated in promoting migration and metastasis in several contexts mainly by downregulating E-Cadherin, a hallmark of EMT, and altering cytoskeletal dynamics. Moreover BM remodelling enzymes are also upregulated downstream of Ras activation [90].

In *Drosophila* Ras has been linked to physiological migration of tracheal cells (see above paragraph, [114]), border cells in the ovary [121] and primordial germ cells in the embryo [122], downregulation of E-Cadherin has also been observed in

scrib$^{-/-}$; *Ras*^{V12} clones [70]. Nevertheless, in imaginal epithelia production of BM-modifying enzymes has been observed in *Ras*^{V12}-expressing cells only in the context of cell polarity loss (see Section 1.2.2).

Metabolism Reprogramming and Immune Surveillance Evasion Several lines of evidence also implicate Ras in the regulation of the two emerging hallmarks: deregulation of metabolism and evasion of immune destruction. Oncogenic Ras-dependent regulation of HIF1α is indeed responsible for the stimulation of the glycolytic shift often observed in tumour develoment, known as the Warburg effect. HIF1α enhances both glucose uptake, metabolism and intermediates processing [90]. Moreover Ras activity was shown to reduce immunogenicity of cancer cells in different ways, for example by decreasing surface antigen-presenting MHC (Major Histocompatibily Complexes) [90]. Neither of these two effects have been observed so far downstream of activated Ras in *Drosophila*.

1.4 Myc and Cell Competition

1.4.1 Myc Oncogene

Myc family proteins are evolutionarily conserved basic helix-loop-helix leucin zipper (bHLH-Zip) transcription factors that coordinate several key cell functions such as cell cycle progression, growth, metabolism, differentiation, apoptosis. Generally they heterodimerise with their binding partners of the Max proteins family and control target genes expression by binding to regulatory regions, called E-Box sequences; E-Box- and Max-independent functions of Myc have however also been reported.

Mammals possess three members of this family: c-Myc, N-Myc and L-Myc. *c-myc* gene is ubiquitously expressed in dividing cells and normally downregulated in quiescent and/or differentiated cells; on the other hand N-Myc and L-Myc are expressed only during particular stages of embryonic development and in some immature hematopoietic and neuronal cells [123–125]. For this reason c-Myc will be further considered in this review and referred to as Myc.

Recently it has been estimated that Myc regulates 10-15% of all genes and is responsible of genome-wide chromatin remodelling and is thus able to promote global

changes in gene expression, confirming its master role in controlling cell physiology and behaviour [123, 125, 126]. Consistently, *Myc* is found deregulated in a strikingly high percentage of human malignancies and is often associated with aggressive and poorly differentiated tumours. For this reason, together with Ras, it is one of the most intensely studied molecules in cancer biology [123, 124, 127].

Oncogenesis Three decades of research have proved that Myc is a master regulator of cell growth and proliferation. From the early observations that Myc expression was sufficient to drive quiescent cells into S-phase in the absence of mitogenic signals, much progress has been made to understand the complex biology behind Myc activity and its substantial implication in tumour development [127].

Myc targets genes involved in cell cycle progression like cyclins, Cdks (cyclin-dependent kinases) and their regulators, it participates in DNA replication and is a key promoter of cell growth; it indeed regulates protein synthesis acting on ribosomal RNA (rRNA) and rRNA-processing factors, ribosomal proteins, tRNAs and translation initiation and elongation factors. Myc is also a positive regulator of the glycolytic pathway as well as of the oxygen-dependent mitochondrial energy production chain. Moreover it has been clearly implicated in maintenance and self-renewal of stem cells and in suppressing differentiative programmes [123, 124].

Evidence exists that Myc can regulate cell migration and invasion in different ways, in some contexts it was shown to promote EMT and to regulate cell adhesion and cytoskeletal dynamics [128]. Myc has been implicated in several events involved in cross-talk with the tumour-microenvironment and a clear and direct link has also been established between Myc activity and both physiological and tumour-associated angiogenesis [129]. Moreover a context dependent interplay between Myc and HIF1α has been described in tumour development: whereas under physiological conditions HIF1α inhibits Myc, it has been reported that in oncogenic contexts they can either cooperate in promoting both the Warburg effect and angiogenesis through the release of factors such as VEGF [130] or antagonise each other [131].

Since very early in the history of its research, Myc has also been shown to counteract senescence and promote immortalisation. Finally, not only Myc contributes to nearly all the hallmarks of cancer, it also activates a complex inflammatory response [129] and intensifies mutation rates by inducing high degree of genomic instability [132], the two characteristics that favour and accelerate tumour development (see

Section 1.1).

Myc is therefore an extremely potent oncogene and its upregulation is often accompanied by increased levels of cell death, most probably as a safe-guard mechanism evolved to protect cells from the detrimental effects of its uncontrolled activity. The detailed mechanisms by which Myc triggers the apoptotic programme are still unclear although its ability to repress transcription of anti-apoptotic genes is well documented [123, 124]. The existence of these tumour-suppressive mechanisms is at the basis of the requirement of multiple genetic lesions for full tumourigenic transformation and accounts for the well-known oncogenic cooperation between activated Ras signalling and Myc in human cell lines: oncogene-induced senescence caused by Ras is suppressed by Myc activity and, in turn, Ras provides cells with strong survival hints which counteract Myc-induced cell death [123, 124].

Regulation Due to its biochemical properties, Myc deregulation in human cancers does not usually derive from activating mutations in its coding sequence as is true for Ras (see Section 1.3) but rather to an increase in its protein levels that can be caused by gross genetic abnormalities such as enhancer insertions, chromosomal translocation and gene amplification, or by deregulation of signalling pathways that control its expression and mRNA and/or protein stability [127]. Since most, if not all, oncogenic signalling pathways regulate Myc at some level, it is not surprising that abnormal Myc levels and activity are found in a strikingly high percentage of human cancers [125]. Indeed, under physiological conditions Myc abundance is tightly regulated through the integration of several signals acting at transcriptional, post-transcriptional, translational, and post-translational levels [123, 125].

myc is generally expressed at extremely low levels in quiescent cells and it is rapidly induced by mitogenic signals. Myc promoter is regulated by a multitude of pathways, depending on cell type and physiological context. A few examples of *myc* transcription activators are Wnt, Notch, interleukins, cytokines, growth factors, hormones, Ras/MAPK and PI3K/Akt, JAK-STAT and NF-kB signalling pathways, all major cell proliferation-promoting pathways; on the other hand it is inhibited by antiproliferative factors such as TGF-β and p53 [125].

Both Ras/MAPK and PI3K/Akt pathways, among many others, also regulate Myc post-transcriptionally. They are able to enhance its translation, increasing ribosomal recruitment of *myc* mRNA, and its protein stability [125, 133]. Myc pro-

tein, in fact, undergoes a very rapid turn-over with a half-life of 20-30 minutes. This turn-over is regulated by phosphorylation events at two conserved sites: threonine 58 (Thr-58) and serine 62 (Ser-62). Phosphorylation at Ser-62 increases its stability whereas concomitant phosphorylation at Thr-58 and dephosphorylation at Ser-62 targets Myc for proteasomal degradation. Indeed, Erk downstream of Ras signalling can increase Myc protein stability by phosphorylating it at Ser-62 whereas PI3K pathway can do so by inhibiting GSK-3β, which is responsible for the phosphorylation event at Thr-58. [123, 125, 133]. Enhanced protein stability is often observed in cancers associated with abnormal Myc levels and its importance is highlighted by the fact that the factors that regulate its proteolytic turn-over are often lost in many malignancies [134].

1.4.2 *Drosophila* Myc

dmyc (also known as *diminutive*, *dm*) encodes the single *Drosophila* homologue of the Myc family of proto-oncogenes [135]. dMyc has proven to be functionally homologous to c-Myc, it can indeed rescue growth defects in *c-Myc* knock out mouse embryo fibroblasts [136], can functionally substitute for c-Myc in transactivation assays in human cell culture [137] and can cooperate with activated Ras to transform rat embryo fibroblasts [138]. Moreover, human c-Myc can rescue *dmyc* loss of function lethality [139]. Similarly to human Myc proteins, dMyc regulates its target genes forming heterodimers with its partner, Max, and binding to the E-boxes [135].

Functions Consistent with a well conserved role in regulating growth and proliferation, *dmyc* loss of function causes strong growth defects; null embryos hatch into larvae but are not able to grow further and die at early second larval instar. Individuals bearing weakest alleles show delayed development and reduced body size. Conversely, overexpression of dMyc increases animal dimensions by 30% [140]. Clonal analysis has revealed that $dmyc^{-/-}$ cells are of smaller size and have an impaired cell cycle progression. Indeed dMyc is required to stimulate G1-S transition; its overexpression increases Cyclin E levels and accelerates S phase entry [140]. Cyclin E regulation appears to be post-transcriptional as mRNA levels do not markedly increase, but other cell cycle regulators, such as CycD and its partner Cdk4, are transcriptionally activated by dMyc. Overall division rate is however not altered probably because G2 inducer Cdc25 phosphatase (String) is not affected by dMyc

levels and a compensatory lengthening of G2 phase occurs [101].

Also in *Drosophila* dMyc plays a fundamental role in regulating basic cellular growth machinery. Its overexpression, as opposite of its loss of function, considerably increases cell size accelerating growth through regulation of several factors involved in RNA binding, rRNA processing, nucleolar function, translation and, above all, ribosomal biogenesis [141, 142].

In the ovary, *dmyc* is required for efficient DNA endoreplication in follicle cells, but it seems not to be essential for their mitotic proliferation. *dmyc*$^{-/-}$ follicle cells are unable to perform more than one cycle of endoreplication, moreover they show a dose-dependent reduction in nuclear and cell size [143].

Another parallel between mammalian and *Drosophila* Myc can be found in the regulation of stemness: high dMyc levels are observed both in germline stem cells [144, 145] and in larval neuroblast [146]. These cells undergo asymmetric cell division that originates another stem cell and a daughter cell, the cystoblast and the ganglion mother cell respectively, which will then commit to a specific cell fate; indeed dMyc levels are dramatically reduced in daughter cells of both types, moreover dMyc constitutive expression in germ line daughter cells confers them stem cell-like features indicating that also in *Drosophila* Myc is able to suppress differentiation [145].

The capability of Myc to sensitise cells to various apoptotic stimuli is another conserved feature of its activity and, consistently, imaginal wing disc cells with increased dMyc expression are subject to high levels of autonomous cell death [147]. It is not clear how dMyc promotes cell death but its overexpression has been linked to the upregulation of dIAP1 inhibitors such as Hid, and Hid function has been shown to be required for dMyc-dependent cell death of imaginal wing disc cells [147, 148].

Regulation *dmyc* transcriptional regulation is not as well understood as it is that of *c-myc* but in recent years a few key signalling pathways have been implicated in the regulation of *dmyc* transcription.

During imaginal wing disc development *dmyc* is initially expressed in all cells starting from the second larval instar (L2), then its expression undergoes dynamic changes and by the third larval instar (L3) it decreases in the ventral and dorsal hinge regions while remaining high in the notum, the dorsal body wall primordium. Concurrently *dmyc* expression increases in the wing pouch, the region that will orig-

inate the wing blade. Towards the end of larval development, at the dorso-ventral border - the future wing margin - *dmyc* is repressed in a stripe of cells, called ZNC (Zone of Non-proliferating Cells) where growth and cell cycle are arrested [149]. This dynamic expression pattern seem to depend, at least in part, on the activity of Wg and Notch pathways. In the ZNC *dmyc* is repressed by Notch signalling [150] whereas in other regions Wg acts through a double repression mechanism, that is to say by repressing Notch pathway which would in turn repress dMyc transcription. Wg-dependent positive regulation of dMyc is also involved in wing disc regenerative growth after damage [151] and in the control of the larval hematopoietic niche in the limph gland [152]. Nevertheless the detailed mechanisms of these regulatory events are still largely unknown, moreover in imaginal wing disc cells Wg has also been implicated in dMyc repression and thus might have context-dependent effects on dMyc transcription [153].

The RNA-recognition motif protein Half pint (Hfp) is a direct regulator of *dmyc* as it binds to *dmyc* promoter and represses its transcription. Indeed, *hfp* knockdown leads to increased dMyc levels and dMyc ablation can rescue *hfp* loss of function phenotypes [154]. Since Hfp is upregulated by Wg signalling, this might account for the repressive effect of this latter on dMyc transcription observed in some contexts [155].

Recently, we and others identified dMyc as a direct transcriptional target of the growth-promoting Hpo pathway (see Section 1.2.1.2) [156, 157]. We found that dMyc protein was upregulated in Yki-overexpressing and in Hpo pathway mutant clones and this correlated with an increase in dMyc mRNA; moreover hyperactivation of Hpo pathway members and thus repression of Yki function led to a reduction in dMyc abundance [156]; *dmyc* promoter has consensus binding motifs for Scalloped (Sd), a Yki DNA-binding partner and indeed these motifs were shown to be directly bound by Yki/Sd complex [157] and consistently, we found that knockdown of Sd in the wing disc prevented dMyc upregulation upon Yki overexpression in the wing pouch; conversely in the notum we found that dMyc regulation depended on the ability of Yki to bind another partner, Homothorax (Hth), highly expressed in this region [156]. dMyc transcriptional upregulation plays a key role in mediating the growth-promoting capabilities of Yki as its ablation was sufficient to abolish the overgrown phenotype due to Yki overexpression; nevertheless dMyc alone is not sufficient to rescue $yki^{-/-}$ growth defects indicating that other Yki targets are required

for an efficient promotion of cell growth [156, 157]. This regulation is likely to be functionally conserved as *c-myc* appears to be upregulated in a murine model of Yki mammalian homologue YAP-induced hepatocarcinoma [158].

Other factors have been shown to regulate *dmyc* expression in various tissues. For example Twist transcription factor binds and activates *dmyc* promoter during early mesoderm development [159] and *dmyc* transcription is systemically regulated by nutrients signalling [160] and, in the fat body, by the moulting hormone Ecdysone [161].

Finally, similarly to c-Myc, dMyc autorepresses it-self by negatively regulating its own transcription [162].

Control over dMyc levels has also been demonstrated to occur via translational repression mechanisms. In the cystoblast originated from the germline stem cell in the *Drosophila* ovary, a translational repression complex containing Brat (encoded by the *brain tumour* gene) has been shown to cause dMyc downregulaton by targeting its mRNA [163]. Interestingly, dMyc repression in the ganglion mother cell (derived from larval neuroblasts) also seems to be mediated by Brat [146] possibly through a similar mechanism.

Like its mammalian counterpart, dMyc protein is subject to a very rapid turnover and has a half-life of 35 minutes in S2 cells [164]. Similarly to mammalian c-Myc, dMyc stability its regulated, *in vitro* and *in vivo*, through phosphorylation by GSK-3β (Shaggy, Sgg, in *Drosophila*) which results in dMyc ubiquitination and proteasomal degradation. Notably, the same effect on dMyc stability is observed upon phosphorylation by a member of the casein kinase 1 family (CK1), encoded by *discs overgrown* (*dco*). Clonal inhibition of both Sgg and Dco causes an increase in dMyc levels in imaginal wing discs, but only in those regions where Wg signalling is not active. In fact, both kinases are negative regulators of Wg pathway and probably since their inactivation leads to increased Wg levels this might lead to a *dmyc* transcriptional repression [164]. dMyc ubiquitination depends on the activity of Archipelago (Ago), the F-box component of the E3 ubiquitin ligase complex SCF (Skp, Cullin, F-box); Ago's human orthologue, Fbw7, is a tumour suppressor and regulates c-Myc protein stability [165].

As mentioned in Section 1.3.2, activated Ras, via Raf/MAPK, increases dMyc protein levels in the wing imaginal disc [92]. Since mammalian c-Myc is phosphorylated and stabilised by Erk (see 1.4.1), a similar mechanism can be hypothesised

for dMyc, however dMyc sequence does not contain Erk phosphorylation consensus sites and therefore other molecules downstream of Ras/Raf probably participate in regulating dMyc stability in *Drosophila* [164]. Ras signalling seems to be required to maintain physiological levels of dMyc in the wing disc cells since this latter is downregulated in $ras^{-/-}$ clones [92]. In that context the authors also investigated a possible cross-talk between dMyc and PI3K signalling but did not find any evidence of reciprocal regulation [92]. Nevertheless, consistently with what is known in mammalian systems, *Drosophila* PI3K pathway was shown to increase dMyc protein stability by inhibiting the GSK-3β Sgg in cultured S2 cells and consistently ectopic activation of PI3K pathway caused dMyc upregulation in imaginal wing disc cells [166]. The discrepancy between these two reports might lie in the fact that the analysis of dMyc levels was carried out with different time scales. In both cases PI3K ectopic activity was clonally induced by overexpressing PI3K catalitic subunit dp110, however, in the first report dMyc levels were analysed 48 hours after clone induction [92] whereas in the second one an inducible system was employed and dMyc abundance was tested after having induced dp110 expression for 5 hours only [166]. This suggests that PI3K pathway transiently affects dMyc stability and that dMyc levels in PI3K-overexpressing clones rapidly adjust to eventually normalise by the end of development. Additionally, Parisi and colleagues showed that the nutrient-sensing TOR pathway also converges on GSK-3β to positively regulate dMyc protein stability [166].

Post-transcriptional regulation of dMyc in the wing imaginal disc may also occur *via* the micro-RNA *bantam*. *bantam* targets Mei-P26 mRNA for degradation. Mei-P26 is the orthologue of mouse TRIM32, a c-Myc-ubiquitinating protein, and its upregulation has been shown to lead to reduction of dMyc [167].

1.4.3 dMyc-Induced Cell Competition

Cell competition is a phenomenon of short-range cell-cell interaction described in *Drosophila* imaginal wing discs over 30 years ago [59]. It consists in the elimination during development of normally viable but slow-dividing cells by the surrounding faster growing populations (Fig. 1.11), ensuring that the adult organ reaches proper size.

It was initially observed analysing a group of dominant mutations called *Minute* (*M*) that concern various ribosomal protein genes. These mutations, affecting more

than 60 *loci* in the *Drosophila* genome [168], are recessive lethal and display a dominant growth defect: $M^{+/-}$ cells are viable but have a slow growing rate and consequently $M^{+/-}$ flies are of normal size but their development is delayed with respect to wild-type counterparts. However, if mitotic clones of $M^{+/-}$ cells are generated in a wild-type wing imaginal disc tissue, they are eliminated by apoptosis. Compensatory proliferation in the wild-type tissue occurs to replace apoptotic cells during competition, the total number of cells in the developing tissue remains unchanged and no morphological alterations are observed in the resulting organ [169].

Moreno and colleagues [170] found in out-competed cells reduction in Dpp signalling. This pro-survival pathway, when activated, inhibits the transcription repressor Brinker, that would otherwise lead to the activation of the JNK pathway, ultimately causing death of the cells under competitive stress, that are eventually lost from the epithelium [171].

Apoptosis is required for cell competition to occur; inhibition of cell death by means of the baculovirus p35 IAP protein not only rescues $M^{+/-}$ cells from death but also decreases neighbouring wild-type cells' proliferation rate [170, 172]. *Minute*-mediated cell competition seems also to require the elimination of apoptotic cells by means of engulfment (phagocytosis) by surrounding tissue, as loss of function of genes involved in this process prevents competition [172]; nevertheless basal extrusion of dead cells, the process by which apoptotic wing disc cells are physiologically eliminated, has also been frequently observed [170].

The non-autonomous elimination of *scrib* mutant clones in the eye imaginal disc is reminiscent of cell competition ([60] and Section 1.2.2). Indeed $scrib^{-/-}$ mutant tissues overgrow in a homotypic context whereas mutant cells undergo JNK-dependent apoptotic cell death if surrounded by wild-type tissue and the resulting adult eye is unaffected. This clearly parallels the effects of $M^{+/-}$-induced cell competition in the wing imaginal disc; competitive interactions have however never been characterised in the eye imaginal disc and their involvement in *scrib* cells elimination can only be hypothesised.

In recent years dMyc has been strongly implicated in the phenomenon of cell competition [148, 171]. Clones bearing hypomorphic *dmyc* mutations, viable in a homotypic environment, were found to be eliminated by non-autonomous cell death when generated in a wild-type imaginal disc [140]. In 2004 two papers were published in which it was clearly demonstrated that this phenomenon is not simply

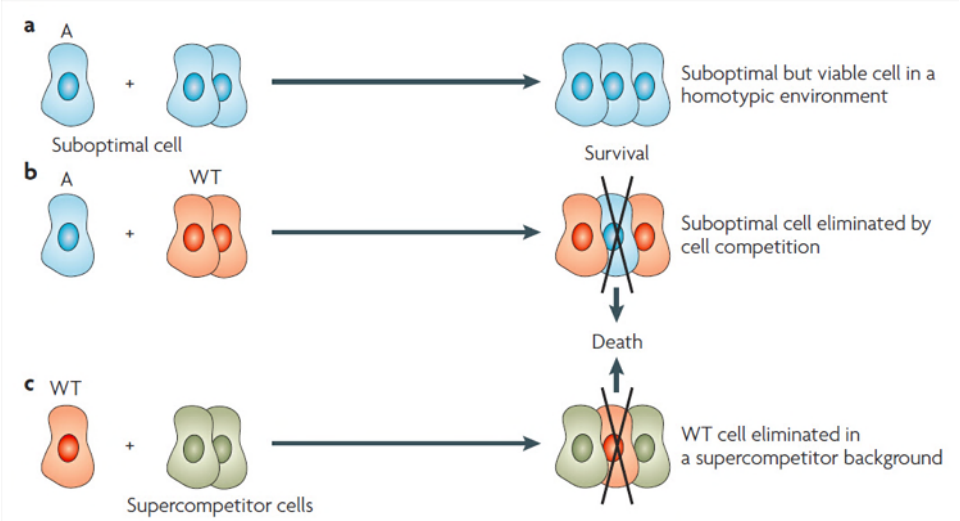

Figure 1.11: Mechanism of cell competition: slow-growing cells survive in a homotypic background (a) but are eliminated when surrounded by wild-type cells (b). However wild-type cells can be outcompeted if surrounded by faster-growing cells (c) [183].

caused by cellular defects associated with *dmyc* loss because, as it was shown, also wild-type cells are out-competed if surrounded by dMyc-overexpressing cells and cell competition is rather triggered by a sharp difference in dMyc protein levels between adjacent populations [148, 171].

de la Cova and colleagues [148] showed that clones overexpressing dMyc were significantly larger than control clones, due to promotion of cellular growth; however, sibling clones generated in recombination events were smaller than control siblings. They also showed that wild-type cells appeared to be subject to competition only if they lied within about eight cell diameters of dMyc-expressing cells (it was indeed later demonstrated that cell competition is mediated by soluble factors [173]), and in the same developmental compartment [148].

Using a *dmyc* tandem duplication, similar results were obtained by Moreno and Basler [171] (Fig. 1.12). Sibling clones were generated that were composed of cells with four (4x*dmyc*) or two copies (2x*dmyc*) of the endogenous *dmyc* gene. Interestingly, not only 4x*dmyc* clones were significantly larger than their 2x*dmyc* wild-type siblings but they were also larger than control clones that were induced simultaneously in different animals in which all cells carried four copies of *dmyc*. Likewise, clones carrying two copies of *dmyc* were not only smaller than their 4x*dmyc* siblings,

but also smaller than control clones growing in a background where all cells had two copies of *dmyc*, demonstrating that clonal growth strongly depends on cellular environment. As for *Minute*-mediated cell competition, Moreno and Basler found reduction of Dpp signalling in out-competed cells. They proposed the so-called "ligand capture" model, according to which cells compete with different success for limiting amounts of extracellular survival and growth factors, such as Dpp, by actively internalising them. "Winner cells", due to their optimal growth status, would be able to capture more survival factors than "loser cells" that, as a consequence, would undergo JNK-mediated apoptosis. Accordingly to this hypothesis, overexpression of the endocytic pathway component Rab5, as well as stimulation of the Dpp signal transduction pathway, rescued wild-type cells from being eliminated by surrounding cells with elevated dMyc levels [171]. Dpp involvement is however still controversial as de la Cova and colleagues neither obtained evidence of Dpp signalling reduction nor found JNK-mediated apoptosis to take place in out-competed cells [148].

Interestingly, Tyler and colleagues [174] demonstrated that mutations in genes belonging to the Hippo pathway were able to protect $M^{+/-}$ cells from being out-competed in a wild-type background and even to provide them with competitive capabilities as indicated by active Caspase 3 staining visible outside the mutant clones [174]. These competitive properties of Hpo mutant cell have been explained by the identification of *dmyc* as a target of this pathway ([156, 157] and Section 1.4.2). Indeed we were able to demonstrate that dMyc upregulation is responsible for Hpo mutant or Yki-overexpressing clones competitive behaviour as their overgrowth was drastically reduced if they were generated in a dMyc-overexpressing background [156].

Similarly, other dMyc regulators have been found to trigger competitive interactions. *ras* loss of function clones were found to be out-competed [92] probably due to their lower levels of dMyc compared to neighbouring wild-type cells and miRNA machinery mutant clones were subject to cell competition because of their inability to repress dMyc negative regulator Mei-P26 [167] (see Section 1.4.2).

The differential expression of splicing variants of Flower (Fwe) surface protein has been shown to be an early event of dMyc-mediated cell competition. Out-competed cells are labelled with a truncated form of Fwe and this is necessary and sufficient to trigger their apoptotic elimination [175]. Moreover in out-competed cells the gene *sparc* is transcriptionally upregulated; it encodes a secreted multifunctional

glycoprotein, Sparc, that seems to transiently protect these cells from apoptosis. This mechanism would hypothetically allow cells that are subject to transient or less intense stress to recover and thus avoid cell death [176]. Interestingly, truncated Fwe and upregulation of Sparc are characteristic of loser cells both in *Minute*- and dMyc-induced cell competition, suggesting that they might be part of a common mechanism that senses differences in cell fitness within a tissue [175, 176].

Similarly to that of *Minute*, also for dMyc-induced cell competition to occur, apoptosis is essential. When cell death is inhibited by reducing the gene dosage of *hid* [148] or by ectopically expressing the antiapoptotic proteins dIAP1 or p35 [171], out-competed clones grew larger while their competitive twins were smaller.

Why differences in dMyc protein levels among cells are able to trigger cell competition is still unclear. A simple difference in growth rate between neighbouring cells is not sufficient to induce the phenomenon: overexpression of Cyclin D and Cdk4 indeed promotes cell autonomous growth but does not trigger competition. The same is true for PI3K: clonal overgrowth is observed upon dp110 overexpression but neighbouring cells do not result to be affected [148]. Thus, cell competition probably depends on Myc ability to influence ribosomal activity. Indeed dMyc overexpressing clones bearing only one copy of the *Minute* gene *M(2)60E* (a known dMyc transcriptional target) were no longer able to out-compete surrounding cells [171]. Since it was demonstrated that raising the copy number or expression level of a *Minute* gene above wild-type had no effect on survival or proliferation properties of imaginal cells [177], it can be hypothesised that a global rise of protein synthesis coordinated by dMyc might be necessary for cell competition to occur. Nevertheless, the ability of Hpo mutant cells to confer competitive capabilities to $M^{+/-}$ cells, which are partially impaired in ribosomal biogenesis, argues against this hypothesis [174].

1.4.3.1 Cell Competition in Mammalian Cells

Evidence exists that cell competition is conserved also in mammals. It has been shown in mice that a deletion within the Rpl24 riboprotein gene significantly impairs ribosome biogenesis and results in decreased rates of protein synthesis and proliferation, clearly mirroring *Drosophila Minute* phenotype. Heterozygous mutant cells, while viable in a homotypic environment, giving rise to almost normal mice, are indeed out-competed by wild-type cells in chimeric blastocysts [178].

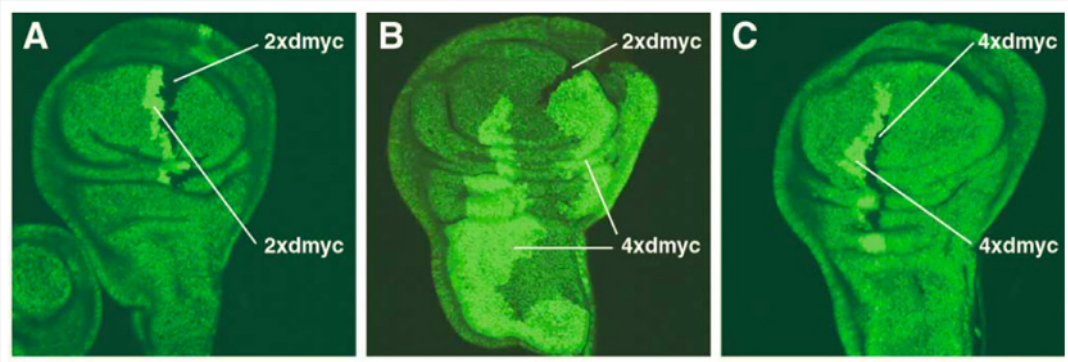

Figure 1.12: The experiment by which Moreno and colleagues showed that cell competition is triggered by relative dMyc levels: clones carrying 4 copies of *dmyc* gene (4x*dmyc*) are larger than their wild-type twin clones, 2x*dmyc* (B) but also larger than 4x*dmyc* clones induced in discs in which all cells were 4x*dmyc* (C). Similarly wild-type (2x*dmyc*) clones were not only smaller than their 4x*dmyc* twins clones (B) but also smaller than wild-type clones induced in a background where all cells carried two copies of *dmyc* (A) [171]

Another example is given by rat liver progenitors transplants: under certain conditions transplanted cells can overproliferate and induce cell death of the host cells to an extent that the entire liver is repopulated by donor-derived cells [179].

Compelling evidence of cell competition occurring in mammalian cell cultures has however been produced in two recent papers [180, 181]. These reports and their implications will be discussed in Chapter 4 in the light of the results presented in this thesis.

On the other hand, clear evidence of Myc-induced cell competition in mammals akin of that described in *Drosophila* epithelia is still missing. Nevertheless, it was demonstrated that in mice intestinal crypt, loss of *APC* (*Adenomatous Polyposis Coli*) leads to unrestricted proliferation and even when only 10% of crypts are *APC* deficient, several lesions and adenomas are recovered in the intestine. However, if these crypts are simultaneously mutant for *APC* and *c-Myc*, they are rapidly replaced by surrounding wild-type stem cells that repopulate the crypts, leading to complete absence of pathological changes [182]. This, far from being a strict demonstration of Myc-mediated cell competition in mammals, might still represent a first hint of the existence of mechanisms, dependent on the coexistence of cell populations with different Myc levels, able to restrain growth of cancerous cells.

1.4.3.2 Cell Competition and its Relevance to Cancer

Myc expression is deregulated in a wide range of human cancers and is often associated with aggressive, poorly differentiated tumours [123]. In the light of the information above reported it is becoming increasingly evident that Myc induced cell competition could play a role in cancer development [183, 184]. Clones of high Myc expressing cells could expand at the expenses of the surrounding normal cells, without generating morphological changes. Further, expansion may increase the probability of accumulation of other mutations in subsets of cells that would confer new oncogenic properties to their descendants, as predicted by the "cancerisation field" theory. On the other hand, cell competition may represent a mechanism of defence that tumour cells need to overcome in the very early steps of cancer onset in order to survive within the tissue [183].

1.5 Aims of the Thesis

Cancer is a complex and heterogeneous disease and its development is linked to dramatic alterations in cell physiology and behaviour. Such alterations arise from the progressive accumulation of genetic lesions within the transforming cells but, as it is becoming increasingly clear, they also strongly depend on the complex interplay that occurs between cancer cells and their environment. Fine *in vivo* modelling of these processes in mammalian systems is still far from being trivial and thus, given the high degree of conservation of most, if not all, signalling pathways and regulatory circuits compromised in cancer, the employment of easily manipulatable invertebrate models represents a golden opportunity towards the understanding of basic cancer cell biology.

During my PhD, I made use of the powerful genetic tools available in *Drosophila* to model different stages of epithelial cancer development.

Loss of function of the conserved tumour suppressor gene *lgl* induces compromission of cell polarity and tissue architecture, hyperproliferation and inhibition of differentiation when mutant cells grow in a homotypic context. When embedded in a wild-type context, however, these cells seem to display a rather different behaviour and fail to develop into tumours. In the first part of this work I aimed to characterise the tumour suppressive mechanisms responsible for counteracting $lgl^{-/-}$-dependent tumour initiation.

As well established in literature, activation of oncogenic Ras signalling within $lgl^{-/-}$ cells unleashes their neoplastic potential and promotes the development of tumorous masses which display many of the hallmarks of human cancers. In the second part of this work I thus employed this oncogenic cooperation model to investigate the role of key signalling pathways in later traits of tumour development such us tissue overgrowth and invasion.

Chapter 2

Materials and Methods

2.1 Model Tissues

2.1.1 The imaginal wing disc

Imaginal discs are larval epithelial organs that, following metamorphosis, give rise to adult structures and appendages. The imaginal wing disc, precursor of the adult wing, appears composed of a pseudostratified columnar epithelium made of undifferentiated, proliferating cells that represent the actual imaginal disc, and by a squamous epithelium that forms the peripodial membrane (Fig. 2.1). The first will originate the integument and the wing, the second will originate the epithelial veil that welds the structures [185].

When it is formed during embryonic development, the wing imaginal disc comprises around 20 cells [185]. These cells intensely proliferate during second and third larval instars to generate a disc of around 50,000 cells in the late third instar (96h after hatching). By this stage, the wing primordium is established and its major elements can be identified. The centrifugal regions will originate the dorsal and ventral body wall thorax structures: notum and pleura. The middle region will give rise to the hinge, while the central region, the wing pouch, is the presumptive territory from which the wing lamina differentiates (Fig. 2.1, [185]); for this reason the wing pouch is defined as the distal region of the wing disc while hinge and pleura are considered as proximal.

The imaginal wing disc represents a widely used excellent model for studying growth and proliferation control in epithelial tissues. It is morphologically and

biochemically very similar to mammalian epithelia and it encounters a dramatic increase in cell number in a relatively short length of time with an average cycle time of 8.5 h [186]. Proliferation is random but uniform across the tissue and uniformly ceases when correct disc size is attained [187].

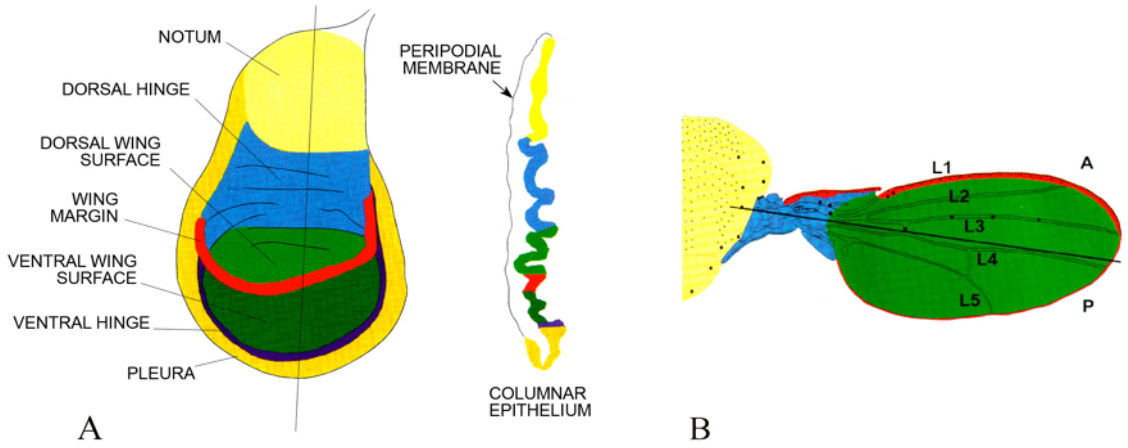

Figure 2.1: A: A third instar imaginal wing disc. The presumptive regions that correspond to the adult wing structures (shown in B) are labelled. Dorsal and ventral wing surfaces compose the wing pouch. A cross section of the epithelium and the peripodial membrane is also shown on the right. B: Adult wing. the different structures are coloured according to the presumptive territories they originate from (shown in A). Longitudinal veins (L 1-5), anterior (A) and posterior (P) compartments are also indicated. Adapted from [185]

2.1.2 The Follicular Epithelium

Drosophila female reproductive system is composed of two ovaries connected through an oviduct to the uterus. The ovary is made of 15-20 ovarioles, each containing a string of developing oocytes of progressive ages and consists of two regions: the germarium, where the pro-oocyte originates, and the vitellarium, where the major phases of oocyte growth and development take place [188] (Fig. 2.2).

In the egg chamber, the functional unit of oogenesis, the oocyte and fifteen germ-line-derived nurse cells (whose function is to synthesise materials to supply the growing oocyte) are surrounded by an epithelium of somatic origin, the follicular epithelium (Fig. 2.3). The follicular epithelium is a monolayered columnar

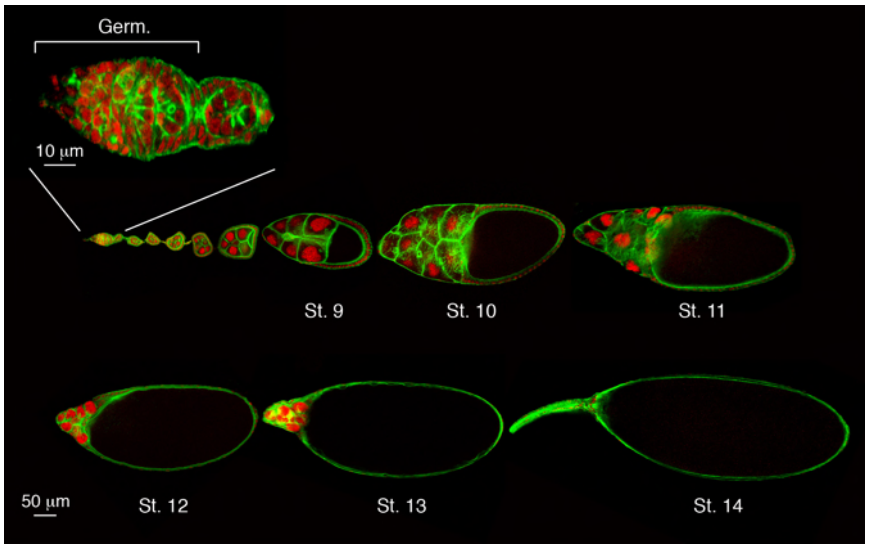

Figure 2.2: Confocal image of an ovariole consisting of egg chambers at progressive stages of development. F-Actin cytoskeleton and nuclei are labelled in green and red respectively. The germarium (Germ.) is shown at higher magnification. Stages (St.) from 9 to 14 are indicated [189].

epithelium that carries out some essential functions in oogenesis: follicular cells secrete the eggshell, produce its specialised structures and, above all, provide oocyte with patterning signals [188]. The majority of follicle cells proliferate until stage 6 to form a uniform epithelium of about 1000 cells. By stage 7, they cease proliferation and enter 4 rounds of endocycle, after which they begin to acquire different cell fates.

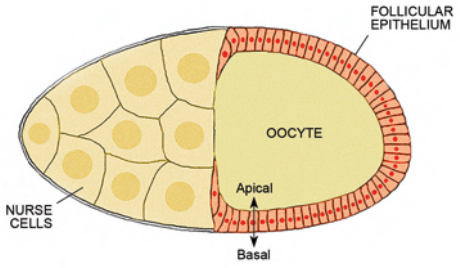

Figure 2.3: Schematics of a stage 10 egg chamber. The oocyte, nurse cells and follicular epithelium are labelled. Apical-basal polarity of follicular cells is also indicated.

2.2 Stocks and Genotypes

Stocks and crosses were raised at 25°C on a growing medium composed of H_2O, agar, corn meal, yeast, glucose and the antifungine Nipagine to avoid mould infection.

2.2.1 Stocks

All stocks are derived from Bloomington Stock Centre strains unless otherwise stated. Stock numbers of key constructs are indicated (Bl = Bloomington Stock Center, VDRC = Vienna *Drosophila* RNAi Center)

w, hs-Flp; arm-LacZ, FRT40A
w; lgl^{27S3} [42], *FRT40A / In(2LR)*[1]
w, hs-Flp; Ubi-GFPnls, FRT40A
yw, hs-Flp, tub-GAL4, UAS-GFP; tub-GAL80, FRT40A
w; lgl^{4}, *FRT40A / In(2LR)*[2]
w, hs-Flp; FRT40A
w; lgl^{4}, *Ubi-GFPnls, FRT40A / In(2LR)*
w; FRT40A
w, P[LacW]l(1)G0354 (dm-LacZ^{G0354}) [193]*/ yw, FM7a; lgl*^{4}, *FRT40A / In(2LR)*
yw, hs-Flp, tub-GAL4; tub-GAL80, FRT40A
w; lgl^{4}, *Ubi-GFPnls, FRT40A / In(2LR); UAS-dIAP1* (Bruce Hay)
yw, UAS-bsk^{DN} [77]; *w; lgl*^{4}, *Ubi-GFPnls, FRT40A / In(2LR)*
w; lgl^{4}, *FRT40A / In(2LR); tub-YFP::Rab5* (L.A. Baena-López)
*w; Ubi-GFPnls, FRT40A / In(2LR); UAS-egr*RNAi (VDRC 45252)
For a validation of *UAS-egr*RNAi construct see Fig. 2.4
w; lgl^{4}, *Ubi-GFPnls, FRT40A / In(2LR); UAS-egr*RNAi
w; lgl^{4}, *Ubi-GFPnls, FRT40A / In(2LR), UAS-YFP::Rab5*^{DN} [192]
yw, hs-Flp; M(2)24F, Ubi-GFPnls, FRT40A / SM5
yw, hs-Flp, tub-GAL4, UAS-GFP; M(2)24F, tub-GAL80, FRT40A / SM5
w; lgl^{4}, *FRT40A / In(2LR); UAS-dmyc*RNAi (VDRC 2947, jumped on III chr.)
For a validation of *UAS-dmyc*RNAi construct see Fig. 2.5

[1] *lgl*^{27S3} is a null allele.
[2] *lgl*^{4} allele is a deletion of the entire *locus*.

yw, hs-Flp; act5c>CD2>GAL4, UAS-GFP / TM6b (B.A. Edgar)
w; UAS-dmyc [190]
w; His2A-GFP
w; FRT40A; UAS-Ras85D^{V12} (*UAS-Ras*^{V12}, Bl 4847)
w; lgl^{4}, *FRT40A / In(2LR); UAS-Ras*^{V12}
yw, UAS-dp110^{CAAX} [191]
For a validation of *UAS-dp110*^{CAAX} construct see Fig. 2.6
yw, UAS-dp110^{CAAX}; *lgl*^{4}, *FRT40A / In(2LR)*
w; en-GAL4, UAS-GFP / In(2LR)
*w; UAS-Ras*RNAi (VDRC 28129)
For a validation of *UAS-Ras*RNAi construct see Fig. 2.7
*yw, hs-Flp, tub-GAL4, UAS-GFP; tub-GAL80, FRT40A; UAS-Ras85D*RNAi
yw, UAS-hRaf^{GOF} (Bl 2074); *lgl*^{4}, *FRT40A / In(2LR)*
For a validation of *UAS-hRaf*^{GOF} construct see Fig. 2.8
*yw, hs-Flp, tub-GAL4, UAS-GFP; tub-GAL80, FRT40A; UAS-dmyc*RNAi
w; lgl^{4}, *FRT40A / In(2LR); UAS-dmyc*
w; lgl^{4}, *FRT40A / In(2LR); UAS-dmyc, UAS-dIAP1*
yw, UAS-hRaf^{GOF}; *lgl*^{4}, *FRT40A / In(2LR); UAS-Yki*RNAi(Bl 31965)
For a validation of *UAS-Yki*RNAi construct see Fig. 2.9
w; lgl^{4}, *FRT40A / In(2LR); UAS-Yki* (Bl 28819)
ry^{506}, *PZ*[*bnl*^{06916}] *(bnl-LacZ) / TM3* (Bl 11704)
yw, hs-Flp, tub-GAL4, UAS-GFP; tub-GAL80, FRT40A; ry^{506}, *PZ*[*bnl*^{06916}] */ TM6b*
w; M(2)24F, en-GAL4, UAS-GFP / In(2LR)
*w; lgl*RNAi (VDRC 51249)
For a validation of *UAS-lgl*RNAi construct see Fig. 2.10
*w; M(2)24F, en-GAL4, UAS-GFP / In(2LR); UAS-dmyc*RNAi

2.2.2 Genotypes

Detailed genotypes of the tissues analised in Chapter 3 are as follows:

- **Figure 3.1**:
A-C: *hsFLP/+; lgl*^{27S3}*, FRT40A/arm-LacZ,FRT40A*
D,E: *w,hsFLP/+; lgl*^{27S3}*, FRT40A/Ubi-GFP,FRT40A*

F,G: *w, hsFLP, tub-Gal4, UAS-GFP/+; lgl^4, FRT40A/tub-Gal80, FRT40A*
- **Figure 3.2**:
A,B and D (left panel): *w, hs-Flp/+; lgl^4, FRT40A/Ubi-GFPnls, FRT40A*
C: *w, hs-Flp/+; lgl^4, Ubi-GFPnls, FRT40A/FRT40A*
D (right panel): *w, hs-Flp/+;Ubi-GFPnls, FRT40A/FRT40A.*
- **Figure 3.3**:
A,B: *w, hs-Flp/+; lgl^4, FRT40A/Ubi-GFPnls, FRT40A*
C: *w, hs-Flp/+; lgl^4, Ubi-GFPnls, FRT40A/FRT40A*
D: *yw, dm-LacZ^{G0354}/w, hs-Flp; lgl^4, FRT40A/Ubi-GFP, FRT40A*
- **Figure 3.4**:
A-C: *w, hsFLP, tub-Gal4, UAS-GFP/+; lgl^4, Ubi-GFPnls, FRT40A/tub-Gal80, FRT40A; UAS-dIAP1/+*
- **Figure 3.5**:
A-C: *w, hsFLP, tub-Gal4, UAS-GFP/UAS-bsk^{DN}; lgl^4, Ubi-GFPnls, FRT40A/tub-Gal80, FRT40A*
- **Figure 3.6**:
A: *w, hsFLP, tub-Gal4/+; lgl^4, FRT40A/tub-Gal80, FRT40A; tub-YFP::Rab5/+*
B,C: *w, hsFLP, tub-Gal4/+; lgl^4, Ubi-GFPnls, FRT40A/tub-Gal80, FRT40A; UAS-egrRNAi/+*
D: *w, hsFLP, tub-Gal4, UAS-GFP/+; lgl^4, FRT40A/tub-Gal80, FRT40A; UAS-YFP::Rab5^{DN}/+*
E,F: *w, hsFLP, tub-Gal4/+; lgl^4, Ubi-GFPnls, FRT40A/tub-Gal80, FRT40A; UAS-YFP::Rab5^{DN}/+*
- **Figure 3.7**:
A-B',D,E: *w, hs-Flp/+; lgl^4, FRT40A/M(2)24F, Ubi-GFPnls, FRT40A*
C:*w, hs-Flp/+; FRT40A/M(2)24F, Ubi-GFPnls, FRT40A*
F: *w, hs-Flp/yw, dm-LacZ^{G0354}; lgl^4, FRT40A/M(2)24F, Ubi-GFPnls, FRT40A*
G,H: *w, hs-Flp/+; lgl^4, FRT40A/M(2)24F, Ubi-GFPnls, FRT40A; UAS-dmyc*RNAi/+
- **Figure 3.8**:
A,B,D,F,G: *w, hs-Flp/+; lgl^4, FRT40A/Ubi-GFPnls, FRT40A*
C: *w; His2A-GFP*
E: *yw, dm-LacZ^{G0354}/w, hs-Flp; lgl^4, FRT40A/Ubi-GFP, FRT40A*
- **Figure 3.9**:

A: *yw, hs-Flp, tub-GAL4, UAS-GFP/+; FRT40A/tub-GAL80, FRT40A*
B: *w, hsFLP, tub-Gal4, UAS-GFP/+; lgl^4, FRT40A/tub-Gal80, FRT40A*
C: *w, hsFLP, tub-Gal4, UAS-GFP/+; FRT40A/tub-Gal80, FRT40A; UAS-Ras^{V12}/+*
D-G: *w, hsFLP, tub-Gal4, UAS-GFP/+; lgl^4, FRT40A/tub-Gal80, FRT40A; UAS-Ras^{V12}/+*
- **Figure 3.12**:
A: *w, hsFLP, tub-Gal4, UAS-GFP/UAS-$dp110^{CAAX}$; lgl^4, FRT40A/tub-Gal80, FRT40A*
B: *w, hsFLP, tub-Gal4, UAS-GFP/UAS-$dp110^{CAAX}$; lgl^4, FRT40A/tub-Gal80, FRT40A; UAS-Ras*RNAi/+
C,D: *w, hsFLP, tub-Gal4, UAS-GFP/UAS-$hRaf^{GOF}$; lgl^4, FRT40A/tub-Gal80, FRT40A*
E,F: *w, hsFLP, tub-Gal4, UAS-GFP/UAS-$hRaf^{GOF}$; lgl^4, FRT40A/tub-Gal80, FRT40A; UAS-Ras*RNAi/+
- **Figure 3.13**:
A: *w, hsFLP, tub-Gal4, UAS-GFP/+; lgl^4, FRT40A/tub-Gal80, FRT40A; UAS-Ras^{V12}/UAS-dmyc*RNAi
B-E: *w, hsFLP, tub-Gal4, UAS-GFP/+; lgl^4, FRT40A/tub-Gal80, FRT40A; UAS-dmyc/+*
F: *w, hsFLP, tub-Gal4, UAS-GFP/+; lgl^4, FRT40A/tub-Gal80, FRT40A; UAS-dmyc, UAS-dIAP1/UAS-Ras*RNAi
- **Figure 3.14**:
A,B: *w, hsFLP, tub-Gal4, UAS-GFP/UAS-$hRaf^{GOF}$; lgl^4, FRT40A/tub-Gal80, FRT40A; UAS-Yki*RNAi/+
C,D: *w, hsFLP, tub-Gal4, UAS-GFP/+; lgl^4, FRT40A/tub-Gal80, FRT40A; UAS-Yki/+*
E,F: *w, hsFLP, tub-Gal4, UAS-GFP/+; lgl^4, FRT40A/tub-Gal80, FRT40A; UAS-Ras*RNAi/*UAS-Yki*
- **Figure 3.15**:
A-D: *w, hsFLP, tub-Gal4, UAS-GFP/+; lgl^4, FRT40A/tub-Gal80, FRT40A; UAS-Ras^{V12}/+*
E: *w, hsFLP, tub-Gal4, UAS-GFP/+; lgl^4, FRT40A/tub-Gal80, FRT40A; UAS-Ras^{V12}/ry^{506}, bnl-LacZ*
F: *ry^{506}, bnl-LacZ / TM3*
- **Figure 3.16**:
A,B: *w, hsFLP, tub-Gal4, UAS-GFP/+; lgl^4, FRT40A/tub-Gal80, FRT40A; UAS-*

Ras^{V12}*/UAS-dmyc*RNAi
C,D: *w, hsFLP, tub-Gal4, UAS-GFP/UAS-hRaf*^{GOF}; *lgl*^{4}, *FRT40A/tub-Gal80, FRT40A; UAS-Yki*RNAi/+
- **Figure 3.17**:
A-C: *w; M(2)24F, en-GAL4, UAS-GFP /+*; *UAS-lgl*RNAi/+
D,D': *w; M(2)24F, en-GAL4, UAS-GFP /+; UAS-lgl*RNAi/*UAS-dmyc*RNAi
E: *w; M(2)24F, en-GAL4, UAS-GFP /+*; *UAS-dmyc*RNAi/+.

2.2.3 Validations

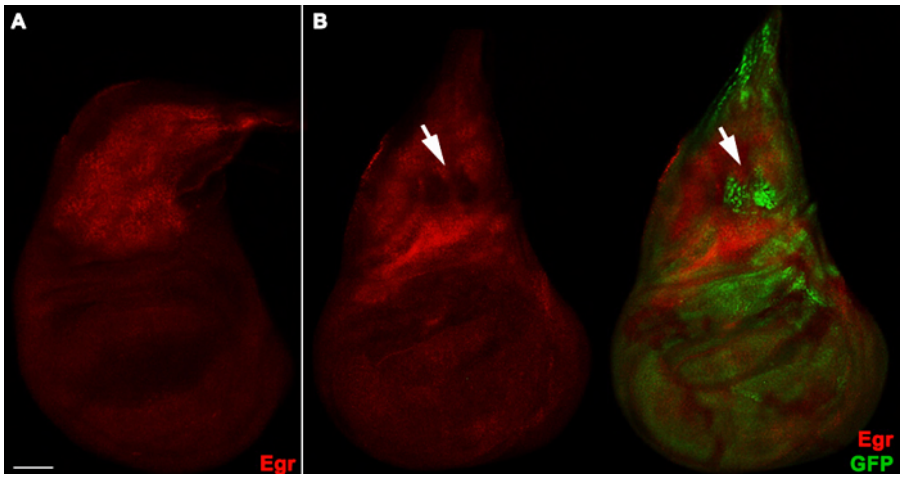

Figure 2.4: **A,B**: Egr staining (red) of a wild-type disc (A) and a disc bearing *egr*RNAi clones (GFP^{2+}). As can be seen in A, Egr is expressed mainly in the notum. In B, the arrows indicate *UAS-egr*RNAi mutant tissue in the notum where downregulation of Egr protein within the mutant clone is clearly visible confirming the efficacy of the RNAi construct. Full genotype of tissues shown in B is *yw, hs-Flp, tub-Gal4/+; Ubi-GFPnls, FRT40A /tub-Gal80, FRT40A; UAS-egr*RNAi/+.

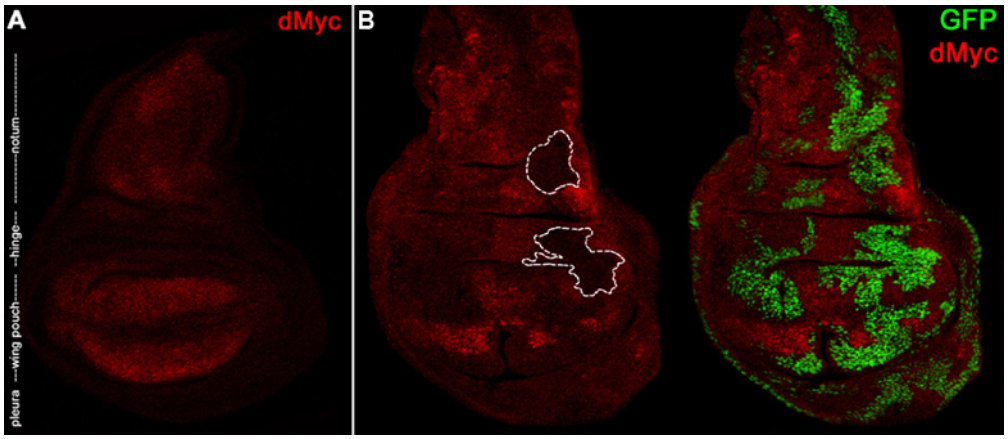

Figure 2.5: **A**: dMyc staining (red) of a wild-type wing disc, the main regions are indicated on the left. dMyc is more abundant in the wing pouch and in the notum while it is expresses at low levels in the hinge and pleura. *B*: dMyc staining (red) of a $M^{+/-}$ wing disc in which lgl^4; *dm*RNAi (GFP^+) were induced (B). dMyc protein levels are reduced in clones throughout the disc, two clones are outlined as an example. Full genotype of the tissue shown in B is *yw, hs-Flp/+, tub-Gal4, UAS-GFP;* lgl^4, *FRT40A/M(2)24F, tub-Gal80, FRT40A; UAS-dmyc*RNAi/+.

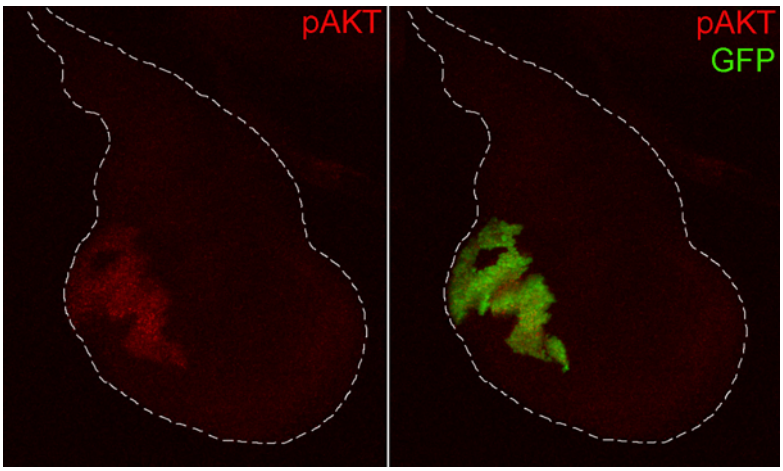

Figure 2.6: A $dp110^{CAAX}$ Flp-out clone (GFP^+). This form of dp110 carries a prenylation motif (CAAX) which targets the protein to the plasma membrane causing constitutive activity. Consistently, high levels of phosphorylated AKt (pAkt, red) are evident within $dp110^{CAAX}$-expressing clone. The wing disc is outlined. Full genotype of the tissue is *yw, hs-Flp / UAS-*$dp110^{CAAX}$; *act5c>CD2>GAL4, UAS-GFP / TM6b.*

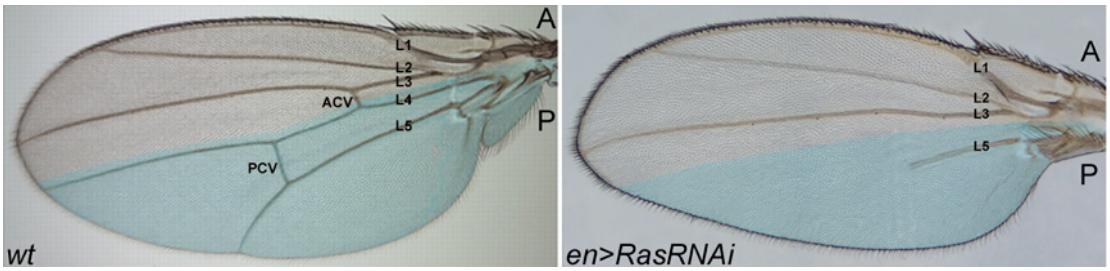

Figure 2.7: An adult wing derived from an individual expressing a *Ras*RNAi construct in the posterior compartment of the wing disc is shown in the right panel. Longitudinal vein 4 (L4), part of longitudinal vein 5 (L5) and both anterior and posterior cross veins (ACV and PCV, respectively) are absent in the corresponding wing compartment (cyan); a wild-type wing is shown in the left panel for comparison. Loss of wing veins is a reported phenotype of Ras loss of function [101], thus confirming the efficacy of the RNAi construct. Longitudinal veins 1-3 (L1-3) are also indicated. A, anterior compartment; P, posterior compartment. Full genotype of tissue shown in the right panel is *w; en-GAL4, UAS-GFP /+; UAS-Ras*RNAi/+.

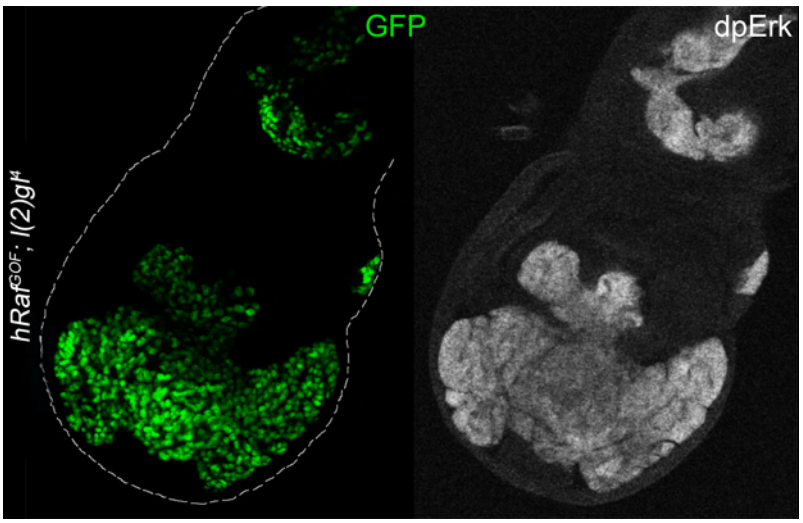

Figure 2.8: dpErk staining of a wing disc in which lgl^4;Raf^{GOF} clones (GFP^+) were induced. High levels of activated Erk are visible within the mutant clone indicating that hRaf can activate MAPK pathway in *Drosophila*. Wing disc is outlined. Full genotype of tissues shown is *yw, hs-Flp, tub-Gal4, UAS-GFP / UAS-Raf*$^{\mathrm{GOF}}$; lgl^4, *FRT40A /tub-Gal80, FRT40A*.

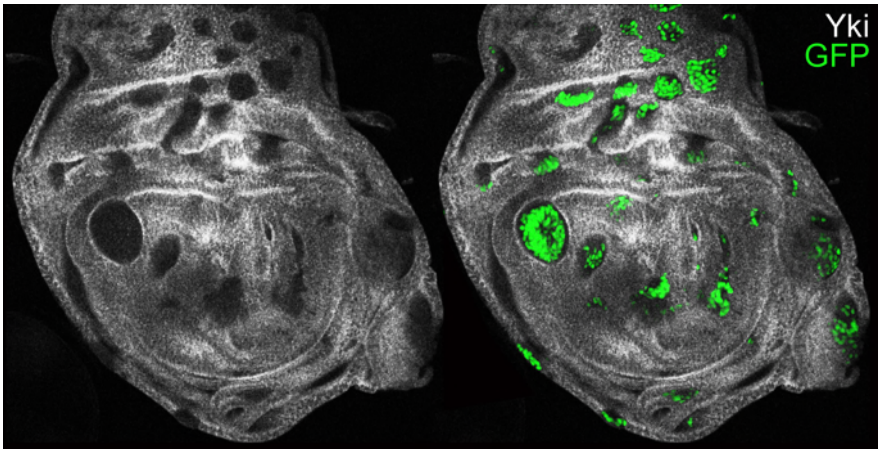

Figure 2.9: Yki staining (white) of a wing disc in which *lgl*^{4};*Raf*$^{\mathrm{GOF}}$; *yki*RNAi clones (GFP$^+$) were induced. Evident downregulation of Yki protein is visible within mutant clones. Full genotype of tissues shown is *yw, hs-Flp, tub-Gal4, UAS-GFP / UAS-Raf*$^{\mathrm{GOF}}$; *lgl*^{4}, *FRT40A /tub-Gal80, FRT40A; UAS-yki*RNAi/+.

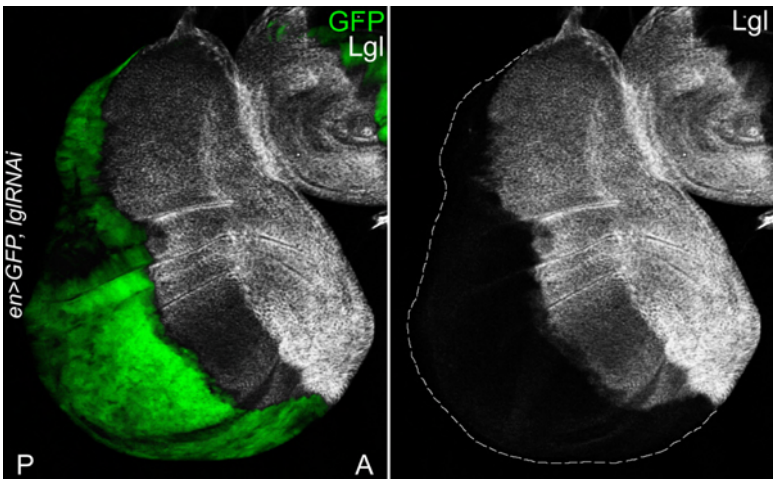

Figure 2.10: An imaginal wing disc in which the *lgl*RNAi construct has been expressed under the control of the *en* promoter. Coexpression of a *UAS-GFP* construct allows to visualise the expression domain (green). Lgl staining is absent in the posterior compartment (P) confirming the efficacy of the construct. Full genotype of tissue shown is *w; en-GAL4, UAS-GFP /+; UAS-lgl*RNAi/+.

2.3 Protocols

2.3.1 Genetic Manipulations

For the twin analysis [58], larvae were heat shocked 48 hours After Egg Laying (AEL) for one hour at 37°C and adult females were heat shocked one to two days after eclosion for one hour at 37°C. For larval staging, freshly hatched larvae were collected in a one-to-four hour time window. For the MARCM clones generation [69], larvae were heat shocked 48 hours AEL for 30 minutes at 37°C and adult females one to two days after eclosion for 30 minutes at 37°C. Minute individuals were always heat shocked at 72 hours AEL to compensate for developmental delay. Flp-out clones [85] were generated heat shocking 48h AEL-larvae and one-two days old females for eight minutes at 37°C. For all the clonal systems used, tissues were collected 72 hours after the heat shock both for larvae and adults, unless otherwise specified.

$M^{+/-}$ larvae expressing either *lgl*RNAi or *lgl*RNAi; *dmyc*RNAi under the control of *en-GAL4* driver were dissected 7 or 11 days AEL (as indicated in the figure legends).

2.3.2 Immunohistochemistry

Larvae and adult females were dissected in PBS (Phosphate Buffer Saline, pH 7.5) and fixed in 3,7% formaldehyde (Sigma) in PBS. Tissues were permeabilised in PBS-Triton 0,3% for 1 hour at room temperature, blocked for 1 hour in PBS-Triton 0,3%, 2% BSA (Bovine Serum Albumine, Sigma) and incubated overnight at 4°C in PBS-Triton 0,3%, 2% BSA with primary antibody. Tissues were then incubated with secondary antibody for 2 hours at room temperature. Accurate washes in PBS-Triton 0,3% were performed following each step. Samples were then mounted on microscopy slides using anti-quenching slide mounting medium Fluoromount (Beckman Coulter).

The following antibodies and dilutions were used: rabbit α-active-Caspase 3 (1:200, 9664S - Cell Signaling Technology); mouse α-dIAP1 (1:100, B.A. Hay); rabbit α-Laminin A (1:200, Y. Kitagawa); rabbit α-Scribble (1:100, C.Q. Doe); mouse α-dMyc (1:5 [92]); mouse α-βGal (1:25, 40-1a - DSHB); rabbit α-βGal (1:50, F. Graziani); rabbit α-aPKCζ (1:200, sc-216 - Santa Cruz Biotechnology); mouse

α-phospho-JNK (1:100, G9 - Cell Signaling Technology); rabbit α-Egr (1:500, M. Miura); mouse α-MMP1 (1:50, 3A6B4 - DSHB); mouse α-dpERK (1:50, MAPK-YT - Sigma); rabbit α-pAkt (1:100, Cell Signaling); rabbit α-Trh (1:10, J. Casanova); rat α-Trh (1:50, L. Jiang); rat α-Ci (1:20, 2A1 - DSHB); mouse α-En (1:50, 4D9 - DSHB); mouse α-Dlg (1:50, 4F3 - DSHB); rabbit α-Yki (1:100, G. Morata); rabbit α-Lgl (1:400, D. Strand). Alexa Fluor 555 or 568 goat α-mouse and α-rabbit (1:200, Invitrogen); Cy3-conjugated goat α-rabbit (1:200, Jackson ImmunoResearch Laboratories); Cy3-conjugated donkey α-rat (1:400, Jackson ImmunoResearch Laboratories); Cy5-conjugated goat α-mouse and α-rabbit (1:200, Jackson ImmunoResearch Laboratories) and DyLight 649-conjugated goat α-mouse and α-rabbit (1:200, Jackson ImmunoResearch Laboratories) were used as secondary antibodies. Nuclei were stained with DAPI (4',6-diamidine-2'-phenylindole dihidrochloride, Sigma) or TOPRO (Invitrogen) and Phalloidin staining (phalloidin-tetramethylrhodamine isothiocyanate, Sigma) was used to to detect F-actin.

Samples were analysed with Leica TSC SP2 laser confocal microscope and entire images were processed with Adobe Photoshop software. All the images shown represent a single confocal stack unless otherwise specified. ImageJ free software from NIH was used for rebuilding the projections along the Z axis starting from 25-45 Z stacks.

2.3.3 Statistics

Clone areas (in pixel^2) were measured using ImageJ free software (NIH) on images captured with 90i widefield fluorescence microscope (Nikon) at a a magnification of 200x. Areas of clones grown as multilayers are likely to be underestimated. Mean, Standard Deviation and the t-Student test P value were calculated with GraphPad Prism software. Clone shapes were measured with ImageJ using the formula $4\pi A/L^2$, in which A = clone area and L = clone circumference [194]. By use of this formula, a perfect circle has a value of 1 and more irregular shapes have values <1.

Chapter 3

Results and Discussion

3.1 Tumour Initiation

Understanding the molecular bases of tumour initiation is of pivotal importance in the field of cancer biology. Human neoplasias are often diagnosed at late stages when the tumour is morphologically and genetically extremely heterogeneous and it is hard, if not impossible, to identify the first hits that led to the development of the tumorous mass. Animal models are thus a precious tool to investigate the first steps of cancer formation. As described in Section 1.2.2 *Drosophila* oncogenic cooperation models faithfully reproduce most of the aspects of human carcinogenesis and offer an ideal genetic approach to address the issue of cancer onset.

Loss of function of *lethal giant larvae*(*lgl*) and the other polarity tumour suppressor genes provides cells with undisputed neoplastic features: mutant epithelia overgrow, lose cell polarity, tissue architecture and the ability to differentiate and are able to invade adjacent tissues, migrate and form metastases. Nevertheless, these neoplastic traits fail to show when mutant cells arise in a clonal context, a condition that most closely resembles the onset of human cancers, indicating the existence of some mechanisms of suppression of tumour initiation (see Sections 1.2.1.2 and 1.2.2).

3.1.1 *lgl* Mutant Clones Die by Apoptosis

To investigate the fate of polarity mutant cells in a clonal condition, the behaviour of *lgl* mutant clones generated in a wild-type imaginal wing disc (Section

2.1.1) was analysed. As can be observed in Figures 3.1 and 3.2, *lgl*$^{-/-}$ clones do not overgrow, on the contrary mutant cells exhibit a rather poor viability: at two days after induction *lgl*$^{-/-}$ clones and their wild-type twins were similar in size (Fig. 3.1A), while at three days *lgl*$^{-/-}$ clones were about half the size of their twins (Fig. 3.1B; n=40 each) and 37% disappeared by the end of larval development leaving only the twin clone (Fig. 3.1B, arrow; n=187). Those which persisted to the end of development resulted in minor scarring of the adult wing (Fig. 3.1C).

lgl mutant clones showed slight defects in disc folding as revealed by F-actin staining (Fig. 3.1D, arrow); however mutant cells did not seem to be strongly compromised in apical-basal polarity as detected by Scribble (Fig. 3.1F and G) and aPKC (Fig. 3.3A and C) polarity markers and no discontinuities of basement membrane were visible (not shown), in agreement with previous observations [70].

In Figure 3.1E many pycnotic nuclei are visible within *lgl*$^{-/-}$ clones in basal sections. As basal extrusion is the process by which apoptotic cells are eliminated in the imaginal wing disc [171] I employed a specific antibody against active effector Caspase 3 to confirm that mutant cells were undergoing apoptosis: indeed many *lgl*$^{-/-}$ cells resulted positive to this staining (Fig. 3.2A), especially at the border of the clone, where mutant and wild-type tissue are in contact (see magnification in Fig. 3.2A*). Coherently, the anti-apoptotic protein *Drosophila* Inhibitor of Apoptosis 1 (dIAP1) was downregulated in *lgl*$^{-/-}$ cells (Fig. 3.2B, arrow). Apoptotic cell death is also known to be induced in the imaginal tissue by the JNK signalling, a conserved stress-induced pathway (see Section 1.2.1.2). To ask whether this pathway was involved in lgl$^{-/-}$ cells death, imaginal wing discs were stained with an antibody against the phosphorylated and thus activated form of JNK; as can be observed in Figure 3.2C mutant clones show a strong activation of JNK signaling pathway (arrow).

3.1.2 *lgl*$^{-/-}$ Cells Are Eliminated by Myc-Induced Cell Competition

As reported in Section 1.4.3, clonal analysis in *Drosophila* imaginal tissues has allowed to discover and characterise a non-cell autonomous developmental phenomenon, named cell competition, which occurs when two cell populations with different growth rates coexist in the same tissue and results in the elimination by

apoptosis of the slow-dividing cells by the surrounding faster-growing population; compensatory proliferation of the so-called "winner cells" ensures that the organ reaches its proper final size.

Since *lgl* mutant tissues have been shown to overgrow but with a much slower proliferation rate with respect to wild-type ones [15], I tested whether competitive interactions were involved in the elimination of $lgl^{-/-}$ cells from the normal tissue by performing a double clonal assay in which $lgl^{-/-}$ clones and wild-type clones were induced in parallel in a wild-type background (Fig. 3.2D). As expected, while no differences were observed between wild-type control clones and their twins (right panel, black and white bars respectively, $P = 0.86$), *lgl* mutant clones were smaller than their wild-type twins (left panel, black and white bars respectively, $P < 0.001$), as well as smaller than wild-type clones induced in control discs (right panel, black bars, $P < 0.001$). The wild-type twins of $lgl^{-/-}$ clones (left panel, white bars) were instead much larger than the wild-type twins from control discs (right panel, white bars, $P < 0.001$). Since no dominant effects on cellular growth rate have been reported for *lgl* null mutations, and developmental stages of $lgl^{+/-}$ animals are of the same duration as those of $lgl^{+/+}$ individuals, even in clonal assays, this result suggests that some non-autonomous mechanisms are at work in $lgl^{-/-}$ clone elimination and that mutant cells are being replaced by the normal surrounding tissue.

Since it is known that differences in dMyc abundance among adjacent cells can trigger competitive behaviour (see Section 1.4.3, [148, 171]), I next analysed dMyc protein levels and found that dMyc was weakly expressed within *lgl* mutant clones with respect to the surrounding tissue (Fig. 3.3A-C). This downregulation does not seem to occur at a transcriptional level: as assayed by a *dm-LacZ* construct (*dm*, *diminutive* is the gene that encodes for dMyc), *dm* promoter results active in mutant cells (Fig. 3.3D) indicating the involvement of a post-transcriptional mechanism.

It is therefore possible to speculate that cells bearing precancerous lesions that do not confer a survival or proliferative advantage relative to neighbouring cells, as with $lgl^{-/-}$ cells that lack dMyc protein, can be eliminated by apoptosis. In the wing disc, dMyc protein accumulates mainly in the distal region, the wing pouch, and is expressed only weakly in the proximal regions, hinge and pleura (Fig. 2.5A). In these proximal regions, no differences in dMyc levels were visible between $lgl^{-/-}$ clones and the adjacent cells (not shown); such clones were larger than those in the wing pouch (Fig. 3.1, compare G with F and 3.3E) and showed low levels of cell

death (not shown), although they never formed tumours (Fig. 3.1G). Thus, low dMyc levels in *lgl*$^{-/-}$ cells seem to affect growth and viability of these cells mainly in the distal region (wing pouch), where the surrounding tissue expresses high levels of dMyc.

3.1.3 Inhibition of Cell Death Is Not Sufficient for Driving Tumourous Growth of *lgl*$^{-/-}$ Clones in the Wing Pouch

Since several molecules associated with cell death were found to be deregulated in *lgl* mutant clones generated in a wild-type background (see Fig. 3.2), I tried to rescue *lgl* mutant clones viability by co-expressing dIAP1 or a dominant negative form of the *Drosophila* JNK, Bsk. As can be seen in Figure 3.4A, *lgl*$^{-/-}$; *dIAP1* clones in the wing pouch still showed active-Caspase 3 signals (arrow) and grew smaller than their wild-type twins (Fig. 3.4D). Since the JNK pathway is activated in *lgl* mutant clones in the wing pouch (Fig. 3.2C, arrow), it could significantly contribute to their death; indeed, as shown in Figure 3.4B, despite dIAP1 expression, active JNK is still present, as detected by pJNK staining (arrow), indicating that it contributes to the elimination of *lgl* mutant clones independently of dIAP1. Both active-Caspase 3 and pJNK were also visible in the mutant clones in the proximal regions of the wing disc (Fig. 3.4A and B, hinge and pleura respectively, white arrowheads), but their phenotype was quite different from that of clones in the wing pouch; they were large, round-shaped and, as can be seen in Figure 3.4A, active-Caspase 3 signal was also present in several cells surrounding the mutant clone (grey arrowheads). A statistical analysis showed that such clones were larger than their wild-type twins (Fig. 3.4D). Interestingly, these phenotypes were associated with higher dMyc levels with respect to the background (Figure 3.4C, arrow); thus JNK signalling may here be subverted from a pro-apoptotic to a pro-growth function, as it has been demonstrated to occur in genetic contexts in which alterations in the polarity genes *lgl*, *scrib* and *dlg* are accompanied by an ectopic expression of oncogenes such as Ras or Notch (see Section 1.2.2, [74, 75, 77]).

I then blocked the JNK pathway inside the *lgl*$^{-/-}$ clones by using a *bsk*$^{\mathrm{DN}}$ transgene and found that the active-Caspase 3 signal was no longer observable in *lgl*$^{-/-}$ clones, regardless of the region in which they were located (not shown), indicating that JNK signalling-induced cell death is the main pathway by which *lgl* mutant

cells die. As can be seen in Figure 3.5A, *lgl*$^{-/-}$; *bsk*^{DN} clones in the wing pouch (outlined) expressed low levels of dMyc and did not form tumours; statistical analysis performed in this region showed that, despite the fact that *lgl*$^{-/-}$; *bsk*^{DN} clones no longer died, their size was smaller than that of their wild-type twins (Fig. 3.5B), demonstrating that even when cell death is blocked *lgl*$^{-/-}$; *bsk*^{DN} cells have a proliferative disadvantage with respect to the wild-type tissue.

In contrast to the wing pouch, *lgl*$^{-/-}$; *bsk*^{DN} clones in the proximal regions (hinge and pleura) showed high dMyc protein levels (Fig. 3.5C), lost polarity and overgrew (not shown), indicating that the pro-growth role of the JNK pathway observed in polarity-compromised clones overexpressing activated Ras or Notch (see Section 1.2.2, [74, 75, 77]) appears not to be necessary in the wing disc for the tumourous growth induced by the cooperation between *lgl* mutation and dMyc oncoprotein.

Altogether, these data show that the difference in clonal growth reported in Section 3.1.2 for *lgl*$^{-/-}$ cells in the wing pouch *versus* the hinge/pleura regions also occurs for *lgl*$^{-/-}$ clones in which cell death has been inhibited and is also associated with the different levels of dMyc protein in the mutant versus the adjacent normal tissue.

3.1.4 Intrinsic Tumour Suppression Is Not Involved in *lgl*$^{-/-}$ Cells Elimination in the Wing Pouch

A recent study demonstrated that clones of *scrib* and *dlg* tumour suppressor mutants generated in wild-type imaginal discs are eliminated by the Intrinsic Tumour Suppressor (ITS) pathway, involving JNK-dependent apoptosis induced by an endocytic accumulation of the TNF homologue, Eiger (Egr) (See Section 1.2.1.2, [61]). Since *scrib* and *dlg* are well-known *lgl* partners in regulating apical-basal cell polarity and proliferation and show similar neoplastic phenotypes in a homotypic background (see Section 1.2.1.1), it could be expected that *lgl*$^{-/-}$ clones could be eliminated by a similar mechanism. To investigate this, I first looked for alterations in endocytosis in *lgl* mutant clones by using an early-endosome reporter, *Rab5*, since Igaki and colleagues [61] observed that Rab5-positive endosomes accumulated in *scrib* mutant clones in the eye disc and correlated with pJNK staining. Nevertheless, in the wing pouch region I did not observe changes in Rab5 levels within *lgl*$^{-/-}$ clones with respect to the neighbours (see Fig. 3.6A, arrowhead, and respective magnification),

whereas outside the wing pouch a moderate increase in Rab5 levels in *lgl*$^{-/-}$ clones was observed (see Fig. 3.6A, arrow, and respective magnification). Since it was also demonstrated that ITS depends on an autocrine TNF signalling [61], I silenced the TNF homologue, *egr*, in *lgl* mutant cells by expressing a *UAS-egr*RNAi construct (for validation see Fig. 2.4 in Section 2.2.3) and scored for changes in clone morphology, but no alterations were observed relative to the *lgl*$^{-/-}$ clonal phenotype (Fig. 3.6B). *lgl*$^{-/-}$; *egr*RNAi clones in the wing pouch were comparable in size to *lgl*$^{-/-}$ clones induced by the same system ($P = 0.58$, n=19 each). Similar effects were seen in *lgl* mutant clones in discs in which the *UAS-egr*RNAi construct was expressed under the control of the *hedgehog* promoter in the whole posterior compartment, thereby also removing Egr protein in the background (not shown). In Figure 3.6B, the apical and basal sections of a wing pouch are shown in which an *lgl* mutant clone is being basally extruded (arrow, the position of the mutant clone with respect to its twin is outlined in the apical section). In Figure 3.6C, an increased pJNK staining is visible in the mutan clone (arrow). The fact that JNK signalling is increased here suggests that, in this case, JNK pathway activation is not triggered by Egr-mediated ITS. I next expressed in *lgl* mutant clones a dominant negative form of *Rab5* to block endocytosis, since it was shown that endocytosis blocking decreased JNK signalling and cell death of *scrib* mutant clones [61]. Indeed, I found that some *lgl*$^{-/-}$ mutant clones expressing *Rab5*$^{\mathrm{DN}}$ in the proximal regions overgrew (48%, n=27 Fig. 3.6D), while clones in the wing pouch never did. Again, *lgl*$^{-/-}$; *Rab5*$^{\mathrm{DN}}$ clones in the wing pouch expressed both active-Caspase 3 (Fig. 3.6E, arrow) and pJNK (Fig. 3.6F, arrow), distinct from what has been observed for *scrib* mutant clones in the eye disc, where *Rab5*$^{\mathrm{DN}}$ expression increased their growth [61]. Notably, all the overgrowing clones observed in the proximal regions of the wing disc were characterised by high dMyc protein levels (Fig. 3.6D).

Taken together, these data exclude *egr*-mediated ITS as the main mechanism responsible for *lgl* mutant clones elimination in the wing pouch.

3.1.5 *lgl*$^{-/-}$ Cells Grown in a *Minute* Background Overexpress dMyc and Form Malignant Tumours

As shown in Section 3.1.3, *lgl*$^{-/-}$ cells grow slower than wild-type cells in a clonal context, which is possibly the main reason why they are eliminated from the ep-

ithelium. To confirm the hypothesis for an active role of cell competition in restraining *lgl*$^{-/-}$ clonal growth, I induced *lgl* mutant clones in the slow-dividing and non-competitive *Minute* background (see Section 1.4.3), to give them a proliferative advantage. As can be seen in Figure 3.7A and B, *lgl* mutant clones in this context were able to overgrow, on average a 5-fold increase in size with respect to *lgl*$^{-/-}$ clones was detected, (n=40 each genotype, $P < 0.001$), displayed rounded cells and lost apical-basal polarity, as can be seen in the Z projection where aPKC apical determinant spreads cortically (Fig. 3.7A). *lgl*$^{-/-}$ clones showed high levels of dMyc protein (Fig. 3.7A, arrow), which accumulated mainly in those outside of the wing pouch. dMyc upregulation is attributable to *lgl* loss of function because wild-type cells did not show any changes in dMyc levels when growing in a $M^{+/-}$ background (Fig. 3.7C). On the other hand, *lgl*$^{-/-}$ clones in the wing pouch did not overgrow, showed a level of dMyc similar to that found in the adjacent cells (Fig. 3.7D, clone outlined) and did not undergo apoptosis (not shown). In large *lgl*$^{-/-}$ clones in the hinge or pleura, dIAP1 was also expressed (Fig. 3.7B') and active-Caspase 3 signal was evident in few cells in the mutant clones, but marked mainly groups of surrounding cells (Fig. 3.7B,B', arrows), which were deficient in dIAP1 (Fig. 3.7B,B', arrowheads). Moreover, basement membrane showed signs of discontinuity (arrows in Fig. 3.7E) as demonstrated by Laminin A staining, a major component of the basement membrane, indicating invasive behaviour.

The upregulation of dMyc protein inside *lgl*$^{-/-}$ proximal clones induced in the $M^{+/-}$ background may be a consequence of an increase in *dmyc* transcript levels, since an upregulation of *dmyc* transcription, assayed by a *dm-LacZ* construct was observed (Fig. 3.7F).

Altogether, these data show that *lgl*$^{-/-}$ cells grown in a $M^{+/-}$ background can acquire a competitive advantage, which correlates with high dMyc expression and polarity loss.

To determine the functional importance of dMyc upregulation in *lgl*$^{-/-}$ clones induced in the $M^{+/-}$ background, I silenced *dmyc* expression inside *lgl*$^{-/-}$ clones using a *UAS-dmyc*RNAi construct (for validation see Fig. 2.5B in Section 2.2.3). Knockdown of *dmyc* in *lgl*$^{-/-}$ clones prevented the cell polarity defects observed with *lgl*$^{-/-}$ clones alone even when the *lgl* mutant tissue occupied a larger proportion of the disc (Fig. 3.7G); no degradation of basement membrane occurred (not shown) and clones did not form tumourous masses, regardless of the region in which they were

located. Concerning the cell death pattern in these clones, it ranged from a complete absence of active-Caspase 3 signal in the majority of discs analysed (not shown) to scattered signals, either in $lgl^{-/-}$ cells, surrounding cells, or in regions distant from mutant clones (Fig. 3.7H, arrows). These results indicate that $lgl^{-/-}$; *dmyc*RNAi and $M^{+/-}$ cells coexist in the same tissue without undertaking competitive interactions, possibly because both populations show a similar impairment in cell proliferation. Similar results were obtained by Wu and Johnston upon the induction of *dm* loss-of-function clones in a $M^{+/-}$ background [149]. $M^{+/-}$ tissue could also intrinsically possess a low level of dMyc protein, but I was not able to detect differences in dMyc protein levels between wild-type and $M^{+/-}$ cells throughout the wing disc by clonal analysis (see Fig. **??**X). Thus, the silencing of *dmyc* in $lgl^{-/-}$ clones and the reduced ribosomal pool in the $M^{+/-}$ background may make their levels of biosynthesis comparable. The ability of *lgl* mutant patches to grow despite dMyc deprivation might also be due to the upregulation of other growth-promoting factors in the $M^{+/-}$ context, which are however *per se* unable to provide $lgl^{-/-}$ cells with tumourigenic features.

3.1.6 The Oncogenic Cooperation Between $lgl^{-/-}$ and dMyc Protein Is Conserved in the Follicular Epithelium

With the aim of assessing whether the oncogenic cooperation between lgl mutation and dMyc protein could be conserved in other *Drosophila* tissues, I investigated $lgl^{-/-}$ clonal behaviour in the ovarian follicular epithelium, a monolayered adult tissue of somatic origin that surrounds the germ line of the egg chamber (see Section 2.1.2). Interestingly, the phenotype of $lgl^{-/-}$ clones in the follicular epithelium reported in literature (see Section 1.2.1.2) appeared to be rather different from that observed in the wing imaginal epithelia, but similar to that of the whole mutant animal; in females bearing a homozygous temperature-sensitive *lgl* mutation, egg chambers invariantly show hyperproliferation of follicular cells that display loss of apical-basal polarity and migrate between the nurse cells [53].

I found that *lgl* mutant clones overproliferated, lost apical-basal polarity and formed multilayers near the chamber poles (Fig. 3.8A), consistent with previous studies [22, 57]. Active-Caspase 3 staining revealed that apoptosis was occasionally observable in egg chambers from stage 8 onward in wild-type cells at the clone

border (Fig. 3.8B). This cell death pattern is reminiscent of a mechanism of dMyc-induced cell competition. Cell competition, however, has never been described in the follicular epithelium, so I induced *dmyc*-overexpressing (*dmyc*^{over}) Flp-out clones [85] in adult females and observed that the wild-type tissue underwent massive cell death (not shown), suggesting that *dmyc* is also able to induce apoptosis in the surrounding cells in this tissue. Indeed, *lgl*$^{-/-}$ clones expressed dMyc protein in early egg chambers as well as at later stages (Fig. 3.8D), where endogenous protein is normally absent (Fig. 3.8C). *dmyc* was also transcriptionally activated, as can be seen from *dm-LacZ* expression in Figure 3.8E. Thus, *lgl*$^{-/-}$ clonal behaviour in the follicular epithelium positively correlates with *dmyc* expression. dIAP1 levels in *lgl*$^{-/-}$ follicular clones were similar to those seen in the wild-type adjacent tissue (Fig. 3.8F), and no autonomous apoptosis was visible in *lgl*$^{-/-}$ follicular cells (not shown). Further, I allowed clones to grow for four additional days in order to obtain stronger phenotypes. As can be seen in Figure 3.8G, dMyc protein was detectable in all *lgl*$^{-/-}$ cells; clonal phenotype varied from larger areas of multilayered tissue (arrowed), which sometimes extended away from the poles (asterisk), to clones that invaded into the nurse cells territory (arrow).

To determine the contribution of *dmyc* to the *lgl* mutant phenotype in this tissue, dMyc levels inside *lgl*$^{-/-}$ cells were lowered using the *UAS-dmyc*RNAi construct. A pronounced decrease both in clone size and number was observed (visible clone area: 44% decrease in 60 clones at chamber poles analysed for each genotype; clone number: 74% decrease on a total of 20 pairs of ovaries for each genotype) and no multilayered tissue was seen (not shown).

Taken together these data demonstrate that also in the follicular epithelium dMyc protein is required for *lgl* mutant clones to grow as malignant tumours.

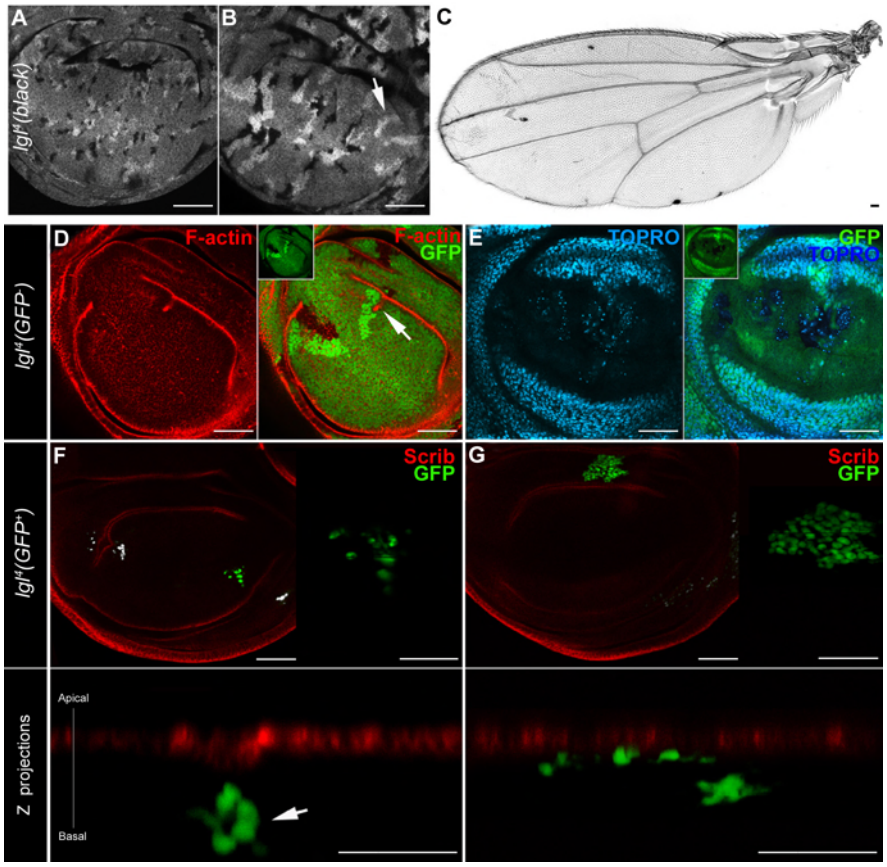

Figure 3.1: **A,B**: 2 (A) and 3 days-old (B) *lgl*$^{-/-}$ clones (black). In B, the arrow indicates a twin clone (bright white) with no *lgl*$^{-/-}$ counterpart; **C**: adult wing from a female of the same genotype as in A and B showing apoptotic scars. **D,E**: apical (D) and basal (E) sections of wing discs bearing *lgl*$^{-/-}$ clones (GFP^{-}); in D, F-actin staining shows there is folding at the clonal boundaries (arrow); in E, pycnotic nuclei inside *lgl*$^{-/-}$ clones (GFP^{-}) are visible. **F,G**: Scrib staining of wing discs bearing *lgl*$^{-/-}$ MARCM clones (GFP^{+}). In the lower panel, the respective projections along the Z axis are shown; no changes in localisation of the subapical marker Scrib are appreciable in the *lgl*$^{-/-}$ cells (GFP^{+}) with respect to the surrounding wild-type tissue (GFP^{-}), even when mutant cell nuclei are being basally extruded (arrow). Scale bars are 35 micron. Experiments shown in A-E have been performed by Nicola A. Grzeschik in Helena Richardson Lab, Peter MacCallum Cancer Center, Melbourne, VIC.

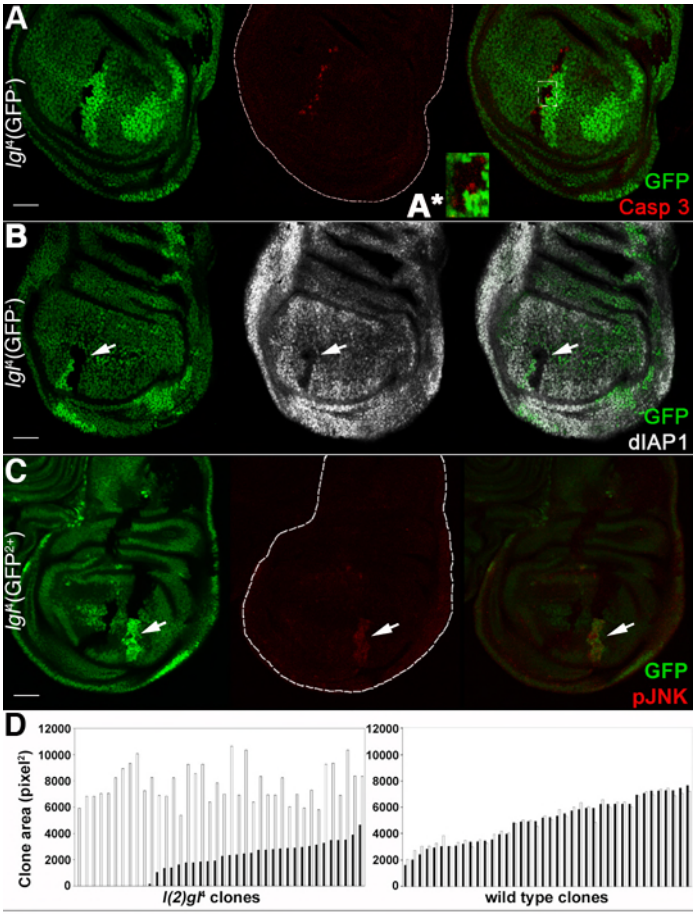

Figure 3.2: **A,B**: $lgl^{-/-}$ clones (GFP^{-}) induced in a wild-type background (GFP^{+}). Wild-type twin clones are GFP^{2+}. A: active-Caspase 3 staining shows that many apoptotic cells are present in $lgl^{-/-}$ clone; in A*, a magnification of the region outlined is shown. B: dIAP1 staining; its expression within the mutant clone (arrow) is visibly lower. **C**: $lgl^{-/-}$ clones (GFP^{2+}) induced in a wild-type background (GFP^{+}). Wild-type twin clones are GFP^{-}. pJNK staining shows that the JNK pathway is activated inside the *lgl* mutant clone (arrow). Wing discs are outlined in A and C. Scale bars are 35 micron. **D**: $lgl^{-/-}$ (left panel) and wild-type (right panel) clone profile from a twin analysis of lgl^{4} or wild-type clones sampled in the wing pouch region induced in a wild-type background. Black bars indicate lgl^{4} (n=40) and wild-type (n=40) clones and white bars indicate the respective twins. For this experiment, freshly hatched larvae were collected in a 1-hour time window and staged on cornmeal medium to 90 hours after hatching before collecting tissues.

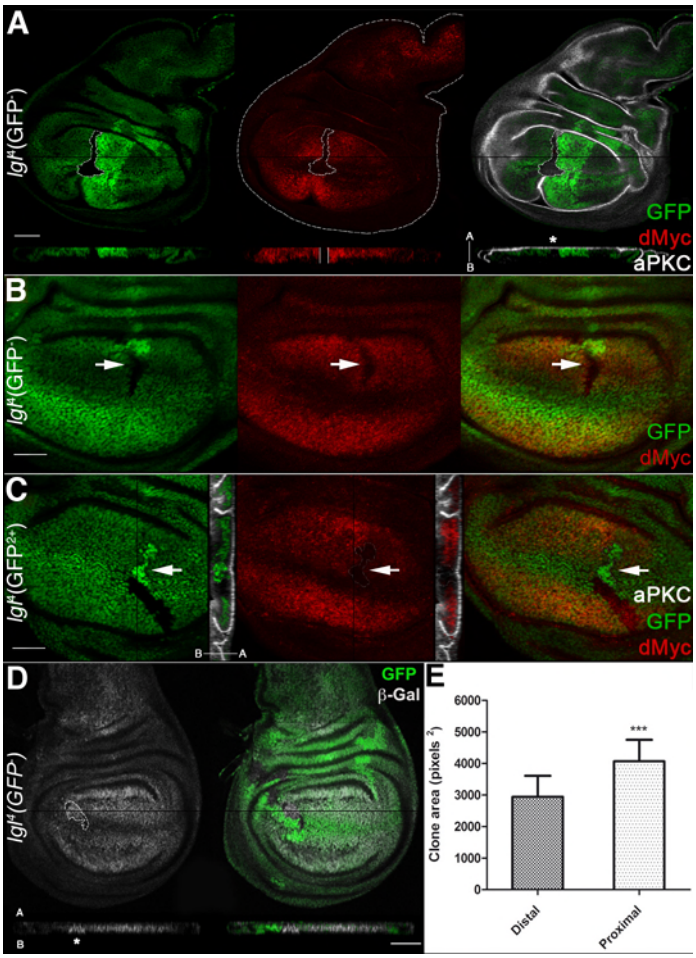

Figure 3.3: **A,B**: *lgl*$^{-/-}$ clones (GFP^{-}) induced in a wild-type background (GFP^{+}). Wild-type twin clones are GFP^{2+}. A: dMyc and aPKC staining; clone is outlined and the projection along the Z axis shows that dMyc expression within the mutant clone is low all along the disc thickness (enclosed between two white bars) and does not show defects in apical-basal cell polarity (asterisk). The apical-basal axis of the disc proper is also shown. Another *lgl*$^{-/-}$ clone showing low dMyc levels (arrow) can be observed in B at higher magnification. **C**: *lgl*$^{-/-}$ clones double positive for GFP (GFP^{2+}, arrow) were also induced to show mutant nuclei. Wild-type twin clones are GFP^{-}. In the projection along the Z axis it can be seen that *lgl*$^{-/-}$ cells are being basally extruded from the epithelium. Wing disc is outlined in A. Scale bars are 35 micron. **D**: β-Gal staining of *lgl*$^{-/-}$ clones induced in *dm-LacZ* individuals showing a mutant clone (outlined) in which *dmyc* transcriptional activity does not seem to be impaired. In the projection along the Z axis, in which the apical (A) and basal (B) sides of the disc proper are shown, note that *lgl* mutant nuclei are more basal with respect to neighbours (asterisk). **E**: A graph showing the average size of *lgl*$^{-/-}$ clones originated in distal and proximal regions of the wing disc: distal clones are significantly smaller than proximal ones; ***= $P < 0.001$, n=15 each.

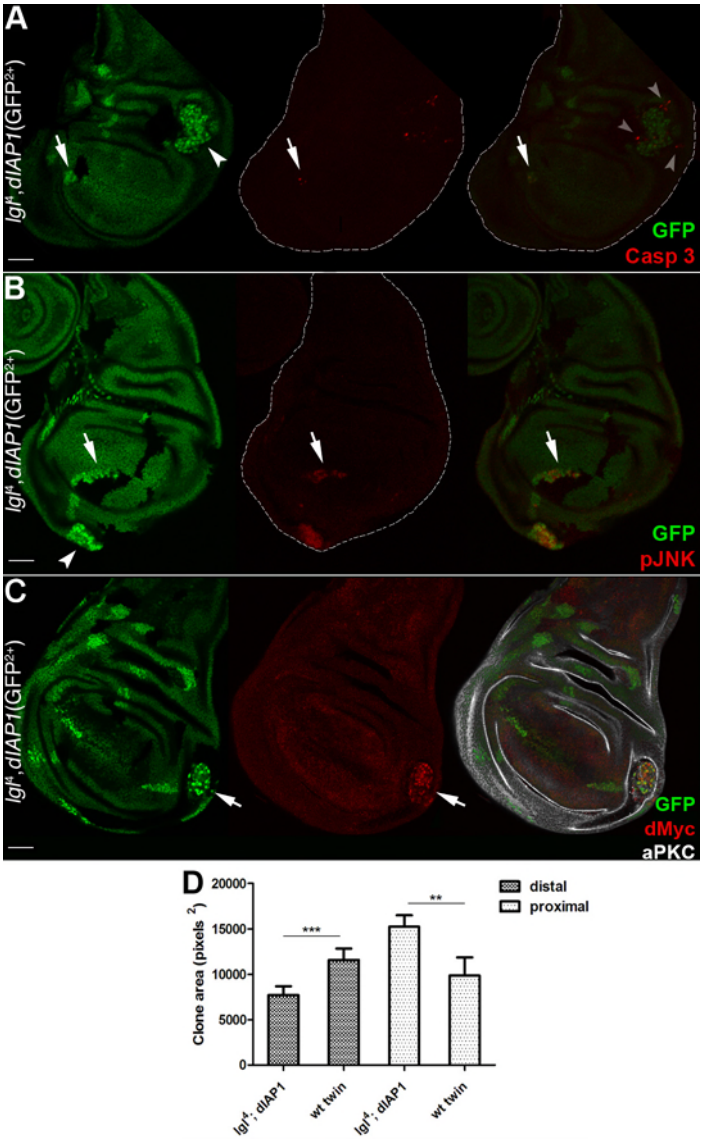

Figure 3.4: **A-C**: *lgl*$^{-/-}$; *dIAP1* clones (GFP^{2+}) induced in a wild-type background (GFP^{+}). Wild-type twin clones are GFP^{-}. Active-Caspase 3 (A) and pJNK (B) signals are both visible inside *lgl* mutant clones (arrows). Arrowheads indicate clones in the proximal regions and grey arrowheads point to active-Caspase 3 signals in wild-type cells surrounding the mutant clone. In C, an *lgl*$^{-/-}$; *dIAP* clone expressing high levels of dMyc protein is shown (arrow). Wing discs are outlined in A and B. Scale bars are 35 micron. **D**: A graph showing the average area of *lgl*$^{-/-}$; *dIAP1* clones and their wild-type twins; while in distal regions (dark bars) mutant clones are smaller than their twins, the opposite is true in proximal regions (light bars), ***= $P < 0.001$, **= $P < 0.01$, n=28 and n=22, respectively.

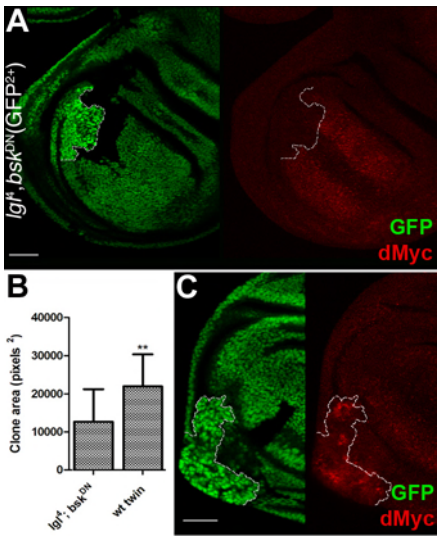

Figure 3.5: **A**: $lgl^{-/-}$; bsk^{DN} clones (GFP^{2+}) induced in a wild-type background (GFP^{+}). Wild-type twin clones are GFP^{-}. dMyc staining shows that the protein is low in the mutant clone in the wing pouch (outlined). **B**: A graph showing the average area of $lgl^{-/-}$; bsk^{DN} clones and their wild-type twins sampled in the distal region of the wing disc, mutant clones are significantly smaller; **= $P < 0.01$, n=15. **C**: a disc of the same genotype as in A is shown in which a $lgl^{-/-}$; bsk^{DN} clone (GFP^{2+}) in the pleura display increased dMyc staining. Clone boundaries are indicated by the white dotted line. Scale bars are 35 micron.

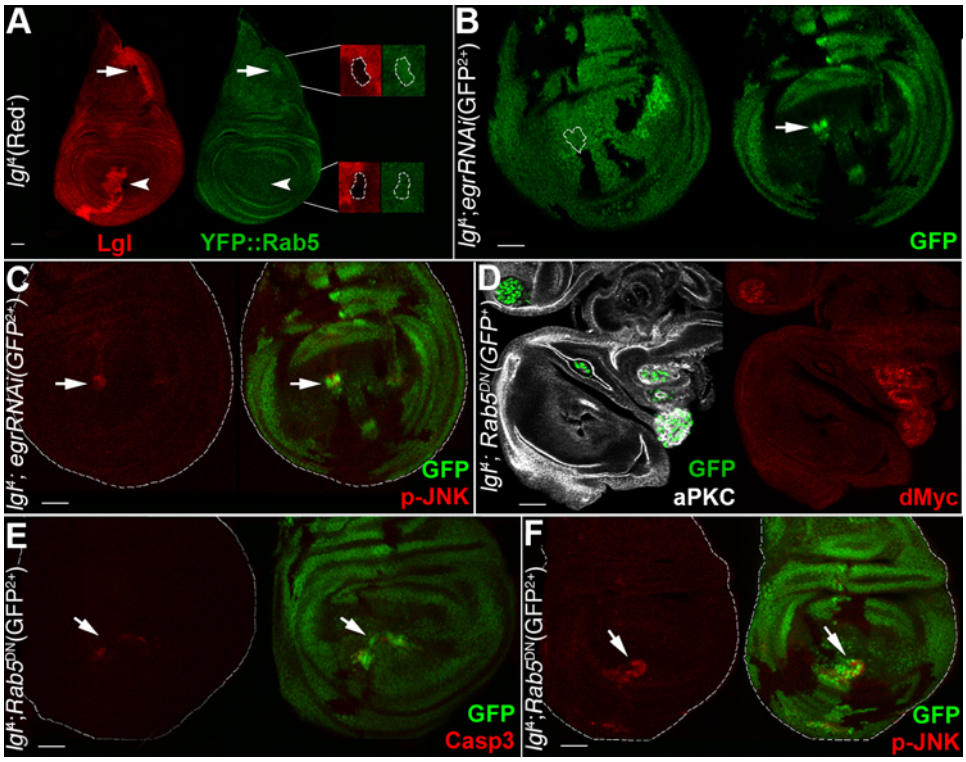

Figure 3.6: **A**: Lgl antibody staining (red) of *tub-YFP::Rab5* discs bearing $lgl^{-/-}$ clones (black). The wild-type twin clones are red^{2+}. The arrow indicates an *lgl* mutant clone in the notum where the *YFP::Rab5* signal is slightly increased and the arrowhead indicates an *lgl* mutant clone in the pouch where the *YFP::Rab5* signal is comparable to that found in the surrounding wild-type tissue. Magnifications of the mutant clones are shown on the right. **B,C**: $lgl^{-/-}$; *egr*RNAi clones (GFP^{2+}) induced in wild-type background (GFP^{+}). Wild-type twin clones are GFP^{-}. In B the apical (left) and basal (right) sections of the same disc are shown; in the basal section a mutant clone contains cells that are basally excluded from the epithelium (arrow) and shows pJNK staining (C). The clone contour is outlined in C. **D**: $lgl^{-/-}$; $YFP::Rab5^{\mathrm{DN}}$ clones (GFP^{+}) induced in a wild-type background (GFP^{-}), stained with aPKC and dMyc. **E,F**: $lgl^{-/-}$; $YFP::Rab5^{\mathrm{DN}}$ clones (GFP^{2+}) induced in a wild-type background (GFP^{+}). Wild-type twin clones are GFP^{-}. In E active-Caspase 3 and in F pJNK signals are visible within the mutant clone (arrows). Wing discs are outlined in C, E and F. Scale bars are 35 micron.

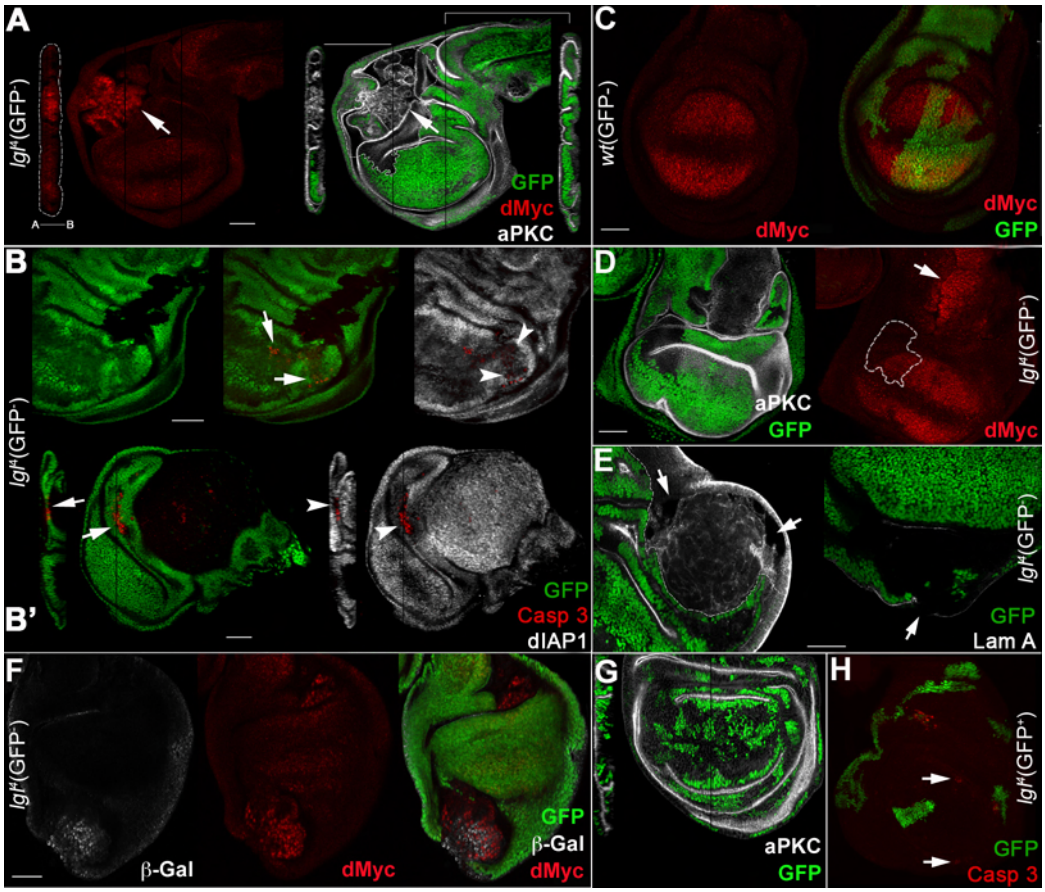

Figure 3.7: **A-B'**: $lgl^{-/-}$ clones (GFP^{-}) in a $M^{+/-}$ background (GFP^{+}). A: dMyc and aPKC staining. A strong dMyc accumulation is visible in the mutant clone located in the hinge region (arrows). A Z projection shows that loss of cell polarity accompanies the dramatic overgrowth. A Z projection of a region of the disc without mutant clones is shown on the right as a control. B-B': Activated Caspase 3 and dIAP1 staining. Arrows indicate $M^{+/-}$ cells dying around the mutant clones; the Z projection confirms that dying cells are outside the $lgl^{-/-}$ tissue. Arrowheads indicate that dying cells are deprived of dIAP1. **C**: wild-type clones (GFP^{-}) induced in a $M^{+/-}$ background (GFP^{+}). No differences in protein level are appreciable in wild-type clones originated in diverse disc regions with respect to the background. **D,E**: $lgl^{-/-}$ clones (GFP^{-}) in a $M^{+/-}$ background (GFP^{+}). In D, dMyc staining shows that while the protein is upregulated in a clone in the notum (arrow) no increase is observed in mutant cells in the wing pouch (clone outlined), aPKC staining is also shown. In E Laminin A staining of $lgl^{-/-}$ clones (GFP^{+}) indicates that basement membrane integrity is lost in several points (arrows). **F**: β-Gal (white) and dMyc (red) staining of of $lgl^{-/-}$ clones induced in *dm-LacZ*-bearing $M^{+/-}$ individuals. The clone in the pleura shows a *dmyc* transcriptional upregulation. **G,H**: $lgl^{-/-}$; *dmyc*RNAi clones (GFP^{+}) in a $M^{+/-}$ background (GFP^{-}).G: aPKC staining reveals that $lgl^{-/-}$; *dmyc*RNAi mutant cells in a $M^{+/-}$ background do not lose apical-basal polarity (Z projection, compare with A). H: Caspase staining shows that apoptosis is scattered throughout the disc (arrows). Scale bars are 35 micron.

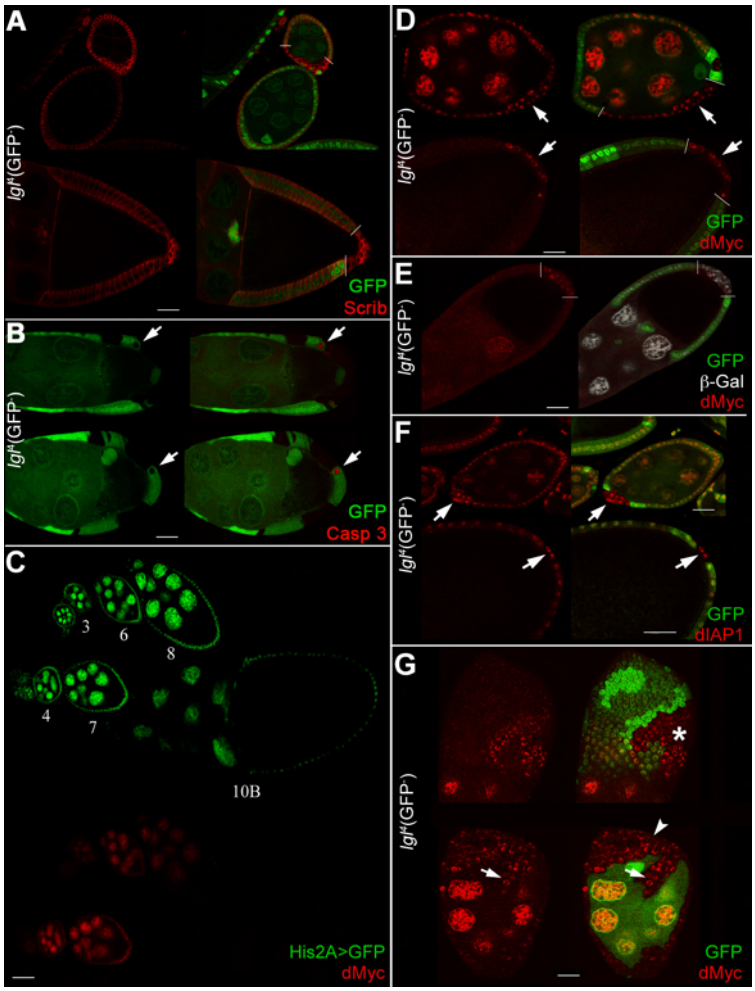

Figure 3.8: **A,B**: Follicular cells' $lgl^{-/-}$ clones (GFP^{-}) induced in a wild-type background (GFP^{+}). Wild-type twin clones are GFP^{2+}. A: $lgl^{-/-}$ clones (bordered by white bars) stained for Scrib are shown in early and late egg chambers. Scrib distribution spreads from lateral to cortical. B: active-Caspase 3 staining of stage 8-9 egg chambers; arrows indicate wild-type cells (GFP^{+}) undergoing apoptosis. **C**: dMyc protein pattern during oogenesis, chamber stages are indicated; from stage 8 onwards dMyc is no longer detectable in follicular cells. **D**: $lgl^{-/-}$ clones (GFP^{-}) stained for dMyc, an early (top) and a late (bottom) egg chamber is shown. Bars mark clone boundaries and arrows indicate dMyc expression inside the mutant clones. **E**: **D**: β-Gal (white) and dMyc (red) staining of $lgl^{-/-}$ clones (marked by bars) induced in *dm-LacZ* females: *dmyc* is transcriptionally upregulated in mutant cells. **F**: $lgl^{-/-}$ clones (GFP^{-}) in early (top) and late (bottom) egg chamber stained with dIAP1. The arrows indicate high dIAP1 expression in the $lgl^{-/-}$ clones. **G**: dMyc staining in older $lgl^{-/-}$ clones; the arrowhead indicates multilayers of mutant follicular cells, the arrow indicates mutant cells migrating into the nurse cell territory and the asterisk refers to a large clone away from the egg chamber pole, where *lgl* mutant clones usually originate. Scale bars are 35 micron.

3.2 Tumour Progression

As described in Section 1.2.2 the oncogenic cooperation between constitutive Ras signalling (Ras^{V12}) and the polarity mutants has been very useful to investigate different aspects of tumour progression such as the genetic requirements for invasion and migration as well as interactions with the innate immune system. I thus took advantage of this model to further analyse the features of *lgl*-induced tumours once the tumour suppressive mechanisms described in the above section have been eluded.

3.2.1 Constitutive Ras Activity Promotes $lgl^{-/-}$ Neoplastic Growth in the Wing Imaginal Disc

Ras^{V12} oncogenic cooperation with either *scrib*, *lgl* or *dlg* loss of function has been extensively described in the eye imaginal disc (Section 1.2.2), however Menéndez and colleagues [82] showed that, at least in the case of *lgl*, this oncogenic cooperation also occurs in the imaginal wing disc: the authors showed that $lgl^{-/-}$; Ras^{V12} clones dramatically overgrow and proliferate with a much higher rate with respect to the surrounding cells.

To further analyse the phenotypes associated to this oncogenic cooperation I generated $lgl^{-/-}$; Ras^{V12} clones (Fig.3.9). As can be seen in Figures 3.9 and 3.10 they are indeed larger than wild-type, $lgl^{-/-}$ or Ras^{V12} clones induced with the same system (also compare in Fig. 3.9 D with A, B and C respectively) and in some cases formed huge tumorous masses that occupied a large percentage of the disc (Fig. 3.9E) possibly because of the phenomenon of clone merging previously described [82]. In $lgl^{-/-}$; Ras^{V12} clones apical-basal cell polarity was compromised as indicated by aPKC cortical spreading (Fig. 3.9D, Z projection) while this was never the case for wild-type, $lgl^{-/-}$ or Ras^{V12} clones (Fig. 3.9A, B and C respectively, Z projections). Ras^{V12} clones, consistent with their documented extrusion from the epithelium [195], formed cyst-like structures (Fig. 3.9C, arrow) in which, however, apical-basal polarity was maintained. Moreover, $lgl^{-/-}$; Ras^{V12} clones in the wing imaginal disc, similarly to what was reported for the eye disc [70, 74, 75] showed signs of invasive behaviour as indicated by the production of the basement membrane-degrading enzyme MMP1 (Fig. 3.9F) that never occurred in wild-type, $lgl^{-/-}$ or Ras^{V12} clones (Fig. 3.9A-C). Activated Caspase-3 positive cells can be seen in wild-type tissue surrounding $lgl^{-/-}$;

Ras^{V12} cells (Fig. 3.9F, arrow), suggesting that these latter can acquire competitive capabilities; nevertheless apoptotic cell death is also present within mutant clones in the wing pouch, where cell competition is fiercer (Fig. 3.9F, arrowhead), confirming the hypothesis that merging of multiple clones could be required for mutant cells to avoid apoptotic elimination [82].

The data presented in Section 3.1 showed that *lgl*$^{-/-}$ overgrowth in all the contexts analysed was always accompanied by high levels of dMyc protein. Indeed, also in *lgl*$^{-/-}$; *Ras*^{V12} mutant clones throughout the disc dMyc was highly expressed (Fig. 3.9D also reported in [82]). Interestingly, while inhibiting cell death (Figures 3.4 and 3.5) or limiting the proliferative drive of the surrounding tissue (Fig. 3.7) was not sufficient to promote *lgl*$^{-/-}$ overgrowth and dMyc upregulation in the wing pouch, *Ras*^{V12} expression in *lgl*$^{-/-}$ cells allowed them to form large, round-shaped clones characterised by high levels of dMyc, loss of apical-basal polarity and invasiveness also in this region (Fig. 3.9D and F)[1]. Since Ras signalling pathway is known to stabilise dMyc at a post-transcriptional level [92, 101] it may allow to counteract *lgl* LOF-dependent downregulation of dMyc protein abundance (see Section 3.1.2) and promote overgrowth in distal regions where surrounding wild-type cells show the highest dMyc expression (Fig. 2.5A in Section 2.2.3).

Altogether these data indicate that *lgl* loss of function and *Ras*^{V12} oncogenic cooperation in the wing disc epithelium is characterised by neoplastic features such as overgrowth, loss of cell polarity and invasiveness and is accompanied by high levels of dMyc even in those regions where *lgl*$^{-/-}$ growth is usually restricted.

3.2.2 Raf/MAPK and not PI3K Signalling Cooperate with *lgl*$^{-/-}$ Downstream of Ras

Activated Ras signals through two main downstream growth-promoting pathways: the Raf/MAPK and the PI3K pathway (Section 1.3.1). Both Ras effectors are activated in *lgl*$^{-/-}$; *Ras*^{V12} clones as can be seen by intense staining of the diphosphorylated form of the MAPK, Erk, (dpErk) and of phosphorylated Akt (pAkt) in Figure 3.9G. I thus investigated how these pathways contribute to the oncogenic cooperation with *lgl* loss of function. As can be seen in Figure 3.12A, expression of

[1]The neoplastic traits described in the text for all the genotypes analysed in this work are summarised in Figure 3.18

an activated form of the catalytic subunit of PI3K, *dp110*$^{\mathrm{CAAX}}$ (see Fig. 2.6 in Section 2.2.3 for a validation) failed to rescue the defective growth of *lgl* mutant cells. Indeed, *lgl*$^{-/-}$; *dp110*$^{\mathrm{CAAX}}$ clones are smaller than *lgl*$^{-/-}$ clones (Fig. 3.10), show a wild-type morphology (Fig. 3.12A) and no significant impairments in cell polarity (Fig. 3.12A, Z projection) or MMP1 expression (not shown) were observed. Consistently, a similar inability of activated PI3K in promoting *lgl*$^{-/-}$ cells growth was also observed upon inhibition of upstream Ras activity by means of an RNAi construct (see Fig. 2.7 in Section 2.2.3 for a validation). *lgl*$^{-/-}$; *dp110*$^{\mathrm{CAAX}}$; *Ras*RNAi clones (Fig. 3.12B) were comparable to *lgl*$^{-/-}$; *dp110*$^{\mathrm{CAAX}}$ (Fig. 3.10) and smaller than *lgl*$^{-/-}$ clones (Fig. 3.10), did not lose apical-basal-polarity (not shown) or showed MMP1 expression (Fig. 3.12B).

On the other hand, expression of a constitutively activated form of human Raf (hRaf$^{\mathrm{GOF}}$) in *lgl*$^{-/-}$ clones fully recapitulated the phenotypes observed for *lgl*$^{-/-}$; *Ras*$^{\mathrm{V12}}$ (Fig. 3.12C and D). hRaf has been demonstrated to be functionally conserved in *Drosophila* [196] and it indeed activated MAPK pathway as shown by dpErk staining (Fig. 2.8 in Section 2.2.3). *lgl*$^{-/-}$; *hRaf*$^{\mathrm{GOF}}$ clones are overgrown and round in shape (Fig. 3.12C and 3.10), lose apical-basal cell polarity (Fig. 3.12C, Z projection) and produce the basement membrane-degrading enzime MMP1 (Fig. 3.12D). Moreover, similarly to *lgl*$^{-/-}$; *Ras*$^{\mathrm{V12}}$ ones, also *lgl*$^{-/-}$; *hRaf*$^{\mathrm{GOF}}$ clones were able to grow in the wing pouch (Fig. 3.11) and extensive tumorous growth with mutant cells taking over half of the entire disc was also observed (Fig. 3.12D). Knockdown of Ras activity in *lgl*$^{-/-}$; *hRaf*$^{\mathrm{GOF}}$ cells did not affect their growth or neoplastic behaviour. As can be observed in Figure 3.10, *lgl*$^{-/-}$; *hRaf*$^{\mathrm{GOF}}$; *Ras*RNAi clones were comparable in size to *lgl*$^{-/-}$; *hRaf*$^{\mathrm{GOF}}$ clones and similarly showed compromised apical-basal cell polarity (Fig. 3.12E, Z projection) and expressed high levels of MMP1 in proximal regions as well as in the wing pouch (Fig. 3.12F, arrow and arrowhead respectively).

Since both Raf/MAPK and PI3K pathways are able to stabilise dMyc protein (see Section 1.4.2, [92, 164, 166]) I analysed dMyc abundance in *lgl*$^{-/-}$ cells in which these pathways were activated. Interestingly, no increase in dMyc levels was detected in *lgl*$^{-/-}$; *dp110*$^{\mathrm{CAAX}}$ clones (Fig. 3.12A) nor in *lgl*$^{-/-}$; *dp110*$^{\mathrm{CAAX}}$; *Ras*RNAi clones (not shown). On the contrary high levels of dMyc were detected both in *lgl*$^{-/-}$; *hRaf*$^{\mathrm{GOF}}$ clones (Fig. 3.12C) and *lgl*$^{-/-}$; *hRaf*$^{\mathrm{GOF}}$; *Ras*RNAi clones (Fig. 3.12E) throughout the wing disc, suggesting that post-transcriptional regulation

of dMyc downstream of Ras signalling is due to the Raf/MAPK activity and that PI3K-dependent stabilisation of dMyc, given its transient nature (see Section 1.4.2, [92, 166]) may not be sufficient to allow a significant accumulation of the protein.

Taken together these data indicate that, similarly to what has been observed for *scrib*$^{-/-}$ clones in the eye disc [60], the Raf/MAPK branch downstream of Ras signalling is responsible for the oncogenic cooperation with *lgl* loss of function. Its activation indeed phenocopied the effect of Ras^{V12} on *lgl* mutant cells while activated PI3K had no effect on mutant clones behaviour. Moreover, once again, neoplastic behaviour of *lgl* mutant clones was found to positively correlate with dMyc protein levels.

3.2.3 dMyc Is Necessary and Sufficient to Promote *lgl*$^{-/-}$ Cells Growth

The fact that high levels of dMyc are found to be associated with neoplastic *lgl*$^{-/-}$; *Ras*^{V12} and *lgl*$^{-/-}$; *hRaf*^{GOF} clones but not with the poorly-grown *lgl*$^{-/-}$; *dp110*^{CAAX} clones (see above) suggests that dMyc might play a key role in the oncogenic cooperation between *lgl* loss and activated Ras signalling as it does in driving tumorous growth of *lgl*$^{-/-}$ clones generated in the *Minute*$^{+/-}$ background in the wing imaginal disc (Section 3.1.5) or in the follicular epithelium (Section 3.1.6). Indeed expression of a *dmyc*RNAi construct in *lgl*$^{-/-}$; *Ras*^{V12} clones drastically reduced their size (Fig. 3.13A) and rescued the defects in apical basal cell polarity (Fig. 3.13A, Z projection); moreover no MMP1 expression was detected in the wing disc proper (Fig. 3.13A) and mutant clones were recovered at an extremely low frequency suggesting that dMyc is required for *lgl*$^{-/-}$; *Ras*^{V12} cells neoplastic behaviour. To test whether dMyc is *per se* sufficient to drive *lgl*$^{-/-}$ cells growth in a wild-type background, I expressed a *UAS-dmyc* construct in *lgl*$^{-/-}$ clones. As can be observed in Figure 3.13B, *lgl*$^{-/-}$; *dmyc* clones were round in shape and massively overgrown, with larger clones located in the proximal regions of the disc (Fig. 3.10 and 3.11). A staining for the apical marker aPKC indicated that *lgl*$^{-/-}$; *dmyc* cells displayed impaired apical-basal polarity (Fig. 3.13D, Z projection) and signs of discontinuity of the basement membrane across the mutant clones were detected by staining for Laminin A (Fig. 3.13E, arrows), indicating that *lgl*$^{-/-}$; *dmyc* cells acquire invasive properties.

As discussed above, *lgl*$^{-/-}$; *dmyc* clones in the wing pouch are on average smaller

than those in wing hinge/pleura (3.11) and also displayed a different behaviour: in Figure 3.13D, the arrow indicates a clone in the wing pouch that does not exhibit evident tumourous properties. Notably, despite expression of *UAS-dmyc* transgene, these clones do not show the high levels of dMyc protein observable in the clone located in the hinge. Since *dmyc* expression was induced using a heterologous promoter, the fact that dMyc protein is low in the *lgl* mutant clones in the wing pouch suggests that in this region the *lgl*-dependent post-transcriptional downregulation of dMyc (see Section 3.1.2) counteracts the accumulation of the protein even when the gene is highly expressed. This probably explains why *dmyc* overexpression in $lgl^{-/-}$ cells had a different outcome depending on the region of the disc where clones were located. In $lgl^{-/-}$; *dmyc* clones in the proximal regions, where the endogenous levels are very low, dMyc is upregulated (Fig. 3.13D) and thus mutant cells are able to overgrow and outcompete surrounding cells as indicated by Caspase 3 staining in wild-type cells at clonal border (Fig. 3.13C, arrowheads). $lgl^{-/-}$; *dmyc* clones located in the distal region instead fail to upregulate dMyc (Fig. 3.13D) and the high levels of the endogenous protein in this region are likely to prevent these $lgl^{-/-}$; *dmyc* clones from acquiring a competitive advantage as suggested by Caspase 3-positive mutant cells (3.13C, arrows).

I then asked if dMyc overexpression was able to cooperate with *lgl* loss of function even in the absence of endogenous Ras signalling. $lgl^{-/-}$; *dmyc*; *Ras*RNAi clones in the proximal regions lost cell polarity and expressed MMP1 (not shown) indicating that they acquired neoplastic features. These clones moderately overgrew (Fig. 3.11), while those located in the wing pouch do not overgrow (Fig. 3.11), do not express MMP1 or lose apical-basal polarity (not shown). Since many pycnotic nuclei were observed in these clones (not shown), the inhibition of Ras signalling and its pro-survival effects (Section 1.3.2) may enhance apoptotic elimination of dMyc-overexpressing cells, possibly causing a reduction in size of proximal clones and completely abolishing growth in the wing pouch, where cell competition is also at work. Indeed coexpression of dIAP1 in $lgl^{-/-}$; *dmyc*; *Ras*RNAi clones significantly increased their size both in the proximal and distal regions (Fig. 3.11 and 3.13F); nevertheless tumorous features such as high MMP1 expression and cell polarity loss were invariantly observed only in clones outside the wing pouch indicating that a favourable dMyc gradient is however necessary for neoplastic growth to occur.

Taken together, these data demonstrate that dMyc is necessary to $lgl^{-/-}$; Ras^{V12}

oncogenic cooperation and its stable upregulation is sufficient to promote tumorous growth of *lgl* mutant cells even in the absence of Ras signalling.

3.2.4 Oncogenic Cooperation between *lgl*$^{-/-}$ and Activated Raf/MAPK Signalling Requires Yki Function

Menéndez and colleagues [82] reported that in *lgl*$^{-/-}$; *Ras*^{V12} clones the transcriptional coactivator Yorkie (Yki) is mainly localised to the nucleus and its target gene *dIAP1* is upregulated, indicating that the Hippo pathway is inactive in these cells (see 1.2.1.2). Since Ras^{V12} clones did not show Yki nuclear enrichment [82], it is plausible that this effect is due to *lgl* mutation. Indeed it has been demonstrated that *lgl* loss of function is able to deregulate this pathway both in the eye [43] and wing imaginal disc (in a condition in which mutant cells growth is not restricted by cell competition) [45] (1.2.1.2). Since I observed an increase in Yki nuclear localisation in *lgl*$^{-/-}$; *hRaf*^{GOF} clones (not shown), it is possible that deregulation of Hpo pathway is a feature of overgrown *lgl* mutant tissues. As we and others demonstrated, *dmyc* is a Yki transcriptional target [156, 157]; this clearly suggests that activation of Yki in *lgl*$^{-/-}$; *Ras*^{V12} or *lgl*$^{-/-}$; *hRaf*^{GOF} clones could significantly contribute to the upregulation of dMyc and to the tumorous features of these cells. To test this hypothesis I lowered Yki levels in *lgl*$^{-/-}$; *hRaf*^{GOF} cells by co-expressing a *Yki*RNAi construct (see Fig. 2.9 in Section 2.2.3 for a validation). In *lgl*$^{-/-}$; *hRaf*^{GOF}; *Yki*RNAi clones growth was drastically reduced (Fig. 3.14A e 3.10), mutant clones were still round in shape but apical-basal polarity of mutant cells was not altered (Fig. 3.14A, Z projection) and no MMP1 expression was detected throughout the wing disc proper, indicating that these clones had lost their tumorous behaviour. Consistently, dMyc levels within *lgl*$^{-/-}$; *hRaf*^{GOF}; *Yki*RNAi clones were comparable to those of the surrounding wild-type tissue (Fig. 3.14B); some accumulation of the protein was detected in wild-type cells at clonal border (Fig. 3.14B, arrow) suggesting that a phenomenon of compensatory proliferation may take place in these cells.

These data indicate that Yki-dependent *dmyc* transcriptional upregulation is required for this oncogenic cooperation to occur, although other Yki targets may also play a role in the tumourigenesis downstream of *lgl*$^{-/-}$; *hRaf*^{GOF}.

I then asked whether Yki could cooperate with *lgl* loss of function in promoting neoplastic growth and overexpressed a wild-type form of *Yki* in *lgl* mutant cells. As

can be appreciated in Fig. 3.14C and 3.11, *lgl*$^{-/-}$; *Yki* clones originated in the proximal regions are overgrown, display strong impairments in apical basal cell polarity and are invasive as indicated by MMP1 staining (Fig. 3.14D). On the other hand, clones generated in the wing pouch are smaller than those in the hinge and pleura (Fig. 3.11) and show, in most cases, dMyc levels comparable to those of the surrounding tissue (not shown). Since Yki overexpression is *per se* able to upregulate dMyc in the wing pouch [156], failure to do so in the context of *lgl* loss of function might be due to the *lgl* LOF-dependent impairment in dMyc post-transcriptional stabilisation reported in other genetic contexts (Sections 3.1.2 and 3.2.3); alternatively *lgl* mutation might deregulate the Hpo pathway, and thus promote Yki activity, to a lesser extent in the wing pouch. It was recently demonstrated that, similarly to *lgl*, *scrib* mutant clones in the wing imaginal disc are subject to cell competition [83]; while in non-competitive conditions *scrib*$^{-/-}$ clones show enhanced Yki activity, when competitive interactions take place upregulation of Yki activity is prevented. A similar mechanism can thus be hypothesised for *lgl* mutant cells in the wing pouch where competitive stress is high. Analysis of dMyc transcription levels by means of the *dmyc-LacZ* reporter and of other Yki transcriptional targets in *lgl*$^{-/-}$; *Yki* clones in the wing pouch or the use of a constitutively active form of Yki will help clarify this issue.

Inhibition of Ras signalling in *lgl*$^{-/-}$; *Yki* clones further enhanced the difference in clonal behaviour in proximal *vs* distal regions: despite expression of *Ras*RNAi led to a reduction in clone size throughout the tissue (Fig. 3.14E and 3.10), clones originated in the wing pouch, besides having a correct apical-basal polarity (Fig. 3.14E, Z projection, arrow) and not showing MMP1 production (Fig. 3.14F, arrow), appeared wild-type in shape and consistently, no upregulation of dMyc was detected in this region (Fig. 3.14E, outlined clone), suggesting that dMyc post-transcriptional stabilisation may indeed play a key role in unleashing the neoplastic features of *lgl*$^{-/-}$ clones in distal regions.

Altogether this data show that *lgl* loss of function-dependent deregulation of the Hpo pathway is required to promote oncogenic cooperation between *lgl*$^{-/-}$ and activated Raf/MAPK signalling, but the expression of a wild-type form of Yorkie is not sufficient to drive neoplastic growth of *lgl*$^{-/-}$ cells in the wing pouch.

3.2.5 *lgl*$^{-/-}$; *Ras*^{V12} Cells Interact With the Tracheal System and Express Tracheal Fate Determinants

In the process of analysing *lgl*$^{-/-}$; *Ras*^{V12} cells clonal behaviour an interesting phenomenon emerged. Basally to the wing disc proper, abnormal tracheal networks were often observed that contained both GFP positive (*lgl*$^{-/-}$; *Ras*^{V12}) and GFP negative cells (Fig. 3.15A). Tracheal tubes are the organs responsible for supplying larval tissues with oxygen and are specified by the expression of the transcription factor Trachealess (Trh, see Section 1.3.2). Staining with a specific antibody revealed that some *lgl*$^{-/-}$; *Ras*^{V12} clones expressed Trh similarly to tracheal cells (Fig. 3.15B and C, arrows). Most of these Trh-expressing mutant clones were clearly interconnected with tracheal segments (Fig. 3.15A, C and D), but in some cases Trh-positive *lgl*$^{-/-}$; *Ras*^{V12} cells that did not undertake obvious interaction with tracheal tubes were also recovered (Fig. 3.15B, arrow). To rule out the possibility that these clones could have originated from tracheal tissue, I stained for Engrailed (En) and Cubitus interuptus (Ci) which mark the posterior and anterior compartments of the imaginal wing disc epithelium respectively; as can be appreciated in Figure 3.15B and C no differences in Ci expression are visible in Trh-positive (arrow) and Trh-negative *lgl*$^{-/-}$; *Ras*^{V12} adjacent clones, suggesting that these cells are of epithelial origin and are probably undergoing a phenomenon of trans-differentiation. Pastor-Pareja and colleagues demonstrated that JAK-STAT pathway is hyperactivated in *lgl*$^{-/-}$; *Ras*^{V12} clones [79] (see Section 1.2.2) and since Trh is a STAT transcriptional target [116], it is possible that activation of this pathway might promote trans-differentiation of mutant cells. Further experiments will be required to confirm and characterise this interesting phenomenon. The acquisition of tracheal fate by *lgl*$^{-/-}$; *Ras*^{V12} would be reminiscent of the recently documented ability of human carcinoma cells to trans-differentiate into endothelial cells and form vascular-like structures to increase oxygen supply in the early stages of tumour development, a process known as vasculogenic mimicry (see Section 1.1).

In the light of these observations it is tempting to speculate that the interactions between *lgl*$^{-/-}$; *Ras*^{V12} clones and the tracheal network described above might serve the tumour to gain access to an oxygen source to sustain extensive growth in a process resembling mammalian neoangiogenesis or vasculogenic mimicry (see Section 1.1). As reported in Section 1.3.2, imaginal wing disc cells that suffer from hypoxia

express *branchless* (bnl) gene, which encodes *Drosophila* FGF homologue; FGF/Bnl production attracts tracheal cells and promotes their migration. To investigate if *lgl*$^{-/-}$; *Ras*^{V12} tumours expressed FGF/Bnl I employed a *bnl-LacZ* reporter construct. As can be seen in Figure 3.15F, wild-type imaginal wing discs possess a region of FGF/Bnl production which is located in the notum and stimulates migration and proliferation of the air sac tracheal cells (arrow). Ectopic expression of FGF/Bnl is clearly visible in *lgl*$^{-/-}$; *Ras*^{V12} cells (Fig. 3.15E); this allows to speculate that indeed *lgl*$^{-/-}$; *Ras*^{V12} tumours might undergo a "tracheogenic switch" to gain access to oxygen sources as it happens for mammalian tumours which secrete pro-angiogenic factors such as VEGF and FGF to attract blood vessels and stimulate their growth or produce vascular structures through a trans-differentiative process. It will thus be interesting to explore a possible correlation between FGF/Bnl production in *lgl*$^{-/-}$; *Ras*^{V12} clones and the interaction with tracheal system or the activation of Trh expression in mutant cells them-selves.

3.2.6 dMyc Is Not Required for Mutant Cells Interactions with the Tracheal System

As I showed in Section 3.2.3, knockdown of *dmyc* expression in *lgl*$^{-/-}$; *Ras*^{V12} clones dramatically abolishes their growth (Fig. 3.13A). Unexpectedly, however, abnormal interactions between mutant cells and the tracheal network were still present and even enhanced as can be appreciated in Figure 3.16A and B where basal sections of discs of the same genotype as in Fig. 3.13A are shown. A continuum of mutant cells (GFP^{+}) from the apical to the basal surface of the epithelium can be observed in the Z projection of these discs (Fig 3.16B) with the basally located cells physically enveloping tracheal tubes. While mutant cells in apical sections do not show MMP1 expression (Fig. 3.13A), those located basally express extremely high levels of basement membrane-remodelling enzyme. This suggests that, since these cells no longer belong to the epithelial sheath but are still in continuity with it, they might be in the process of active migration over the tracheal segment.

Interestingly, similar interactions between mutant cells and the tracheal network were observed for *lgl*$^{-/-}$; *hRaf*^{GOF}; *Yki*RNAi clones (Fig. 3.16C and D): wing discs bearing clones of this genotype invariantly showed mutant cells contacting tracheal

tubes (outlined) and forming a network that links several distant clones. Notably also in these clones dMyc levels are reduced (Fig. 3.14B) further suggesting that dMyc is probably dispensable for this phenomenon to occur and might even counteract it.

Since *lgl*$^{-/-}$; *Ras*^{V12}; *dmyc*RNAi clones were recovered at an extremely low frequency, to confirm this hypothesis, a more efficient genetic system was used. A *lgl*RNAi construct was expressed in the posterior compartment of the imaginal wing disc, under the control of the *engrailed*, *en*, promoter (see Fig. 2.10 in Section 2.2.3 for a validation of the RNAi construct and for *en* expression pattern). Since cell competition does not affect cells belonging to different compartments [148], *lgl*-deficient cells are viable and able to grow in this context; moreover these experiments were carried out using $M^{+/-}$ individuals that show a delay in development (Section 1.4.3) and thus allow tumorous growth to proceed for up to 11 days. In these conditions, as can be seen in Figure 3.17A, *lgl*RNAi-expressing compartments massively overgrow, lose cell polarity and express high levels of dMyc, thus recapitulating many of the features of *lgl*$^{-/-}$; *Ras*^{V12} clones. Indeed, extensive interaction with the tracheal network is reproducibly observed in basal section of these discs with large clusters of mutant cells migrating and extending cytonemes towards tracheal tubes (Fig. 3.17B and B'). Extreme phenotypes in which tumorous cells formed tubular structures them-selves where also observed (Fig. 3.17C). Strikingly, expression of the *dmyc*RNAi construct in these tumorous discs totally abolished growth leading to a severe reduction of the posterior compartment (Fig. 3.17D) but did not prevent *lgl*RNAi; *dmyc*RNAi cells from migrating towards and interacting with tracheal tubes as can be seen in Fig. 3.17D' where basal sections are shown. Since expression of *dmyc*RNAi alone in the same genetic system does not induce any of these phenotypes (Fig. 3.17E), the effect of dMyc reduction is specific to *lgl*-deprived tissue.

Altogether these data indicate that dMyc is dispensable for the extensive interaction that tumorous *lgl*-deficient cells undertake with the tracheal system.

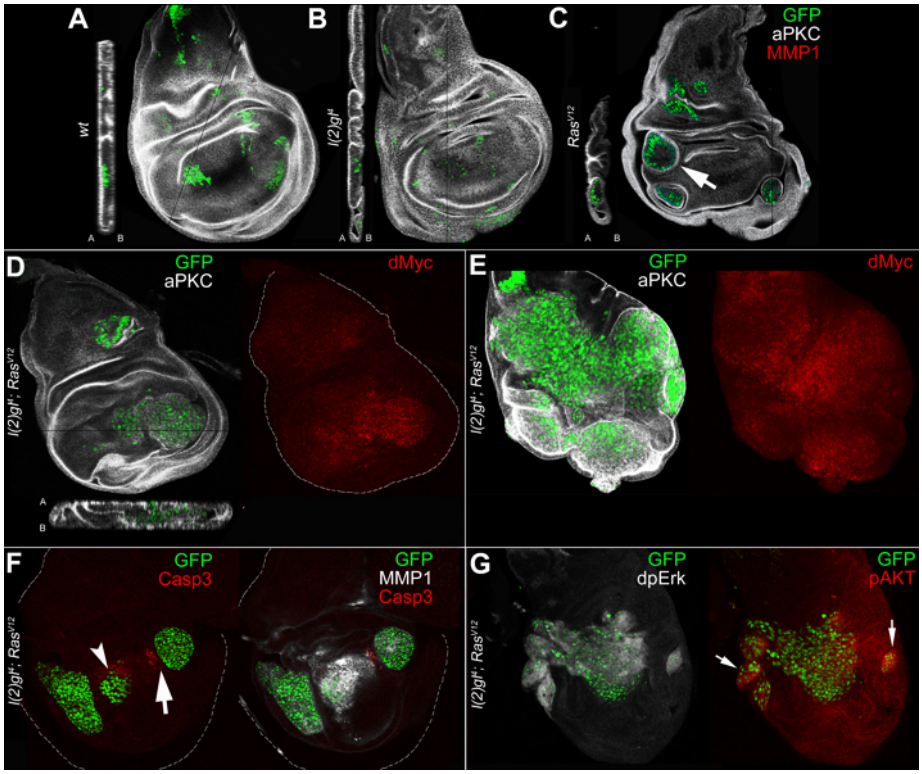

Figure 3.9: **A-C**: aPKC (white) and MMP1 (red) staining of wild-type (A), $lgl^{-/-}$ (B) and Ras^{V12} (C) clones (GFP^{+}) induced in a wild-type background (GFP^{-}). The Z projections of each disc are shown (apical, A, and basal, B, polarity is indicated). Neither impairments in aPKC localisation nor MMP1 expression are visible in clones of these genotypes. In C the arrow indicates a Ras^{V12} clone forming a cyst-like structure. **D-G**: $lgl^{-/-}$; Ras^{V12} clones (GFP^{+}) generated in a wild-type background (GFP^{-}). In D and E, aPKC (white) and dMyc (red) staining are reported. A Z projection in D shows that loss of cell polarity accompanies the overgrowth; the apical-basal axis of the disc proper is shown. Increased dMyc levels are visible in $lgl^{-/-}$; Ras^{V12} clones both in proximal and distal regions. In E an extreme phenotype in which mutant cells occupy a large proportion of the disc is observable. F: Caspase 3 (red) and MMP1 (white) staining: the arrow indicates wild-type cells undergoing cell death at the clonal border, while arrowheads points towards Caspase 3-positive cells within the mutant clone. MMP1 is expressed at high levels in $lgl^{-/-}$; Ras^{V12} clones. G: dpErk (white) and pAkt (red) staining. Arrows indicate mutant clones where pAkt staining is particularly intense. All images are 400x.

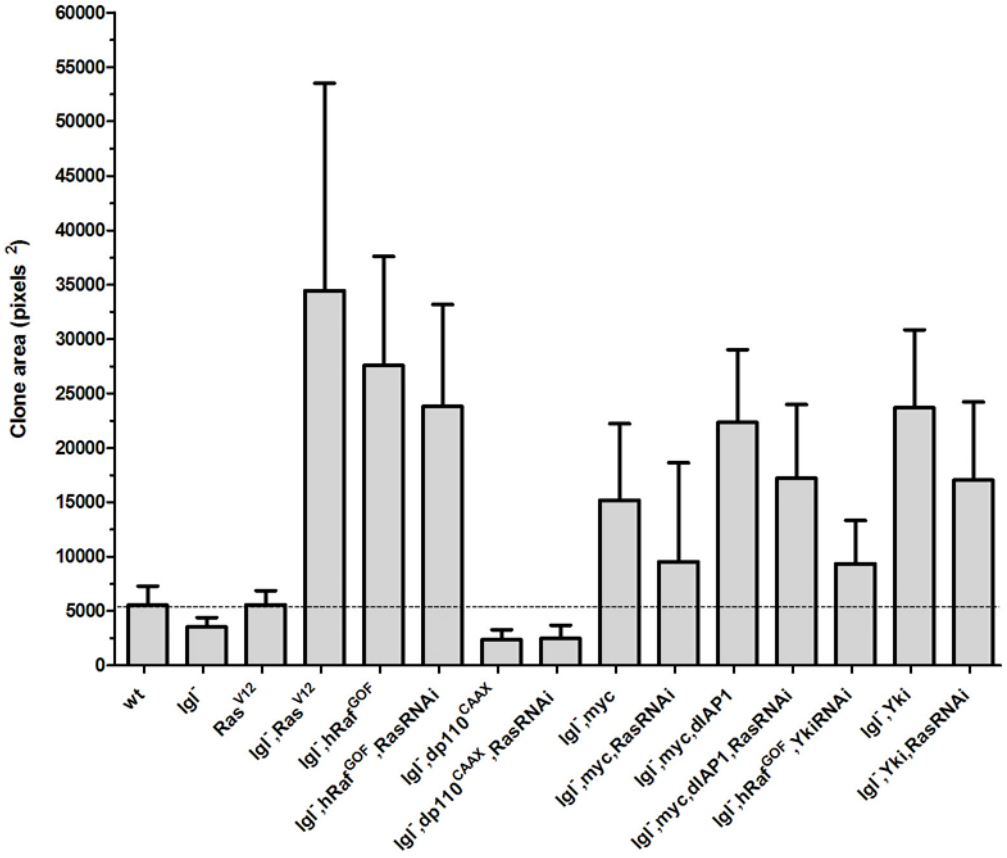

Figure 3.10: A graph showing the average clone area of all the genotypes analysed in Section 3.2 sampled all across the imaginal wing disc. The dotted line is referred to the area of wild-type clones. Areas of clones growing as multilayers are likely to be underestimated. Error bars indicate the standard deviation of the mean; n=26 each genotype. Due to low sample number, the data concerning $lgl^{-/-}$; Ras^{V12}; *dmyc*RNAi were not included in the analysis. All the comparisons described in the text are statistically significant with a $P < 0.001$ except for that between $lgl^{-/-}$; *dmyc* and $lgl^{-/-}$; *dmyc*; *Ras*RNAi clones for which $P < 0.01$. No statistical difference was found for the following comparisons: $lgl^{-/-}$; Ras^{V12} *versus* $lgl^{-/-}$; $hRaf^{GOF}$ and $lgl^{-/-}$; $hRaf^{GOF}$ *versus* $lgl^{-/-}$; $hRaf^{GOF}$; *Ras*RNAi.

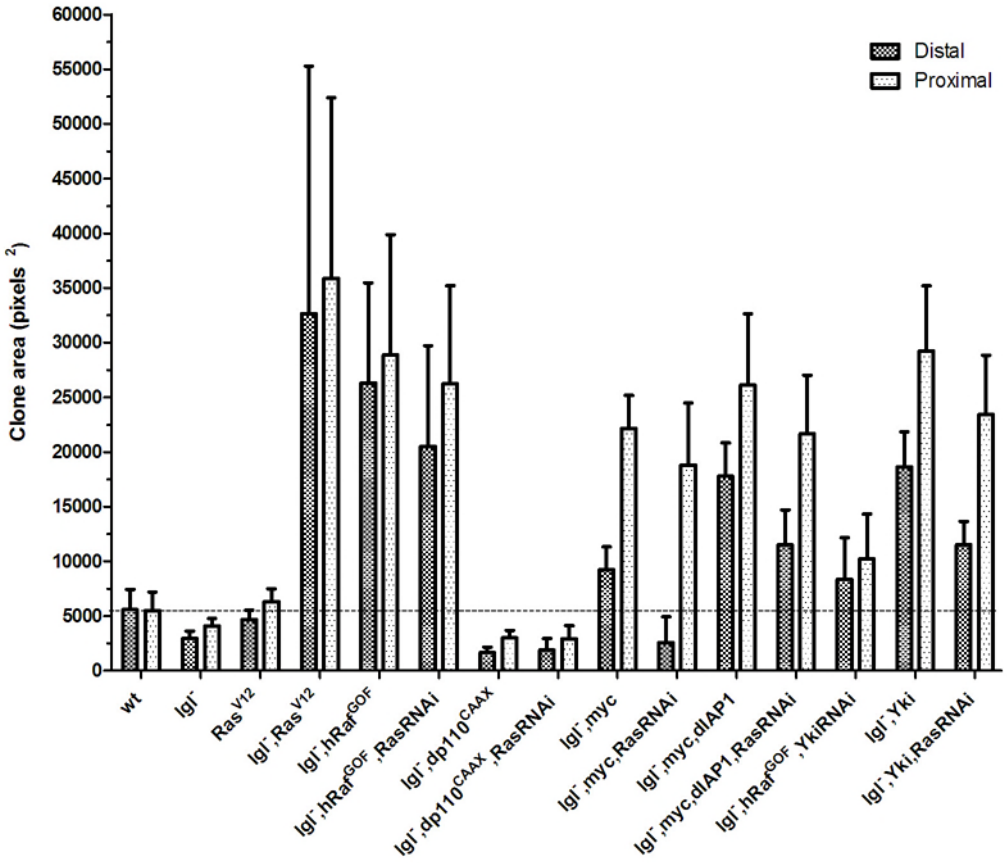

Figure 3.11: A graph showing the average clone area of all the genotypes analysed in Section 3.2 sampled in distal (dark bars) and proximal (light bars). The dotted line is referred to the area of wild-type clones. Error bars indicate the standard deviation of the mean; n=13 each genotype for both regions. All the comparisons described in the text are statistically significant with a $P < 0.001$. No statistical difference was found between the average areas of proximal and distal clones of the following genotypes: wild-type, *lgl*$^{-/-}$; *Ras*$^{\mathrm{V12}}$, *lgl*$^{-/-}$; *hRaf*$^{\mathrm{GOF}}$, *lgl*$^{-/-}$; *hRaf*$^{\mathrm{GOF}}$, *Ras*RNAi, *lgl*$^{-/-}$; *hRaf*$^{\mathrm{GOF}}$, *Ras*RNAi and *lgl*$^{-/-}$; *hRaf*$^{\mathrm{GOF}}$, *Yki*RNAi.

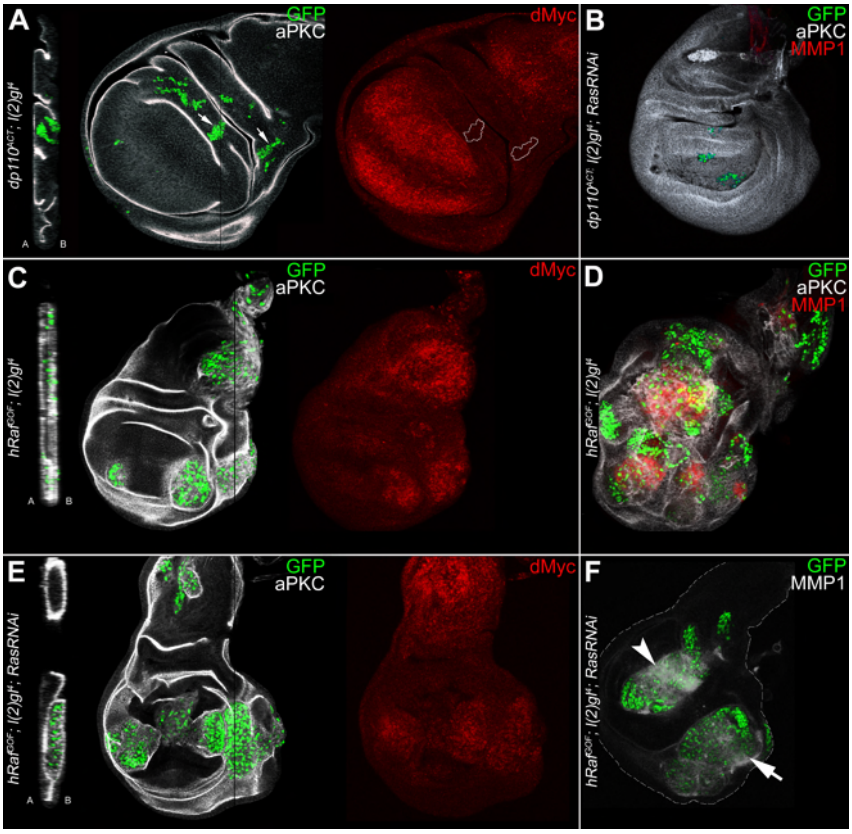

Figure 3.12: **A**: *lgl*$^{-/-}$; *dp110*$^{\mathrm{CAAX}}$ clones (GFP^{+}) generated in a wild-type background (GFP^{-}). aPKC staining (white) in the Z projection shows that mutant cells do not have impaired apical-basal polarity (indicated with A-B). dMyc staining (red) is also shown; two clones are outlined (arrowed in A, left) as an example in which no increase in dMyc levels is observed. **B**: *lgl*$^{-/-}$; *dp110*$^{\mathrm{CAAX}}$; *Ras*RNAi clones (GFP^{+}) generated in a wild-type background (GFP^{-}) stained with aPKC (white) and MMP1 (red). No MMP1 expression is visible in mutant cells. MMP1 signal in the notum corresponds to a tracheal tube [197]. **C,D**: *lgl*$^{-/-}$; *hRaf*$^{\mathrm{GOF}}$ clones (GFP^{+}) generated in a wild-type background (GFP^{-}). C: aPKC (white) and dMyc (red) staining: Z projection shows that loss of cell polarity accompanies the overgrowth of these clones (the apical-basal axis of the disc proper is shown); increased expression of dMyc is visible in mutant clones regardless of the region they are located. D: aPKC (white) and MMP1 (red) staining, high levels of MMP1 are associated to *lgl*$^{-/-}$; *hRaf*$^{\mathrm{GOF}}$ clones. **E,F**: *lgl*$^{-/-}$; *hRaf*$^{\mathrm{GOF}}$; *Ras*RNAi clones (GFP^{+}) generated in a wild-type background (GFP^{-}). In E loss of apical-basal cell polarity (aPKC staining, white, in the Z projection) and dMyc upregulation (red) are observable in mutant tissue all across the disc. F: MMP1 staining, both in distal (arrowhead) and in proximal (arrow) clones MMP1 production is evident; wing disc is outlined. Apical-basal polarity of the wing disc proper is indicated in the Z projections. All images are 400x.

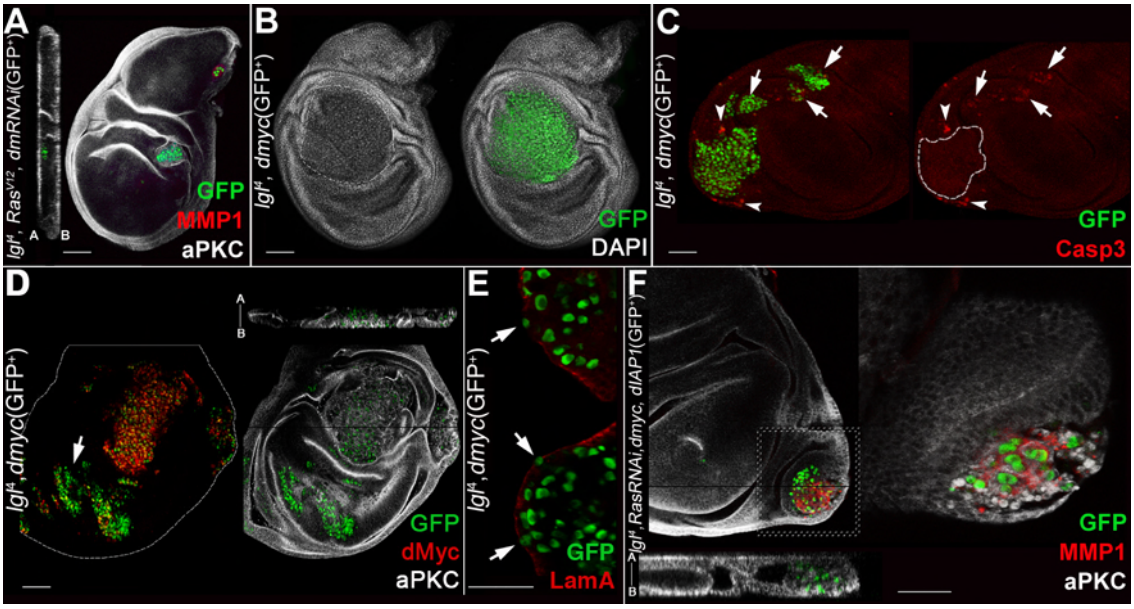

Figure 3.13: **A**: *lgl*$^{-/-}$; *Ras*^{V12}; *dmyc*RNAi clones (GFP^{+}) generated in a wild-type background (GFP^{-}). aPKC staining (white) indicates that mutant cells are not impaired in apical-basal polarity as can be observed in the Z projection. No positivity in MMP1 staining (red) is detected in these cells. **B-E**: *lgl*$^{-/-}$; *dmyc* clones (GFP^{+}) in a wild-type background (GFP^{-}). B: clone morphology, DAPI marks nuclei. C: active-Caspase 3 and dIAP1 staining; the arrows indicate groups of mutant cells undergoing autonomous apoptosis and the arrowheads indicate wild-type cells dying outside a mutant clone. D: dMyc and aPKC staining; the projection along the Z axis shows loss of cell polarity; the multilayered nature of the epithelium inside the mutant clone is also visible. The arrows indicate clones in the wing pouch that show low levels of dMyc protein. E: Laminin A staining; the arrows indicate regions of discontinuity. Wing disc is outlined in D. **F**: *lgl*$^{-/-}$; *dmyc*; *dIAP1*; *Ras*RNAi clones (GFP^{+}) in a wild-type background (GFP^{-}). aPKC staining reveal impairments in cell polarity (Z projection) and discontinuities in the epithelial sheath (see magnification of the region outlined). MMP1 antibody positively stains mutant cells as visible in the red channel. The apical-basal axis of the disc proper is indicated in all Z projections. Scale bars are 35 micron.

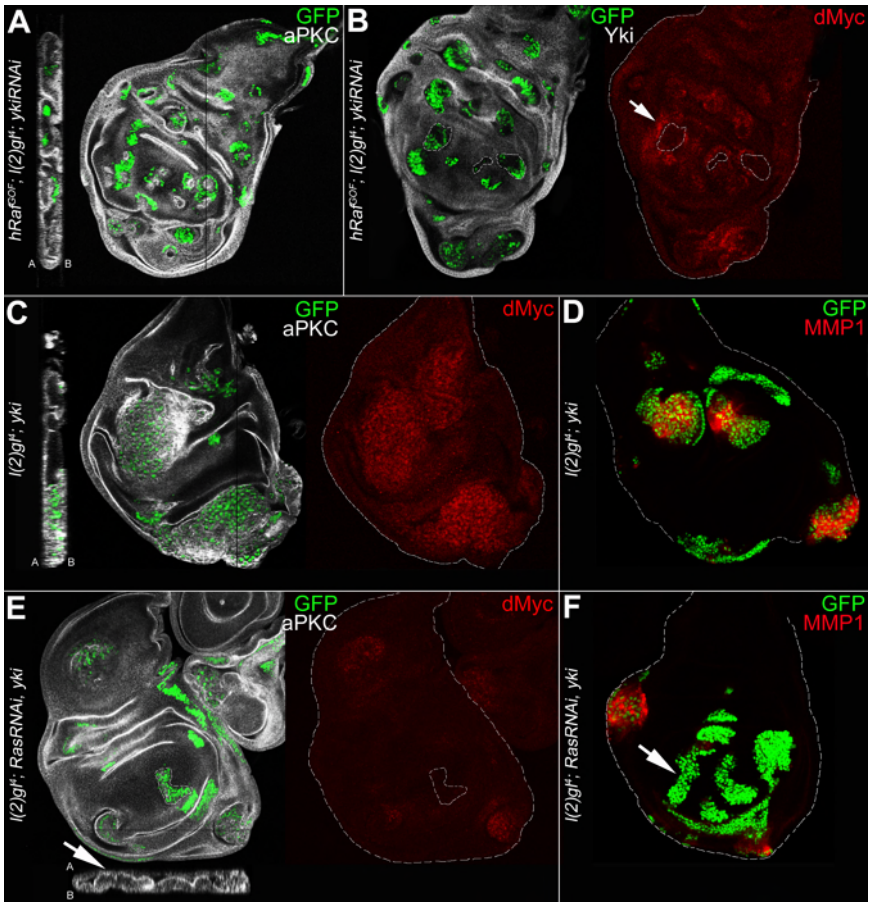

Figure 3.14: **A,B**: *lgl*$^{-/-}$; *hRaf*$^{\mathrm{GOF}}$; *Yki*RNAi clones (GFP^{+}) generated in a wild-type background (GFP^{-}). A: aPKC staining: as can be observed in the Z projection aPKC is correctly localised to the apical surface of mutant clones in all regions of the disc. B: Yki (white) and dMyc (red) staining; a few clones in the wing pouch are outlined as an example which show low levels of dMyc, the arrow indicates an enrichment of this latter in the wild-type tissue at the clonal border. **C,D**: *lgl*$^{-/-}$;*Yki* clones (GFP^{+}) generated in a wild-type background (GFP^{-}). In C loss of cell polarity, as indicated by aPKC staining, as well as multilayered growth are clearly visible in the Z projection. dMyc staining is also shown in red: mutant clones express high levels of the protein. D: MMP1 expression is high in clones grown in the proximal regions. **E,F**: *lgl*$^{-/-}$; *Yki*; *Ras*RNAi clones (GFP^{+}) generated in a wild-type background (GFP^{-}). E: aPKC (white) and dMyc (red) staining. Correct apical-basal polarity is maintained in distal mutant clones as shown in the Z projection (the arrow indicates the position of the GFP^{+} cells). A clone in the wing pouch is outlined which shows a wild-type morphology and no upregulation of dMyc. In F, the arrow indicates a clone in the wing pouch that does not express MMP1 and has a wild type morphology; MMP1 signal is observable in proximal clones. The apical-basal axis of the disc proper is indicated in all Z projections. All images are 400x.

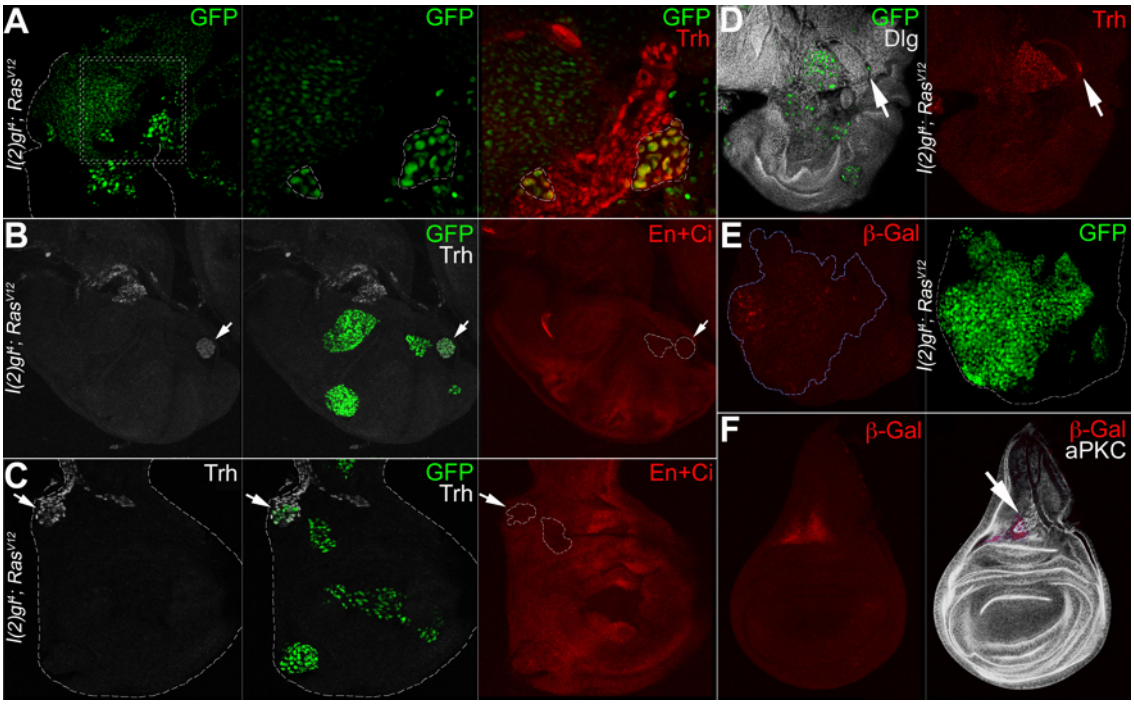

Figure 3.15: **A-D**: $lgl^{-/-}$; Ras^{V12} clones (GFP^{+}) generated in a wild-type background (GFP^{-}). A-D: Trh staining. In A, the basal section and relative magnification of a disc in which mutant cells (outlined) express Trh and are in contact with the tracheal segment are shown. Similar interactions are also shown in C (the arrow indicates a Trh-positive mutant clone contacting a tracheal branch) and D (the arrow indicates the tracheal segment). In B a Trh-positive clone not interacting with tracheal tubes is indicated by the arrow. Staining with En and Ci (both red) in B and C shows that the Trh-positive clone (outlined and arrow) express Ci similarly to an adjacent Trh-negative clone (outlined). Wing disc is outlined in A and C. **E**: $lgl^{-/-}$; Ras^{V12} clones (GFP^{+}) generated in *bnl-LacZ* individuals. Many cells in the mutant clone (outlined) are positive to β-Gal staining indicating that the FGF/Bnl promoter is active. **F**: β-Gal (red) and (aPKC) staining of *bnl-LacZ* wing discs: endogenous FGF/Bnl is produced in a limited area located in the notum, in proximity of which the air sac develops (arrow). All images are 400x except for magnification in A.

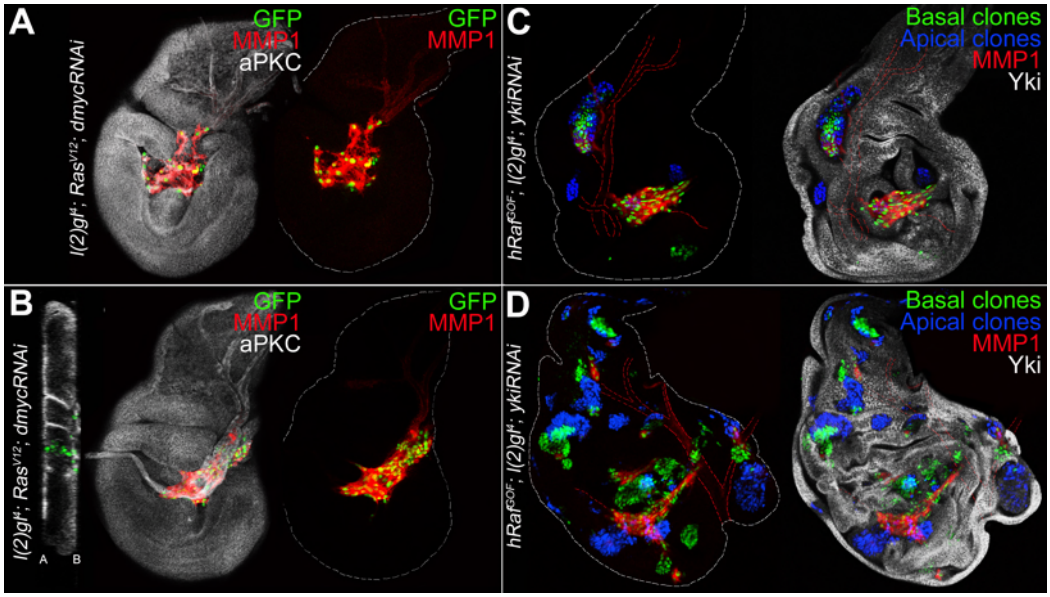

Figure 3.16: **A,B**: *lgl*$^{-/-}$; *Ras*^{V12}; *dmyc*RNAi clones (GFP^{+}) generated in a wild-type background (GFP^{-}). aPKC (white) and MMP1 (red) staining in basal sections of the disc are shown. Mutant cells are clearly interconnected with the tracheal segments and show high levels of MMP1 (less intense staining is also visible in GFP-negative tracheae). In B a Z projection resulting from superimposition of several Z stacks is shown in which continuity between the apical and the basal GFP^{+} cells is appreciable. Apical-basal polarity of the wing disc proper is also shown. **C,D**: *lgl*$^{-/-}$; *hRaf*^{GOF}; *Yki*RNAi clones (GFP^{+}) generated in a wild-type background (GFP^{-}). Superimposition of a basal (clones in green) and an apical (clones in blue) section of the disc (outlined) is shown. Stainings are: Yki (white, apical) and MMP1 (red, basal). Basal clones are coplanar with the tracheal branches (outlined in red). In A-D wing discs are outlined. All images are 400x.

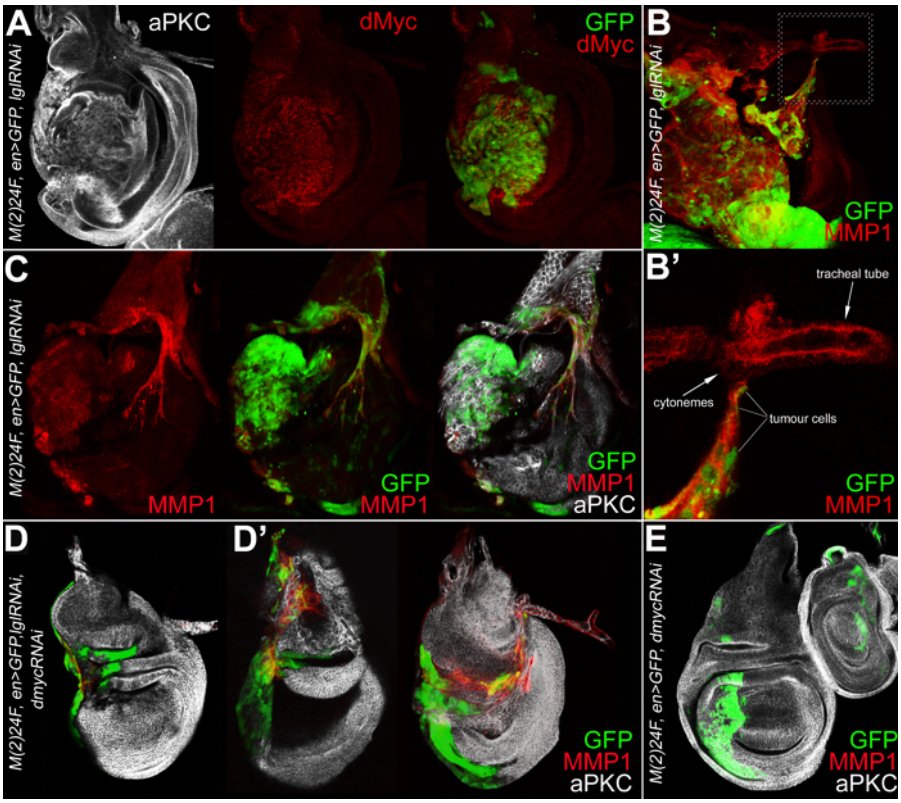

Figure 3.17: **A,C**: *lgl*RNAi expression in the posterior compartment (GFP^+) of $M^{+/-}$ wing discs. A: aPKC (white) and dMyc (red) staining. The compartment overgrowth is accompanied by loss of tissue architecture and dMyc accumulation. B: MMP1 staining reveals interactions between mutant cells and tracheal tubes, the outlined region is magnified in B'. C: *lgl*-deprived cells form tracheal-like structures; stainings are MMP1 (red) and aPKC (white). **D,D'**: *lgl*RNAi, *dmyc*RNAi expression in the posterior compartment (GFP^+) of $M^{+/-}$ wing discs. In D an apical section is shown in which a reduction in compartment size is evident, in D' MMP1 staining (red) shows that mutant cells migrate towards and contact tracheal segments; aPKC staining (white) is also shown. **E**: *dmyc*RNAi expression in the posterior compartment (GFP^+) of $M^{+/-}$ wing discs. No major alterations in disc morphology are visible as indicated by aPKC and MMP1 staining, white and red respectively. All images are 400x, except for magnification in B'. The experiments shown in this Figure have been carried out by Elisabetta Fontana, an undergraduate student in our lab.

	Roundness§		BM degradation		A/B polarity loss		dMyc expression	
	D	P	D	P	D	P	D	P
wild-type	0.42	0.47	no	no	no	no	~	~
lgl⁻	0.30	0.50	no	no	no	no	↓	~
Ras^{V12}	0.70	0.69	no	no	no	no	Ref [92]	
lgl⁻, Ras^{V12}	0.82	0.74	yes	yes	yes	yes	↑↑	↑↑
lgl⁻, hRaf^{GOF}	0.78	0.75	yes	yes	yes	yes	↑↑	↑↑
lgl⁻, hRaf^{GOF}, RasRNAi	0.66	0.76	yes	yes	yes	yes	↑↑	↑↑
lgl⁻, dp110^{CAAX}	0.34	0.45	no	no	no	no	~	~
lgl⁻, dp110^{CAAX}, RasRNAi	0.27	0.38	no	no	no	no	-	-
lgl⁻, myc	0.52	0.75	yes	yes	yes	yes	↑	↑↑
lgl⁻, myc, RasRNAi	0.31	0.65	no	yes	no	yes	-	-
lgl⁻, myc, dIAP1	0.65	0.69	no	yes	-	yes	-	-
lgl⁻, myc, dIAP1, RasRNAi	0.34	0.72	no	yes	no	yes	-	-
lgl⁻, hRaf^{GOF}, YkiRNAi	0.38	0.60	no	no	no	no	~	~
lgl⁻, Yki	0.69	0.74	v	yes	v	yes	v	↑↑
lgl⁻, Yki, RasRNAi	0.52	0.67	no	yes	no	yes	~	↑

§ roundness = 1 for perfect circles
↑ increased
↑↑ highly increased
~ comparable to surrounding tissue
- not determined
v variable

Figure 3.18: Summary of the neoplastic traits analysed for the genotypes discussed in Section 3.2. Note that roundness is a parameter of non-wild-type shape and characterises both hyperplastic and neoplastic growth. Detailed description in given in the text. BM, basement membrane; A/B, apical/basal.

Chapter 4

Conclusions and Perspectives

Deciphering the molecular crosstalk occurring between genetically different cell populations growing within a tissue is relevant to both developmental and cancer biology. A world of intimate and extensive interactions between transformed and normal cells has been unveiled in the past decades and has revolutionised the field of cancer biology. Much has been done towards the understanding of how the tumour microenvironment promotes and sustains tumour development whilst very little is known about possible safe-guard mechanisms that might counteract cancer development. Due to the conservation of signalling pathways involved in cell growth, cell proliferation and cell death between fly and humans, *Drosophila* represents an ideal system for analysing the early events occurring in tumourigenesis upon the confrontation of different cell populations.

In *Drosophila*, *lgl* mutant larvae show neoplastic overgrowth of the epithelial tissues, whereas $lgl^{-/-}$ cells growing in mosaic larvae are usually eliminated by cell death; thus this opposite phenotype results from mechanisms triggered by the confrontation of lgl^{-} and lgl^{+} cells. In literature, two main processes have been described to mediate the elimination of unfit/polarity-deficient cells from *Drosophila* imaginal epithelia: Cell Competition (Section 1.4.3) and Intrinsic Tumour Suppression (ITS) (Section 1.2.1.2). Both mechanisms work by the induction of cell death in the mutant population; in addition, in the first one normal tissue grows at the expense of the unfit cells. There is suggestive evidence in literature regarding the relevance of cell competition to cancer biology 1.4.3.2, however a clear connection between cell competition and tumour development is yet to be made.

dMyc oncoprotein has been shown to play a leading role in cell competition:

cells bearing low levels of this protein die by apoptosis if growing in a high dMyc-expressing context [148, 171]. In ITS, cell death is instead triggered in the presence of cells with impaired polarity in an otherwise normal epithelium [61]. I found that JNK-mediated apoptosis is the main process through which *lgl* mutant clones are eliminated from imaginal wing epithelia. Clonal phenotype is however different in the distal (wing pouch) and proximal (hinge/pleura) regions of the wing disc: *lgl* mutant clones located in the wing pouch showed massive cell death and were rapidly extruded from the epithelium, while clones located in the hinge/pleura grew to a larger extent, although they never formed tumours. This regional difference in clonal behaviour could depend on dMyc protein pattern in the wing disc; the protein is highly expressed in the wing pouch and very low in the hinge/pleura. Indeed $lgl^{-/-}$ clones in the wing pouch expressed very low levels of dMyc protein relative to the background; such clones died and were replaced by the surrounding wild-type tissue. Moreover, $lgl^{-/-}$ clonal behaviour in the slow-dividing *Minute* background or in the follicular epithelium switched from "outcompeted" to "overgrown and invasive", with the tumourous mutant clone invariantly showing high dMyc levels relative to the neighbouring tissue. Lowering dMyc abundance inside those clones prevented the tumourous phenotype, whereas dMyc overexpression in *lgl* mutant clones in a wild-type background was able to confer increased proliferation, survival and invasive properties clearly demonstrating that dMyc plays a key role in $lgl^{-/-}$ cells behaviour. Notably, dMyc effect on *lgl* clonal behaviour seems very specific as activation of a growth-promoting pathway that however failed to increase dMyc levels within mutant cells, such as PI3K, was unable to promote their neoplastic growth. I also showed that ITS is not responsible for *lgl* mutant cells elimination in the wing pouch, in contrast to what was observed for the other two neoplastic tumour suppressor mutants *scrib* and *dlg* [61]; $lgl^{-/-}$ clones located in the distal regions still died even upon ITS inhibition. On the other hand, its blockade in *lgl* mutant tissue located outside of the wing pouch resulted in clonal overgrowth (accompanied by dMyc upregulation), indicating that ITS and cell competition are likely to be involved in the elimination of *lgl* mutant cells in complementary regions.

This is first evidence that cell competition functions as a tumour suppressive mechanisms in preserving epithelial integrity in *Drosophila*. Besides a well established role in favouring expansion of cells with supercompetitive abilities at the expenses of the surrounding tissue, it also serves the elimination of damaged and

potentially harmful cells before they acquire additional oncogenic mutations.

Several reports have been published that confirmed that polarity-deficient cells are subject to cell competition, both in *Drosophila* [82, 83, 180] and mammalian epithelia [180, 181]. Indeed, inducible cell culture systems have been employed to demonstrate that such non-cell autonomous phenomenon is conserved. Tamori and colleagues knocked down the Lgl interactor Mahjong (that they proved to be involved in *lgl*-mediated cell competition in *Drosophila*) in Madin-Darby canine kidney epithelial cells and showed that Mahjong-deficient cells undergo apoptotic cell death only when surrounded by wild-type cells [180]. Similar results were obtained by Norman and colleagues upon *scrib* knockdown in the same cell line: the authors demonstrated that while Scrib^{KD} cells were viable when surrounded by cells of the same kind, they died and were apically extruded in presence of Scrib^{WT} cells. In addition, in a murine model of familial polyposis, APC^{-} cells deprived of *c-Myc* were out-competed by surrounding, *c-Myc*-expressing wild-type cells, thereby reverting the malignant phenotype, suggesting that Myc-induced cell competition could play a role in mammalian carcinogenesis [182]. Hence, given the high degree of conservation of these processes and of the molecules involved, the results I showed are likely to be relevant to human cancer biology.

The work I presented also demonstrates that dMyc protein not only affects the ability of $lgl^{-/}$ to overcome tissue constraints and avoid elimination, but also influence the behaviour of mutant cells in later phases of tumour development. High levels of the oncoprotein were indeed found to be associated with neoplastic behaviour induced by the cooperation between *lgl* loss of function and activated Ras signalling and reduction of dMyc abundance abolished clonal expansion of mutant cells.

Ras cooperation with *lgl* mutation resulted in massive overgrowth of mutant tissues accompanied by loss of cell polarity and invasive behaviour indicated by the secretion of basement membrane-degrading enzymes. These phenotypes were found to be dependent on the activation of the Ras effector Raf/MAPK pathway. Expression of a constitutively active form of Raf kinase in *lgl* mutant cells fully recapitulated the phenotypes observed in $lgl^{-/-}$; Ras^{V12} clones, including dMyc upregulation, even when upstream Ras signalling was completely abolished by co-expression of a *Ras*RNAi construct. On the other hand, despite its role in promoting cell growth,

constitutive activation of PI3K failed to induce overgrowth and invasiveness of *lgl* mutant cells. Notably no dMyc upregulation was observed in *lgl*$^{-/-}$; *dp110*^{CAAX} clones. Since activated PI3K signalling has been shown to increase dMyc levels in a transient manner (see Section 1.4.2, [92, 166]), this might indicate that dMyc protein must be stably upregulated in *lgl* mutant clones in order to trigger overgrowth; this mirrors the condition observed in many human cancers, where Myc protein is highly and stably overexpressed [134]. Consistently, constitutive *dmyc* expression was sufficient to promote *lgl* mutant cells neoplastic growth in those regions of the epithelium where accumulation of the protein occurred (hinge and pleura); conversely, in the distal region of the wing disc, *dmyc* transcriptional overexpression did not result in a consistent increase in protein abundance and tumorous traits failed to appear in these clones. Similar restriction of *dmyc* post-transcriptional accumulation in the wing pouch was also observed for *lgl*$^{-/-}$ clones generated both in a wild-type and *Minute*$^{+/-}$ background. *lgl* loss of function might therefore interfere with *dmyc* mRNA stability or translation or might block the activity of molecules that enhance dMyc protein stability or promote that of pathways involved in dMyc degradation. Further work is required to address this issue.

Whatever the mechanism of *lgl* LOF-dependent post-transcriptional downregulation of dMyc is, constitutive activity of the Ras/Raf/MAPK pathway is able to counteract it. *lgl*$^{-/-}$; *Ras*^{V12} or *lgl*$^{-/-}$; *hRaf*^{GOF} clones in the wing pouch were indeed able to overgrow and form large masses of neoplastic tissue in which high levels of dMyc were observed. Post-transcriptional stabilisation of dMyc by activated Erk may thus be sufficient to ensure high levels of the oncoprotein despite the *lgl*LOF-dependent destabilisation effect; in alternative this latter might be somehow abolished by the activation of Ras/Raf/MAPK.

The elevated levels of dMyc observed in *lgl* mutant clones with constitutive Ras/Raf/MAPK activity, besides being due to post-transcriptional regulation of the protein, also depend on increased transcription of *dmyc* gene. Loss of function of *lgl* and *scrib* has been demonstrated to lead to the deregulation of the Hpo pathway (Sections 1.2.1.2 and 1.2.2) and activation of the transcriptional co-factor Yki (indicated by its nuclear localisation) was observed in both in *lgl*$^{-/-}$; *Ras*^{V12} and *scrib*$^{-/-}$; *Ras*^{V12}. As we recently demonstrated [156], *dmyc* is a Yki transcriptional target and I was able to show that knockdown of Yki levels in *lgl*$^{-/-}$; *hRaf*^{GOF} clones (which also displayed Yki nuclear enrichment) dramatically reduced dMyc levels suggesting that

Yki-dependent transcriptional upregulation of *dmyc* is required for elevated dMyc levels to accumulate in *lgl* mutant cells with activated Ras/Raf/MAPK signalling. Reduction of Yki in *lgl*$^{-/-}$; *hRaf*$^{\mathrm{GOF}}$ clones also abolished their neoplastic behaviour indicating that deregulation of Hpo pathway, also by virtue of is positive effect on dMyc levels, plays a key role in the oncogenic cooperation model here analysed. Surprisingly however, overexpression of a wild-type form of Yki failed to increase dMyc abundance above wild-type levels in the majority of *lgl*$^{-/-}$ clones grown in the wing pouch, leading to the speculation that increased post-transcriptional stabilisation by Ras/Raf/MAPK signalling may play a key role in allowing dMyc accumulation in this region. Accordingly, silencing of endogenous Ras signalling in *lgl*$^{-/-}$; *Yki* clones completely reverted clonal phenotype in the wing pouch and reduced growth and dMyc upregulation even in the distal territories. It is however also possible that *lgl* mutation in the wing pouch is not able to deregulate the Hpo pathway due to competitive stress as it has been demonstrated for *scrib* LOF clones [83] and thus even if overexpressed, a substantial fraction of Yki pool might still be phosphorylated and sequestered in the cytoplasm, impeding its transcriptional activity. Nevertheless, consistent with dMyc levels of these clones being comparable to those of the surrounding tissue in the wing pouch, neoplastic behaviour was not triggered in *lgl*$^{-/-}$; *hRaf*$^{\mathrm{GOF}}$; *Yki*RNAi nor in *lgl*$^{-/-}$; *Yki*; *Ras*RNAi indicating that both pathways are required in this region for *lgl* cells to acquire malignant features.

I can therefore conclude that when dMyc is highly expressed it cooperates with *lgl* loss of function in a cell-autonomous manner, driving malignant growth in different contexts and organs; when dMyc levels in *lgl*$^{-/-}$ tissue are comparable to those of the wild-type surrounding cells, the two populations "peacefully" coexist and no major alterations of epithelial integrity occur; where dMyc protein abundance is lower in the *lgl* mutant cells with respect to the surrounding tissue, these cells undergo apoptotic cell death and are eliminated by cell competition.

Given the high incidence of dMyc upregulation in human cancers, understanding how this key molecule is regulated in the process of transformation and how it influences the crosstalk with the tumour microenvironment represents an important goal in the field of molecular oncology. As shown in this work, the employment of a genetically tractable model like *Drosophila*, that closely recapitulates the features of human carcinogenesis, may help gain insight into the complex biology of Myc oncoproteins.

Interestingly, from the analysis presented in this thesis a novel aspect of the oncogenic cooperation between *lgl* loss of function and activated Ras signalling has emerged: tumorous cells have been found to interact with the tracheal tubes, the organs which supply larval tissues with oxygen, and to produce the diffusible factor, FGF, that stimulate tracheogenesis and tracheal cells migration. Further analysis is required to better characterise this phenomenon; nevertheless given the similarities, it is possible to speculate that it might represent a process analogous to that of mammalian tumour-associated angiogenesis. It is indeed well known that cancer cells produce pro-angiogenic factors that stimulate the blood vessels in order to vascularise the growing tumorous mass. In imaginal wing disc cells, hypoxia triggers cellular responses very similar to those of mammalian epithelial cells (Section 1.3.2), it is therefore plausible that also in the fly, cells within an expanding mass may sense oxygen deprivation and trigger cellular responses that promote the interaction with the respiratory system.

Extensive crosstalk with tracheal tubes was also observed in another genetic model of *lgl* deprivation-induced tumourigenesis. With this system, the sole knockdown of *lgl* in the posterior compartment of the imaginal wing disc in individuals in which larval life is extended is sufficient to drive a severe neoplastic growth as cell competition is avoided and tumour development is allowed to progress longer in time. In this context large clusters of tumorous cells invariantly migrate towards and contact tracheal segments, indicating that this interaction may also depend on an active movement of cancer cells towards the oxygen source. The fact that interaction between mutant cells and the tracheal system is clearly evident also in this genetic system may indicate that it does not depend on active Ras signalling but is instead a feature of *lgl*-deprived cells that are allowed to grow and acquire neoplastic traits. Surprisingly, while elevated dMyc levels are required for the growth of *lgl*-deprived cells and are consistently associated with increased clone size and defects in apical-basal cell polarity, dMyc seems to be dispensable for their interaction with the tracheal network as in both the genetic contexts analysed knockdown of *dmyc* did not affect the ability of cells to migrate towards tracheal tubes.

Further to interacting with the tracheal system, I also showed that $lgl^{-/-}$; Ras^{V12} clones can express the tracheal fate determinant, Trachealess. This interesting finding opens the possibility that a trans-differentiation occurs in some mutant cells.

In human cancers such phenomenon has been attributed to the multipotent cancer stem cells which produce high levels of pro-angiogenic factors and trans-differentiate into different cell types including endothelial cells to form a vascular-like structure that supplies oxygen and nutrients to the tumour before the normal vasculature is recruited (see Section 1.1). Further analysis of this phenomenon in the oncogenic model here presented may help shed light on these still poorly characterised events in human carcinogenesis.

As described in Section 1.2.2 many of the hallmarks of cancer have been faithfully recapitulated in the cooperative oncogenesis models in *Drosophila*. The preliminary data described above seem to indicate that also the strategies that cancer cells enforce to overcome oxygen deprivation may be profitably investigated in this model animal.

Appendix

Preliminary Studies in Human Cells

Introduction

The results presented in this thesis clearly highlight the importance of dMyc regulation in *lgl*-induced tumourigenesis, even in the context of the oncogenic cooperation with activated Ras.

Given the high degree of conservation of the signalling pathways involved in these events (see Chapter 1), it is likely that similar genetic interactions also take place in mammalian cells. To test this hypothesis I aimed to analyse the relationship between Lgl-1/2, Myc and Ras in a human epithelial cell line: MCF10A.

MCF10A are immortalised, non-transformed mammary epithelial cells that, if cultured in reconstituted basement membrane (3D culture), recapitulate many features of mammary epithelium *in vivo* such as the formation of acini with a hollow lumen and an evident apical-basal polarisation [198]. These organotypic cultures are therefore a system of election for the analysis of the effect of tumour-inducing mutations on epithelial architecture.

Indeed, *Scrib* knockdown ($Scrib^{KD}$) was shown to cooperate with both Ras and c-Myc in 3D cultured MCF10A [71, 199]. As reported in Section 1.2.2, $Scrib^{KD}$; Ras^{V12} acini display an invasive behaviour with the projection of protrusions in the basement membrane [71]. On the other hand, $Scrib^{KD}$ seems to suppress the high levels of cell death induced by c-Myc in the same cell system [199].

Overexpression of Scrib is able to suppress most of Ras^{V12} induced phenotypes both in 2D and 3D cultured MCF10A [71]. Interestingly, knockdown of Lgl-1 or Lgl-2 is able to bypass Scrib-mediated suppression of Ras^{V12} transforming capabilities in these acini (Patrick Humbert, personal communication). This demonstrates that Lgl-1/2 can cooperate with oncogenic Ras also in human epithelial cells.

To test whether c-Myc plays a role in this oncogenic cooperation, as it does in *Drosophila* imaginal wing disc epithelium, I decided to employ the commercially-available low molecular weight Myc inhibitor 10058-F4. 10058-F4 is a cell-permeable thioxothiazolidinone compound that specifically inhibits the c-Myc-Max interaction, thereby preventing the transactivation of c-Myc target genes [200]. Treatment of Lgl-1/2^{KD}; Ras^{V12}-expressing acini could help clarify whether c-Myc is necessary to promote tumourigenesis downstream of Lgl-1/2 loss in human cells.
I thus tested the efficacy of c-Myc inhibitor in 2D and 3D cultured MCF10A and found that, while 10058-F4 efficiently blocks proliferation and c-Myc target genes expression in monolayer-grown MCF10A, even in a c-Myc-overexpressing context, its effects are ambiguous on acini grown on Matrigel. It will therefore be necessary to better characterise 10058-F4 activity on MCF10A acini or to device alternative strategies in order to test this hypothesis.

Results

Lgl1-2 KD Affects Myc Levels in MCF10A

To investigate if Lgl-1 and/or Lgl-2 knockdown affects c-Myc (hereafter referred as Myc) levels in MCF10 cultured as a monolayer (2D) I transiently transfected them with a pool of siRNAs (short interfering RNAs) against Lgl-1, Lgl-2 or both. Transfection of siRNAs against GFP was used as a control.

qRT-PCR showed that while Lgl-1 mRNA was reduced by 64% relative to the transfection control (Fig IA), knockdown of Lgl-2 was less efficient and mRNA levels were reduced by 24% only (Fig IB). Interestingly some compensatory mechanisms might occur since silencing of one gene induced increased mRNA levels of the other (Fig. IA-B). Simultaneous knockdown of Lgl-1 and Lgl-2 led to a significant reduction of Lgl-1 mRNA abundance and abrogated the compensatory effect of Lgl-1 knockdown on Lgl-2 mRNA which levels were brought back to control levels (Fig IA-B).

As can be observed in Fig IC, in Lgl-1 depleted cells Myc mRNA levels are significantly higher than in control transfected cells and this increase is even more pronounced upon Lgl-2 knockdown. This effect does not seem to be due to the

reciprocal compensatory effect since higher Myc mRNA levels are also observed upon simultaneous Lgl-1 and Lgl-2 silencing where mRNA levels of both genes are equal to or lower than in control transfected cells.

The effect of Lgl-1 and/or Lgl-2 depletion on Myc is also observed at protein level. As essayed by western blot on whole cell lysates of siRNA transfected cells, Myc is significantly upregulated with respect to the control (see Fig. ID).

Since Myc mRNA and protein levels were assayed in asynchronously cycling cells, the effect is likely to be underestimated.

This data indicate that perturbation of Lgl-1 and Lgl-2 expression levels, even to a low extent as for Lgl-2, affects Myc mRNA and protein abundance. It is thus possible that the genetic interactions between *lgl* and dMyc in *Drosophila* reported in this thesis are conserved in MCF10A. It will be interesting to test whether these effects are mediated by similar pathways.

10058-F4 Efficiently Inhibits Myc Activity in 2D Cultures

To test whether 10058-F4 is able to knockdown Myc activity in MCF10A, I treated 2D cultured cells with increasing concentrations of the inhibitor and 24 hours post treatment I assayed proliferation levels by staining for the mitotic marker KI67. As can be observed in Fig. IIA treatment with 10058-F4 led to a severe concentration-dependent inhibition of proliferation. Representative stainings are reported in Fig IIB. Cells treated with 120μM inhibitor present pycnotic nuclei indicating at this concentration 10058-F4 might have a toxic effect. 60-120μM is the widely reported effective concentration range in literature [200–202] and 60μM was thus chosen as the starting point. It indeed reduced KI67-positive nuclei of over 60%; it is however possible that lower concentrations could still be effective in this context.

10058-F4 efficacy was confirmed by qRT-PCR of Myc target genes (Fig. IIC). In 2D cultured MCF10A, 24 hours post treatment with 60μM and 80μM 10058-F4, Myc target genes are specifically downregulated in a concentration dependent manner. B2M (β2 microglobulin), a house keeping gene, was used as a control and its mRNA levels did not vary upon inhibitor treatment. Consistently with other reports [201, 203], Myc mRNA also was found to be affected by 10058-F4.

To further asses 10058-F4 specificity I generated a cell line stably expressing an inducible form of Myc, Myc:ER. Myc:ER is a fusion of Myc and the oestrogen receptor ligand-binding domain. Upon induction with 4-hydroxytamoxifen (4-OHT) MYC:ER fusion protein can transactivate Myc target genes [204, 205]. The cell line produced expresses the fusion protein (not shown) and this latter is functional as treatment with 4-OHT can promote cell cycle re-entry and proliferation of Myc:ER expressing cells following 48 hours of starvation to a similar extent as serum/EGF stimulation does to starved control cells (Fig. IIIA-C). This is achieved at a concentration of 200nM 4-OHT and for higher concentrations no further effect is observed (Fig. IIIA). Noticeably, the percentage of KI67 nuclei in starved non-induced Myc:ER-expressing cells (EtOH treated) is higher than that of starved control cells indicating that some basal activity of the fusion protein is present even in the absence of 4-OHT induction (Fig. IIIA). Consistently with Myc:ER being functional, Myc transcriptional targets are specifically upregulated upon treatment with 200nM or 500nM 4-OHT (Fig. IVC).

Increasing concentrations of 10058-F4 drastically reduced proliferative rates of Myc:ER cells induced with 200nM 4-OHT (Fig. IVA-B) as well as mRNA levels of Myc transcription targets while it did not affect B2M expression (Fig. IVC). In this case no differences in Myc mRNA abundance can be detected as the mRNA highly transcribed downstream of Myc:ER heterologous promoter possibly masks differences in endogenous levels (Fig. IVC).

All together, these data demonstrate that 10058-F4 can efficiently and specifically interfere with Myc function in monolayer-grown MCF10A.

10058-F4 does not have specific effects in 3D cultures

Since 10058-F4 proved to be effective in inhibiting Myc activity in 2D-cultured MCF10A I tested its effects on differentiated acini grown on Matrigel. Differently from what was observed for monolayer-grown MCF10A, 10058-F4 at concentration of 60μM was toxic and completely inhibited acini formation (Fig.VA) indicating that cells grown in 3D are more sensitive to this chemical inhibitor.

I then performed a 10058-F4 titration on MCF10 acini. As can be observed in Fig.VA at day 4 of Matrigel culture treatment with 10μM and, more prominently, 20μM Myc inhibitor caused the formation of acini reduced in size. Similar observations where made at day 6 of culture (Fig. VA, lower panel). To investigate

whether this effect was specifically due to inhibition of Myc activity I analysed its target genes expression (Fig. VB). mRNA levels of Myc target genes did not seem to change in accordance to the phenotype observed. While BRCA-1 and BRCA-2 mRNA levels showed a significant decrease following 100nM and 500nM inhibitor treatment, they raised back to control levels for higher concentrations. CycD2 was not significantly affected at any inhibitor concentration. This might indicate that, at low concentrations, 10058-F4 is able to specifically interfere with the transcription of only some Myc targets without affecting overall acini size or morphology. On the other hand B2M and Myc mRNA levels show inconsistent fluctuations at the different concentrations of 10058-F4 and the reduction in size observed upon treatment with 10-20μM inhibitor does not seem to depend on a decrease of target genes mRNA, or at least of those tested, and thus might be a non-specific effect.

This data highlight the different sensitivity that MCF10A cells show towards treatment with 10058-F4 Myc inhibitor when cultured as a monolayer or as three-dimensional differentiated acini. Further analysis will be required to characterise the effect of this inhibitor on Matrigel-grown cells in order to be able to use it to specifically knockdown Myc activity in Lgl-1/2^{KD}; Ras^{V12} organotypic cultures. Alternatively stable cell lines simultaneously expressing Lgl-1/2^{KD}; Ras^{V12} and Myc^{KD} constructs could be generated for this purpose.

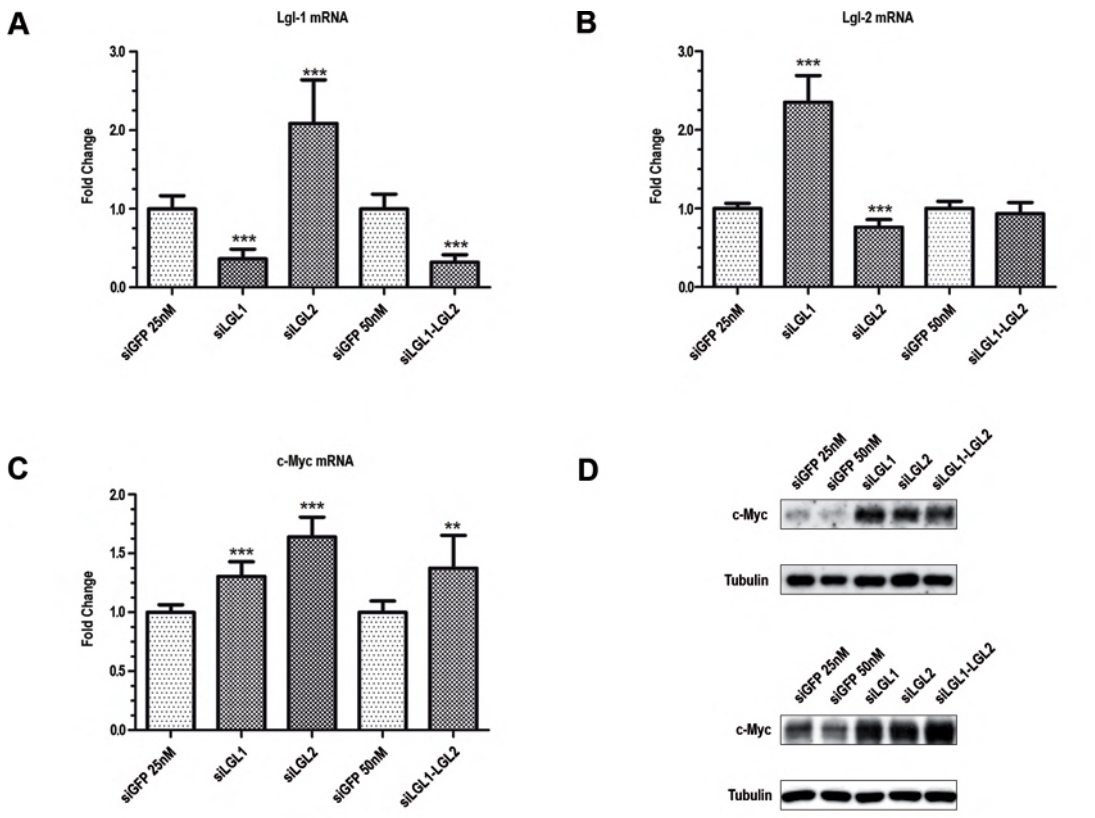

Figure I: A-C: qRT-PCR of Lgl-1 (A), Lgl-2 (B) and c-Myc (C) mRNA 72 hours post Lgl-1 and/or Lgl-2 specific siRNA pools transfection. mRNA levels are represented as the fold change relative to the appropriate control. Error bars represent the standard deviation of the mean for three independent experiments performed in triplicate. ***= $p<0.001$; **= $p<0.01$ (Student T-test). D: Western Blot analysis on whole cell lysates harvested 72 hours post Lgl-1 and/or Lgl-2 specific siRNA pools transfection. The results of two independent experiments are shown. α-Tubulin (Tubulin) was used as a loading control.

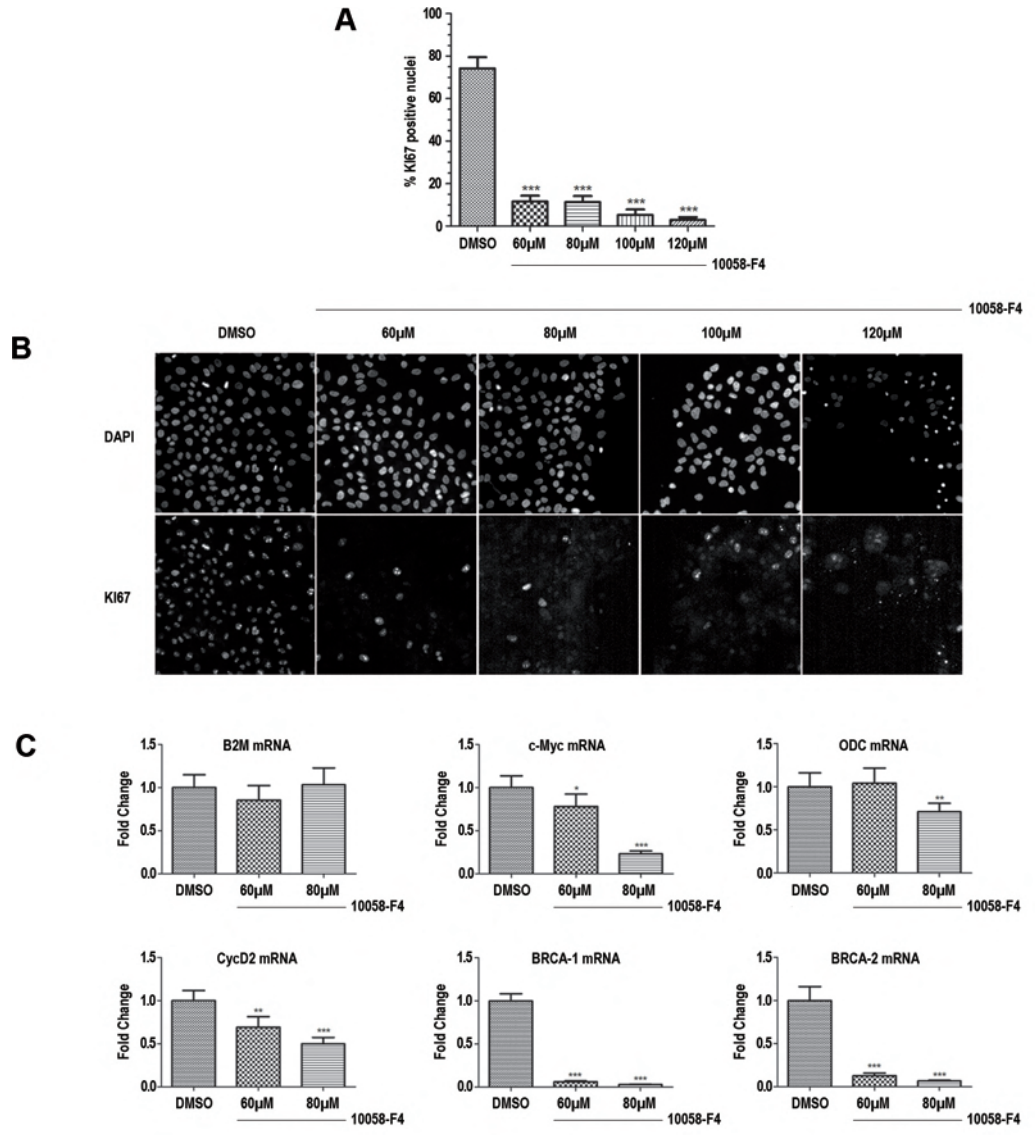

Figure II: A: Percentage of KI67-positive nuclei following 24 hours treatment with the indicated concentrations of 10058-F4 in 2D-cultured MCF10A. Error bars represent the standard deviation of the mean for two independent experiments performed in triplicate. ***= $p<0.001$ (Student T-test) relative to the carrier-only control (DMSO). B: Representative images of KI67 staining quantified in A, all nuclei are counterstained with DAPI. C: qRT-PCR of c-Myc target genes (http://www.myccancergene.org) upon 24 hours treatment with the indicated concentrations of 10058-F4. Error bars represent the standard deviation of the mean for two independent experiments performed in triplicate. ***= $p<0.001$; **= $p<0.01$; *= $p<0.05$ (Student T-test) relative to the carrier-only control (DMSO).

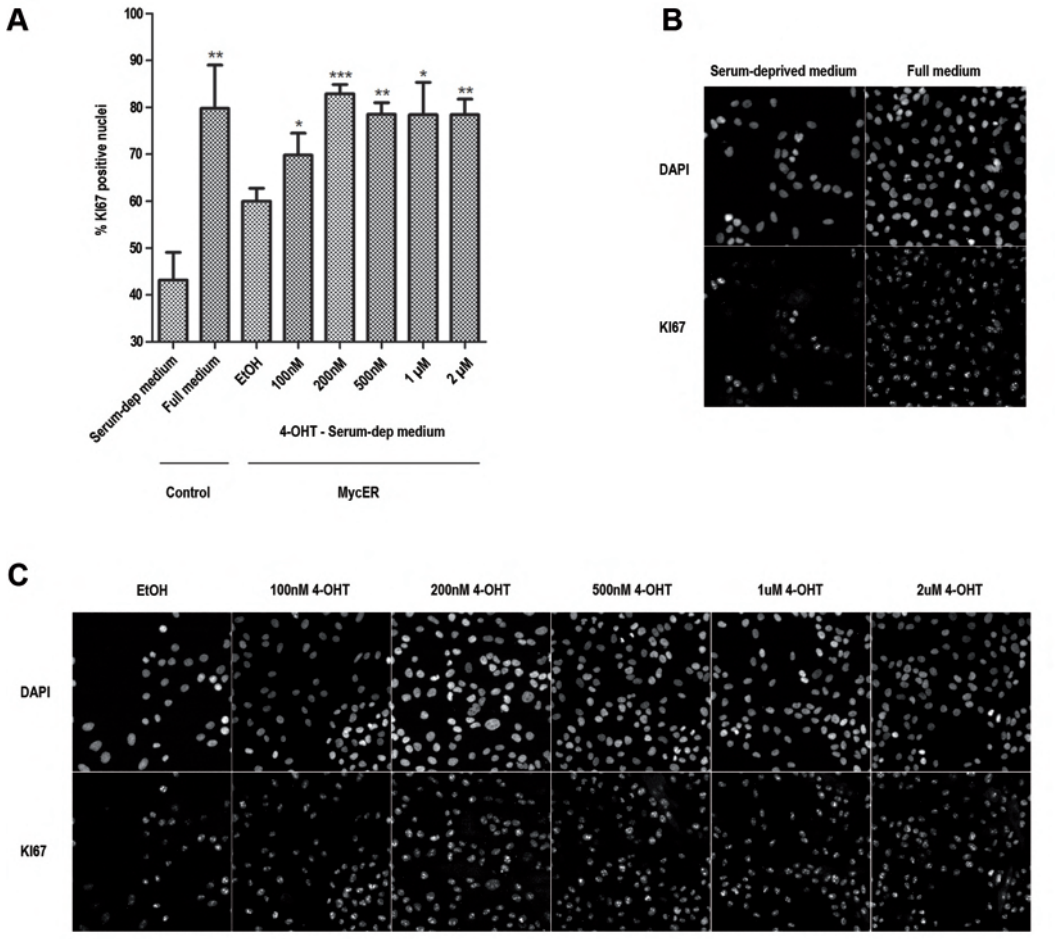

Figure III: A: Percentage of KI67-positive nuclei in 2D-cultured Myc:ER-expressing MCF10A upon 24 hours treatment with the indicated concentrations of 4-OHT in serum/EGF-deprived medium. Treatment of empty vector-expressing (control) cells with full medium after 48 hours starvation was used as a control. Error bars represent the standard deviation of the mean for two independent experiments performed in triplicate. ***= $p<0.001$; **= $p<0.01$; *= $p<0.05$ (Student T-test) relative to the carrier-only control (EtOH). B-C: Representative images of KI67 staining quantified in A of control (B) and Myc:ER-expressing (C) cells following the indicated treatment. All nuclei are counterstained with DAPI.

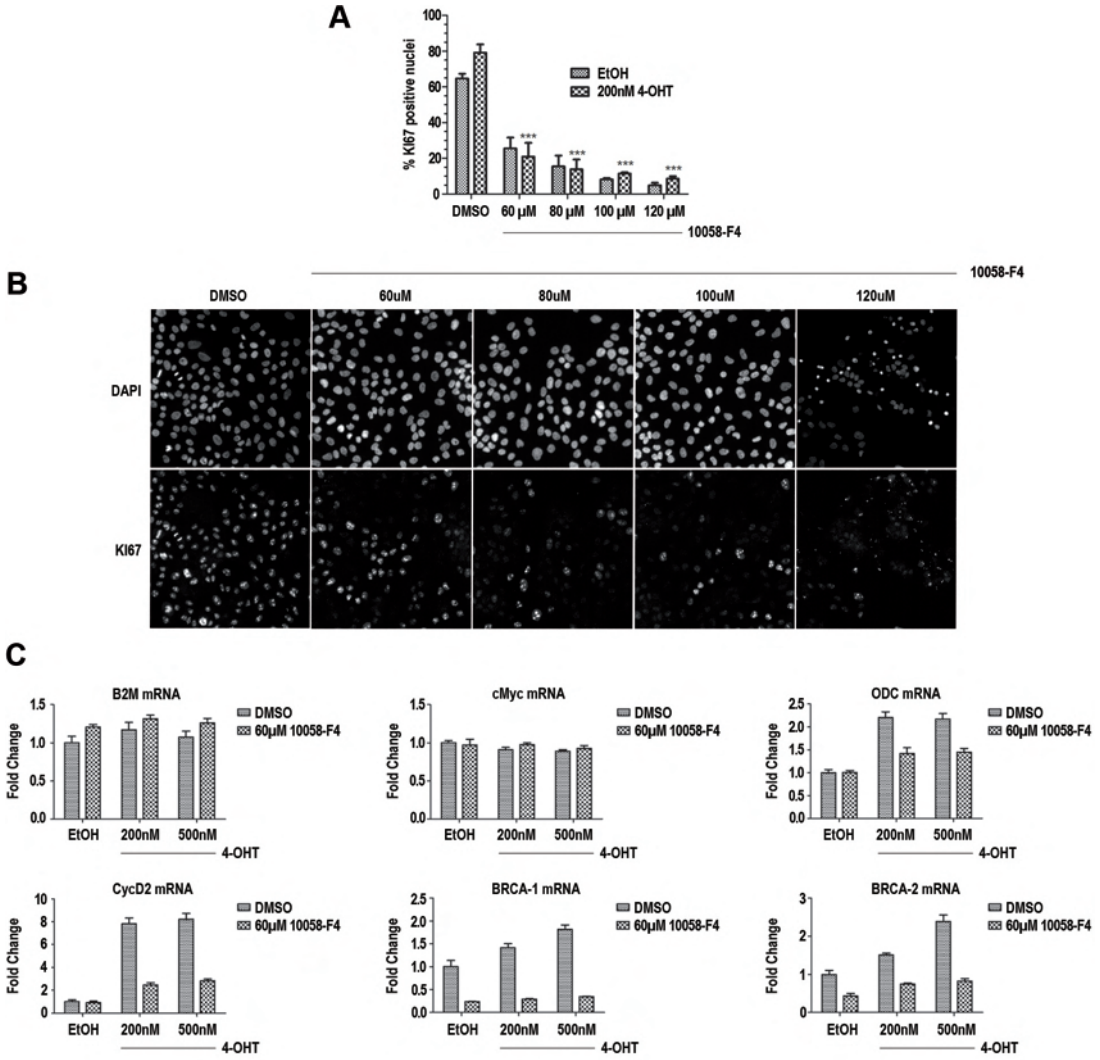

Figure IV: A: Percentage of KI67-positive nuclei in 2D-cultured Myc:ER-expressing MCF10A induced with 200nM 4-OHT and treated with the indicated concentrations of 10058-F4. Error bars represent the standard deviation of the mean for two independent experiments performed in triplicate. Statistical significance of 10058-F4 effect was calculated for the 200nM 4-OHT-treated samples only ***= $p<0.001$ (Student T-test) relative to the carrier-only control (DMSO). B: Representative images of KI67 staining quantified in A of Myc:ER-expressing cells induced with 200nM 4-OHT following treatment with the indicated concentrations of 10058-F4. All nuclei are counterstained with DAPI. C: qRT-PCR of c-Myc target genes (http://www.myccancergene.org) in Myc:ER expressing cells induced with 200 or 500nM 4-OHT upon 24 hours treatment with 60μM 10058-F4. Error bars represent the standard deviation of the mean for an experiment performed in triplicate.

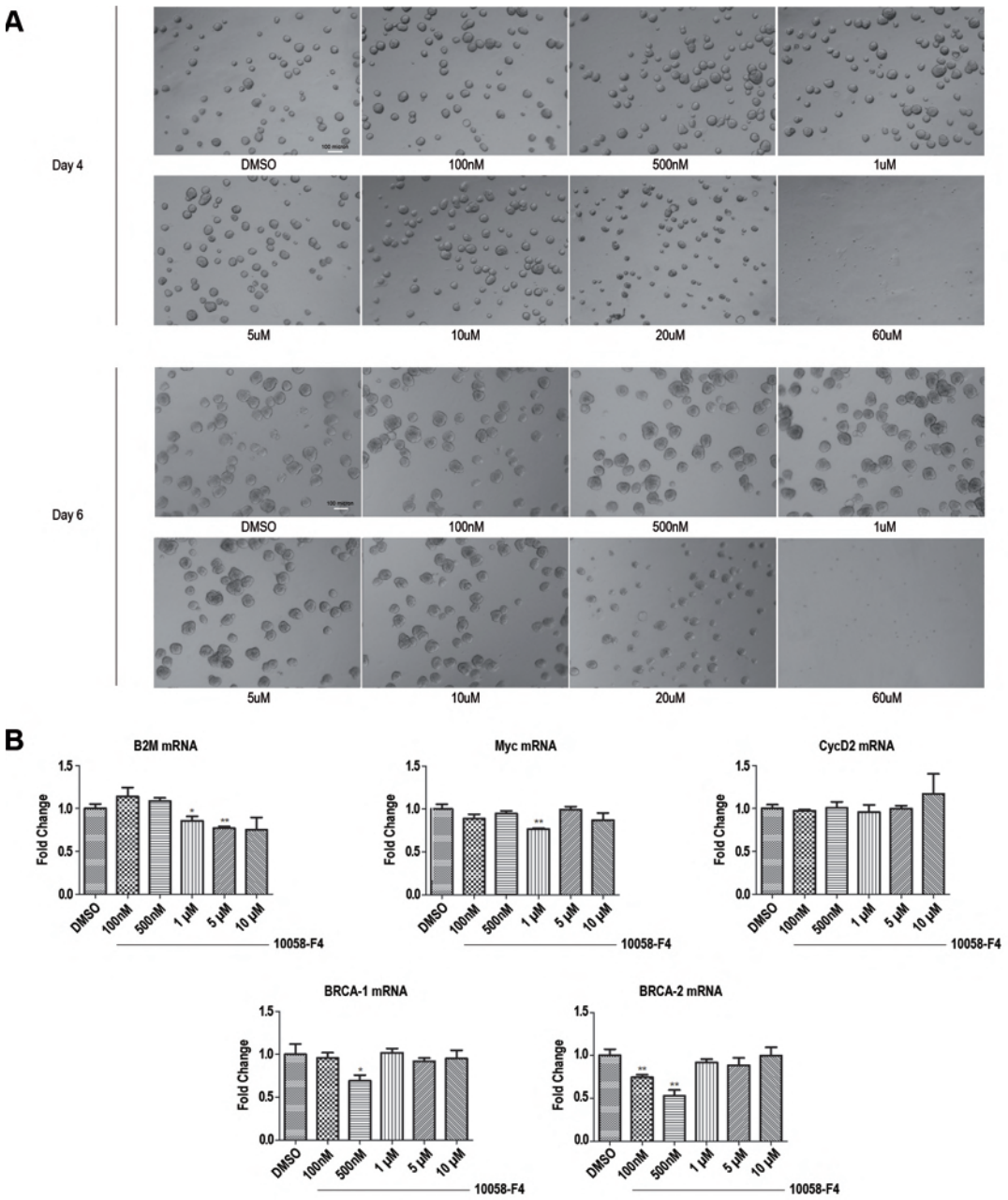

Figure V: A: Bright field images of acini cultured with the indicated concentrations of 10058-F4 for 4 (upper panel) and 6 (lower panel) days. B: qRT-PCR of c-Myc target genes (http://www.myccancergene.org) upon 7 days of culture in presence of 10058-F4. Error bars represent the standard deviation of the mean for two independent experiments performed in duplicate. **= $p<0.01$; *= $p<0.05$ (Student T-test) relative to the carrier-only control (DMSO).

Materials and Methods

Cell Maintenance MCF10A were cultured in DMEM:F12 (Dulbecco's Modified Eagle Medium:F12) supplemented with 5% Donor Horse Serum (Invitrogen), 10μg/ml Insulin (Novo Nordisk), 100ng/ml Cholera Toxin (Sapphire Bioscience), 0.5μg/ml Hydrocortisone (Sigma Aldrich), 20ng/ml EGF (Australian Laboratory Services), 100U/ml Penicillin and 100U/ml Streptomycin (Invitrogen). HEK-293T cells were cultured in DMEM with 10% Foetal Bovine Serum (JRH Biosciences), 100U/ml Penicillin and 100U/ml Streptomycin (Invitrogen). All cultures were maintained at 37°C in 5% CO_2.

Generation of Stable Cell Lines Myc:ER- or empty vector- MCF10A cells were generated by retroviral infection. HEK-293T were used as packaging cells for virus production. 1x10^6 cells were plated in a 10 cm dish and 24 hours later were co-transfected with either $MSCV_{Cherry}$-empty (Patrick Humbert Lab) or $MSCV_{Cherry}$-c-Myc:ER (Gretchen Poortinga, G. McArthur Lab) vector and the RD114 amphotrophic packaging vector using the calcium phosphate technique. 1 ml of $CaCl_2$ 0.24M solution containing 10μg of packaging vector and 10μg of DNA vector was added dropwise to 1ml of HEBS (0.3M NaCl, 0.06M Hepes, 0.45mM Na_2HPO_4, pH 7.09-7.12), gently mixing. The mixture was then distributed evenly across the plate. 18 hours post transfection HEK-293T cells were washed with PBS and fresh MCF10A medium was applied. Virus-containing supernatant was collected three/four times, at 8-12 hours intervals, and filtered using 0.22μm filters. 20ng/ml EGF and 1μ/ml Polybrene (Sigma Aldrich) were added each time. For transduction, 7.5x10^4 early passage MCF10A were plated in 6-well plates and allowed to settle for 24 hours. Freshly collected viral supernatant was applied three/four times at 8-12 hours intervals and cells were allowed to recover in fresh medium for 48 hours after the last viral hit. Infected cells were then selected with a Vantage SE DiVa cell sorter for Cherry expression.

siRNA Transfections MCF10A were plated in antibiotic free medium at a density of 1.1x10^5 per well in six-well plates 24 hours prior transfection. Dharmafect SMARTpool siRNA pools (ThermoScientific) specific for hLgl-1 or hLgl-2 were used at a final concentration of 25nM; when used in combination, the total final

concentration was 50nM. GFP-directed siRNA pools were used as a control at a final concentration of 25nM or 50nM respectively. Transfections were performed as follows: siRNA and Dharmafect lipid (0.15% final concentration) were diluted in OPTImem, mixed, allowed to complex for 20 minutes at room temperature and added dropwise to the plate. Transfection solution was replaced after 24 hours with fresh medium and cells were harvested for RNA or protein extraction 72 hours post transfection. Knockdown efficiency was assessed by quantitative real-time PCR (qRT-PCR).

3D Organotypic Cultures 3D organotypic cultures were performed using the overlay method described in [198]. 40μl of Growth Factor Reduced (GFR) Matrigel (Becton Dickinson) was dispensed to each well of an 8-well chamber slide and allowed to gel for 30 minutes at 37°C. Subconfluent MCF10A were resuspended in 3D culture medium (2% GFR Matrigel, 2% Donor Horse Serum, 5ng/ml EGF, 10μg/ml Insulin, 0.5μg/ml Hydrocortisone, 100ng/ml Cholera Toxin, 100U/ml Penicillin and 100U/ml Streptomycin) and plated over Matrigel at a density of 3000 cells per well. Medium was replaced every 4 days for the duration of the culture period. Images were taken with a Leica DMIRB inverted microscope and RNA extraction was performed using the TRizol reagent (Invitrogen).

RNA Extraction, Reverse Transcription and qRT-PCR RNA was harvested using TRizol reagent (Invitrogen). Cells grown on plates were scraped directly into TRizol whilst cells grown in 3D were lysed by dissolving the matrigel in Trizol. RNA was purified using chloroform extraction and ethanol precipitation following the manufacturer's instructions (Invitrogen). Isolated, dried RNA was resuspended in RNase-free H_2O and the concentration and purity of RNA was determined using a Nanodrop ND-1000 spectrophotometer (Labtech). cDNA was made from 1μg RNA using 1μg Random Primers (Promega). RNA-Random Primers solution was heated at 70°C for 5 minutes, cooled on ice for 5 minutes. A mix containing 200U M-MLV Reverse Transcriptase, M-MMV Buffer and dNTP (0.5mM final concentration) was added, mixing well. The reaction was carried out at 40°C for 50 minutes after having sat 10 minutes at room temperature. cDNA samples were amplified in triplicate reactions using the SYBER Green dye detection method (Applied Biosystems). qRT-PCR reactions were run on a StepOnePlus Real-Time PCR System (Applied

Biosystems) with the following programme: 95°C for 10 minutes (denaturation), 40 cycles of 95 °C for 15 seconds (denaturation), 60°C for 1 minute (annealing and extension). Samples were normalised to GAPDH control and relative differences between samples were calculated ($2^{\Delta CT}$, where CT, Cycle Threshold, is the number of cycles required for the fluorescent signal to cross an arbitrary threshold). Statistical significance was calculated using the Student T-test with GraphPad Prism software. The following primers have been used:
Lgl-1 (Patrick Humbert Lab)
Fw: TGCCATCCTGATCAAATGAGG
Rv: CAGTGGAGCCTACAGGTTAGCA
Lgl-2 (Patrick Humbert Lab)
Fw: GAGACCCCAACCAGATCCTGAT
Rv: GATGTTCTCCAGTTGCTGGCTG
c-Myc (Gretchen Poortinga, G. McArthur Lab)
Fw: GGAGACGAGACCTTCATCAA
Rv: CCAGCTTCTCTGAGACGAGCTT
B2M (Gretchen Poortinga, G. McArthur Lab)
Fw: TCACCCCCACTGAAAAAGATGAGTA
Rv: GAATTCTCTGCTCCCCACCTCTAAG
GAPDH (Patrick Humbert Lab)
Fw: AAGGTGAAGGTCGGAGTCAAC
Rv: GAGTTAAAAGCAGCCCTGGTG
ODC (Gretchen Poortinga, G. McArthur Lab)
Fw: TGAGGTTGGTTTCAGCATGTATCT
Rv: GGTTGATTACGCCGGTGATCT
CycD2 (Patrick Humbert Lab)
Fw: CTGTGTGCCACCGACTTTAAGTT
Rv: GATGGCTGCTCCCACACTTC
BRCA-1 (Patrick Humbert Lab)
Fw: GGTGGTACATGCACAGTTGC
Rv: ACTCTGGGGCTCTGTCTTCA
BRCA-2 (Christine Hauser, R. Hannan Lab)
Fw: CCACAGCCAGGCAGTCTGTAT
Rv: AGAACACGCAGAGGGAACTTG

Protein Extraction, SDS PAGE and Western Blotting Cells were lysed in SDS Sample Buffer (250mM Tris-HCl pH 6.8, 30% Glycerol, 10% SDS) supplemented with the phosphatase inhibitor sodium vanadate (100μM) and Complete Mini Protease Inhibitor cocktail (Roche Diagnostics). Quantitation of protein concentrations was carried out using Lowry Protein Assay (BioRad). Lysates were resolved on pre-cast acrylamide gradient gels (Invitrogen) and trasferred to PVDF membrane (Millipore). Membranes were blocked in 5% skim milk in PBST (0.5% Tween PBS) in agitation for 1 hour at room temperature. Incubation with the primary antibody was performed overnight at 4°C in agitation. Membranes were then washed four times in PBST over a period of 1 hour and incubated with the appropriate HRP-conjugated secondary antibody (1:5000, Biorad) in 5% skim milk in PBST for 1 hour at room temperature, in agitation. Membranes were then washed four times over a period of 1 hour and developed with LumiLight (Roche) following manufacturer's instructions.
The following antibodies were used:
Mouse monoclonal α c-Myc (1:500, 9E11 clone - Invitrogen)
Mouse monoclonal α α-Tubulin (1:40000, B512 clone - Sigma Aldrich)

Drug Treatments MCF10A were plated in 6-well, 12-well or 96-well plate at a density of $5x10^4$, $3x10^4$ or $4.5x10^3$ cells per well respectively and allowed to settle for 24 hours. 10058-F4 was then applied at the indicated concentration with fresh medium. Cells were treated for RNA harvesting or fixed for immunofluorescence staining 24 hours post drug treatment. In case of starvation, 24 hours post seeding, cells were rinsed in PBS and serum/EGF-deprived medium (1% Donor Horse Serum, 10μg/ml Insulin, 0.5μg/ml Hydrocortisone, 100ng/ml Cholera Toxin, 100U/ml Penicillin and 100U/ml Streptomycin) was added. Cells were cultured in starving conditions for 48 hours before serum/EGF-deprived medium containing 4-OHT (Sigma) and/or 10058-F4 (Sigma) at the indicated concentrations or full medium was added. Cells were treated for RNA harvesting or fixed for immunofluorescence staining 24 hours post drug treatment. 4-OHT is solubilised in ethanol (EtOH) whilst 10058-F4 in dimethyl-sulphoxide (DMSO). For 10058-F4 treatment in 3D cultured MCF10A, the indicated concentration of the inhibitor was added to the cell suspension before plating on Matrigel and it was freshly applied at every medium change.

KI67 Staining After drug treatments, MCF10A cultured on black immunofluorescence 96-well plates were rinsed with PBS, fixed with 4% paraformaldehyde for 15 minutes and washed three times with PBS. Cells were then permeabilised in 0.3% Triton-PBS for 10 minutes, washed with PBS again and blocked for 1 hour in 2% BSA-PBS. Primary antibody (rabbit polyclonal α KI67, Abcam, 1:500) incubation was performed over night at 4°C in 2% BSA-PBS. Subsequently, cells were washed three times with PBS and incubated with the secondary antibody (α rabbit AlexaFluor 647, Invitrogen, 1:1000) in 2% BSA-PBS for 1 hour at room temperature in dark. Cells were washed three times with PBS and nuclei were stained with DAPI (1:1000, Molecular Probes). Imaging was performed with a Cellomics Arrayscan VTi microscope. KI67 positive nuclei were manually counted (at least 500 nuclei per well were scored) and the average value of triplicate wells was calculated.

Bibliography

[1] Grosberg R.K. and Strathmann R.R. The evolution of multicellularity: A minor major transition? *Annual Review of Ecology Evolution and Systematics* 2007, 38:621-654

[2] Jemal A., Bray F., Center M.M., Ferlay J., Ward E. and Forman D. Global Cancer Statistics. *A Cancer Journal For Clinicians* 2011, 61:69-90

[3] Weinberg R.A. The Biology of Cancer. *Garland Science* 2007, New York, NY

[4] Thiery J.P. Epithelial-mesenchymal transition in tumour progression. *Nature Reviews Cancer* 2002, 2:442-454

[5] Hanahan D. and Weinberg R.A. The Hallmarks of Cancer. *Cell* 2000, 100:57-70

[6] Merlo M.M.F., Pepper J.W. Reid B.J and Maley C.C. Cancer as an evolutionary and ecological process. *Nature Reviews Cancer* 2006, 6:924-935

[7] Hanahan D. and Weinberg R.A. Hallmarks of Cancer: The Next Generation. *Cell* 2011, 144:646-674

[8] Roberts P.J. and Der C.J. Targeting the Raf-MEK-ERK mitogen activated protein kinase cascade for treatment of cancer. *Oncogene* 2007, 26:3291-3310

[9] Yao X.H., Ping Y.F. and Bian X.W. Contribution of cancer stem cells to tumor vasculogenic mimicry. *Protein & Cell* 2011, 2:266-272

[10] Valastyan S. and Weinberg R.A. Tumor Metastasis: Molecular Insights and Evolving Paradigms. *Cell* 2011, 147:275-292

[11] Pietras K. and Östman A. Hallmarks of cancer: Interactions with the tumor stroma. *Experimental Cell Research* 2010, 316:1324-1331

[12] McAllister S. and Weinberg R.A. Tumor-Host Interactions: A Far-Reaching Relationship. *Journal of Clinical Oncology* 2010, 28:4022-4028

[13] Mareel M. and Leroy A. Clinical, cellular, and molecular aspects of cancer invasion. *Physiological Reviews* 2003, 83:337-376

[14] Gateff E. The genetics and epigenetics of neoplasms in *Drosophila*. *Biological Reviews of the Cambridge Philosophical Society* 1978, 53:123-68

[15] Bilder D. Epithelial polarity and proliferation control:links from the *Drosophila* neoplastic tumor suppressors. *Genes and Development* 2004, 18:1909-1925

[16] Brumby A.M. and Richardson H.E. Using *Drosophila melanogaster* to map human cancer pathways. *Nature Reviews Cancer* 2005, 5:626-639

[17] Froldi F., Ziosi M., Tomba G., Parisi F., Garoia F., Pession A. and Grifoni D. *Drosophila Lethal Giant Larvae* Neoplastic Mutant as a Genetic Tool for Cancer Moldeling. *Current Genomics* 2008, 9:147-154

[18] Dow L.E. and Humbert P.O.Polarity Regulators and the Control of Epithelial Architecture, Cell Migration and Tumorigenesis. *International Review of Cytology* 2007, 262:253-302

[19] Wodartz A. and Näthke I. Cell polarity in development and cancer. *Nature Cell Biology* 2007, 9:1016-1024

[20] Müller H.A. Genetic Control of Epithelial Cell Polarity: Lessons From *Drosophila*. *Developmental Dynamics* 2000, 218:52-67

[21] Tervonen T.A., Partanen J.I., Saarikoski S.T., Myllyen M., Marques E., Paasonen K., Moilanen A., Wohlfahrt G., Kovanen P.E. and Klefstrom J. Faulty Epithelial Polarity Genes and Cancer. *Advances in CANCER RESEARCH* 2011, 111:98-161

[22] Bilder D., Li M. and Perrimon N. Cooperative regulation of cell polarity and growth by *Drosophila* tumor suppressors. *Science* 2000, 289:113-116

[23] Grifoni D., Garoia F., Schimanski C.C., Schmitz G., Laurenti E., Galle P.R., Pession A., Cavicchi S. and Strand D. The human protein Hugl-1 substitutes for *Drosophila lethal giant larvae* tumour suppressor function in vivo. *Oncogene* 2004, 23:8688-8694

[24] Thomas U., Phannavong B., Muller B., Garner C.C. and Gundelfinger E.D. Functional expression of rat synapse-associated proteins SAP97 and SAP102 in *Drosophila dlg-1* mutants: effects on tumor suppression and synaptic bouton structure. *Mechanisms of Development* 1997, 62:161-174

[25] Dow L.E., Brumby A.M., Muratore R., Coombe M.L., Sedelies K.A., Trapani J.A., Russell S.M., Richardson H.E. and Humber P.O. hScrib is a functional homologue of the *Drosophila* tumour suppressor Scribble. *Oncogene* 2003, 22:9225-9230

[26] Humbert P.O., Dow L. E. and Russel S.M. The Scribble and Par complexes in polarity and migration: friends or foes? *TRENDS in Cell Biology* 2006, 16:622-629

[27] Betschinger J., Mechtler K. and Knoblich J.A. The Par complex directs asymmetric cell division by phosphorylating the cytoscheletal protein Lgl. *Nature* 2003, 422:326-330

[28] Wodarz A. Molecular control of cell polarity and asymmetric cell division in *Drosophila* neuroblasts. *Current Opinion in Cell biology* 2005, 17:475-481

[29] Betschinger J., Eisenhaber F. and Knoblich J.A. Phosphorylation-induced autoinhibition regulates the cytoskeletal protein Lethal (2) giant larvae. *Current Biology* 2005, 15:276-282

[30] Lee C.Y., Robinson K.J. and Doe C.Q. Lgl, Pins and aPKC regulate neuroblast self-renewal versus differentiation. *Nature* 2006, 439:594-598

[31] Grifoni D., Garoia F., Bellosta P., Parisi F., De Biase D., Collina G., Strand D., Cavicchi S. and Pession A. aPKCζ cortical loading is associated with Lgl cytoplasmic release and tumor growth in *Drosophila* and human epithelia. *Oncogene* 2007, 26:5960-5965

[32] Rolls M.M., Albertson R., Shih H.P., Lee C.Y. and Doe C.Q. Drosophila aPKC regulates cell polarity and cell proliferation in neuroblasts and epithelia. *Journal of Cell Biology* 2003, 163:1089-1098

[33] Hutterer A., Betschinger J., Petronczki M. and Knoblich J.A. Sequential roles of Cdc42, Par-6, aPKC, and Lgl in the establishment of epithelial polarity during *Drosophila* embryogenesis. *Developmental Cell* 2004, 6:845-54

[34] Strand D., Unger S., Corvi R., Hartenstein K., Schenkel H., Kalmes A., Merdes G., Neumann B., Krieg-Schneider F., Coy J.M., Poustka A., Schwab M. and Mechler B.M. A human homologue of the *Drosophila* tumour suppressor gene l(2)gl maps to 17p11.2-12 and codes for a cytoskeletal protein that associates with nonmuscle myosin II heavy chain. *Oncogene* 1995, 11:291-301

[35] Peng C.Y., Manning L., Albertson R. and Doe C.Q. The tumour-suppressor genes *lgl* and *dlg* regulate basal protein targeting in*Drosophila* neuroblasts. *Nature* 2000, 408:596-600

[36] Lehman K., Rossi G., Adamo J.E. and Brennwald P. Yeast homologues of *tomosyn* and *lethal giant larvae* function in exocytosis and are associated with the plasma membrane SNARE, Sec9. *Journal of Cell Biology* 1999, 146:125-140

[37] Arquier N., Perrin L., Manfruelli P. and Semeriva M. The *Drosophila* tumor suppressor gene *lethal(2)giant larvae* is required for the emission of the *decapentaplegic* signal. *Development* 2001, 128:2209-2220

[38] Mechler B.M., McGinnis W. and Gehring W.J. Molecular cloning of *lethal(2)giant larvae*, a recessive oncogene of*Drosophila melanogaster*. *EMBO Journal* 1985, 4:1551-1557

[39] Agrawal N., Kango M., Mishra A. and Sinha P. Neoplastic transformation and aberrant cell-cell interactions in genetic mosaics of *lethal(2)giant larvae* (*lgl*), a tumor suppressor gene of *Drosophila*. *Developmental Biology* 1995, 172:218-229

[40] Knox A.L. and Brown N.H. Rap1 GTPase regulation of adherens junction positioning and cell adhesion. *Science* 2002, 295:1285-1288

[41] Brumby A., Secombe J., Horsfield J., Coombe M., Amin N., Coates D., Saint R. and Richardson H. A genetic screen for dominant modifiers of a *cyclin E* hypomorphic mutation identifies novel regulators of S-phase entry in *Drosophila*. *Genetics* 2004, 168:227-251

[42] Grzeschik N.A., Amin N., Secombe J., Brumby A.M. and Richardson H.E. Abnormalities in cell proliferation and apico-basal cell polarity are separable in *Drosophila lgl* mutant clones in the developing eye. *Developmental Biology* 2007, 311:106-123

[43] Grzeschik N.A, Parsons L., Allot M., Harvey K.F. and Richardson H.E. Lgl, aPKC and Crumbs regulate the Salvador/Warts/Hippo pathway through two distinct mechanisms. *Current Biology* 2010, 20:573-581

[44] Halder G. and Johnson R.L. Hippo signaling: growth control and beyond. *Development* 2011, 130:9-22

[45] Sun G. and Irvine K. Regulation of Hippo signaling by Jun kinase signaling during compensatory cell proliferation and regeneration, and in neoplastic tumors. *Developmental Biology* 2011, 350:139-151

[46] Igaki T. Correcting developmental errors by apoptosis: lessons from *Drosophila* JNK signaling. *Apoptosis* 2009, 14:1021-1028

[47] Dogget K., Grusche F.A., Richardson H.E. and Brumby A.M. Loss of the *Drosophila* cell polarity regulator Scribbled promotes epithelial tissue overgrowth and cooperation with oncogenic Ras-Raf through impaired Hippo pathway signaling. *BMC Developmental Biology* 2011, 11:57

[48] Woodhouse E., Hersperger E. and Shearn A. Growth, metastasis, and invasiveness of *Drosophila* tumors caused by mutations in specific tumor suppressor genes. *Development Genes and Evolution* 1998, 207:542-550

[49] Beaucher M., Goodliffe J., Hersperger E., Trunova S., Frydman H. and Shearn A. *Drosophila* brain tumor metastases express both neuronal and glial cell type marker. *Developmental Biology* 2007, 301:287-297

[50] Woodhouse E., Hersperger E., Stetler-Stevenson W.G., Liotta L.A. and Shearn A. Increased type IV collagenase in *lgl*-induced invasive tumors of *Drosophila*. *Cell Growth and Differentiation* 1994, 5:151-159

[51] Beaucher M., Hersperger E., Page-McCaw A. and Shearn A. Metastatic ability of*Drosophila* tumors depends on MMP activity. *Developmental Biology* 2007, 303:625-634

[52] Woodhouse E.C., Fisher E., Bandle R.W., Bryant-Greenwood B., Charboneau L., Petricoin III E.F. and Liotta L.A. *Drosophila*screening model for metastasis: Semaphorin 5c is required for *l(2)gl* cancer phenotype. *Proceedings of the National Academy of Science USA* 2003, 100:11463-11468

[53] Manfruelli P., Arquier N., Hanratty W.P. and Sémériva M. The tumor suppressor gene *lethal(2)giant larvae* (*l(2)gl*) is required for cell shape changes of epithelial cells during *Drosophila* development. *Development* 1996, 122:2283-2294

[54] Szafranski P. and Goode S. Basolateral junctions are sufficient to suppress epithelial invasion during *Drosophila* oogenesis. *Developental Dynamics* 2007, 236:364-373

[55] Goode S., Wei J. and Kishore S. Novel spatiotemporal patterns of epithelial tumor invasion in *Drosophila dics large* egg chambers. *Developental Dynamics* 2005, 232:855-864

[56] Szafranski P. and Goode S. A Fasciclin 2 morphogenetic switch organizes epithelial cell cluster polarity and motility. *Development* 2004, 131:2023-2036

[57] Zhao M., Szafranski P., Hall C.A. and Goode S. Basolateral junctions utilize Warts signaling to control epithelil-mesenchimal transition and proliferation crucial for migration and invasion of *Drosophila* ovarian epithelial cells. *Genetics* 2008, 178:1947-1971

[58] Xu T. and Rubin G.M. Analysis of genetic mosaics in developing and adult *Drosophila* tissues. *Development* 1993, 117:1223-1237

[59] Morata G. and Ripoll P. Minutes: mutants of Drosophila autonomously affecting cell division rate. *Developmental Biology* 1975, 42:211-221

[60] Brumby A.M. and Richardson H.E. scribble mutants cooperate with oncogenic Ras or Notch to cause neoplastic overgrowth in *Drosophila*. *EMBO Journal* 2003, 22:5769-5779

[61] Igaki T., Pastor-Pareja J.C., Aonuma H., Miura M. and Xu T. Intrinsic Tumor Suppression and Epithelial Maintenance by Endocytic Activation of Eiger/TNF signaling in *Drosophila*. *Developmental Cell* 2009, 16:458-465

[62] Sinha P., Joshi S., Radhakrishnan V. and Mishra A. Developmental effects of $l(2)gl^4$ and *l(2)gd* recessive oncogenes on imaginal discs of *D. melanogaster*. *Cell Differentiation and Development* 1989, Suppl 577

[63] Kuphal S., Wallner S., Schimanski C.C., Bataille F., Hofer P., Strand S., Strand D. and Bosserhoff A.K. Expression of Hugl-1 is strongly reduced in malignant melanoma. *Oncogene* 2006, 25:103-110

[64] Schimanski C.C., Schmitz G., Kashyap A., Bosserhoff A.K., Bataille F., Schäfer S.C., Lehr H.A., Berger M.R., Galle P.R., Strand S. and Strand D. Reduced expression of Hugl-1, the human homologue of *Drosophila* tumour suppressor gene *lgl*, contributes to progression of colorectal cancer. *Oncogene* 2005, 24:3100-3109

[65] Korshunov A., Sycheva R. and Golanov A. Genetically distinct and clinically relevant subtypes of glioblastoma defined by array-based comparative genomic hybridization (array-CGH). *Acta Neuropathologica* 2006, 111:465-474

[66] Lu X., Feng X., Man X., Yang G., Tang L., Du D., Zhang F., Yuan H., Huang Q., Zhang Z., Liu Y., Strand D. and Chen Z. Aberrant splicing of Hugl-1 is associated with epatocellular carcinoma progression. *Clinical Cancer Research* 2009, 15:3287-3296

[67] Klezovitch O., Fernandez T.E., Tapscott S.J. and Vasioukhin V. Loss of cell polarity causes severe brain dysplasia in *Lgl1* knockout mice. *Genes and Development* 2004, 18:559-571

[68] Aigner K., Dampier B., Descovich L., Mikula M., Sultan A., Schreiber M., Mikulits W., Brabletz T., Strand D., Obrist P., Sommergruber W., Schweifer N., Wernitznig A., Beug H., Foisner R. and Eger A. The transcription factor ZEB1 (δEF1) promotes tumour cell dedifferentiation by repressing master regulators of epithelial polarity. *Oncogene* 2007, 26:6979-6988

[69] Lee T. and Luo L. Mosaic analysis with a repressible cell marker (MARCM) for *Drosophila* neural development. *Trends in Neuroscience* 2001, 24:251-254

[70] Pagliarini R.A. and Xu T. A genetic screen in *Drosophila* for metastatic behavior. *Science* 2003, 302:1227-1231

[71] Dow L.E., Elsum I.A., King C.L., Kinross K.M., Richardson H.E. and Humbert P.O. Loss of human Scribble cooperates with H-Ras to promote cell invasion through deregulation of MAPK signalling. *Oncogene* 2008, 27:5988-6001

[72] Uhlirova M., Jasper H. and Bohmann D. Non-cell-autonomous induction of tissue overgrowth by JNK/Ras cooperation in a *Drosophila* tumor model. *Proceedings of the National Academy of Science USA* 2005, 102:13123-13128

[73] Ryoo H.D., Gorenc T. and Steller H. Apptotic cells can induce compensatory cell proliferation through the JNK and Wingless signaling pathways. *Developmental Cell* 2004, 7:491-501

[74] Igaki T., Pagliarini R.A. and Xu T. Loss of Cell Polarity Drives Tumor Growth and Invasion through JNK Activation in *Drosophila*. *Current Biology* 2006, 16:1139-1146

[75] Uhlirova M. and Bohmann D. JNK- and Fos-regulated Mmp1 expression cooperates with Ras to induce invasive tumors in *Drosophila*. *EMBO Journal* 2006, 25:5294-5304

[76] Srivastava A., Pastor-Pareja J.C. Igaki T., Pagliarini R. and Xu T. Basement membrane remodelling is essential for *Drosophila* disc eversion and tumor invasion. *Proceedings of the National Academy of Science USA* 2007, 104:2721-2726

[77] Leong G.R., Goulding K.R. Amin N., Richardson H.E and Brumby A.M. *Scribble* mutants promote aPKC and JNK-dependent epithelial neoplasia independently of Crumbs. *BMC Biology* 2009, 7:62

[78] Brumby A.M., Goulding K.R., Schlosser T., Loi S., Galea R., Khoo P., Bolden J.E., Aigaki T., Humbert P.O. and Richardson H.E. Identification of Novel Ras-Cooperating Oncogenes in *Drosophila melanogaster*: a RhoGEF/Rho-Family/JNK Pathway Is a Central Driver of Tumorigenesis. *Genetics* 2011, 188:105-125

[79] Wu M., Pastor-Pareja J.C. and Xu T. Interaction between Ras^{V12} and *scribbled* clones induces tumour growth and invasion. *Nature* 2010, 463:545-549

[80] Zhu M., Xin T., Weng S., Gao Y., Zhang Y., Li Q. and Li M. Activation of JNK signaling links *lgl* mutations to disruption of the cell polarity and epithelial organization in *Drosophila* imaginal discs. *Cell Research* 2010, 20:242-245

[81] Wagner E.F and Nebreda A.R. Signal integration by JNK and p38 MAPK patways in cancer development. *Nature Reviews Cancer* 2009, 9:537-549

[82] Menéndez J., Pérez-Garijo A., Calleja M. and Morata G. A tumor-suppressing mechanism in *Drosophila* involving cell competition and the Hippo pathway. *Proceedings of the National Academy of Science USA* 2010, 107:14651-14656

[83] Chen C., Schroeder M.C., Kango-Singh M., Tao C. and Halder G. Tumor suppression by cell competition through regulation of the Hippo pathway. *Proceedings of the National Academy of Science USA* 2011, 109:484-489

[84] Willecke M., Toggweiler J. and Basler K. Loss of PI3K blocks cell-cycle progression in a *Drosophila* tumor model. *Oncogene* 2011, 30:4067-4074

[85] Struhl G. and Basler K. Organizing activity of Wingless protein in *Drosophila*. *Cell* 1993, 72:527-540

[86] Pastor-Pareja J.C., Wu M. and Xu T. An innate immune response of blood cells to tumors and tissue damage in *Drosophila*. *Disease Models and Mechanisms* 2008, 1:144-154

[87] Cordero J.B., Macagno J.P. Stefanatos R.K., Strathdee K.E., Cagan R.L. and Vidal M. Oncogenic Ras Diverts a Host TNF Tumor Suppressor Activity into Tumor Promoter. *Developmental Cell* 2010, 18:999-1011

[88] Chi C., Zhu H., Han M., Zhuang Y., Wu X. and Xu T. Disruption of lysosome function promotes tumor growth and metastasis in*Drosophila*. *The Journal of Biological Chemistry* 2010, 285:21817-21823

[89] Fernández-Medarde A. and Santos E. Ras in Cancer and Developmental Deseases *Genes & Cancer* 2011, 2:344-358

[90] Pylayeva-Gupta Y., Grabocka E. and Bar-Sagi D. RAS oncogenes: weaving a tumorigenic web. *Nature Reviews Cancer* 2011, 11:761-774

[91] Neuman-Silberberg F.S., Schejter E., Hoffmann F.M. and Shilo B.Z. The *Drosophila ras* oncogenes: Structure and nucleotide sequence. *Cell* 1984, 37:1027-1033

[92] Prober D.A. and Edgar B.A. Interactions between Ras1, dMyc, and dPI3K signaling in the developing *Drosophila* wing. *Genes & Development* 2002, 16:2286-2299

[93] Malumbres M. and Barbacid M. *RAS* oncogenes: the first 30 years. *Nature Reviews Cancer* 2003, 3:459-465

[94] Rajalingam K., Schreck R., Rapp U.R. and Albert S. *RAS* oncogenes and their downstream targets. *Biochimica et Biophysica Acta* 2007, 1773:1177-1195

[95] Repasky G.A., Chenette E.J. and Der C.J. Renewing the conspiracy theory debate: does Raf function alone to mediate Ras oncogenesis?. *TRENDS in Cell Biology* 2004, 14:639-647

[96] Liu P., Cheng H., Roberts T.M. and Zhao J.J. Targeting the phosphoinositide 3-kinase (PI3K) pathway in cancer. *Nature Reviews Drug Discovery* 2009, 8:627-644

[97] Orme M.H., Alrubaie S., Bradley L.G., Walker C.D. and Leevers S.J. Input from Ras is required for maximal PI(3)K signalling in *Drosophila*. *Nature Cell Biology* 2006, 8:1298-1302

[98] James K.E., Dorman J.B and Berg C.A. Mosaic analyses reveal the function of *Drosophila* Ras in embryonic dorsoventral patterning and dorsal follicle cell morphogenesis. *Development* 2002, 129:2209-2222

[99] Mollerau B and Domingos P.M. Photoreceptor differentiation in *Drosophila*: from immature neurons to functional photoreceptors. *Developmental Dynamics* 2005, 232:585-592

[100] Karim F.D. and Rubin G.M. Ectopic expression of activated Ras1 induces hyperplastic growth and increased cell death in *Drosophila* imaginal tissues. *Development* 1998, 125:1-9

[101] Prober D.A. and Edgar B.A. Ras1 Promotes Cellular Growth in the *Drosophila* Wing. *Cell* 2000, 100:435-446

[102] Sturtevant M.A., Roark M. and Bier E. The *Drosophila rhomboid* gene mediates the localized formation of wing veins and interact genetically with components of the EGF-R signaling pathway. *Genes & Development* 1993, 7:961-973

[103] Xu N., Wang S.Q., Tan D., Gao Y., Lin G. and Xi R. EGFR, Wingless and JAK/STAT signaling cooperatively maintain*Drosophila* intestinal stem cells. *Developmental Biology* 2011, 354:31-43

[104] Jiang H., Grenley M.O., Bravo M.J., Blumhagen R.Z. and Edgar B.A. EGFR/Ras/MAPK signaling mediates adult midgut epithelial homeostasis and regeneration in *Drosophila*. *Cell Stem Cell* 2011, 8:84-95

[105] Shaul Y.D. and Senger R. The MEK/ERK cascade: From signaling specificity to diverse functions. *Biochimica et Biophysica Acta* 2007, 1773:1213-1216

[106] Brown M.D. and Sacks D.B. Protein Scaffolds in MAP Kinase Signalling. *Cell Signaling* 2009, 21:462-469

[107] MAP kinase subcellular localization controls both pattern and proliferation in the developing *Drosophila* wing. *Development* 2006, 133:43-51

[108] Kurada P. and White K. Ras Promotes Cell Survival in *Drosophila* by Downregulating *Hid* Expression. *Cell* 1998, 95:319-329

[109] Bergmann A., Agapite J., McCall K. and Steller H. The *Drosophila* Gene *hid* Is a Direct Molecular Target of Ras-Dependent Survival Signal. *Cell* 1998, 95:331-341

[110] Wu Y., Zhuang Y., Han M., Xu T and, Deng K. Ras promotes cell survival by antagonizing both JNK and Hid signals in the *Drosophila* eye. *BMC Developmental Biology* 2009, 9:53

[111] Hickey M.M. and Simon M.C. Regulation of angiogenesis by hypoxia and hypoxia-inducible factors. *Current Topics in Developmental Biology* 2006, 76:217-257

[112] Petit V., Ribeiro C., Ebner A. and Affolter M. Regulation of cell migration during tracheal development in *Drosophila melanogaster*. *International Journal of Developmental Biology* 2002, 46:125-132

[113] Ghabrial A., Luschnig S., Metzstein M.M. and Krasnow M.A. Branching morphogenesis of the *Drosophila* tracheal system. *Annual Review of Cell and Develpmental Biology* 2003, 19:623-647

[114] Petit V., Nussbaumer U., Dossenbach C. and Affolter M. Downstream-of-FGFR Is a Fibroblast Growth Factor-Specific Scaffolding Protein and Recruits Corkscrew upon Receptor Activation. *Molecular and Cellular Biology* 2004, 24:3769-3781

[115] Wilk R., Weizman I., Shilo B.Z. *trachealess* encodes a bHLH-PAS protein that is an inducer of tracheal cell fates in *Drosophila*. *Genes & Development* 1996, 10:93-102

[116] Sotillos S., Espinosa- Vázquez J.M., Foglia F., Hu N. and Castelli-Gair Hombría J. An efficient approach to isolate STAT regulated enhancers uncovers STAT92E fundamental role in *Drosophila* tracheal development. *Developmental Biology* 2010, 340:571-582

[117] Jin J., Anthopoulos N., Wetsch B., Binari R.C., Isaac D.D. Andrew D.J., Woodgett J.R. and Manoukian A.S. Regulation of *Drosophila* Tracheal System Development by Protein Kinase B. *Developmental Cell* 2001, 1:817-827

[118] Sato M. and Kornberg T.B. FGF Is an Essential Mitogen and Chemoattractant for the Air Sacs of the *Drosophila* Tracheal System. *Developmental Cell* 2002, 3:195-207

[119] Yan D. and Lin X. *Drosophila* glypican Dally-like acts in FGF-receiving cells to modulate FGF signaling during tracheal morphogenesis. *Developmental Biology* 2007, 312:203-216

[120] Gervais L. and Casanova J. The *Drosophila* homologue of SRF acts as a boosting mechanism to sustain FGF-induced terminal branching in the tracheal system. *Development* 2011, 138:1269-1274

[121] Lee T., Feig L. and Montell D.J. Two distinct roles for Ras in a developmentally regulated cell migration. *Development* 1996, 122:409-418

[122] Li J., Xia F. and Li W.X. Coactivation of STAT and Ras Is Required for Germ Cell Proliferation and Invasive Migration in *Drosophila*. *Developmental Cell* 2003, 5:787-798

[123] Albihn A., Johnsen J.I. and Henriksson M.A. MYC in Oncogenesis and as a Target for Cancer Therapies. *Advances in Cancer Research* 2010, 107:163-224

[124] Larsson L., Henriksson M.A. The Yin and Yang functions of the Myc oncoprotein in cancer development and as targets for therapy. *Experimental Cell Research* 2010, 316:1429-1437

[125] Wierstra I. and Alves J. The *c-myc* Promoter: Still *M*yster*Y* and *C*hallenge. *Advances in Cancer Research* 2008, 99:113-133

[126] Jagruti P.H., Loboda A.P., Showe M.K., Showe L.C., McMahon S.B. Analysis of genomic targets reveals complex functions of MYC. *Nature Reviews Cancer* 2004, 4:562-568

[127] Meyer N. and Penn L.Z. Reflecting on 25 years with MYC. *Nature Reviews Cancer* 2008, 8:976-990

[128] Wolfer A. and Ramaswamy S. MYC and Metastasis. *Cancer Research* 2011, 71:2034-2037

[129] Whitfield J.R. and Soucek L. Tumor microenvironment: becoming sick of Myc. *Cellular and Molecular life Sciences* 2011, DOI: 10.1007/s00018-011-0860-x

[130] Podar K. and Anderson K.C. A therapeutic role for targeting c-Myc/Hif-1-dependent signaling pathways. *Cell Cycle* 2010, 9:1722-1728

[131] Dang C.V., Kim J., Gao P. and Yustein J. The interplay between MYC and HIF in cancer. *Nature Reviews Cancer* 2008, 8:51-56

[132] Kuttler F. and Mai S. c-Myc, Genomic Instability and Disease. *Genome Dynamics* 2006, 1:171-190

[133] Thomas L.R. and Tansey W.P. Proteolytic Control of the Oncoprotein Transcription Factor Myc. *Advances in Cancer Research* 2011, 110:77-106

[134] Junttila M.R. and Westermarck J. Mechanisms of MYC stabilization in human malignancies. *Cell Cycle* 2008, 7:592-596

[135] Gallant P. *Drosophila* Myc. *Advances in Cancer Research* 2009, DA COMPLETARE

[136] Trumpp A., Refaeli Y., Oskarsson T., Gasser S., Murphy M., Martin G.R. and Bishop J.M. c-Myc regulates mammalian body size by controlling cell number but not cell size. *Nature* 2010, 414:768-773

[137] Gallant P., Shiio Y., Cheng P.F., Parkhurst S.M. and Eisenman R.N. Myc and Max homologs in *Drosophila*. *Science* 1996, 274:1523-1527

[138] Schreiber-Agus N., Stein D., Chen K., Goltz J.S., Stevens L. and DePinho R.A. *Drosophila* Myc is oncogenic in mammalian cells and plays a role in the diminutive phenotype. *Proceedings of the National Academy of Science, USA* 1997, 94:1235-1240

[139] Benassayag C., Montero L., Colombie N., Gallant P., Cribbs D. and Morello D. Human c-Myc isoforms differentially regulate cell growth and apoptosis in *Drosophila melanogaster*. *Molecular and Cellular Biology* 2005, 25:9897-9909

[140] Johnston L.A., Prober D.A., Edgar B.A., Eisenman R.N. and Gallant P. *Drosophila myc* regulates cellular growth during development. *Cell* 1999, 98:779-790

[141] Grewal S.S., Li L., Orian A., Eisenman R.N. and Edgar B.A. Myc-dependent regulation of ribosomal RNA synthesis during *Drosophila* development. *Nature Cell Biology* 2005, 7:295-302

[142] Oskarsson T. and Trumpp A. The Myc trilogy: lord of RNA polymerases. *Nature Cell Biology* 2005, 7:215-217

[143] Maines J.Z., Stevens L.M., Tong X. and Stein D. *Drosophila* dMyc is required for ovary cell growth and endoreplication. *Development* 2004, 131:775-786

[144] Neumuller R.A., Betschinger J., Fischer A., Bushati N., Poernbacher I., Mechtler K., Cohen S. M. and Knoblich J.A. Mei-P26 regulates microRNAs and cell growth in the *Drosophila* ovarian stem cell lineage. *Nature* 2008, 241-245

[145] Rhiner C., Diaz B., Portela M., Poyatos J.F., Fernandez-Ruiz I., Lopez-Gay J.M., Gerlitz O. and Moreno E. Persistent competition among stem cells and their daughters in the *Drosophila* ovary germline niche. *Development* 2009, 995-1006

[146] Betschinger J., Mechtler K. and Knoblich J.A. Asymmetric segregation of the tumor suppressor *brat* regulates self-renewal in *Drosophila* neural stem cells. *Cell* 2006, DA COMPLETARE

[147] Montero L., Müller N. and Gallant P. Induction of apoptosis by *Drosophila* Myc. *Genesis* 2008, 46:104-111

[148] de la Cova C., Abril M., Bellosta P., Gallant P. and Johnston L.A. *Drosophila* Myc regulates organ size by inducing cell competition. *Cell* 2004, 117:107-116

[149] Wu C. and Johnston L.A. Control of Wing Size and Proportions by *Drosophila* Myc. *Genetics* 2010, 184:199-211

[150] Herranz H., Pérez, Martín F.A. and Milán M. A Wingless and Notch double-repression mechanism regulates G1-S transition in the *Drosophila* wing. *The EMBO Journal* 2008, 27:1633-1645

[151] Smith-Bolton R.K., Worley M.I., Kanda H. and Hariharan K. Regenerative Growth in *Drosophila* Imaginal Discs Is Regulated by Wingless and Myc. *Developmental Cell* 2009, 16:797-809

[152] Pennetier D., Oyallon J., Morin-Poulard I., Dejean S., Vincent A. and Crozatier M. Size control of the *Drosophila* hematopoietic niche by bone morphogenetic protein signaling reveals parallels with mammals. *Proceedings of the National Academy of Science, USA* 2012, doi: 10.1073/pnas.1109407109

[153] Duman-Scheel M., Johnston L. and Du W. Repression of dMyc expression by Wingless promotes Rbf-induced G1 arrest in the presumptive *Drosophila* wing margin. *Proceedings of the National Academy of Science, USA* 2004, 101:3857-3862

[154] Mitchell N.C., Johanson T.M., Cranna N.J., Er A.L., Richardson H.E., Hannan R.D. and Quinn L.M. Hfp inhibits [**?**] transcription and cell growth in a TFIIH/Hay-dependent manner. *Development* 2010, 137:2875-2884

[155] Quinn L.M., Dickins R.A., Coombe M., Hime G.R., Bowtell D.D. and Richardson H. *Drosophila* Hfp negatively regulates *dmyc* and *stg* to inhibit cell proliferation . *Development* 2004, 131:1411-1423

[156] Ziosi M., Baena-López L.A., Grifoni D., Froldi F., Pession A., Garoia F., Trotta V., Bellosta P., Cavicchi S. and Pession A. dMyc Functions Downstream of Yorkie to Promote the Supercompetitive Behavior of Hippo Pathway Mutant Cells. *PLoS Genetics* 2010, 6:e1001140

[157] Neto-Silva R.M., de Beco S. and Johnston L.A. Evidence for a Growth-Stabilizing Regulatory Feedback Mechanism between Myc and Yorkie, the *Drosophila* Homolog of Yap. *Developmental Cell* 2010, 19:507-520

[158] Dong J., Feldmann G., Huang J., Wu S., Zhang N., Comerford S.A., Gayyed M.F., Anders R.A., Maitra A. and Pan D. Elucidation of a Universal Size-Control Mechanism in *Drosophila* and Mammals. *Cell* 2007, 130:1120-1133

[159] Sandmann T., Girardot C., Brehme M., Tongprasit W., Stolc V. and Furlong E.E. A core transcriptional network for early mesoderm development in *Drosophila melanogaster*. *Genes & Development* 2007, 21:436-449

[160] Teleman A.A., Hietakangas V., Sayadian A.C. and Cohen S.M. Nutritional Control of Protein Biosynthetic Capacity by Insulin via Myc in *Drosophila*. *Cell Metabolism* 2007, 7:21-32

[161] Delanoue R., Slaidina M. and Léopold P. The Steroid Hormone Ecdysone Controls Systemic Growth by Repressing dMyc Function in *Drosophila* Fat Cells. *Developmental Cell* 2010, 18:1012-1021

[162] Goodliffe J.M., Wieschaus E. and Cole M.D. Polycomb mediates Myc autorepression and its transcriptional control of many loci in *Drosophila*. *Genes & Development* 2005, 19:2941-2946

[163] Harris R.E., Pargett M., Sutcliffe C., Umulis D. and Ashe H.L. Brat Promotes Stem Cell Differentiation via Control of a Bistable Switch that Restricts BMP Signaling. *Developmental Cell* 2011, 20:72-83

[164] Galletti M., Riccardo S., Parisi F., Lora C., Saqcena M.K., Rivas L., Wong B., Serra A., Serras F., Grifoni D., Pelicci P., Jiang J. and Bellosta P. Identification of Domains Responsible for Ubiquitin-Dependent Degradation of dMyc by Glycogen Synthase Kinase 3β and Casein Kinase 1 Kinases. *Molecular and Cellular Biology* 2009, 29:3424-3434

[165] Moberg K.H., Mukherjee A., Veraksa A., Artavanis-Tsakonas S. and Hariharan I.K. The *Drosophila* F Box Protein Archipelago Regulates dMyc Protein Levels In Vivo. *Current Biology* 2004, 14:965-974

[166] Parisi F., Riccardo S., Daniel M., Saqcena M., Kundu N., Pession A., Grifoni D., Stocker H., Tabak E. and Bellosta P. *Drosophila* insulin and target of rapamycin (TOR) pathways regulate GSK3 beta activity to control Myc stability and determine Myc expression in vivo. *BMC Biology* 2011, 9:65

[167] Herranz H., Hong X., Pérez L., Ferreira A., Olivieri D., Cohen S.M. and Milán M. The miRNA machinery targets Mei-P26 and regulates Myc protein levels in the *Drosophila* wing. *EMBO Journal* 2010, 29:1688-1698

[168] Marygold S.J., Roote J., Reuter G., Lambertsson A., Ashburner M., Millburn G.H., Harrison P.M., Yu Z., Kenmochi N., Kaufman T.C., Leevers S.J. and Cook K.R. The ribosomal protein genes and *Minute* loci of *Drosophila melanogaster*. *Genome Biology* 2010, 8:R216

[169] Gallant P. Myc, cell competition, and compensatory proliferation. *Cancer Research* 2005, 6485-6487

[170] Moreno E., Basler K. and Morata G. Cells compete for *decapentaplegic* survival factor to prevent apoptosis in *Drosophila* wing development. *Nature* 2002, 416:755-759

[171] Moreno E. and Basler K. dMyc transforms cells into super-competitors. *Cell* 2004, 117:117-129

[172] Li W. and Baker N.E. Engulfment is required for cell competition. *Cell* 2007, 129:1215-1225

[173] Senoo-Matsuda N. and Johnston L.A. Soluble factors mediate competitive and cooperative interactions between cells expressing different levels of *Drosophila* Myc. *Proceedings of the National Academy of Science, USA* 2007, 104:18543-18548

[174] Tyler D.M., Li W., Zhuo N., Pellock B. and Baker N.E. Genes affecting cell competition in *Drosophila*. *Genetics* 2007, 175:643-657

[175] Rhiner C., López-Gay J.M., Soldini D., Casas-Tinto S., Martín F.A., Lombardía L. and Moreno E. Flower Forms an Extracellular Code that Reveals the Fitness of a Cell to its Neighbors in *Drosophila*. *Developmental Cell* 2010, 18:985-998

[176] Portela M., Casas-Tinto S., Rhiner C., López-Gay J.M., Domínguez O., Soldini D. and Moreno E. *Drosophila* SPARC is a self-protective signal expressed by loser cells during cell competition. *Developmental Cell* 2010, 19:562-573

[177] Simpson P. Parameters of cell competition in the compartments of the wing disc of *Drosophila*. *Developmental Biology* 1979, 69:182-193

[178] Oliver E. R., Saunders T. L., Tarle S. A. and Glaser T. Ribosomal protein L24 defect in belly spot and tail (Bst), a mouse Minute. *Development* 2005, 131:3907-3920

[179] Oertel M., Menthena A., Dabeva M.D. and Shafritz D.A. Cell competition leads to a high level of normal liver reconstitution by transplanted fetal liver stem/progenitor cells. *Gastroenterology* 2006, 130:507-520

[180] Tamori Y., Bialucha C.U., Tian A.G., Kajita M., Huang Y.C., Norman M., Poulton J., Ivanovitch K., Disch L., Liu T., Deng W.M. and Fujita Y. Involvement of Lgl and Mahjong/VprBP in cell competition. *PLoS Biology* 2010, 8:e1000422

[181] Norman M., Wisniewska K.A., Lawrenson K., Garcia-Miranda P., Tada M., Kajita M., Mano H., Ishikawa S., Ikegawa M., Shimada T and Fujita Y. Loss of Scribble causes cell competition in mammalian cells. *Journal of Cell Science* 2012, 125:59-66

[182] Sansom O.J., Meniel V.S., Muncan V., Phesse T.J., Wilkins J.A., Reed K.R., Vass J.K., Athineos D., Clevers H. and Clarke A.R. Myc deletion rescues Apc deficiency in the small intestine. *Nature* 2007, 446:676-679

[183] Moreno E. Is cell competition relevant to cancer?. *Nature Reviews Cancer* 2008, 8:141-147

[184] Baker N.E. and Li W. Cell competition and its possible relation to cancer. *Cancer Research* 2008, 68:5505-5507

[185] Bate M. and Martinez-Árias A. The Development of *Drosophila melanogaster*. *Cold Spring Harbor Laboratory Press* 1993, Volume II

[186] Garcia-Bellido A. and Merriam J. R. Parameters of the wing imaginal disc development of *Drosophila melanogaster*. *Developmental Biology* 1971, 24:61-87

[187] Johnston L.A. and Gallant P. Control of growth and organ size in *Drosophila*. *Bioessays* 2002, 24:54-64

[188] Wilkins A.S. Genetic Analysis of Animal Development. *Wiley-Liss*, New York, NY, 1993 (second edition)

[189] Cavaliere V., Bernardi F., Romani P., Duchi S. and Gargiulo G. Building up the *Drosophila* eggshell: First of all the eggshell genes must be transcribed. *Developmental Dynamics* 2008, 237:2061-2072

[190] Bellosta P., Hulf T., Balla Diop S., Usseglio F., Pradel J., Aragnol D. and Gallant P. Myc interacts genetically with Tip48/Reptin and Tip49/Pontin to control growth and proliferation during *Drosophila* development. *Proceedings of the National Academy of Science, USA* 2005, 102:11799-11804

[191] Leevers S.J., Weinkove D., MacDougall L.K., Hafen E. and Waterfield M.D. The*Drosophila* phosphoinositide 3-kinase Dp110 promotes cell growth. *EMBO Journal* 1996, 15:6584-6594

[192] Woolworth J.A., Nallamothu G. and Hsu T. The *Drosophila* metastasis suppressor gene *Nm23* homolog, *awd*, regulates epithelial integrity during oogenesis. *Molecular and Cellular Biology* 2009, 29:4679-4690

[193] Cranna N. and Quinn L. Impact of steroid hormone signals on *Drosophila* cell cycle during development. *cell Division* 2009, 4:3

[194] Lawrence P.A., Casal J. and Struhl G. The Hedgehog morphogen and gradients of cell affinity in the abdomen of *Drosophila*. *Development* 1999, 126:2441-2449

[195] Hogan C., Dupré-Crochet S., Norman M., Kajita M., Zimmermann C., Pelling A.E., Piddini E., Baena-López L.A., Vincent J.P., Itoh Y., Hosoya H., Pichaud F. and Fujita Y. Characterization of the interface between normal and transformed epithelial cells. *Nature Cell Biology* 2009, 11:460-467

[196] Brand A.H. and Perrimon N. Raf acts downstream of the EGF receptor to determine dorsoventral polarity during *Drosophila* oogenesis. *Genes & Development* 1993, 8:629-639

[197] Page-McCaw A., Ewald A.J. and Werb Z. Matrix metalloproteinases and the regulation of tissue remodelling. *Nature Reviews Molecular Cell Biology* 2007, 8:221-233

[198] Debnath J., Muthuswamy S.K. and Brugge J.S. Morphogenesis and oncogenesis of MCF-10A mammary epithelial acini grown in three-dimensional basement membrane cultures. *Methods* 2003, 30:256-68

[199] Zhan L., Rosenberg A., Bergami K.C., Yu M., Xuan Z., Jaffe A.B., Allred C. and Muthuswamy S.K. Deregulation of Scribble Promotes Mammary Tumorigenesis and Reveals a Role for Cell Polarity in Carcinoma. *Cell* 2008, 135:865-878

[200] Wang H., Hammoudeh D.I., Follis A.V., Reese B.E. Lazo J.S., Metallo S.J. and Prochownik E.V. Improved low molecular weight Myc-Max inhibitors. *Molecular Cancer Therapeutics* 2007, 6:2399-2408

[201] Sampson V.B., Rong N.H., Han J., Yang Q., Aris V., Soteropoulos P., Petrelli N.J. Dunn S.P. and Krueger L.J. MicroRNA Let-7a Down-regulates MYC and Reverts MYC-Induced Growth in Burkitt Lymphoma Cells. *Cancer Research* 2007, 67:9762-9770

[202] Khanna A., Böckelman C., Hemmes A., Junttila M.R., Wiksten J., Lundin M., Junnila S., Murphy D.J., Evan G.I., Haglund C., Westermarck J. and Ristimäki. MYC-Dependent Regulation and Prognostic Role of CIP2A in Gastric Cancer. *Journal of the National Cancer Institute* 2009, 101:793-805

[203] Gomez-Curet I., Perkins R.S., Bennet R., Feidler K.L. Dunn S.P. and Krueger L.J. c-Myc inhibition negatively impacts lymphoma growth. *Journal of Pediatric Surgery* 2006, 41:207-211

[204] Littlewood T.D., Hancock D.C., Danielian P.S., Parker M.G. and Evan G.I. A modified oestrogen receptor ligand-binding domain as an improved switch for the regulation of heterologous proteins. *Nucleic Acids Research* 1995, 23:1686-1690

[205] Wall M., Poortinga G., Hannan K.M., Pearson R.B., Hannan R.D. and McArthur G.A. Translational control of c-MYC by rapamycin promotes terminal myeloid differentiation. *Blood* 2008, 112:2305-2317

Acknowledgements

First and foremost, my sincere gratitude goes to Daniela Grifoni; without her this thesis would not exist. She has introduced me to the fly world and has encouraged, challenged and guided me throughout this PhD. She is a great mentor and a great friend.

I am also grateful to professor Annalisa Pession for supervising and supporting my work in these three years.

A warm thanks goes to past and present members of my research group, to the fly lab in Bologna and to all the people with whom I shared my experience at the "fourth floor"and made it a fantastic environment to work in.

My PhD would not have been the same without the "Australian adventure" and thus a special thanks goes to Helena Richardson for having hosted me at Peter MacCallum Cancer Center in Melbourne and to Patrick Humbert for having welcomed me in his lab and having given me the opportunity to take my first steps into the world of "non-drosophilid" biology.

A big thanks to all the members of their labs who have been extremely supportive throughout my stay and in particular to Tanja Kinwel and Lorey Smith for their unlimited patience.

I am also grateful to Kate Hannan and Gretchen Poortinga for sharing reagents and their expertise.

BMC Biology

RESEARCH ARTICLE Open Access

The *lethal giant larvae* tumour suppressor mutation requires dMyc oncoprotein to promote clonal malignancy

Francesca Froldi[1,2], Marcello Ziosi[1,2], Flavio Garoia[3], Andrea Pession[4], Nicola A Grzeschik[5], Paola Bellosta[6], Dennis Strand[7], Helena E Richardson[5,8], Annalisa Pession[†1] and Daniela Grifoni[*†1,2]

Abstract

Background: Neoplastic overgrowth depends on the cooperation of several mutations ultimately leading to major rearrangements in cellular behaviour. Precancerous cells are often removed by cell death from normal tissues in the early steps of the tumourigenic process, but the molecules responsible for such a fundamental safeguard process remain in part elusive. With the aim to investigate the molecular crosstalk occurring between precancerous and normal cells *in vivo*, we took advantage of the clonal analysis methods that are available in *Drosophila* for studying the phenotypes due to *lethal giant larvae* (*lgl*) neoplastic mutation induced in different backgrounds and tissues.

Results: We observed that *lgl* mutant cells growing in wild-type imaginal wing discs show poor viability and are eliminated by Jun N-terminal Kinase (JNK)-dependent cell death. Furthermore, they express very low levels of dMyc oncoprotein compared with those found in the surrounding normal tissue. Evidence that this is a cause of *lgl* mutant cells elimination was obtained by increasing dMyc levels in *lgl* mutant clones: their overgrowth potential was indeed re-established, with mutant cells overwhelming the neighbouring tissue and forming tumourous masses displaying several cancer hallmarks. Moreover, when *lgl* mutant clones were induced in backgrounds of slow-dividing cells, they upregulated dMyc, lost apical-basal cell polarity and were able to overgrow. Those phenotypes were abolished by reducing dMyc levels in the mutant clones, thereby confirming its key role in *lgl*-induced tumourigenesis. Furthermore, we show that the *eiger*-dependent Intrinsic Tumour Suppressor pathway plays only a minor role in eliminating *lgl* mutant cells in the wing pouch; $lgl^{-/-}$ clonal death in this region is instead driven mainly by dMyc-induced Cell Competition.

Conclusions: Our results provide the first evidence that dMyc oncoprotein is required in *lgl* tumour suppressor mutant tissue to promote invasive overgrowth in larval and adult epithelial tissues. Moreover, we show that dMyc abundance inside *versus* outside the mutant clones plays a key role in driving neoplastic overgrowth.

Background

In *Drosophila*, the tumour suppressor gene *lethal giant larvae* (*lgl*) functions together with *scribble* (*scrib*) and *discs large* (*dlg*) to link apical-basal cell polarity regulation to cell proliferation control in epithelial tissues [1,2]. Lgl, Dlg and Scrib are scaffold proteins associated with septate junctions at the lateral membrane, where they function in establishing basolateral domain identity by antagonising the activity of two other complexes: the Bazooka (Baz/Par3)/Par6/atypical Protein Kinase C (aPKC) and the Crumbs (Crb)/Stardust (Sdt)/PATJ complexes, which define the apical membrane domain [3]. Alterations to this process compromise apical-basal and cytoskeletal structure and eventually disrupt epithelial integrity [2]. When the whole individual is mutant for *lgl*, loss of cell structure and neoplastic overgrowth indeed occur, despite a low proliferation rate, in larval imaginal epithelia, monolayered diploid organs which give rise to the adult appendages. These epithelia grow as highly disorganised, multistratified masses in which cell differenti-

* Correspondence: daniela.grifoni@unibo.it
[1] Alma Mater Studiorum, Dipartimento di Patologia Sperimentale, Via S. Giacomo 14, 40126 Bologna, Italy
[†] Contributed equally
Full list of author information is available at the end of the article

ation does not occur and the animal dies after a prolonged larval stage [1,2]. Furthermore, when these tumourous tissues are transplanted into wild-type recipients, they overgrow and cells migrate to distant sites where they are able to form secondary tumours [4], thus showing some of the properties of mammalian metastatic cancers. The function of *lgl* as a tumour suppressor is evolutionarily conserved, since the human orthologue, *Hugl-1*, can rescue *Drosophila lgl* mutants, and downregulation of its activity in human cells results in cell polarity and proliferation defects and is associated with cancer [5,6]. Despite the malignant behaviour (increased tumour growth and survival and invasive properties) of *lgl* mutant tissues, adult wings from $lgl^{+/-}$ individuals in which $lgl^{-/-}$ clones had been generated at the larval stage by X-rays did not display tumourous growth [7], raising the possibility that *lgl* mutant cells could be eliminated through a mechanism induced by the surrounding tissue.

There are two mechanisms described in the literature that may act to prevent $lgl^{-/-}$ clones from developing into tumours. First, it has been recently shown that the growth of polarity-deficient *scrib* or *dlg* mutant clones is counteracted by the so-called *Intrinsic Tumour Suppression* (ITS) mechanism, which functions by triggering in the mutant cells both endocytic uptake and endosomal activation of the Eiger protein (homologue of the mammalian Tumour Necrosis Factor), which in turn leads to activation of pro-apoptotic JNK signaling [8,9]. However, when normal tissue surrounding the mutant clones is removed, mutant cells are no longer eliminated and grow into tumours [8]. ITS can be thus classified as a non-autonomous process, in which an as yet unknown signal from the normal tissue acts to induce the mutant cells to undergo apoptosis. Second, it has long been known that relatively slow-growing cells are eliminated from developing tissues by a phenomenon termed *Cell Competition* (CC), where slow-dividing cells are killed and replaced by the surrounding faster-growing populations, eventually giving rise to an organ of proper size [10]. CC was first described by analysing *Minute* (*M*) mutations in *Drosophila* [11], a group of dominant, homozygous-lethal mutations of various ribosomal genes. *M/+* cells are viable in a homotypic context (that is, all the cells composing the tissue are of the same genotype) though showing a reduced rate of cell proliferation; however, when juxtaposed to wild-type cells, they are eliminated by apoptosis and the wild-type cells overtake the *M/+* cells so that the organ eventually reaches normal size. It has been recently speculated that these competitive interactions could have evolved as a mechanism ensuring that viable but unfit, damaged or potentially harmful cells do not accumulate within a growing tissue, and this could be the case in normal development as well as in tumourigenesis [12,13]. During recent years it has become evident that different levels of dMyc protein in adjacent cell populations can trigger competitive interactions; cells with higher dMyc levels are able to out-compete those showing lower levels by inducing apoptotic death [14,15]. Both *Minute* and dMyc-induced CC are assumed to depend on a local difference in ribosome biogenesis or function that affects cell growth and proliferation [13]. Clonal alterations in dMyc expression are indeed detrimental due to its key role in cell growth, proliferation and biosynthesis [16] and upregulation of this protein is associated with almost all human cancers [17], among which carcinomas show in addition alterations in apical-basal cell polarity [18,19]. *lgl* mutant cells have both abnormal polarity and a reduced proliferation rate, so both ITS and CC may be involved in their elimination. In *Drosophila* epithelia, two main pathways are known to trigger apoptosis upon polarity alteration: the JNK signalling and the Hid/dIAP1 pathways [20]. JNK signalling has been clearly associated to ITS, while its involvement in dMyc-induced CC is still controversial [14,15].

In order to identify possible molecules and mechanisms associated with the phenotype of *lgl* mutant cells, we induced $lgl^{-/-}$ clones in diverse backgrounds and tissues. We show that $lgl^{-/-}$ clonal phenotype strictly depends on dMyc oncoprotein levels: when $lgl^{-/-}$ cells have lower levels of dMyc with respect to the surrounding tissue, their clonal growth is restricted by JNK-mediated apoptosis, whereas when $lgl^{-/-}$ cells have high levels of dMyc, mutant clones survive and proliferate to form invasive tumours.

Results and Discussion

lgl mutant clones die by caspase-dependent apoptosis when induced in an $lgl^{+/-}$ background

In order to investigate the proliferation and polarity phenotypes of *lgl* mutant cells during development, we induced clones of two different *lgl* null mutations in *Drosophila* wild-type wing discs, larval proliferating epithelia where competitive mechanisms between genetically different cell populations have been extensively characterised [14,15]. As can be observed in Figure 1A and Figure S1A, B in Additional File 1, lgl^{4} [21] or lgl^{27S3} [22] mutant clones grew preferentially in the proximal-distal direction, in a pattern similar to that of wild-type clones [23]. At two days after induction $lgl^{-/-}$ clones and their twin $lgl^{+/+}$ clones were similar in size (Figure S1A in Additional file 1), while at three days $lgl^{-/-}$ clones were about one half the size of their twins (bright white, compare Figure S1B and Figure S1A in Additional file 1, n = 40 each) and many of them (37%, n = 287) disappeared by the end of larval development, leaving only the twin clone (Figure S1B in Additional file 1, arrow). However, some persisted to the end of development, resulting in scarring of the adult wing (Figure S1C in Additional file 1).

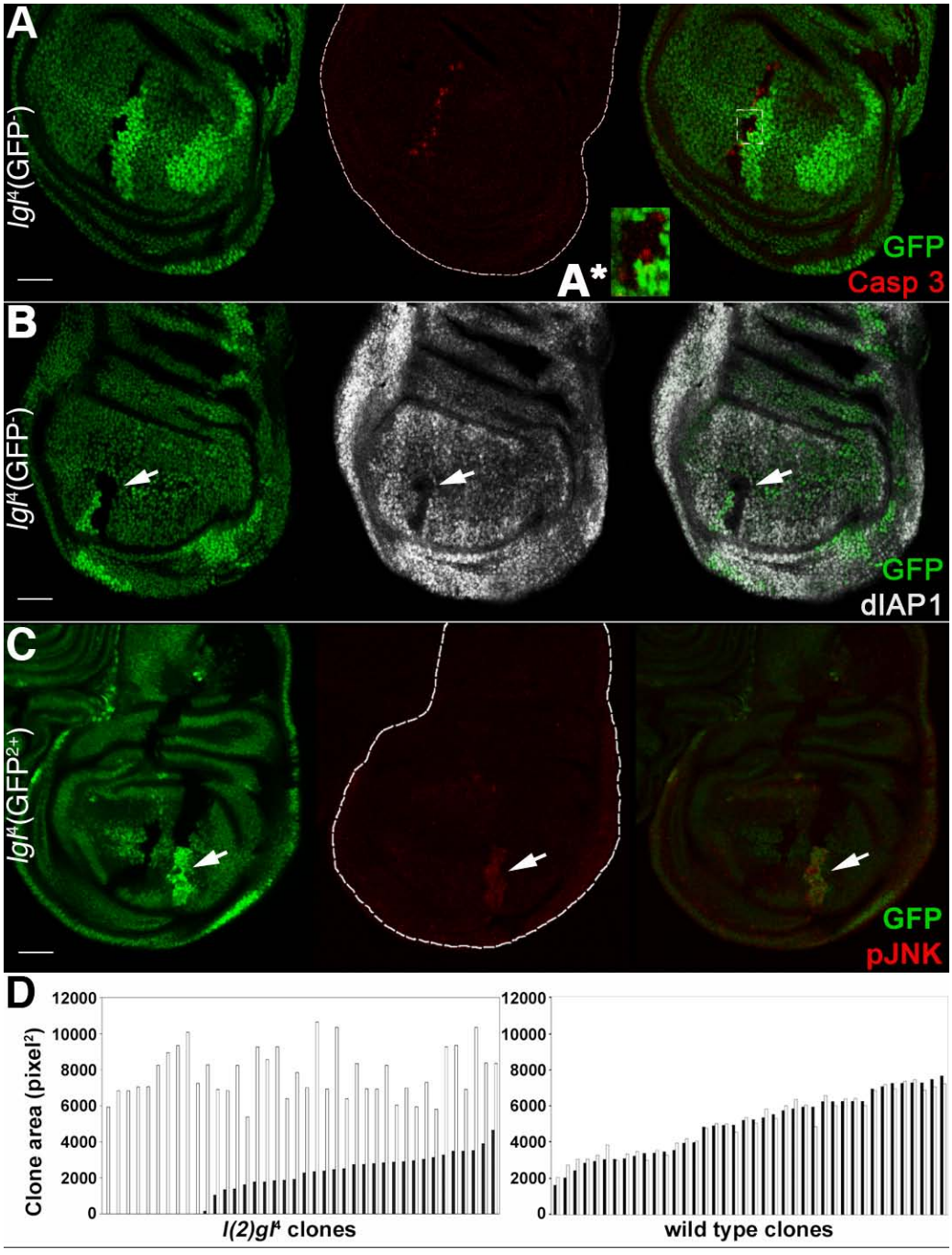

Figure 1 *lgl*$^{-/-}$ clones induced in *lgl*$^{+/-}$ imaginal wing discs die by apoptosis and the surrounding tissue grows at their expense. **A, B**: *lgl*$^{-/-}$ clones (GFP^{-}) induced in a *w, hs-Flp/+*; *l(2)gl*^{4}, FRT40A/*Ubi>GFPnls*, FRT40A background (GFP^{+}). Wild-type twin clones are GFP^{2+}. A: active-Caspase 3 staining; in A*, a magnification of the region outlined is shown. B: dIAP1 staining; its expression within the mutant clone (arrow) is visibly lower. **C**: *lgl*$^{-/-}$ clones (GFP^{2+}) induced in a *w, hs-Flp/+*; *l(2)gl*^{4}, *Ubi>GFPnls*, FRT40A/FRT40A background (GFP^{+}). Wild-type twin clones are GFP^{-}. pJNK staining shows that the JNK pathway is activated inside the *lgl* mutant clone (arrow). Wing discs are outlined in A and C. Scale bars are 35 μm. Mutant clone genotypes are indicated. **D**: *lgl*$^{-/-}$ (left panel) and wild-type (right panel) clone profile from a twin analysis of *l(2)gl*^{4} or wild-type clones sampled in the wing pouch region induced in a *w, hs-Flp/+*; *l(2)gl*^{4}, FRT40A or FRT40A/*Ubi>GFPnls*, FRT40A background. Black bars indicate *lgl*^{4} (n = 40) and wild-type (n = 40) clones and white bars indicate the respective twins. For this experiment, freshly hatched larvae were collected in a one-hour time window and staged on cornmeal medium to 90 hours after hatching before collecting tissues.

Staining for active-Caspase 3 revealed that *lgl*$^{-/-}$ cells die by apoptosis (Figure 1A) and in basal sections many pycnotic nuclei were visible within *lgl*$^{-/-}$ clones (Figure S1E in Additional file 1), confirming the presence of dying cells. Caspase activation occurred mostly in mutant cells at clonal boundaries, where mutant and normal tissues were in close contact (outlined, magnified in Figure 1A*). The anti-apoptotic protein *Drosophila* Inhibitor of Apoptosis 1 (dIAP1), ubiquitously expressed in imaginal tissues [24], was downregulated in *lgl*$^{-/-}$ cells (Figure 1B, arrow), whereas the JNK pathway was activated (as detected by phospho-JNK staining) in the mutant clones (Figure 1C, arrow). Possible crosstalk among these pathways in inducing cell death in *lgl* mutant clones will be discussed in detail in Section 5.

lgl mutant clones showed slight defects in disc folding, as revealed by F-actin staining (Figure S1D in Additional file 1, arrow); however, mutant cells did not seem to be strongly compromised in apical-basal polarity (as detected by aPKC and Scribble staining), at least up to 72 hrs after clone induction (Figures 2C and S1F, G in Additional file 1), and no discontinuities in basement membrane were visible (not shown), in agreement with previous observations [22,25].

lgl mutant cells express low levels of dMyc oncoprotein compared with the adjacent epithelium, and the latter grows at the expense of the lgl$^{-/-}$ clones

To test whether competitive interactions were involved in the elimination of *lgl*$^{-/-}$ cells from the normal tissue, we performed a double clonal assay in which *lgl*$^{-/-}$ clones were induced in an *lgl*$^{+/-}$ background in parallel to wild-type clones induced in a wild-type background (Figure 1D). As expected, while no differences were observed between wild-type control clones and their twins (right panel, black and white bars respectively, $P = 0.86$), *lgl* mutant clones were smaller than their wild-type twins (left panel, black and white bars respectively, $P < 0.001$), as well as smaller than wild-type clones induced in control discs (right panel, black bars, $P < 0.001$). The wild-type twins of *lgl*$^{-/-}$ clones (left panel, white bars) were instead much larger than the wild-type twins from control discs (right panel, white bars, $P < 0.001$). Since no dominant effects on cellular growth rate have been reported for *lgl* null mutations, and developmental stages of *lgl*$^{+/-}$ animals are of the same duration as those of *lgl*$^{+/+}$ individuals, even in clonal assays, this result suggests that some non-autonomous mechanisms are at work in *lgl*$^{-/-}$ clone elimination and that mutant cells are being replaced by the normal surrounding tissue.

Since it is known that differences in dMyc abundance among adjacent cells can trigger competitive behaviour [14,15], we next analysed dMyc protein levels and found that dMyc was weakly expressed within *lgl* mutant clones with respect to the surrounding *lgl*$^{+/-}$ tissue (Figure 2). We therefore speculated that cells bearing precancerous lesions that do not confer a survival or proliferative advantage relative to neighbouring cells, as with *lgl*$^{-/-}$ cells that lack dMyc protein, can be eliminated by apoptosis. In the wing disc, dMyc protein accumulates mainly in the distal region, the wing pouch, and is expressed only weakly in the proximal regions, hinge and pleura (see Figure S2A in Additional File 1). In these proximal regions, no differences in dMyc levels were visible between *lgl*$^{-/-}$ clones and the adjacent cells; such clones were larger than those in the wing pouch, although they never formed tumours (Figure S1G in Additional File 1. Proximal: 3,254 ± 1,129 pixels *vs* distal: 2,197 ± 756 pixels, n = 35 each; $P < 0.001$) and showed low levels of cell death (not shown). Thus, low dMyc levels in *lgl*$^{-/-}$ cells seem to affect growth and viability of these cells mainly in the distal region (wing pouch), where the surrounding tissue expresses high levels of dMyc.

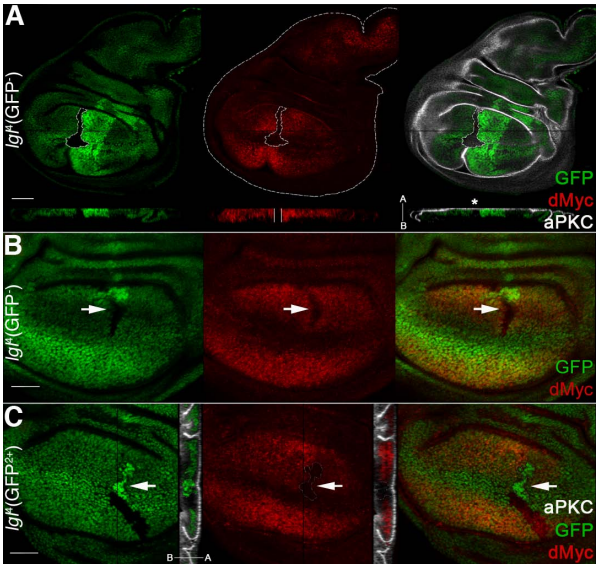

Figure 2 *lgl* mutant clones show low levels of dMyc oncoprotein with respect to the surrounding tissue. **A, B**: *lgl*$^{-/-}$ clones (GFP^{-}) induced in a *w, hs-Flp/+; l(2)gl*^{4}, FRT40A/*Ubi>GFPnls*, FRT40A background (GFP^{+}). Wild-type twin clones are GFP^{2+}. A: dMyc and aPKC staining; clone is outlined and the projection along the Z axis shows that dMyc expression within the mutant clone is low all along the disc thickness (enclosed between two white bars) and does not show strong defects in apical-basal cell polarity (asterisk). The apical-basal axis of the disc proper is also shown. Another *lgl*$^{-/-}$ clone showing low dMyc levels (arrow) can be observed in B at higher magnification. **C**: To show mutant nuclei, *lgl*$^{-/-}$ clones (GFP^{2+}, arrow) were also induced in a *w, hs-Flp/+; l(2)gl*^{4}, *Ubi>GFPnls*, FRT40A/FRT40A background (GFP^{+}). Wild-type twin clones are GFP^{-}. In the projection along the Z axis it can be seen that *lgl*$^{-/-}$ cells are being basally extruded from the epithelium. Wing disc is outlined in A. Scale bars are 35 μm. Mutant clone genotypes are indicated.

dMyc overexpression within lgl mutant clones unleashes their neoplastic potential

To investigate if the reduced level of dMyc protein in *lgl* mutant cells could be a cause of their elimination from the epithelium, we took advantage of the MARCM system [26] to express the *UAS-dmyc* construct [27] in $lgl^{-/-}$ clones. As can be observed in Figure 3A, $lgl^{-/-}$; *UAS-dmyc* (*dmyc*^{over}) clones were round in shape and massively overgrown, with the largest clones located in the proximal regions of the disc. A 10-fold increase in clone area was observed with respect to $lgl^{-/-}$ control clones induced through the same genetic system (average area of clones sampled in the hinge/pleura: 24,518 ± 4,237 pixels *vs* 2,725 ± 1,146 pixels respectively, n = 68 each). A gain in cell size has been reported for *dmyc*^{over} cells [28], raising the question of whether this could contribute in a significant way to $lgl^{-/-}$; *dmyc*^{over} clone area. Our analysis confirmed that cells in $lgl^{-/-}$; *dmyc*^{over} clones were larger than in $lgl^{-/-}$ control clones (83 ± 41 pixels vs 67 ± 32, n = 80 each), but this gain in cell size accounts only for a small fraction of clone expansion, indicating that the massive

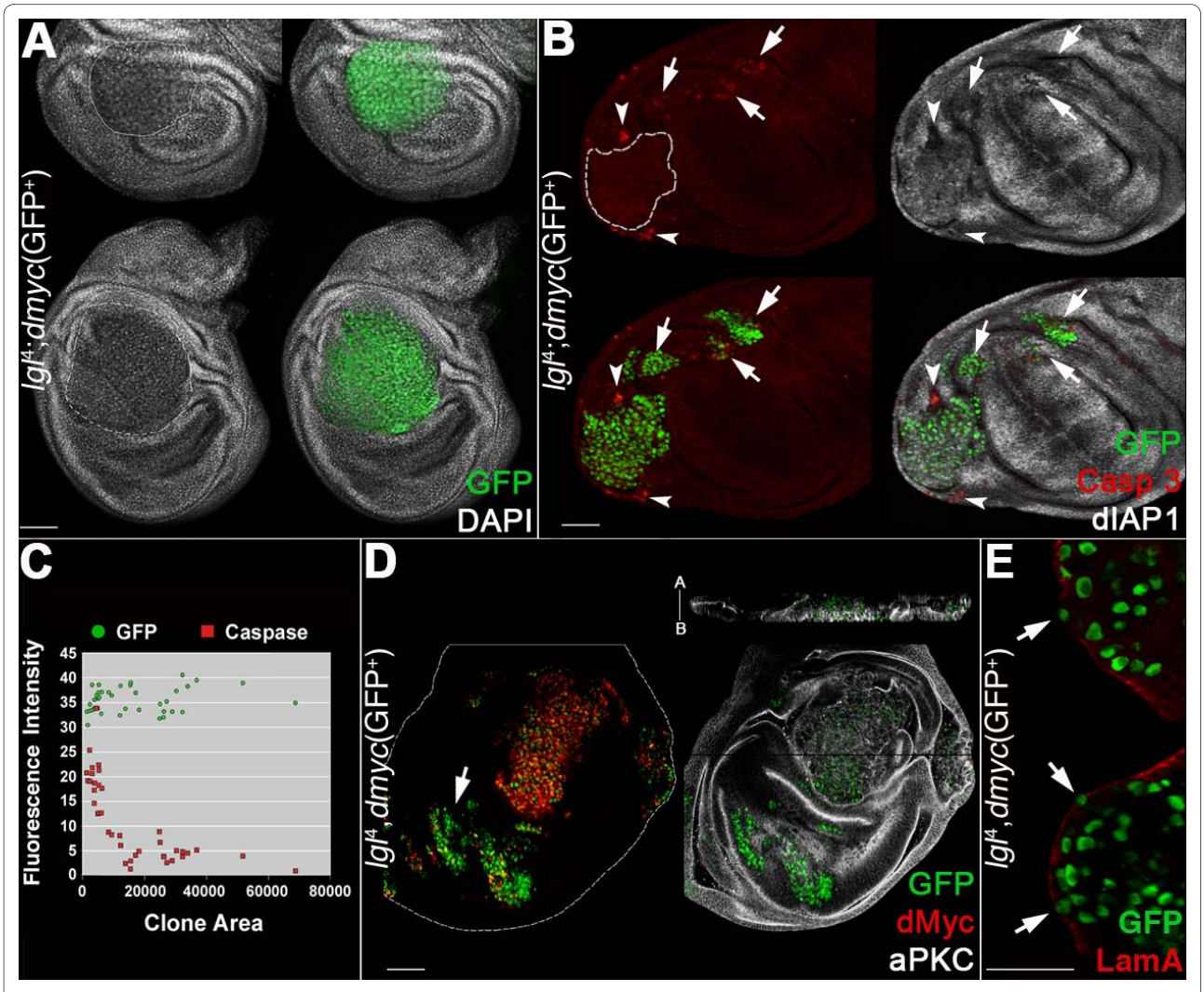

Figure 3 dMyc expression in $lgl^{-/-}$ clones induced in an $lgl^{+/-}$ background promotes overgrowth and invasive behaviour. **A-E**: $lgl^{-/-}$; *UAS-dmyc* clones (GFP^{+}) in a *yw*, *hs-Flp*, *tub>Gal4*, *UAS-GFP/+*; *l(2)gl*^{4}, FRT40A/*tub>Gal80*, FRT40A; *UAS-dmyc/+* background (GFP^{-}). A: clone morphology. B: active-Caspase 3 and dIAP1 staining; the arrows indicate groups of mutant cells undergoing autonomous apoptosis and the arrowheads indicate $lgl^{+/-}$ cells dying outside a mutant clone. C: distribution of the ratios 'clone area/active Caspase 3 fluorescence intensity' (red squares) and 'clone area/GFP fluorescence intensity' (green circles) as a control (n = 40); D: dMyc and aPKC staining; the projection along the Z axis shows the multilayered nature of the epithelium inside the mutant clone. The apical-basal axis of the disc proper is also indicated. The arrows indicate clones in the wing pouch that show low levels of dMyc protein. E: Laminin A staining; the arrows indicate regions of discontinuity. Wing disc is outlined in D. Scale bars are 35 μm. Mutant clone genotypes are indicated.

overgrowth of *lgl*$^{-/-}$; *dmyc*^{over} clones is due mainly to a substantial increase in cell number.

dMyc ectopic expression is associated with an autonomous increase in apoptosis [29], so we expected to find high levels of cell death within *lgl*$^{-/-}$; *dmyc*^{over} clones. However, while small clones showed many active-Caspase 3 positive cells (Figure 3B, arrows), the majority of the large clones showed little or no active-Caspase 3 staining (Figure 3B, clone outlined). We indeed found a significant negative correlation between clone size and active-Caspase 3 staining (Figure 3C, Spearman's rank correlation coefficient 0.716, $P < 0.001$). Furthermore, active-Caspase 3 staining was evident immediately outside the overgrown clones (Figure 3B, arrowheads), indicating that dMyc overexpression conferred *lgl*$^{-/-}$ cells the ability to out-compete neighbouring cells. dIAP1 protein was expressed in the overgrowing mutant clones (Figure 3B), but was undetectable in the smallest clones, where the active-Caspase 3 signal is the strongest (Figure 3B, arrows).

dmyc overexpression in *lgl*$^{-/-}$ cells therefore had a different outcome depending on the region of the disc where clones were located. In the proximal regions (hinge and pleura), where the endogenous dMyc levels are very low and competitive interactions between *lgl*$^{-/-}$ and wild-type cells are relaxed, some *lgl*$^{-/-}$; *dmyc*^{over} cells survived and formed clonal progeny that expressed dIAP1 and was therefore able to take advantage of dMyc's role in promoting biosynthesis and proliferation to out-compete surrounding cells (Figure 3B, arrowheads; see also the large clone in the hinge region in Figure 3D). *lgl*$^{-/-}$; *dmyc*^{over} clones located in the distal region (pouch) instead grew poorly, did not express dIAP1 protein and underwent untimely cell death (Figure 3B, arrows); the explanation for this behaviour could be because endogenous dMyc is expressed at high levels here, which is likely to prevent these *lgl*$^{-/-}$; *dmyc*^{over} clones from acquiring a competitive advantage. Other mechanisms could also be involved in generating such regional diversity in clonal growth, and further work is required to address this complex issue.

A staining for the apical marker aPKC indicated that *lgl*$^{-/-}$; *dmyc*^{over} cells displayed impaired apical-basal polarity (Figure 3D, see in particular the Z projection), a typical hallmark of epithelial neoplasias [30]. Staining for Laminin A, a major component of the basement membrane in both *Drosophila* and mammalian epithelia, revealed signs of discontinuity across the mutant clones (Figure 3E, arrows), suggesting that *lgl*$^{-/-}$; *dmyc*^{over} cells can acquire invasive properties, as has been demonstrated with other cooperative oncogenic models in *Drosophila* [25,31,32]. No pharate adults were recovered from larvae carrying *lgl*$^{-/-}$; *dmyc*^{over} clones (not shown), indicating that the differentiation of adult structures was impaired.

As discussed above, *lgl*$^{-/-}$; *dmyc*^{over} clones in the wing pouch behave differently from those in the wing hinge/pleura. In Figure 3D, the arrow indicates a clone in the wing pouch that does not exhibit tumourous properties. Notably, despite expression of *UAS-dmyc* transgene, clones do not show the high levels of dMyc protein observable in the clone located in the hinge. Since *dmyc* expression was induced using a heterologous promoter, the fact that dMyc protein is low in the *lgl* mutant clones in the wing pouch suggests that in this region an *lgl*-dependent regulation of *dmyc* at a post-transcriptional level is at work. Moreover, this result suggests that dMyc protein must be stably upregulated in *lgl* mutant clones in order to trigger overgrowth. This observation is similar to that of many human cancers, where Myc protein is highly and stably overexpressed [33]. Altogether, these data highlight a key role for *dmyc* in cooperating with the loss of a tumour suppressor to promote proliferation and to unleash the invasive potential of mutant cells.

dp110 kinase expression fails to rescue the defective growth of lgl mutant cells

To understand whether dMyc could be substituted in rescuing the defective growth of *lgl*$^{-/-}$ cells in an *lgl*$^{+/-}$ background by other growth-promoting molecules, we expressed in *lgl*$^{-/-}$ clones an activated form of the catalytic subunit of the Phosphoinositide-3 Kinase, *dp110*^{CAAX} [34], whose well-known role in cell growth and proliferation does not involve CC [14]. As can be observed in Figure S3B in Additional File 1, *dp110* is not able to rescue the defective growth of *lgl*$^{-/-}$ cells. Indeed, *UAS-dp110*^{CAAX}; *lgl*$^{-/-}$ clones are comparable in size to *lgl*$^{-/-}$ clones induced through the same technique (average area 1,974 ± 753 pixels *vs* 1,894 ± 916 pixels respectively, n = 40 each, $P = 0.67$); moreover, no significant impairments in cell polarity were observed (see Figure S3B in additional file 1, Z projection). As a control, a disc bearing *dp110*^{CAAX} clones is shown (Figure S3A in Additional file 1). Since it has been demonstrated that the ectopic expression of genes in the Insulin pathway, such as *dp110*, has no effect on ribosome biogenesis in *Drosophila* [35], it is plausible that the competitive properties of dMyc are due mainly to an increase in ribosome biogenesis [13,15]; its effect in increasing growth, proliferation and survival of *lgl* mutant cells could be due to the boosting of their biosynthetic rates.

Inhibition of cell death is not sufficient for driving tumourous growth of lgl mutant clones in the wing pouch region

Since several molecules associated with cell death were found to be deregulated in *lgl* mutant clones generated in an *lgl*$^{+/-}$ background (see Figure 1), we tried to rescue *lgl* mutant clones viability by co-expressing *dIAP1* or a dom-

inant negative form of the *Drosophila* JNK, *basket (bsk)*. As can be seen in Figure 4A, *lgl*$^{-/-}$; *UAS-dIAP1* clones in the wing pouch still showed active-Caspase 3 signals (arrow). A statistical analysis performed on clones found in the wing pouch indeed demonstrated that they are smaller than their wild-type twins (average area 7,721 ± 944 pixels *vs* 11,583 ± 1,248 pixels respectively, n = 28; $P < 0.001$). Since the JNK pathway is activated in *lgl* mutant clones in the wing pouch (Figure 1C, arrow), it could significantly contribute to their death. It has however previously been reported that JNK activation also occurs in response to dIAP1 inactivation [36,37]; therefore if the reverse interaction occurred it may be expected that JNK signalling would be absent in *lgl*$^{-/-}$; *UAS-dIAP1* cells but, as shown in Figure 4B, there is strong upregulation of active JNK, as detected by pJNK staining (arrow), indicating that it contributes to the elimination of *lgl* mutant clones independently of dIAP1. Both pJNK and active-Caspase 3 were also visible in the mutant clones in the proximal regions of the wing disc (Figure 4A, B, hinge and pleura respectively, white arrowheads), but their phenotype was quite different from that of clones in the wing pouch; they were large, round-shaped and, as can be seen in Figure 4A, active-Caspase 3 signal was also present in several cells surrounding the mutant clone (grey arrowheads). A statistical analysis showed that such clones were larger than their wild-type twins (average area 15,243 ± 1,228 pixels *vs* 9,855 ± 1,991 pixels respectively, n = 22; $P < 0.01$) These phenotypes were associated with high dMyc levels, as shown in Figure 4C (arrow); thus JNK signalling may here be subverted from a pro-apoptotic to a pro-growth function, as has been demonstrated to occur in genetic contexts in which alterations in the polarity genes *lgl*, *scrib* and *dlg* are accompanied by an ectopic expression of activated (oncogenic) Ras or Notch [32,38,39].

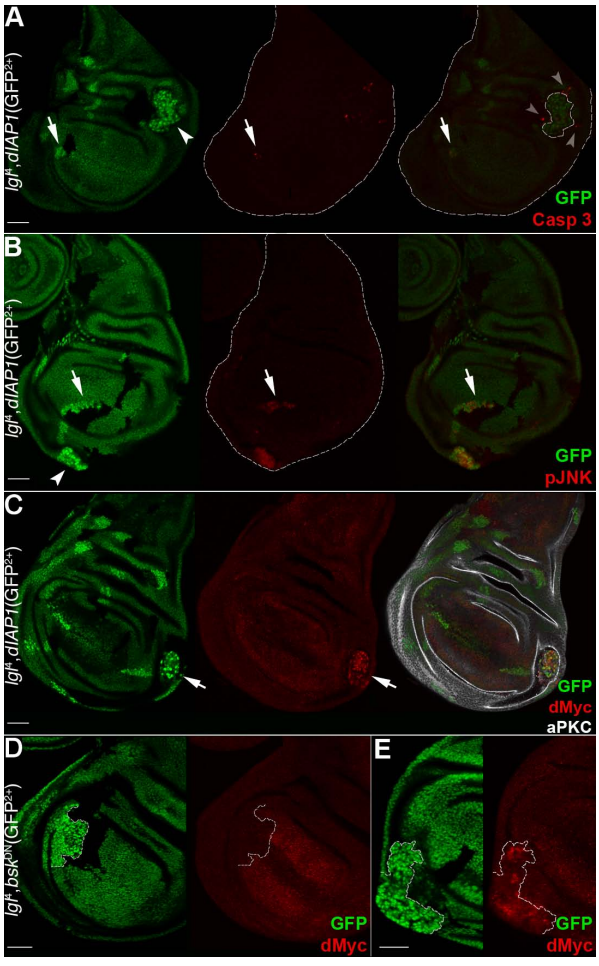

Figure 4 Inhibition of cell death is not sufficient to unveil the malignant potential of the *lgl*$^{-/-}$ clones in the wing pouch region. **A-C:** *lgl*$^{-/-}$; *UAS-dIAP* clones (GFP^{2+}) induced in a *yw*, *hs-Flp*, *tub>Gal4/+*; *l(2)gl*^{4}, *Ubi>GFPnls*, FRT40A/*tub>Gal80*, FRT40A; *UAS-dIAP/+* background (GFP^{+}). Wild-type twin clones are GFP^{-}. Active-Caspase 3 (A) and pJNK (B) signals are both visible inside *lgl* mutant clones (arrows). Arrowheads indicate clones in the proximal regions and grey arrowheads point to active-Caspase 3 signals in *lgl*$^{+/-}$ cells surrounding the mutant clone (outlined). In C, an *lgl*$^{-/-}$ clone expressing high levels of dMyc protein is shown (arrow). **D, E**: *UAS-bsk*^{DN}; *lgl*$^{-/-}$ clones (GFP^{2+}) induced in a *yw*, *hs-Flp*, *tub>Gal4/UAS-bsk*^{DN}; *l(2)gl*^{4}, *Ubi>GFPnls*, FRT40A/*tub>Gal80*, FRT40 background (GFP^{+}). Wild-type twin clones are GFP^{-}. dMyc protein is low in the mutant clone in the wing pouch (D) but is high in the clone in the pleura (E). Clone boundaries are indicated by the white dotted line. Wing discs are outlined in A and B. Scale bars are 35 μm. Mutant clone genotypes are indicated.

We then blocked the JNK pathway inside the *lgl*$^{-/-}$ clones by using a *bsk*^{DN} transgene [39] and found that the active-Caspase 3 signal was no longer observable in *lgl*$^{-/-}$ clones, regardless of the region in which they were located (not shown), indicating that JNK signalling-induced cell death is the main pathway by which *lgl* mutant cells die. As can be seen in Figure 4D, *UAS-bsk*^{DN}; *lgl*$^{-/-}$ clones in the wing pouch (outlined) expressed low levels of dMyc and did not form tumours; statistical analysis performed in this region showed that, despite the fact that *UAS-bsk*^{DN}; *lgl*$^{-/-}$ clones no longer died, their size was smaller than that of their wild-type twins (average area 12,697 ± 8,491 pixels *vs* 21,957 ± 8,372 pixels respectively, n = 15, $P < 0.001$), demonstrating that even when cell death is blocked *UAS-bsk*^{DN}; *lgl*$^{-/-}$ cells have a proliferative disadvantage with respect to the wild-type tissue.

In contrast to the wing pouch, *UAS-bsk*^{DN}; *lgl*$^{-/-}$ clones in the proximal regions (hinge and pleura) showed high dMyc protein levels, lost polarity and overgrew (Figure 4E), indicating that the pro-growth role of the JNK pathway observed in polarity-compromised clones overexpressing activated Ras or Notch [32,38,39] appears not to be necessary in the wing disc for the tumourous growth induced by the cooperation between *lgl* mutation and dMyc oncoprotein. Altogether, these data show that the

difference in clonal growth reported in section 2 for *lgl*$^{-/-}$ cells in the wing pouch *versus* the hinge/pleura regions also occurs for *lgl*$^{-/-}$ clones in which cell death has been inhibited and is also associated with the different levels of dMyc protein in the mutant *versus* the adjacent normal tissue.

The Intrinsic Tumour Suppressor pathway does not appear to be involved in lgl$^{-/-}$ cells elimination in the wing pouch region

A recent study demonstrated that clones of *scrib* and *dlg* tumour suppressor mutants generated in wild-type imaginal discs are eliminated by the Intrinsic Tumour Suppressor (ITS) pathway, involving JNK-dependent apoptosis induced by an endocytic accumulation of the TNF homologue, Eiger (Egr) [8]. Since *scrib* and *dlg* are well-known *lgl* partners in regulating apical-basal cell polarity and proliferation and show similar neoplastic phenotypes in a homotypic background [2], it could be expected that *lgl*$^{-/-}$ clones could be eliminated by a similar mechanism. To investigate this, we first looked for alterations in endocytosis in the *lgl* mutant clones by using an early-endosome reporter, *Rab5*, since it was observed by Igaki et al. [8] that Rab5-positive endosomes accumulated in *scrib* mutant clones in the eye disc correlating with pJNK staining. However, in the wing pouch region we did not observe changes in Rab5 levels within *lgl*$^{-/-}$ clones with respect to the neighbours (see Figure 5A, arrowhead, and respective magnification), whereas outside the wing pouch a moderate increase in Rab5 levels in *lgl*$^{-/-}$ clones was observed (see Figure 5A, arrow, and respective magnification). Since Igaki et al. [8] demonstrated that ITS depends on an autocrine TNF signalling, we then silenced the TNF homologue, *egr*, in *lgl* mutant cells by expressing a *UAS-egr*RNAi construct (for validation see Figure S4A, B in Additional File 1) and scored for changes in clone morphology, but no alterations were observed relative to the *lgl*$^{-/-}$ clonal phenotype (Figure 5B-B"). *lgl*$^{-/-}$; *UAS-egr*RNAi clones in the wing pouch were comparable in size to *lgl*$^{-/-}$ clones induced through the same system (average area pixels 2,954 ± 876 *vs* 3,177 ± 1,028 pixels respectively, n = 19 each; P = 0,58). Similar effects were seen in *lgl* mutant clones in discs in which the *UAS-egr*RNAi construct was expressed under the control of the *hedgehog* promoter in the whole posterior compartment, thereby also removing Egr protein in the *lgl*$^{+/-}$ background (not shown). In Figure 5B and 5B', the apical and basal sections of a wing pouch are shown in which an *lgl* mutant clone is being basally extruded (in Figure 5B the position of the mutant clone is outlined), which also showed increased pJNK staining (Figure 5B"). The fact that JNK signalling is increased here suggests that, in this case, JNK pathway activation is not triggered by *egr*-mediated ITS. We next expressed in *lgl* mutant clones a dominant negative form of *Rab5* [40] to block endocytosis, since in the Igaki et al. study [8] it was shown that blocking endocytosis decreased JNK signalling and cell death of *scrib* mutant clones. Indeed, we found that some *lgl*$^{-/-}$ mutant clones expressing *Rab5*^{DN} in the proximal regions overgrew (13 out of 27 scored, Figure 5C), while clones in the wing pouch never did. Again, *lgl*$^{-/-}$; *UAS-Rab5*^{DN} clones (arrows) in the wing pouch were much smaller than the wild-type twins (see Figure S4C in Additional File 1) and expressed both active-Caspase 3 (Figure 5D, arrow) and pJNK (Figure 5E, arrow), distinct from what has been observed for *scrib* mutant clones in the eye disc, where *Rab5*^{DN} expression increased their growth [8]. Notably, all the overgrowing clones observed in the proximal regions of the wing disc were characterised by high dMyc protein levels (Figure 5C). Taken together, these data exclude *egr*-mediated ITS as the main mechanism responsible for *lgl* mutant clones elimination, at least in the wing pouch.

lgl$^{-/-}$ cells grown in a Minute background overexpress dMyc, display a competitive behaviour and form malignant tumours

As we showed in section 5, *lgl*$^{-/-}$ cells grew slower than wild-type cells in a clonal context, which is possibly the main reason why they are eliminated from the epithelium. To confirm the hypothesis for an active role of CC in restraining *lgl*$^{-/-}$ clonal growth, we induced *lgl* mutant clones in the slow-dividing *Minute* background, to give them a proliferative advantage. As can be seen in Figure 6A-C"' and in the Additional File 2, *lgl* mutant clones in these larvae were able to overgrow (average area of clones sampled all across the wing disc: 12,974 ± 3,427 pixels *vs* 2,648 ± 1,211 pixels of *lgl* mutant clones in a wild-type background, n = 40 each) and cells became rounded, indicating that apical-basal polarity was lost, as can be seen in the Z projection where aPKC apical determinant spreads cortically. *lgl*$^{-/-}$ clones showed high levels of dMyc protein (Figure 6A, arrow), which accumulated mainly in those outside of the wing pouch (see also Figure S5 in Additional File 1). dMyc upregulation is attributable to *lgl* loss of function because wild-type cells did not show any changes in dMyc levels when growing in a *M/+* background (Figure S6 in Additional file 1; in particular, no dMyc accumulation was visible in a large clone in the hinge region, S6A, arrow). *lgl*$^{-/-}$ clones in the wing pouch did not overgrow, showed a level of dMyc similar to that found in the *M/+*, *lgl*$^{+/-}$ adjacent cells (Figure S5A in Additional File 1, clone outlined) and did not undergo apoptosis (not shown). In that region, dMyc endogenous expression is high (see Figure S5A in Additional File 1), so it is plausible that its upregulation by the loss of function of *lgl* was not sufficient to trigger the cell growth advan-

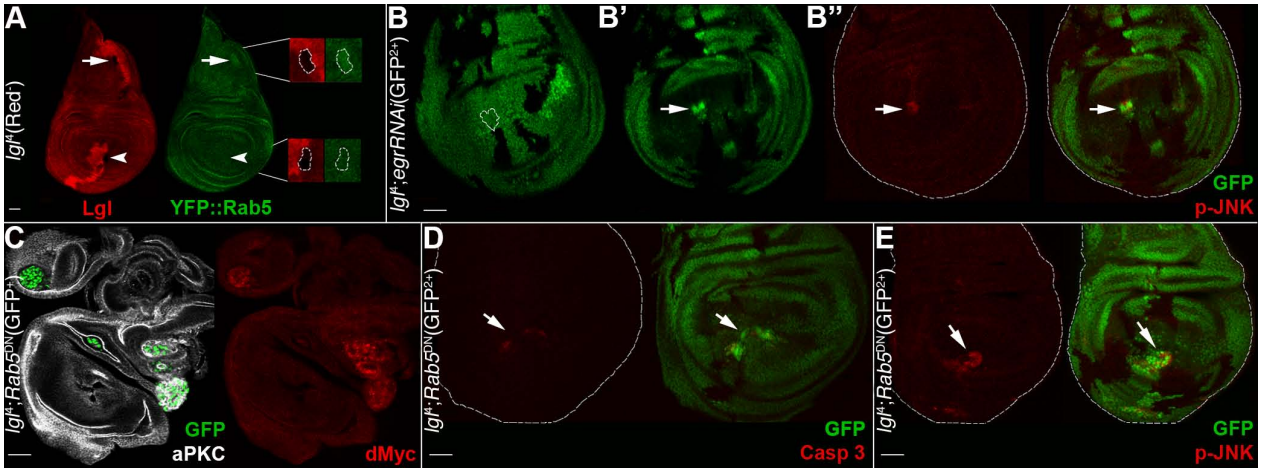

Figure 5 Intrinsic Tumour Suppression is not responsible for *lgl*$^{-/-}$ clonal death in the wing pouch region. **A:** Lgl antibody staining (red) of *lgl*$^{-/-}$ clones (black) induced in a *yw*, *hs-Flp*, *tub>Gal4/+*; *l(2)gl*^{4}, FRT40A/*tub>Gal80*, FRT40; *tub>YFP::Rab5/+*background (red^{+}). The wild-type twin clones are red^{2+}. The arrow indicates an *lgl* mutant clone in the notum where the *YFP::Rab5* signal is slightly increased and the arrowhead indicates an *lgl* mutant clone in the pouch where the *YFP::Rab5* signal is comparable to that found in the surrounding *lgl*$^{+/-}$ tissue. Magnifications of the mutant clones are shown on the right. **B-B":** *lgl*$^{-/-}$;*UAS-egr*RNAi clones (GFP^{2+}) induced in a *yw*, *hs-Flp*, *tub>Gal4/+*; *l(2)gl*^{4}, *Ubi>GFPnls*, FRT40A/*tub>Gal80*, FRT40A; *UAS-egr*RNA *i/+* background (GFP^{+}). Wild-type twin clones are GFP^{-}. B and B' show the apical and basal sections of the same disc; in the basal section a mutant clone contains cells that are basally excluded from the epithelium (arrow) and shows pJNK staining (B", arrow). The clone contour is outlined in B. **C:**, *lgl*$^{-/-}$; *UAS-YFP::Rab5*^{DN} clones (GFP^{+}) induced in a *yw*, *hs-Flp*, *tub>Gal4, UAS-GFP/+*; *l(2)gl*^{4}, FRT40A/*tub>Gal80*, FRT40A; *UAS-YFP::Rab5*^{DN}/+ background (GFP^{-}), stained with aPKC and dMyc. Due to high staining intensity inside the mutant clones, dMyc signal has been kept very low to avoid overexposure, so its endogenous expression is barely visible. **D, E**: *lgl*$^{-/-}$; *UAS-YFP::Rab5*^{DN} clones (GFP^{2+}) induced in a *yw*, *hs-Flp*, *tub>Gal4/+*; *l(2)gl*^{4}, *Ubi>GFPnls*, FRT40A/*tub>Gal80*, FRT40A; *UAS-YFP::Rab5*^{DN}/+ background (GFP^{+}). Wild-type twin clones are GFP^{-}. D: active-Caspase 3; E: pJNK. Wing discs are outlined in B", D and E. Scale bars are 35 μm. Mutant clone genotypes are indicated.

tage necessary for driving clonal expansion at the expense of the adjacent tissue.

In contrast, in regions where dMyc abundance is very low, such as the hinge and the pleura, dMyc upregulation by *lgl* mutation might be sufficient for clone overgrowth. In large *lgl*$^{-/-}$ clones in the hinge or pleura, dIAP1 was also expressed (Figure 6B') and active-Caspase 3 signal was evident in few cells in the mutant clones, but marked mainly groups of surrounding cells (Figure 6B, B', arrows), which were deficient in dIAP1 (Figure 6B, B', arrowheads). Moreover, cells lost polarity (Figure S5 in Additional file 1) and the basement membrane showed signs of discontinuity (arrows in Figure 6C'-C'", compared with the wild-type disc shown in C), indicating invasive behaviour. No pharate adults were recovered from mosaic larvae (not shown). Altogether, these data show that *lgl*$^{-/-}$ cells grown in a *M/+*, *lgl*$^{+/-}$ background can acquire a competitive advantage, which correlates with high dMyc expression and polarity loss. The upregulation of dMyc protein inside *lgl*$^{-/-}$ clones induced in the *M/+* background may be a consequence of an increase in *dmyc* transcript levels, since an upregulation of *dmyc* transcription, assayed by a *dm>LacZ* construct [41] (*dm* stands for *diminutive*, the gene encoding dMyc protein) was observed (Figure S7B in Additional File 1). In contrast, there was no correlation between *dmyc* transcription and protein abundance in *lgl*$^{-/-}$ clones grown in the *lgl*$^{+/-}$ background; the reduced levels of dMyc protein observed (Figure 2) did not result from a decrease in *dmyc* transcription (Figure S7A in Additional File 1), therefore post-transcriptional mechanisms must be at work in this case.

To determine the functional importance of dMyc upregulation in *lgl*$^{-/-}$ clones induced in the *M/+*, *lgl*$^{+/-}$ background, we silenced *dmyc* inside *lgl*$^{-/-}$ clones using a *UAS-dm*RNAi construct (for validation, see Figure S2C in Additional File 1). Knockdown of *dmyc* expression in *lgl*$^{-/-}$ clones prevented the cell polarity defects observed with *lgl*$^{-/-}$ clones alone (Figure 6D, compared with Figure 6A-C, Z projections), even when the *lgl* mutant tissue occupied a larger proportion of the disc (Figure 6D'); no degradation of basement membrane occurred (not shown) and clones did not form tumourous masses, regardless of the region in which they were located. Adults were indeed recovered at the expected frequency (not shown). Concerning the cell death pattern in these clones, it ranged from a complete absence of active-Caspase 3 signal in the majority of discs analysed (Figure 6E) to scattered signals, either in *lgl*$^{-/-}$ cells, surrounding cells, or in regions distant from mutant clones (Figure 6E', arrows). These results indicate that *lgl*$^{-/-}$; *UAS-dm*RNAi and *M/+*, *lgl*$^{+/-}$ cells coexist in the same tissue without undertaking competi-

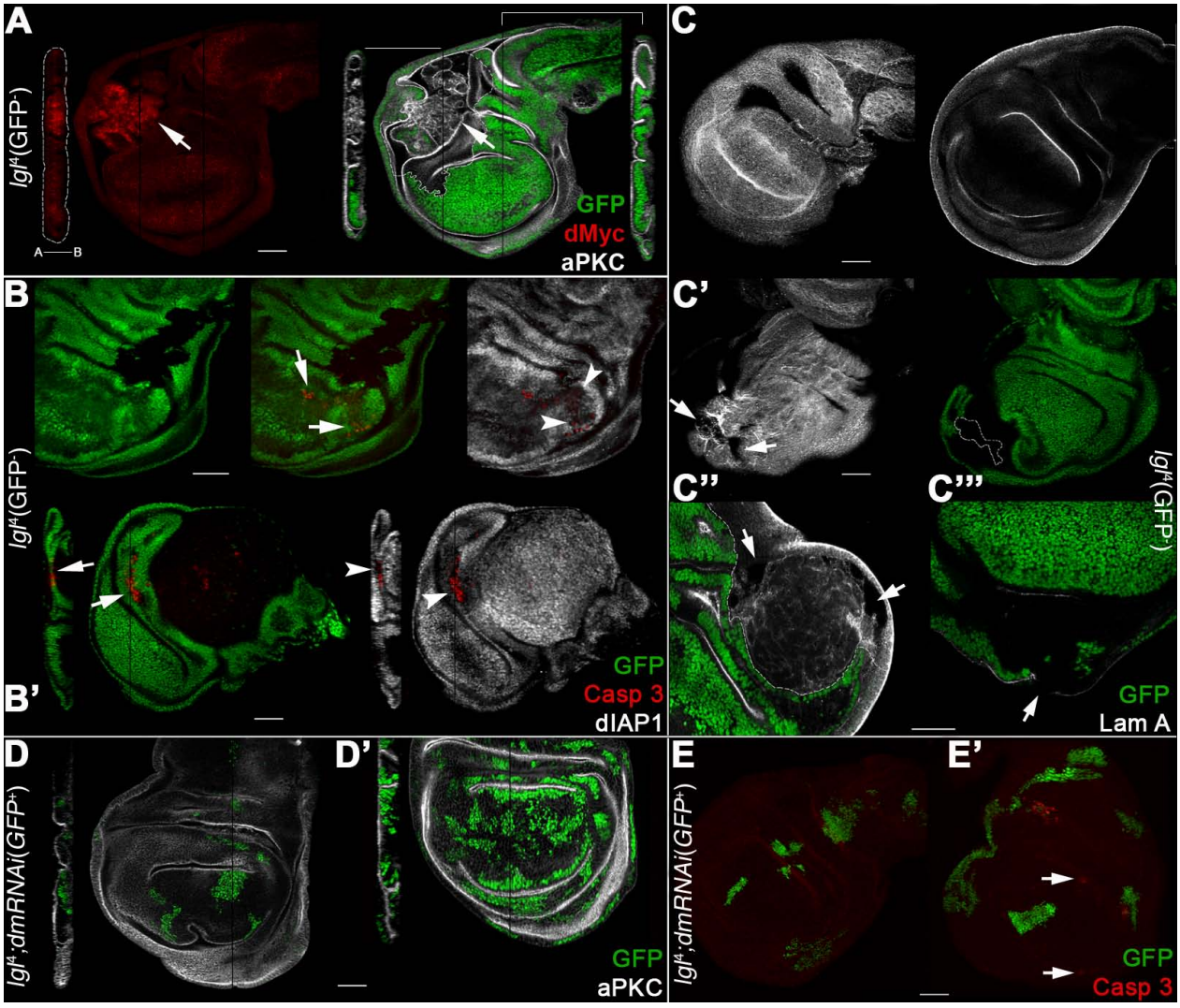

Figure 6 *lgl*$^{-/-}$ malignant behaviour in a *Minute* background depends on dMyc protein levels. **A-C''':** *lgl*$^{-/-}$ clones (GFP^{-}) in a *w, hs-Flp/+;l(2)gl*^{4}, FRT40A/*M(2)24F, Ubi>GFPnls*, FRT40A background (GFP^{+}). A: dMyc and aPKC staining. A strong dMyc accumulation is visible in the part of the mutant clone located in the hinge region (arrows). A Z projection of the mutant clone shows that loss of cell polarity accompanies the dramatic overgrowth; the apical-basal axis of the disc proper is shown. A Z projection of a region of the disc without mutant clones is shown on the right as a control. B: Activated Caspase 3 and dIAP1 staining. Arrows indicate *M/+*, *lgl*$^{+/-}$ cells dying around the mutant clones; the Z projection confirms that dying cells are outside the *lgl*$^{-/-}$ tissue. Arrowheads indicate that dying cells are deprived of dIAP1. C: Surface and cross sections of a wild-type disc stained with Laminin A. C'-C''': Laminin A staining of *lgl*$^{-/-}$ clones in a *M/+*, *lgl*$^{+/-}$ background; arrows indicate several points in which basement membrane integrity is lost. **D-E':** *lgl*$^{-/-}$; *UAS-dm*RNAi clones (GFP^{+}) in a *yw, hs-Flp, tub>Gal4, UAS-GFP/+;l(2)gl*^{4}, FRT40A/*M(2)24F, tub>Gal80*, FRT40A; *UAS-dm*RNAi/+ background (GFP^{-}). D, D': aPKC staining reveals that *lgl*$^{-/-}$; *UAS-dm*RNAi mutant cells in a *M/+*, *lgl*$^{+/-}$ background do not lose apical-basal polarity (compare with 6A). Heat shock pulses were 20 minutes (D) and 1 hour duration (D'). E, E': Caspase staining shows that apoptosis is either absent (E) or scattered throughout the disc (E', arrows). Scale bars are 35 μm. Mutant clone genotypes are indicated.

tive interactions, possibly because both populations show a similar impairment in cell proliferation. Similar results were obtained by Wu and Johnston upon the induction of *dm* loss-of-function clones in a *M/+* background [42]. *M/+* tissue could also intrinsically possess a low level of dMyc protein, but we were not able to detect differences in dMyc protein levels between wild-type and *M/+* clones throughout the wing disc (see Figure S6 in Additional File 1). Thus, the silencing of *dmyc* in *lgl*$^{-/-}$ clones and the reduced ribosomal pool in the *M/+*, *lgl*$^{+/-}$ background may make their levels of biosynthesis comparable. The ability of *lgl* mutant patches to grow despite dMyc deprivation might be due to the upregulation of other growth-promoting factors in the *M/+*, *lgl*$^{+/-}$ context, which are however *per se* unable to provide *lgl*$^{-/-}$ cells with tumourigenic features.

The oncogenic cooperation between lgl mutation and dMyc protein is not tissue-specific

With the aim of assessing whether the oncogenic cooperation between *lgl* mutation and dMyc protein could be conserved in other *Drosophila* tissues, we investigated *lgl*$^{-/-}$ clonal behaviour in the ovarian follicular epithelium, a monolayered adult tissue of somatic origin that surrounds the germ line of the egg chamber. Interestingly, the phenotype of *lgl*$^{-/-}$ clones in the follicular epithelium appeared to be rather different from that observed in the wing imaginal epithelia, but similar to that previously reported in the whole mutant animal; in females bearing a homozygous temperature-sensitive *lgl* mutation, egg chambers invariantly show hyperproliferation of follicular cells that display loss of apical-basal polarity and migrate between the nurse cells [43]. We found that *lgl* mutant clones overproliferated and formed multilayers near the chamber poles (Figure 7A), consistent with previous studies [2,44]. Active-Caspase 3 staining revealed that apoptosis was occasionally observable in egg chambers from Stage 8 onward in *lgl*$^{+/-}$ cells at the clone border (Figure 7B). This cell death pattern is reminiscent of a mechanism of dMyc-induced CC. CC, however, has never been described in the follicular epithelium, so we induced *dmyc*^{over} Flp-out clones [45] in adult females and observed the cell death pattern in their egg chambers. As can be seen in Figure S8 in Additional File 1, the wild-type tissue underwent massive cell death, particularly when it was completely surrounded by *dmyc*^{over} cells (arrows), suggesting that *dmyc* is able to induce apoptosis in the surrounding cells also in this tissue. Indeed, *lgl*$^{-/-}$ clones expressed dMyc protein in early egg chambers (Figure 7C) as well as at later stages (Figure 7C'), where endogenous protein is normally absent (see Figure S2B in Additional file 1). *dmyc* was also transcriptionally activated, as can be seen from *dm>LacZ* expression in Figure S7C in Additional file 1. Thus, *lgl*$^{-/-}$ clonal behaviour in the follicular epithelium positively correlates with *dmyc* expression. dIAP1 levels in *lgl*$^{-/-}$ follicular clones were similar to those seen in the *lgl*$^{+/-}$ adjacent tissue (see Figure 7E), and no autonomous apoptosis was visible in *lgl*$^{-/-}$ follicular cells (not shown). Further, we allowed clones to grow for four additional days in order to obtain stronger phenotypes. As can be seen in Figure 7D-D", dMyc protein was detectable in all *lgl*$^{-/-}$ cells; clonal phenotype varied from larger areas of multilayered tissue (Figure 7D), which sometimes extended away from the poles (Figure 7D'), to clones that invaded into the nurse cells territory (Figure 7D", arrow). To determine the contribution of *dmyc* to the *lgl* mutant phenotype in this tissue, we lowered dMyc levels inside *lgl*$^{-/-}$ cells using the *UAS-dm*RNAi construct. We observed a pronounced decrease both in clone size and number (visible clone area: 44% decrease in 60 clones at chamber poles analysed for each genotype; clone number: 74% decrease on a total of 20 pairs of ovaries for each genotype) and no multilayered tissue was seen, demonstrating that also in this epithelium dMyc protein is required for *lgl* mutant clones to grow as malignant tumours.

Conclusions

Deciphering the molecular crosstalk occurring between genetically different cell populations growing within a tissue is relevant to both developmental and cancer biology. In *Drosophila*, *lgl* mutant larvae show neoplastic overgrowth of the epithelial tissues, whereas *lgl*$^{-}$ cells growing in mosaic larvae are usually eliminated by cell death; thus this opposite phenotype results from mechanisms triggered by the confrontation of *lgl*$^{-}$ and *lgl*$^{+}$ cells. In the literature, two main processes have been described to mediate the elimination of unfit/polarity-deficient cells from *Drosophila* imaginal epithelia: *Cell Competition* (CC) and *Intrinsic Tumour Suppression* (ITS) [9]. Both mechanisms work by the induction of cell death in the mutant population; in addition, normal tissue grows at the expense of the unfit cells in CC [15], while this has not been shown for ITS [8]. There is suggestive evidence in the literature regarding the relevance of CC to cancer biology [12,13,46], however a clear connection between CC and tumour development is yet to be made.

dMyc oncoprotein has been shown to play a leading role in CC, in the sense that cells bearing low levels of this protein die by apoptosis if growing in a high dMyc-expressing context [14,15]. In ITS, cell death is instead triggered in the presence of cells with impaired polarity in an otherwise normal epithelium [8]. Here we found that JNK-mediated apoptosis is the main process through which *lgl* mutant clones are eliminated from imaginal wing epithelia (Figures 1C and 4D). Clonal phenotype is however different in the distal (wing pouch) and proximal (hinge/pleura) regions of the wing disc: *lgl* mutant clones located in the wing pouch showed massive cell death and were rapidly extruded from the epithelium (Figures 1 and S1E-F in Additional file 1), while clones located in the hinge/pleura grew to a larger extent, although they never formed tumours (Figure S1G in Additional file 1). This regional difference in clonal behaviour could depend on dMyc protein pattern in the wing disc; the protein is highly expressed in the wing pouch and very low in the hinge/pleura (Figure S2A in Additional file 1). We indeed found that *lgl*$^{-}$ clones in the wing pouch expressed very low levels of dMyc protein relative to the background (Figure 2); such clones died and were replaced by the surrounding wild-type tissue (Figure 1D). Moreover, *lgl*$^{-}$ clonal behaviour in the slow-dividing *Minute* background (Figure 6) or in the follicular epithelium (Figure 7) switched from *out-competed* to *overgrown and invasive*,

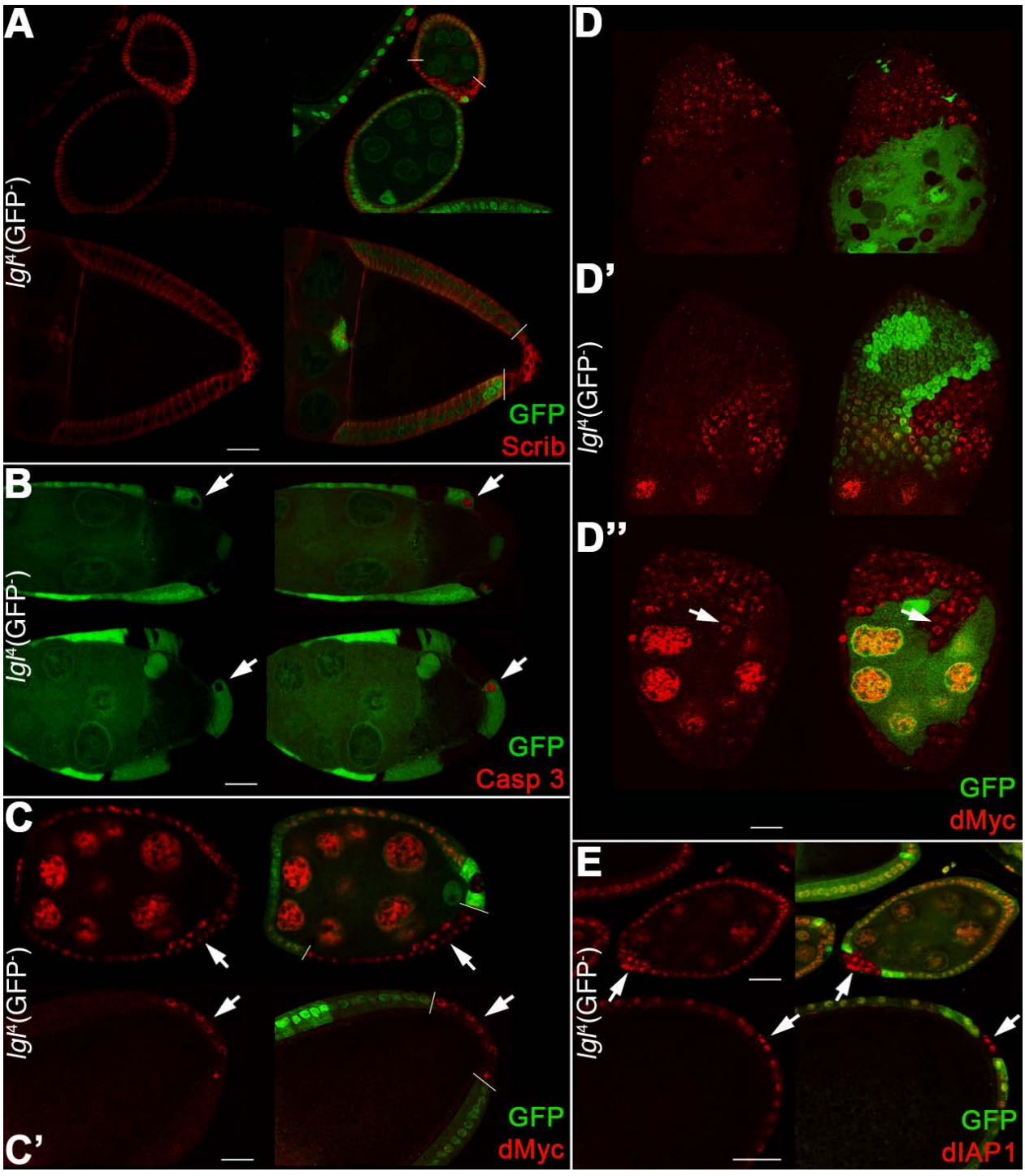

Figure 7 *lgl*$^{-/-}$ clonal overgrowth is sustained by dMyc expression also in the follicular epithelium. **A-E:** Twin-clone analysis of *lgl*$^{-/-}$ clones (GFP^{-}) induced in a *w, hs-Flp/+; l(2)gl*^{4}, FRT40A/*Ubi>GFPnls*, FRT40A background (GFP^{+}). Wild-type twin clones are GFP^{2+}. A: *lgl*$^{-/-}$ clones (bordered by white bars) stained for Scrib are shown in early and late egg chambers. Scrib distribution spreads from lateral to cortical as mutant cells become round. B: active-Caspase 3 staining of Stage 8 to 9 egg chambers; arrows indicate wild-type cells undergoing apoptosis. C: dMyc staining of early (C) and late (C') egg chambers. Bars mark clone boundaries and arrows indicate dMyc expression inside the mutant clones. D-D": dMyc staining in older *lgl*$^{-/-}$ clones; in D" the arrow indicates mutant cells migrating into the nurse cell territory. E: dIAP1 staining of early and late egg chambers. The arrows indicate high dIAP1 expression in the *lgl*$^{-/-}$ clones. Mutant clone genotypes are indicated.

with the tumourous mutant clone invariantly showing high dMyc levels relative to the neighbouring tissue. Lowering dMyc abundance inside those clones prevented the tumourous phenotype (Figure 6D and data not shown), whereas dMyc overexpression in *lgl*$^{-}$ mutant clones in a wild-type background was able to confer increased proliferation, survival and invasive properties (Figure 3), clearly demonstrating that dMyc plays a key role in *lgl*$^{-}$ cells behaviour. In all the cases analysed, clonal overgrowth of *lgl*$^{-}$ *dmyc*^{over} tissue was observed in the proximal regions of the wing disc, where endogenous dMyc is poorly expressed, underlining the importance of a favourable dMyc gradient between the mutant clone and the surrounding tissue in triggering *lgl*-induced malignancy. We also showed that ITS is not responsible for *lgl* mutant cells elimination in the wing pouch, in contrast to what was observed for the other two neoplastic tumour suppressor mutants *scrib* and *dlg* [8]; *lgl*$^{-}$ clones located in the distal regions still died even upon *egr* silencing or endocytosis inhibition (Figure 5B-D). In the pouch, where dMyc protein is highly expressed, *lgl*$^{-}$ cells instead underwent apoptosis due to low levels of dMyc protein relative to their neighbours, since when dMyc levels were restored in the mutant clones, as happens in a slow-growing *Minute* background, *lgl* mutant cells no longer died. This is first evidence that dMyc-induced CC protects tissues from tumourous growth. On the other hand, blockade of endocytosis in *lgl* mutant tissue located outside of the wing pouch resulted in clonal overgrowth, indicating that ITS is likely to be involved in the elimination of *lgl* mutant cells in this region. Also in this case, dMyc upregulation was observed in the overgrown mutant tissue (Figure 5C).

The main conclusion of our work is that dMyc protein levels dictate the behaviour of *lgl*$^{-}$ tissue: when dMyc is highly expressed it cooperates with *lgl* mutations in a cell-autonomous manner, driving malignant growth in different contexts and organs, whereas when dMyc is downregulated in *lgl*$^{-}$ tissue relative to the wild-type surrounding cells, the *lgl* mutant cells are eliminated by CC. Moreover, it appears that CC and ITS play an important role in epithelial integrity, eliminating potentially harmful cells in complementary regions of the wing disc.

How does Lgl depletion lead to dMyc upregulation in particular tissues? Recent analysis [47] has revealed that depletion of Lgl in the eye disc leads to deregulation of the Salvador-Warts-Hippo (SWH) tumour suppressor pathway, an evolutionarily conserved signalling pathway that controls organ size and prevents hyperplastic diseases from flies to humans by restricting the activity of the transcriptional coactivator Yorkie [48]. Further to this, we found that *dmyc* is a transcriptional target of the SWH pathway, and dMyc protein is strongly upregulated in mutant clones of many members of the pathway (unpublished data). Consistent with the SWH pathway being deregulated, the *bona fide* Yorkie target, dIAP1 [49,50] was upregulated in larger *lgl*$^{-}$ clones that overgrew and expressed dMyc (Figure 6B' and data not shown), although further analysis of this in wing disc clones using other SWH targets is required to confirm this. We also note that the upregulation of dMyc in *lgl*$^{-}$ tissue correlates with a loss in apico-basal polarity (Figures 6A and S5B in Additional file 1, arrow). Although in the eye disc *lgl*$^{-}$ clones deregulate the SWH pathway without polarity loss [47], this does not seem to be the case in the wing, since the SWH target dIAP1 was only upregulated in *lgl*$^{-}$ tissue where polarity is lost. The results of our study suggest that upon Lgl depletion, to the extent that apical-basal cell polarity is compromised, that is, in a *Minute* context in the wing disc or in the ovarian follicular cells, deregulation of the SWH pathway occurs and, as a consequence, upregulates *dIAP1* and *dmyc*. The activity of the *dmyc* promoter is indeed increased in *lgl*$^{-}$ clones induced in a *Minute* background and in follicular cells (Figure S7B, C in Additional file 1). In *lgl*$^{-}$ clones induced in a wild-type context, where *lgl* mutant cells do not lose polarity (Figure S1F, G in Additional file 1), *dmyc* transcription is not altered (Figure S7A In Additional file 1). In these clones, dMyc protein is downregulated, which could occur by post-transcriptional mechanisms affecting protein stability [51].

Examples of these complex behaviours are also present in the literature describing mammalian carcinogenesis, in which the role of polarity proteins is still not well understood. It has been recently shown that *c-myc* cooperates with *scribble* tumour suppressor to induce the neoplastic progression observed during mammary tumourigenesis [52]. On the other hand, in a murine model of FAP, *APC*$^{-}$ cells deprived of *c-myc* were out-competed by surrounding, *c-myc*-expressing wild-type cells, thereby reverting the malignant phenotype, suggesting that CC could play a role in mammalian carcinogenesis [53].

Complex molecular interactions among genetically different cells growing in an organ emerge from our study, which in turn activate several safeguard mechanisms to restrict overgrowth and preserve epithelial integrity. Due to the conservation of signalling pathways, cell proliferation, and cell death pathway genes between fly and humans, *Drosophila* represents an ideal system for analysing the early events occurring in tumourigenesis upon the confrontation of different cell populations, and further analysis will help dissect these mechanisms.

Methods

Mosaic analyses

For the list of mutant and transgenic flies utilised, please see Additional File 1.

lgl^{27S3} and *lgl*^{4} mutant phenotypes are fully rescued by expression of *UAS-lgl* transgenes, resulting in normal larval and adult structures [22,5].

For mosaic analyses, either the Flp-FRT [54] or MARCM [26] systems were used. For larval staging, freshly hatched larvae were collected in a one-to-four hour time window. For the twin analysis, larvae were heat shocked 48 hours After Egg Laying (AEL) for one hour at 37°C and adult females were heat shocked one to two days after eclosion for one hour at 37°C. For the MARCM system, larvae were heat shocked 48 hours After Egg Laying (AEL) for 20 minutes at 37°C. *Minute* individuals were always heat shocked at 72 hours AEL to compensate for developmental delay. For the Flp-out system [45], adult females were heat shocked one to two days after eclosion for eight minutes at 37°C. For all the systems used, tissues were collected 72 hours after the heat shock both for larvae and adults, unless otherwise specified. All crosses were kept at 25°C.

Immunofluorescence

Imaginal discs and ovaries were fixed and stained according to standard protocols. The following antibodies and dilutions were used: rabbit anti-active-Caspase 3 (1:200, (9664S) Cell Signaling Technology, Inc., Danvers, MA, USA); mouse anti-dIAP1 (1:100, BA Hay); rabbit anti-Laminin A (1:200, Y Kitagawa); rabbit anti-Scribble (1:100, CQ Doe); mouse anti-dMyc (1:5) [55]; mouse anti-βGal (1:25, [40-1a] DSHB, University of Iowa, Iowa City, IA, USA); rabbit anti-βGal (1:50, F Graziani); rabbit anti-aPKCζ (1:200, [sc-216] Santa Cruz Biotechnology, Inc., Santa Cruz, CA, USA); mouse anti-phospho-JNK (1:100, [G9 clone] Cell Signaling Technology Inc., Danvers, MA, USA); rabbit a-Egr (1:500, M Miura). Alexa Fluor 555 or 568 goat anti-mouse and anti-rabbit (1:200, Invitrogen Corporation, Carlsbad, CA, USA) and Cy5-conjugated goat anti-mouse and anti-rabbit (1:100, Jackson ImmunoResearch Laboratories, Inc., West Grove, PA, USA) were used as secondary antibodies. DAPI and TOPRO staining were used to detect DNA and phalloidin staining to detect F-actin. Samples were analysed by laser confocal microscopy (Leica TSC SP2, Leica Microsystems SpA, Milan, Italy) and entire images were processed with Adobe Photoshop software. ImageJ free software from NIH, Bethesda, MD, USA was used for rebuilding the projections along the Z axis starting from 25-45 Z stacks.

Measurements and statistical analysis

To measure clone area (in pixel^2) and fluorescence intensity (in calibrated units), ImageJ free software from NIH, Bethesda, MD, USA, was used. Fluorescence intensity (signal intensity) was calculated as the average gray value within the selection. The average and the standard deviation alone or the t-Student test *P* value are given in the text. For the correlation between clone size and active-Caspase 3 staining in Figure 3, the Spearman's rank correlation coefficients were calculated using the software XLSTAT (available at http://www.xlstat.com). To measure average cell area in wing disc clones, TOPRO stained nuclei and clone area were scored in confocal series and the relative cell area (in pixels^2) was calculated.

Additional material

Additional file 1 Fly stocks and additional figures and legends in Portable Document Format. Stock list and Eight additional figures with respective legends.

Additional file 2 Movie. Movie of a *M/+* imaginal wing disc in which a large *lgl* mutant clone (GFP-) is visible. The whole thickness of the disc is shown in which the overgrowth of the mutant clone is clearly observable.

Abbreviations

AEL: After Egg Laying; APC: Adenomatous Polyposis Coli; aPKC: atypical Protein Kinase C; bGal: beta Galactosidase; Bsk: Basket; Baz: Bazooka; CC: Cell Competition; Crb: Crumbs; DAPI: 4',6-Diamidino-2-Phenylindole; Dlg: Discs large; dIAP1: drosophila Inhibitor of Apoptosis 1; dm: diminutive; DN: Dominant Negative; Egr: Eiger; FAP: Familial Adenomatous Polyposis; Flp: Flippase; FRT: Flippase Recognition Targets; GFP: Green Fluorescent Protein; Hid: Head Involution Defective; hrs: hours; hs: heat shock; Hugl-1: Human giant larvae 1; ITS: Intrinsic Tumour Suppression; JNK: Jun N-terminal Kinase; Lgl: Lethal giant larvae; M: Minute; MARCM: Mosaic Analysis with a Repressible Cell Marker; nls: nuclear localisation signal; Over: Overexpressed; PATJ: Pals 1-Associated Tight Junction protein; PAR3: Partitioning defective 3; PAR6: Partitioning defective 6; Scrib: Scribble; Sdt: Stardust; UAS: Upstream Activating Sequences; vs: versus; pJNK: phosphoJNK; TNF: Tumour Necrosis Factor; RNAi: RNA interference; SWH: Salvador Warts Hippo; tub: tubulin; Ubi: Ubiquitin; YFP: Yellow Fluorescent Protein.

Authors' contributions

FF, MZ and NAG carried out the experiments; FG participated in conceiving the project. PB, DS, HER, AP and AP* participated in designing the experimental layout and DG conceived the study and wrote the paper.

Acknowledgements

We thank Chris Q Doe, Bruce A Hay, Masayuki Miura, Yasuo Kitagawa and the DSHB for reagents; Luis Alberto Baena-López, the Bloomington Stock Center and the VDRC for fly strains, Giuseppe Gargiulo and Valeria Cavaliere for sharing their laboratory. This work was supported by a grant from the Italian AIRC (RG 6238) to AP and from the Australian NHMRC to HER and NAG. FF is a Fellow of the PhD Program in "Cell Biology and Physiology", Alma Mater Studiorum; MZ is supported by the "Fondazione Cassa di Risparmio in Bologna"; HER is supported by a NHMRC Senior Research Fellowship and DG is supported by a Senior Research Fellowship from Alma Mater Studiorum.

Author Details

[1]Alma Mater Studiorum, Dipartimento di Patologia Sperimentale, Via S. Giacomo 14, 40126 Bologna, Italy, [2]Alma Mater Studiorum, Dipartimento di Biologia Evoluzionistica Sperimentale, Via Selmi 3, 40126 Bologna, Italy, [3]NGB Genetics s.r.l., University of Ferrara, Via Borsari 46, 44100 Ferrara, Italy, [4]Alma Mater Studiorum, Dipartimento di Ginecologia, Ostetricia e Pediatria, Via Massarenti 9, 40138 Bologna, Italy, [5]Peter MacCallum Cancer Centre, Research Division, 7 St Andrew's Place, East Melbourne, Victoria 3002, Australia, [6]City College of the City University of New York, Department of Biology, Convent Ave at 138th, New York, NY 10031, USA, [7]Johannes Gutenberg University, First Department of Internal Medicine, 63 Obere Zahlbacherstr, 55131 Mainz, Germany and [8]Department of Anatomy and Cell Biology and Department of Biochemistry and Molecular Biology, University of Melbourne, Parkville, Victoria 3052, Australia

Received: 9 November 2009 Accepted: 7 April 2010
Published: 7 April 2010

References

1. Humbert P, Russel S, Richardson H: **Dgl, Scribble and Lgl in cell polarity, cell proliferation and cancer.** *Bioessays* 2003, **25:**542-553.
2. Bilder D: **Epithelial polarity and proliferation control: links from the *Drosophila* neoplastic tumor suppressors.** *Genes Dev* 2004, **18:**1909-1925.
3. Dow LE, Humbert PO: **Polarity regulators and the control of epithelial architecture, cell migration, and tumorigenesis.** *Int Rev Cytol* 2007, **262:**253-302.
4. Woodhouse E, Hersperger E, Shearn A: **Growth, metastasis and invasiveness of *Drosophila* tumors caused by mutations in specific tumor suppressor genes.** *Dev Genes Evol* 1998, **207:**542-550.
5. Grifoni D, Garoia F, Schimanski CC, Schmitz G, Laurenti E, Galle PR, Pession A, Cavicchi S, Strand S: **The human protein Hugl-1 substitutes for *Drosophila lethal giant larvae* tumour suppressor function *in vivo*.** *Oncogene* 2004, **23:**8688-8694.
6. Grifoni D, Garoia F, Bellosta P, Parisi F, De Biase D, Collina G, Strand D, Cavicchi S, Pession A: **aPKCζ cortical loading is associated with Lgl cytoplasmic release and tumor growth in *Drosophila* and human epithelia.** *Oncogene* 2007, **26:**5960-5965.
7. Sinha P, Joshi S, Radhakrishnan V, Mishra A: **Developmental effects of *l(2)gl* ^{4} and *l(2)gd* recessive oncogenes on imaginal discs of *D. melanogaster*.** *Cell Differ Dev* 1989:S.577.
8. Igaki T, Pastor-Pareja JC, Aonuma H, Miura M, Xu T: **Intrinsic Tumor Suppression and Epithelial Maintenance by Endocytic Activation of Eiger/TNF Signaling in *Drosophila*.** *Dev Cell* 2009, **16:**458-465.
9. Igaki T: **Correcting developmental errors by apoptosis: lessons from *Drosophila* JNK signaling.** *Apoptosis* 2009, **14:**1021-1028.
10. Lecuit T, Le Goff L: **Orchestrating size and shape during morphogenesis.** *Nature* 2007, **450:**189-192.
11. Morata G, Ripoll P: **Minutes: mutants of *Drosophila* autonomously affecting cell division rate.** *Dev Biol* 1975, **42:**211-221.
12. Moreno E: **Is cell competition relevant to cancer?** *Nat Rev Cancer* 2008, **8:**141-147.
13. Johnston LA: **Competitive interactions between cells: death, growth, and geography.** *Science* 2009, **324:**1679-1682.
14. de la Cova C, Abril M, Bellosta P, Gallant P, Johnston LA: ***Drosophila* Myc regulates organ size by inducing cell competition.** *Cell* 2004, **117:**107-116.
15. Moreno E, Basler K: **dMyc tansforms cells into super-competitors.** *Cell* 2004, **117:**117-129.
16. de la Cova C, Johnston LA: **Myc in model organisms: A view from the flyroom.** *Semin Cancer Biol* 2006, **16:**303-312.
17. Vita M, Henriksson M: **The Myc oncoprotein as a therapeutic target for human cancer.** *Semin Cancer Biol* 2006, **16:**318-330.
18. Hanahan D, Weinberg RA: **The hallmarks of cancer.** *Cell* 2000, **100:**57-70.
19. Thiery JP: **Epithelial-mesenchymal transition in development and pathologies.** *Curr Opin Cell Biol* 2003, **15:**740-746.
20. Herz HM, Chen Z, Scherr H, Lackey M, Bolduc C, Bergmann A: **vps25 mosaics display non-autonomous cell survival and overgrowth, and autonomous apoptosis.** *Development* 2006, **133:**1871-1880.
21. Gateff E: **Malignant neoplasms of genetic origin in *Drosophila melanogaster*.** *Science* 1978, **200:**1448-1459.
22. Grzeschik NA, Amin N, Secombe J, Brumby AM, Richardson HE: **Abnormalities in cell proliferation and apico-basal cell polarity are separable in *Drosophila lgl* mutant clones in the developing eye.** *Dev Biol* 2007, **311:**106-123.
23. Resino J, Salama-Cohen P, Garcìa-Bellido A: **Determining the role of patterned cell proliferation in the shape and size of the *Drosophila* wing.** *Proc Natl Acad Sci USA* 2002, **99:**7502-7507.
24. Yoo SJ, Huh JR, Muro I, Yu H, Wang L, Wang SL, Feldman RM, Clem RJ, Muller HA, Hay B: **Hid, Rpr and Grim negatively regulate DIAP1 levels through distinct mechanisms.** *Nat Cell Biol* 2002, **4:**416-424.
25. Pagliarini RA, Xu T: **A genetic screen in *Drosophila* for metastatic behavior.** *Science* 2003, **302:**1227-1231.
26. Lee T, Luo L: **Mosaic analysis with a repressible cell marker (MARCM) for *Drosophila* neural development.** *Trends Neurosci* 2001, **24:**251-254.
27. Bellosta P, Hulf T, Balla Diop S, Usseglio F, Pradel J, Aragnol D, Gallant P: **Myc interacts genetically with Tip48/Reptin and Tip49/Pontin to control growth and proliferation during *Drosophila* development.** *Proc Natl Acad Sci USA* 2005, **102:**11799-11804.
28. Johnston LA, Prober DA, Edgar BA, Eisenman RN, Gallant P: ***Drosophila myc* regulates cellular growth during development.** *Cell* 1999, **98:**779-790.
29. Montero L, Müller N, Gallant P: **Induction of apoptosis by *Drosophila* Myc.** *Genesis* 2008, **46:**104-111.
30. Bissell MJ, Radisky D: **Putting tumours in context.** *Nat Rev Cancer* 2001, **1:**46-54.
31. Srivastava A, Pastor-Pareja JC, Igaki T, Pagliarini R, Xu T: **Basement membrane remodelling is essential for *Drosophila* disc eversion and tumor invasion.** *Proc Natl Acad Sci USA* 2007, **104:**2721-2726.
32. Uhlirova M, Bohmann D: **JNK- and Fos-regulated Mnp1 expression cooperates with Ras to induce invasive tumors in *Drosophila*.** *EMBO J* 2006, **25:**5294-5304.
33. Junttila MR, Westermarck J: **Mechanisms of MYC stabilization in human malignancies.** *Cell Cycle* 2008, **7:**592-596.
34. Leevers SJ, Weinkove D, MacDougall LK, Hafen E, Waterfield MD: **The *Drosophila* phosphoinositide 3-kinase Dp110 promotes cell growth.** *EMBO J* 1996, **15:**6584-6594.
35. Grewal SS, Li L, Orian A, Eisenman RN, Edgar BA: **Myc-dependent regulation of ribosomal RNA synthesis during development.** *Nat Cell Biol* 2005, **7:**295-302.
36. Kuranaga E, Kanuka H, Igaki T, Sawamoto K, Ichijo H, Okano H, Miura M: **Reaper mediated inhibition of DIAP-1-induced DTRAF1 degradation results in activation of JNK in *Drosophila*.** *Nat Cell Biol* 2002, **4:**705-710.
37. Ryoo HD, Gorenc T, Steller H: **Apoptotic cells can induce compensatory cell proliferation through the JNK and Wingless signaling pathways.** *Dev Cell* 2004, **7:**491-501.
38. Igaki T, Pagliarini RA, Xu T: **Loss of cell polarity drives tumor growth and invasion through JNK activation in *Drosophila*.** *Curr Biol* 2006, **16:**1139-1146.
39. Leong GR, Goulding KR, Amin N, Richardson HE, Brumby AM: **Scribble mutants promote aPKC and JNK-dependent epithelial neoplasia independently of Crumbs.** *BMC Biol* 2009, **7:**62.
40. Woolworth JA, Nallamothu G, Hsu T: **The *Drosophila* metastasis suppressor gene Nm23 homolog, awd, regulates epithelial integrity during oogenesis.** *Mol Cell Biol* 2009, **29:**4679-4690.
41. Cranna N, Quinn L: **Impact of steroid hormone signals on *Drosophila* cell cycle during development.** *Cell Div* 2009, **4:**3.
42. Wu DC, Johnston LA: **Control of wing size and proportions by *Drosophila myc*.** *Genetics* 2010, **184:**199-211.
43. Manfruelli P, Arquier N, Hanratty WP, Sémériva M: **The tumor suppressor gene, lethal(2)giant larvae (1(2)g1), is required for cell shape change of epithelial cells during *Drosophila* development.** *Development* 1996, **122:**2283-2294.
44. Zhao M, Szafranski P, Hall CA, Goode S: **Basolateral junctions utilize Warts signaling to control epithelial-mesenchymal transition and proliferation crucial for migration and invasion of *Drosophila* ovarian epithelial cells.** *Genetics* 2008, **178:**1947-1971.
45. Struhl G, Basler K: **Organizing activity of wingless protein in *Drosophila*.** *Cell* 1993, **72:**527-540.
46. Baker NE, Li W: **Cell competition and its possible relation to cancer.** *Cancer Res* 2008, **68:**5505-5507.
47. Grzeschik NA, Parsons LM, Allott M, Harvey KF, Richardson HE: **Lgl, aPKC and Crumbs regulate the Salvador/Warts/Hippo pathway through two distinct mechanisms.** *Curr Biol* in press.
48. Harvey K, Tapon N: **The Salvador-Warts-Hippo pathway - an emerging tumour-suppressor network.** *Nat Rev Cancer* 2007, **3:**182-191.
49. Wu S, Liu Y, Zheng Y, Dong J, Pan D: **The TEAD/TEF family protein Scalloped mediates transcriptional output of the Hippo growth-regulatory pathway.** *Dev Cell* 2008, **14:**388-398.
50. Zhang L, Ren F, Zhang Q, Chen Y, Wang B, Jiang J: **The TEAD/TEF family of transcription factor Scalloped mediates Hippo signaling in organ size control.** *Dev Cell* 2008, **14:**377-387.
51. Galletti M, Riccardo S, Parisi F, Lora C, Saqcena MK, Rivas L, Wong B, Serras F, Grifoni D, Pelicci P, Jiang J, Bellosta P: **Identification of domains responsible for ubiquitin-dependent degradation of dMyc by Glycogen Synthase Kinase 3b and Casein Kinase 1 kinases.** *Mol Cell Biol* 2009, **29:**3424-3434.
52. Zhan L, Rosenberg A, Bergami KC, Yu M, Xuan Z, Jaffe AB, Allred C, Muthuswamy SK: **Deregulation of scribble promotes mammary tumorigenesis and reveals a role for cell polarity in carcinoma.** *Cell* 2008, **135:**865-878.

53. Sansom OJ, Meniel VS, Muncan V, Phesse TJ, Wilkins JA, Reed KR, Vass JK, Athineos D, Clevers H, Clarke AR: **Myc deletion rescues Apc deficiency in the small intestine.** *Nature* 2007, **446:**676-679.
54. Xu T, Rubin GM: **Analysis of genetic mosaics in developing and adult *Drosophila* tissues.** *Development* 1994, **117:**1223-1237.
55. Prober DA, Edgar BA: **Interactions between Ras1, dMyc, and dPI3K signaling in the developing *Drosophila* wing.** *Genes Dev* 2002, **16:**2286-2299.

doi: 10.1186/1741-7007-8-33
Cite this article as: Froldi *et al.*, The lethal giant larvae tumour suppressor mutation requires dMyc oncoprotein to promote clonal malignancy *BMC Biology* 2010, **8**:33